



University
of Glasgow

Moreaux, Guenievre (2012) Investigating downstream effectors of KRas signalling in vivo: Dusp6 and Fra1. PhD thesis

<http://theses.gla.ac.uk/4056/>

Copyright and moral rights for this thesis are retained by the author

A copy can be downloaded for personal non-commercial research or study, without prior permission or charge

This thesis cannot be reproduced or quoted extensively from without first obtaining permission in writing from the Author

The content must not be changed in any way or sold commercially in any format or medium without the formal permission of the Author

When referring to this work, full bibliographic details including the author, title, awarding institution and date of the thesis must be given.

Investigating downstream effectors of KRas signalling *in vivo*: Dusp6 and Fra1

Guenièvre Moreaux, B.Sc.

Thesis submitted to the University of Glasgow for the degree of Doctor
of Philosophy

October 2012

Beatson Institute for Cancer Research
Garscube Estate
Switchback road
Glasgow, G61 1BD

ABSTRACT

Despite the high frequency of oncogenic *KRas* mutations in cancer, the precise mechanistic consequences of these mutations are unclear. In pancreatic cancer *KRas* mutation is thought to initiate tumourigenesis. In colorectal cancer *KRas* mutation causes tumour progression following an initiating mutation of Adenomatous Polyposis Coli (*Apc*).

In this thesis, in these two distinct scenarios, I examined the functional importance of, two downstream transcription targets of *KRas* signalling: Dual specificity phosphatase 6 (*Dusp6*) and Fos related antigen 1 (*Fra1*). *Dusp6* is a phosphatase specific for Erk 1/2 and therefore is predicted to be a tumour suppressor. On the other hand, *Fra1* is part of the AP-1 complex and is predicted to drive invasion and metastasis.

The aim of this work was to:

- Determine the implication of the MAPK pathway in colorectal cancer
- Determine the functional significance of *Dusp6* and *Fra1* deletion in two *in vivo* models
- Understand the mechanism of action of *Dusp6* and *Fra1* deletion

In colorectal cancer, *KRas* activation did not appear to robustly activate MAPK pathway and moreover pharmacological inhibition of this pathway had no impact upon cells carrying mutations in both *Apc* and *KRas*. Mechanistically this was associated with increased levels of *Dusp6* and *Dusp6* deletion increased proliferation and tumourigenesis in a MAPK dependent manner.

In pancreatic cancer, *KRas* mutation stimulated MAPK pathway and *Dusp6* deletion accelerated tumourigenesis. This again was partly dependant on the MAPK signalling pathway.

Surprisingly, *Fra1* deletion did not have expected consequences in the intestine. Here *Fra1* deletion did not modify invasion and instead accelerated tumourigenesis. Within the pancreas, *Fra1* deletion strongly suppressed tumourigenesis though not metastasis. Further mechanistic studies are required to elucidate the mechanism to explain these phenomena.

Overall, the deregulation of these two genes appears to be important events in cancer progression following *KRas* mutation. Importantly I have identified that *Dusp6* can act as a potential tumour suppressor protein downstream of *KRas* mutation, whilst *Fra1* can act as a context specific tumour suppressor or oncogene.

TABLE OF CONTENT

Abstract.....	2
Table of content	4
List of figures	8
Acknowledgements	11
Author's declaration.....	12
Abbreviations	13
Introduction.....	16
1 Introduction to colon cancer	16
1.1 Colorectal cancer.....	16
1.2 Biology of the Intestinal epithelium	18
1.2.1 Organisation of the intestinal epithelium.....	18
1.2.2 Intestinal stem cells.....	21
1.2.3 Identifying different epithelial lineages within the intestinal epithelium	27
1.3 The WNT signalling cascade.....	29
1.3.1 The canonical WNT pathway.....	29
1.3.2 Adenomatous Polyposis Coli (APC)	31
2 Introduction to pancreatic cancer	34
2.1 Pancreatic cancer	34
2.1.1 Biology of the pancreas.....	34
2.1.2 Pancreatic cancer (PC)	35
2.2 The oncogene <i>Ras</i>	37
2.2.1 KRas in CRC.....	37
2.2.2 KRas in PC	38
2.3 The MAPK pathway	38
2.3.1 The MAPKs	40
2.3.2 ERK 1/2	40
2.4 Other Ras effector pathways	42
2.4.1 The PI3K/Akt pathway	42
2.4.2 The Tiam/Rac pathway.....	43
3 The dusp family	44
3.1 MKP proteins	45
3.1.1 Structure.....	45
3.1.2 Subcellular localisation	46
3.2 MKPs and cancer	47
3.2.1 Dusp1	47
3.2.2 Other MKPs	48

3.3	Dusp6	49
3.3.1	Structure of dusp6.....	49
3.3.2	Subcellular localisation	51
3.3.3	Dusp6 targets specifically Erk	51
3.3.4	Regulation of DUSP6	52
3.3.5	Reciprocal activation and inactivation relationship between ERK and DUSP6..	54
3.3.6	Dusp6 and cancer.....	55
4	Fra1, a Ras pathways target	56
4.1	The AP-1 transcription factor.....	56
4.2	Fra1	57
5	Murine models of cancer	57
5.1	Cre Recombinase constructs:	58
5.1.1	Intestinal model: Vil-cre-ER system (VilCreER ⁺)	58
5.1.2	Intestinal model: AH-Cre system (AhCre ⁺)	58
5.1.3	Pancreatic model: Pdx-Cre system (PdxCre ⁺)	59
5.2	Modified alleles:	60
5.2.1	Dusp6	60
5.2.2	Fra1.....	60
5.2.3	Apc	61
5.2.4	KRas	61
5.2.5	p53.....	62
6	Thesis aim.....	63
	Materials and methods	64
7	<i>In vivo</i> experiments	64
7.1	Drug treatments	64
7.1.1	Induction reagents	64
7.1.2	MEK inhibitors.....	65
7.2	Mouse experiments.....	65
7.2.1	Time point experiments	65
7.2.2	Survival experiments:.....	66
8	Mouse genotyping	66
8.1	DNA isolation:	66
8.2	Genotyping via Polymerase Chain Reaction (PCR)	67
8.2.1	Primers for the <i>Dusp6</i> construct.....	67
8.2.2	PCR reactions	67
9	Primary cell culture	68
9.1	Media for cell culture	68
9.2	Experiments on PDAC cell primary culture	69
9.2.1	PDAC culture	69
9.2.2	Organotypic collagen I Invasion Assay	69
9.3	Villi culture	70
9.4	Crypt culture	70

10	Epithelial extraction	71
11	Tissue isolation.....	72
12	Immunohistochemistry on paraffin sections	73
12.1	Histochemistry	73
12.2	Immunohistochemistries (IHCs).....	73
12.2.1	β-Catenin IHC	73
12.2.2	pErk and pMek IHCs.....	75
12.2.3	β-galactosidase IHC.....	76
13	Protein analysis	77
13.1	Protein extract preparation.....	77
13.2	Protein concentration measurement	77
13.3	Western Blot	77
14	Statistics:.....	79
Results	80
15	Oncogenic <i>KRas</i> phenotype in the CRC mouse model	80
15.1	Oncogenic <i>KRas</i> mutation increases proliferation rates of intestinal cells following <i>Apc</i> deletion.	80
15.1.1	Influence of <i>KRas</i> mutations on tumourigenesis	80
15.1.2	Influence of <i>KRas</i> mutation on the phenotype after an acute <i>Apc</i> deletion	82
15.2	Oncogenic <i>KRas</i> allows an expansion of the cell of origin of the tumour	86
15.3	<i>KRas</i> activation signature	90
15.3.1	Wnt pathway signature	90
15.3.2	Stem cell signature	95
15.3.3	MAPK pathway signature.....	97
16	<i>Dusp6</i> deletion effects in the context of <i>Apc</i> deletion driven tumourigenesis associated with <i>KRas</i> activation	101
16.1	<i>Dusp6</i> deletion effects during oncogenic <i>KRas</i> driven tumourigenesis .	101
16.1.1	<i>Dusp6</i> loss effects in VilCreER ⁺ Apc ^{fl/+} KRas ^{LsL-G12D/+} mice	101
16.1.2	<i>Dusp6</i> loss effects in VilCreER ⁺ Apc ^{fl/+} KRas ^{LsL-G12V/+} mice.....	108
16.2	<i>Dusp6</i> deletion effects on CPL phenotype	110
16.2.1	<i>Dusp6</i> loss effects on proliferation.....	110
16.2.2	<i>Dusp6</i> loss effects on cell differentiation	112
16.3	<i>Dusp6</i> loss signature.....	114
16.3.1	Wnt pathway signature	114
16.3.2	Stem cell signature	118
16.3.3	MAPK pathway signature.....	120
17	The functional outcome of Mek inhibition following <i>Dusp6</i> loss	123
17.1	The chemoprevention effects of Mek inhibition are <i>Dusp6</i> loss dependent	123
17.2	Mek inhibition affects the CPL phenotype only when <i>Dusp6</i> is deleted	126

18	Dusp6 deletion effects on tumourigenesis.....	130
18.1	Dusp6 deletion effects in the context of Apc deletion alone	130
18.2	Dusp6 deletion effects in the context of <i>KRas</i> activation alone	131
19	Effects of <i>Dusp6</i> deletion on MAPK pathway	134
20	Impact of Mek inhibition on gene signature	138
20.1	Wnt pathway signature	138
20.2	Stem cell signature.....	145
20.3	MAPK pathway signature	148
21	Dusp6 in Pancreatic tumourigenesis	154
21.1	<i>Dusp6</i> loss increases tumourigenesis following <i>KRas</i> activation	154
21.2	<i>Dusp6</i> heterozygosity allows the formation of metastases.....	158
21.3	Effects of <i>Dusp6</i> deletion on MAPK pathway	164
21.3.1	Erk activation is independent of <i>Dusp6</i> status	164
21.3.2	Effect of Mek inhibition on tumourigenesis.....	165
22	The role of Fra1 in two <i>in vivo</i> cancer models - a paradox	168
22.1	Fra1 deletion impacts on intestinal homeostasis	168
22.2	Fra1 deletion can accelerate tumourigenesis	172
22.2.1	The effect of Fra1 deletion following <i>Apc</i> deletion	172
22.2.2	<i>Fra1</i> deletion in the context of <i>KRas</i> activation	174
22.3	<i>Fra1</i> deletion can increase tumour free survival	176
22.4	Conclusion and discussion	180
	Discussion	182
23	Colorectal cancer and the MAPK cascade	182
23.1	Current CRC chemotherapy treatments.....	182
23.2	Finding new chemotherapy agents.....	184
24	Is <i>Dusp6</i> a tumour suppressor gene?	189
24.1	<i>Dusp6</i> can act as a tumour suppressor	189
24.2	<i>Dusp6</i> can promote tumourigenesis.....	191
	Appendix.....	195
	List of References.....	205

LIST OF FIGURES

Figure 1: Overview of the evolution of CRC	17
Figure 2: Gut epithelium organisation.....	18
Figure 3: Mouse gut epithelium	19
Figure 4: Cell migration in mouse intestinal epithelium.....	28
Figure 5: The Wnt pathway	31
Figure 6: Structure of the Apc protein	32
Figure 7: The CPL phenotype	33
Figure 8: The mouse pancreas organisation	35
Figure 9: Overview of the evolution of PDAC	36
Figure 10: Overview of the MAPK pathway	39
Figure 11: Dual Specificity Phosphatases classification:.....	45
Figure 12: The MKPs classification and their human chromosome localisation ..	46
Figure 13: The MKPs specific targets and their cellular localisation.....	47
Figure 14: Structure of Dusp6/Mkp3.....	50
Figure 15: Representation of the MKB/KIM domain of Dusp6.	51
Figure 16: Overview of MAPK pathway and Dusp6 interactions.....	53
Figure 17: Erk-induced activation of Dusp6	54
Figure 18: Autoinhibition of Dusp6.....	55
Figure 19: Recombination in the pancreatic model	59
Figure 20: Dusp6 null allele.....	60
Figure 21: PCR mix	67
Figure 22: Crypt culture	71
Figure 23: Immunoblot antibodies	78
Figure 24: Effect of <i>KRas</i> activation on the tumour free survival	81
Figure 25: Quantification of proliferation	83
Figure 26: Effects of <i>KRas</i> activation on CPL phenotype following <i>Apc</i> deletion	85
Figure 27: Effects of <i>KRas</i> activation on CPL phenotype area	86
Figure 28: <i>KRas</i> activation allows tumours to form in the villus	87
Figure 29: Tumour formation in the colon of <i>KRas</i> activated mice	88
Figure 30: Effect of <i>KRas</i> activation on spheroid formation from the villus epithelium.....	89
Figure 31A: WNT pathway signature.....	92
Figure 31B: WNT pathway signature.....	94
Figure 32: WNT pathway signature: confirmation of targets by qRT-PCR.....	95
Figure 33: Stem cell signature.....	96
Figure 34: MAPK pathway signature	99
Figure 35: Levels of Dusp6 protein.....	100
Figure 36: Effects of <i>Dusp6</i> deletion on tumour free survival	102
Figure 37: <i>KRas</i> activation allows tumours to form in the villus independently of <i>Dusp6</i> status.....	103
Figure 38: Wnt pathway activation following <i>Apc</i> deletion and <i>KRas</i> activation	104
Figure 39: Effects of <i>Dusp6</i> deletion in the context of slower tumourigenesis .	105
Figure 40: Effects of <i>Dusp6</i> deletion in the context of slower tumourigenesis .	107
Figure 41: <i>Dusp6</i> deletion decreases survival following <i>KRas</i> activation (<i>KRas</i> ^{L^{SL}- G12V} allele).	108
Figure 42: Tumour formation following <i>KRas</i> activation (<i>KRas</i> ^{L^{SL}-G12V} allele). ...	109

Figure 43: The effects of <i>Dusp6</i> deletion on the CPL phenotype.....	111
Figure 44: Comparison of the CPL phenotype of AK and AKD mice	113
Figure 45A: WNT pathway signature.....	115
Figure 45B: WNT pathway signature.....	117
Figure 46: Stem cell signature.....	119
Figure 47: MAPK pathway signature	122
Figure 48: Effects of Mek inhibition on survival.....	124
Figure 49: Effects of Mek inhibition on tumourigenesis in <i>Dusp6</i> null mice	125
Figure 50: Effects of Mek inhibition on tumourigenesis.....	125
Figure 51: Effects of Mek inhibition on proliferation in the CPL phenotype of <i>Dusp6</i> null mice.....	127
Figure 52: Effects of Mek inhibition on proliferation in the CPL phenotype of <i>KRas</i> activated mice	128
Figure 53: <i>Dusp6</i> deletion has no effect following <i>Apc</i> deletion alone.....	130
Figure 54: <i>Dusp6</i> deletion reduces the survival following <i>KRas</i> activation	132
Figure 55: <i>Dusp6</i> deletion allows tumour formation following <i>KRas</i> activation .	132
Figure 56: Activation of Wnt signalling in <i>KRas</i> activated mice	133
Figure 57: MAPK pathway activation following <i>Apc</i> deletion and <i>KRas</i> activation	135
Figure 58: MAPK pathway activation in the intestinal epithelium	137
Figure 59: MAPK pathway activation in CPL phenotype	137
Figure 60A: WNT pathway signature.....	140
Figure 60B: WNT pathway signature.....	144
Figure 61: Stem cell signature.....	147
Figure 62: MAPK pathway signature	152
Figure 63: Effects of <i>Dusp6</i> deletion on survival in the context of tumourigenesis driven by the <i>KRas</i> ^{L^{SL}-G12D/+} allele.....	155
Figure 64: Multiple cells of origin for pancreatic lesions	156
Figure 65: Senescence	157
Figure 66: Effects of <i>Dusp6</i> loss on survival in the context of tumourigenesis driven by the <i>KRas</i> ^{L^{SL}-G12V/+} allele.....	158
Figure 67: Activation of the TGF β pathway	160
Figure 68: Liver metastasis	161
Figure 69: Organotypic assay	163
Figure 70: Activation of Erk in early pancreatic lesions	164
Figure 71: PDAC characteristics	165
Figure 72: Allograft experiment.....	166
Figure 73: <i>Fra1</i> deletion does not affect differentiation.....	169
Figure 74: <i>Fra1</i> deletion affects proliferation	170
Figure 75: <i>Fra1</i> deletion affects mitosis	171
Figure 76: <i>Fra1</i> deletion affects mitosis	172
Figure 77: <i>Fra1</i> deletion decreases survival	173
Figure 78: <i>Fra1</i> deletion decreases survival.....	175
Figure 79: <i>Fra1</i> deletion decreases survival.....	176
Figure 80: <i>Fra1</i> deletion increases survival in a pancreatic cancer model.....	177
Figure 81: <i>Fra1</i> deletion increases survival in a pancreatic cancer model.....	178
Figure 82: The effects of <i>Fra1</i> deletion are partially rescued by a p53 mutation	179
Figure 83: Targeting Wnt pathway.....	188
Supplementary figure 1: Wnt signature; Clustering WT, A and AK mice samples	196

Supplementary figure 2: Stem cells signature; Clustering WT, A and AK mice samples	197
Supplementary figure 3: MAPK signature; Clustering WT, A and AK mice samples	198
Supplementary figure 4: Wnt signature; Clustering AK and AKD mice samples ..	199
Supplementary figure 5: Stem cells signature; Clustering AK and AKD mice samples	200
Supplementary figure 6: MAPK signature; Clustering AK and AKD mice samples	201
Supplementary figure 7: Wnt signature; Clustering AK and AKD mice samples treated with CI1040	202
Supplementary figure 8: Stem cells signature; Clustering AK and AKD mice samples treated with CI1040	203
Supplementary figure 9: MAPK signature; Clustering AK and AKD mice samples treated with CI1040	204

ACKNOWLEDGEMENTS

I would like to thank my supervisor Owen Sansom for the help and support he has given me in the last 4 years, for being patient and for believing in me when I lost belief in myself (especially during write-up!). I would also like to thank my past and present advisors Walter Kolch, Brad Ozanne and Jim Norman, you have taken the time to listen and encourage me along the way.

A special thanks to my examiners, Marcos Vidal and Farhat Din, who have kindly agreed to review my thesis.

A “mulțumesc” to my lovely Sorina for your help all along the PhD and especially for your thesis proof reading. But “merci” mostly for being who you are: my very special vampire friend. A big thank you to everybody in the R18, R14 and Y35 labs (both past and present) as well as all the animal house staff, everybody in histology (Colin you are a histology star and a very quiet neighbour!), Gabriela and Ann for being wonderful bioinformaticians and most importantly the mice. I could not have done any of this without you!

I also want to thank the Beatson for providing great science but also making me meet other fantastic people who have given me great support and entertainment: the "coffee girls" and the poker/night out/climbing folks. Thank you to all the dance people who have been oxygen for the artist in me for the last 4 years. Thanks to the two other S of the “triple S” trio who can be far in distance but always close in mind and thanks to Pierre for taking with him a piece of me around the world.

And last but not least thank you to my family: my mother for great and unconditional support, my "second parents" Sylvie and Jean-Luc for their good care and affection, my Babe sister for keeping my mind busy, my cousins Martin and Alexia for great pieces of advice and great phone discussions as well as IT support and finally my 3 grandmothers for being my eternal inspiration. And of course, a very special thank you to Robert Hulk.

AUTHOR'S DECLARATION

I'm the sole author of the thesis and all the work presented is my own unless stated otherwise. No part of this work has been submitted for consideration as part of any other degree or award.

ABBREVIATIONS

4EBP1	4E Binding Protein 1
AH	Aryl Hydrocarbon
AMPK	Adenosine Monophosphate-activated Protein Kinase
AP-1	Activator Protein 1
APC	Adenomatous Polyposis Coli
ACF	Aberrant Crypt Focus
Ascl2	Achaete scute-like 2
Asef	Apc-Stimulated guanine nucleotide Exchange Factor
BCR-ABL	Philadelphia Chromosome
BRaf	V-raf murine sarcoma viral oncogene homolog B1
BRCA	Breast Cancer (gene)
BrdU	Bromodeoxyuridine
β -TRCP	F-box β -transducin repeats-containing protein
C-Ter	C-Terminal
CBC	Crypt Base Columnar
CD	Cluster of Differentiation
CDC	Cell Division Cycle (gene)
CDK	Cyclin-Dependent Kinase
CK1	Casein Kinase 1
CPL	Crypt Progenitor-Like
CRC	Colorectal Cancer
Cyp1A1	Cytochrome p450 subfamily A1
DAB	3,3'-Diaminobenzidine
Dkk	Dickkopf
DMBA	7,12-dimethylbenzanthracene
DNA	Deoxyribonucleic Acid
Dsh	Dishevelled
DUSP	Dual-Specificity Phosphatase
EB1	End Binding 1
EGFR	Epithelial Growth Factor Receptor
EphB2	Ephrin B2
ER	Estrogen Receptor
ErbB2	Erythroblastic leukemia viral oncogene homolog 2
ERK	Extracellular-signal Regulated Kinase
ESCC	Oesophageal Squamous Cell Carcinoma
ETS	ERK-responsive Transcription factor
Etv4	ETS translocation variant 4
FAP	Familial Adenomatous Polyposis
FGF	Fibroblast Growth Factor
FLIM	Fluorescence Lifetime Imaging Microscopy
FOXO3A	Forkhead box O3
FRA1	Fos Related Antigen 1
FRET	Forster Resonance Energy Transfer
Fz	Frizzled receptor
GAP	GTPase Activating Protein
GDP	Guanosine-Diphosphate

GEF	Guanine nucleotide Exchange Factor
GFP	Green Fluorescent Protein
Grb2	Growth factor receptor bound 2
GSK3B	Glycogen Synthase Kinase 3B
GTP	Guanosine-Triphosphate
H2B	Histone 2B
HNPCC	Hereditary Non-Polyposis Colorectal Cancer
HRas	Ha Ras
IGFR	Insulin Growth Factor Receptor
IHC	Immunohistochemistry
IκB	Inhibitor of kappa B
IKK	IκB Kinase
Int 1	Integration 1
IP	Intra-peritoneal
IRES	Internal Ribosomal Entry Site
JNK	cJun N-Terminal Kinase
KDa	Kilo Dalton
KIM	Kinase Interaction Motif
KRas	Kirsten Ras
LCR	Label-Retaining Cell
LEF	Lymphoid Enhancer Factor
LGR	Leucine-rich repeat containing G-protein coupled receptor
LKB1	Liver Kinase B1
LOH	Loss Of Heterozygosity
LPS	Bacterial Lipopolysaccharide
LRC	Label-Retaining Cell
LRP5/6	Lipoprotein Receptor-related Protein 5/6
LSL	LoxP-STOP-LoxP
MAP	Mitogen-Activated Protein
MAPK	Mitogen-Activated Protein Kinase
MEF	Mouse Embryonic Fibroblasts
MEK	Mitogen-associated Extracellular regulated Kinase
MKB	MAP Kinase Binding
MKP	MAP Kinase Phosphatase
mTOR	mammalian Target Of Rapamycin
mRNA	messenger Ribonucleic Acid
NES	Nuclear Export Signal
Nfe2l2	Nuclear factor erythroid-derived 2-like 2 (also called Nrf2)
NFκB	Nuclear Factor kappa-light-chain-enhancer of activated B cells
NGF	Nerve Growth Factor
NLS	Nuclear Localisation Signal
NPC	Nasopharyngeal Carcinoma
NRas	Neuroblastoma Ras
N-Ter	N-Terminal
NTS	Nuclear Translocation Signal
Olfm4	Olfactomedin 4
PanIN	Pancreatic Intraepithelial Neoplasia
PC	Pancreatic Cancer
PDAC	Pancreatic Ductal Adenocarcinoma
PDGF	Platelet-derived Growth Factor
PDGFR	Platelet-derived Growth Factor Receptor

PDK1	Phosphoinositide Dependent protein Kinase 1
Pdx1	Pancreatic and duodenal homeobox 1
PEST	Proline-Glutamate-Serine-Threonine
PI3K	Phosphatidylinositol 3-Kinase
PKB	Protein Kinase B
PMA	Phorbol 12-myristate 13-acetate
PP2	Phosphatidylinositol biphosphate
PP3	Phosphatidylinositol triphosphate
PP2A	Protein phosphatase 2A
Prom1	Prominin 1 (also called CD133)
PTEN	Phosphatase and Tensin homologue
qRT-PCR	quantitative Real-Time Polymerase Chain Reaction
R26	Rosa 26
Rac	RAS-related C3 botulinum substrate
Ral	Ras Related
RNA	Ribonucleic Acid
ROS	Reactive Oxygen Species
R-Spondin	Roof plate-specific Spondin
RTK	Receptor Tyrosine Kinases
S6K1	S6 Kinase 1
SAMP	Serine-Alanine-Methionine-Proline
Shc	Src homology 2 domain-containing protein
Smad3	Mothers against decapentaplegic homolog
SOS	Son Of Sevenless
Src	Sarcoma (gene)
STAT	Signal Transducer and Activator of Transcription
TAC	Transient Amplifying Cell
TCF	T-Cell Factor
TGFB	Transforming Growth Factor β
Tiam	T lymphoma invasion and metastasis
TMA	Tissue Microarray
TNF	Tumour Necrosis Factor
TNKi	Tankyrase inhibitors
TPA	12-O-tetradecanoylphorbol-13-acetate
TRAIL	TNF Related Apoptosis-inducing Ligand
UK	United Kingdom
UTR	Untranslated Region
VEGF	Vascular Endothelial Growth Factor
VEGFR	Vascular Endothelial Growth Factor Receptor
Vil	Villin
Wg	Wingless
WT	Wild Type

INTRODUCTION

1 Introduction to colon cancer

1.1 Colorectal cancer

Colorectal cancer (CRC) is one of the most commonly diagnosed cancers in UK. It is the second most commonly diagnosed cancer for women and the third for men according to Cancer Research UK statistics for 2009 (<http://www.cancerresearchuk.org/cancer-info/cancerstats/>). It is the third cause of cancer death for both women and men and represents 10% of the total mortality by cancer in UK. However, comparing the statistics from 1999-2001 with the 2008-2010 statistics there is a 14% reduction in the number of deaths from CRC.

There are two types of CRC: sporadic and hereditary. Most cases of CRC are sporadic and multiple factors such as diet or alcohol consumption can contribute towards this, while familial CRC can be divided in 2 groups: Familial Adenomatous Polyposis (FAP) and Hereditary Non-Polyposis Colorectal Cancer (HNPCC). HNPCC patients have germline mutations in mismatch repair genes which lead to microsatellite instability. These germline mutations give an 80% chance of developing CRC, 60% for endometrial cancers and less than 20% for gastric, ovarian and bladder cancer (Lynch and de la Chapelle 2003). FAP is an autosomal dominant disease and is due to a germline mutation in the chromosome 5q where the gene *Adenomatous polyposis Coli* (*Apc*) is found (Bodmer, Bailey et al. 1987; Lynch and de la Chapelle 2003). This renders this hereditary disease the closest to sporadic CRC as mutations in the *Apc* tumour suppressor have been found in over 80% of sporadic CRC cases.

The progression of CRC from benign adenoma to invasive carcinoma has been extensively studied and at the molecular level several genetic mutations have been shown to contribute in this process (Figure 1). The most frequent

mutations are in the genes *Apc*, *KRas*, *p53* and *smad4* (Vogelstein, Fearon et al. 1988; Vogelstein, Fearon et al. 1989; Fodde, Smits et al. 2001). The first visible lesion in the colonic epithelium is the aberrant crypt focus (ACF). This consists of early microscopic lesions where dysplastic cells are found surrounded by normal non-dysplastic cells. These lesions progress into a polyp or adenoma. An adenoma is a benign tumour composed of dysplastic cells and starts to protrude into the lumen of the gut. These adenomas will then evolve progressively to adenocarcinoma, consisting of a malignant lesion made of a disorganised epithelium containing cells which have lost nuclear polarity, are poorly differentiated and can secrete mucus. These malignant lesions finally lead to metastases formation mostly in the liver. Given the frequency of the *Apc* mutation in human tumours and the fact that in murine models loss of *Apc* leads directly to ACF and adenoma formation (Sansom, Reed et al. 2004) it is often considered that this mutation may be the initiating event of CRC. Furthermore, a sequential model of the evolution of CRC has been proposed (Vogelstein, Fearon et al. 1988; Vogelstein, Fearon et al. 1989). However, there is no real proof of a defined mutational sequence even if for example the *p53* mutation is believed to be a late event as it correlates with more advanced stages (Baker, Preisinger et al. 1990).

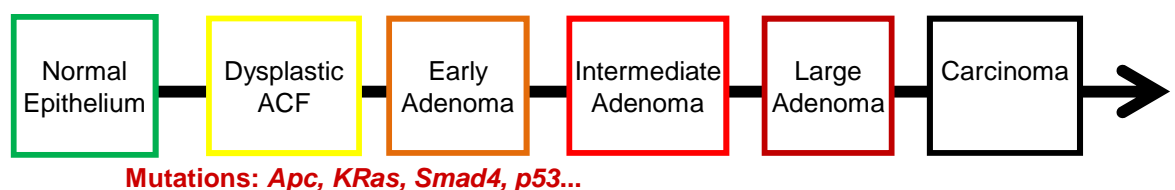


Figure 1: Overview of the evolution of CRC

Initiating mutations allow formation of aberrant crypt foci (ACF) evolving into benign early adenomas. Then accumulation of mutations allows the progression of adenomas to aggressive and invasive carcinomas.

1.2 Biology of the Intestinal epithelium

In order to understand the carcinogenesis process within the intestinal epithelium, it is important to have an overview of the normal homeostasis (for review: (de Santa Barbara, van den Brink et al. 2003; Sancho, Batlle et al. 2004; Pinto and Clevers 2005)).

1.2.1 Organisation of the intestinal epithelium

The intestinal tract is composed of three layers: an inner mucosa absorbing the nutrients protected by a stroma layer surrounded by an external smooth muscle layer responsible for peristalsis. The gut epithelium is composed of luminal villi and crypts of Lieberkühn which are invaginations into the submucosa. These crypt-villus units are conserved through the entire small intestine whereas the colon contains only crypts with a flat surface epithelium. These units are composed of epithelial cells which are organised as monolayer which covers the surface of the gut (Figures 2 and 3).

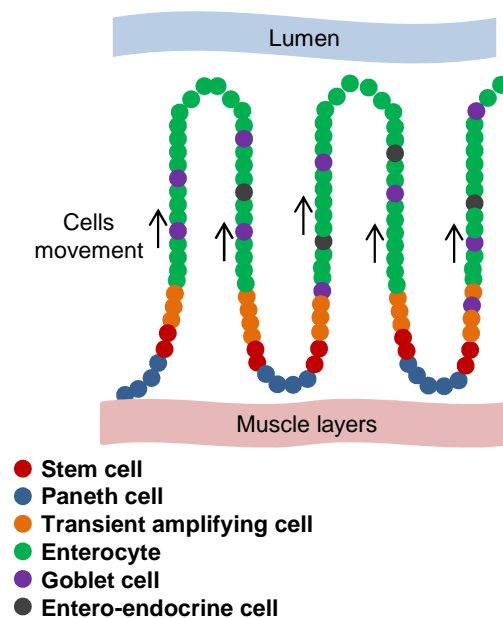


Figure 2: Gut epithelium organisation

Stem cells produce transient amplifying cells which then actively generate other cell types which are progressively moving up the crypt-villus axis to be shed off in the gut lumen.

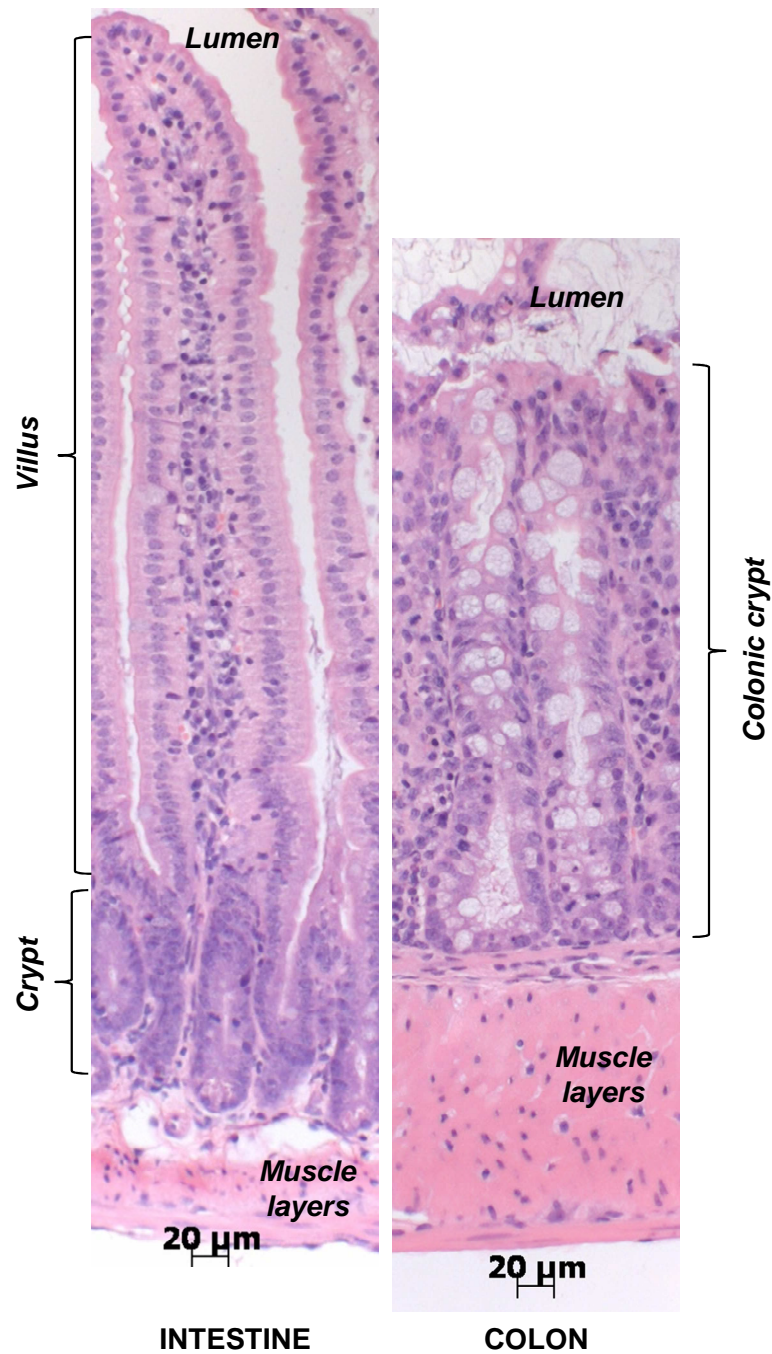


Figure 3: Mouse gut epithelium

H&E of intestine (left panel) and colon (right panel) of a wild type mouse. In the intestine the cells are organised in a single cell layer from the bottom of the crypt in contact with the muscle layers to the top of the villus reaching the gut lumen. The colonic epithelium consists in long crypts organised in a similar way to the crypt-villus axis of the intestine.

The epithelial cells are highly specialised and are continuously produced and discarded throughout the life of the organism. The turnover of intestinal cells is estimated to three days in mice and five days in humans. Epithelial stem cells (four to six stem cells per crypts are estimated) are located at the bottom of the crypt and, undergoing asymmetric division, continuously produce undifferentiated progenitors named transient amplifying cells (TAC) leading to the four intestinal cell types: enterocytes, Goblet cells, Paneth cells and entero-endocrine cells. Recently the Clevers laboratory generated a very elegant new mouse model that allows lineage tracing from individual Lgr5 positive epithelial stem cells, namely the *Cre*-reporter allele R26R-Confetti (Snippert, van der Flier et al. 2010). To do so, they integrated into the Rosa26 locus a CAG promoter followed by a LoxP-flanked Neo cassette (serving as a STOP cassette) and the Brainbow 2.1 construct (Livet, Weissman et al. 2007). The R26R-Confetti allele functions as a stochastic multicolour *Cre* recombinase reporter of multiple fluorescent proteins from a single genomic locus. These R26R-Confetti mice allow a way to label and distinguish individual cells with nuclear localized, membrane-targeted, or cytoplasmic fluorescent proteins in recombined cells. *Cre*-mediated recombination will remove the STOP cassette and a fluorescent marker will be expressed in the newly produced cells allowing us to distinguish between the stem cells and their progeny. This work allowed the Clevers laboratory to show that although there are many intestinal stem cells per crypts, crypts purify through a stochastic process so all cells will be the daughters of a single Lgr5 positive intestinal stem cell.

Within the intestinal epithelium many of the cell types have a specific position through the crypt-villus axis as well as a defined number and their mislocalisation and/or change in number indicate a disturbed homeostasis which may be linked to cancer.

In the small intestine, up to 80% of epithelial cells are enterocytes. They are columnar cells with apical microvilli helping the absorption of nutrients going through the intestinal tract. The Goblet cells are responsible for mucus production. They can represent up to 5% of the cells and they are spread from the crypt to the top of the villi. They are characterised by mucous granules in

their cytoplasm. The entero-endocrine cells are responsible for the secretion of hormones important in the censoring of the luminal content such as cholecystokinin, glucagon-like peptide-1 and oxyntomodulin. Their number is very low and they are located predominantly in the villus. Paneth cells express the marker cluster of differentiation 24 (CD24), are located at the bottom of the crypts and their original function was proposed to be associated with the antimicrobial barrier because of enzyme production such as defensins and lysozyme, however, they are now also thought to be an important component of the stem cell niche (Sato, van Es et al. 2011). Moreover, they are not found in the villus and seem restricted to the crypt compartment despite the cell migration from the crypt to the top of the villus.

In the colon, the differentiated cells are mainly enterocytes and Goblet cells. However a CD24 positive cell population located between stem cells is believed to play the role of Paneth cells (Sato, van Es et al. 2011). The Goblet cells are found in a higher proportion compared to the intestine and are located in the mid-crypt area. Some endocrine cells can be found at the base of the crypt nearby the stem cells.

The epithelium renewal is achieved by cell migration from the crypt to the villus while proliferation and differentiation is constantly maintained (Potten and Loeffler 1990). The TACs undergo up to seven divisions before they terminally differentiate into their progeny which will be move higher on the crypt-villus axis. This constant cell renewal leads to the elimination of the old cells placed at the top of the villi into the lumen. Any modification of this tightly regulated process is a sign of a potentially malignant lesion.

1.2.2 Intestinal stem cells

Intestinal stem cells are self-renewing undifferentiated cells able to give rise to all cell types within a tissue and which function as a reservoir of new cells in normal tissue homeostasis and injury. They are usually long lived and can either be quiescent or actively cycling. They are located within a stem cell niche thought to be constituted by Paneth cells (Sato, van Es et al. 2011). They are also thought to undergo asymmetric division to generate the fast cycling

transient amplifying cells (TAC) which are responsible for the maintenance of the villus by dividing and differentiating when at the crypt villus junction. However, identifying stem cells remains difficult and controversial, and in the intestine at least two distinct populations of cells have been classified as stem cells.

Crypt base columnar, Lgr5⁺ stem cells

In 1974 Cheng and Leblond first described the crypt base columnar (CBC) cells as occupying the nine lowest positions of the crypt interspersed among the Paneth cells (Cheng and Leblond 1974; Bjerknes and Cheng 2005). These cells were marked by a one hour radioactive ³H-Thymidine labelling targeting cells undergoing DNA replication. Furthermore, a continuous labelling with ³H-Thymidine showed that these cells were actively dividing and able to generate all the epithelial cells (Cheng and Leblond 1974). Recently Leucine-rich repeat containing G-protein coupled receptor 5 (*Lgr5*) has been described as a robust marker of these stem cells (Barker and Clevers 2007; Barker, van Es et al. 2007). *Lgr5* expression has been confirmed in transgenic *Lgr5*-EGFP⁺ mice where GFP fluorescence was observed at the bottom of intestinal crypts. Furthermore, elegant experiments have shown that *Lgr5* is a bona fide stem cell marker via lineage tracing. Here, *Lgr5*-EGFP⁺-Cre^{ER} mice were intercrossed with the *Cre* activable lox-STOP-lox ROSA26 (R26R)-LacZ reporter which facilitated the visualisation of *Lgr5* positive cells progeny (Soriano 1999; Barker, van Es et al. 2007). Tamoxifen injection activated the Lac-Z reporter specifically in *Lgr5* positive CBC cells allowing the tracking of daughter cells (Barker and Clevers 2007). This proved the ability of CBC cells to generate all intestinal epithelium cells.

Lgr5 is a target and a component of the Wnt pathway. Wnt signalling is essential for intestinal homeostasis, with the highest levels specifying both the Paneth and stem cell fate. Transgenic mice expressing, under the control of the villin promoter, *Dickkopf* (*Dkk*), a secreted inhibitor of the Wnt pathway, have a strong reduction of crypt formation and shortened villus structures in adult mice intestine (Pinto, Gregorieff et al. 2003). In *Lgr5*-GFP transgenic mice the expression of *Dkk* by adenovirus induced a drastic loss of *Lgr5* expression (Yan,

Chia et al. 2012). Furthermore, a conditional deletion of *B-Catenin* within the adult intestine rapidly leads to crypt death by increased apoptosis and mislocalisation of Paneth cells (Ireland, Kemp et al. 2004). Following crypt death, a rapid repopulation of the epithelium by unrecombined cells was observed. *Lgr5* function, by binding the Wnt agonist R-Spondin, allows maximal activation of the Wnt signalling pathway (de Lau, Barker et al. 2011; Glinka, Dolde et al. 2011). Thus this may explain why intestinal stem cells have the highest levels of Wnt signalling in the adult intestine. Deletion of *Lgr5* has little phenotype alone in the adult intestine, presumably due to compensation by the other *Lgr6* (de Lau, Barker et al. 2011). Deletion of both *Lgr5* and *Lgr4* rapidly leads to crypt death suggesting that *Lgr5* is not only a marker of intestinal stem cells but also an important specifier of intestinal stem cell fate (de Lau, Barker et al. 2011).

As well as a stem cell marker, it appears that *Lgr5* positive cells may be the cell of origin for intestinal adenomas (Barker, Ridgway et al. 2009). Using *Lgr5*-EGFP-IRES-cre^{ER} knock-in mice (where *Lgr5* positive cells are specifically targeted), *Apc* deletion was targeted to the stem cells and led rapidly to large highly proliferative adenomas. In contrast targeting *Apc* deletion outside of the stem cell region led to small lesions that very rarely formed adenomas and if so these took much longer.

Given the lack of antibodies to *Lgr5*, the *Lgr5*-EGFP mouse has been very useful to isolate stem cells from the murine intestine and further define this intestinal stem cell population. This has led to a number of other markers that are highly enriched in the crypt columnar cells such as Achaete scute-like 2 (*Ascl2*) and Olfactomedin 4 (*Olfm4*). These markers are not only enriched in stem cells but also in colorectal cancer. In human CRC both *Lgr5* and *Ascl2*, another Wnt target gene (Sansom, Reed et al. 2004), are highly expressed (over 70%) and correlated (Ziskin, Dunlap et al. 2012). *Ascl2* co-localises with *Lgr5* positive cells and is located at the base of the crypts as shown by *in situ* hybridisation. Furthermore *Ascl2* deletion leads to intestinal stem cell loss (van der Flier, van Gijn et al. 2009). Therefore *Ascl2* is considered as another CBC stem cell population marker. *Olfm4* is expressed in *Lgr5* positive cells of the bottom of the crypt (van

der Flier, Haegebarth et al. 2009; van der Flier, van Gijn et al. 2009) yet its expression is interestingly Wnt independent. Prominin 1 (Prom1, also named CD133) is expressed in cells with the same characteristics as the CBC cell and co-expresses with Lgr5 at the bottom of the crypt. Moreover, CD133 positive cells were able to generate all intestinal cell types (Zhu, Gibson et al. 2009). It is important to note that Ascl2, Olfm4 and CD133 overlap CBC Lgr5 positive cells but also mark cells further up in the crypt and therefore are thought to be conserved in daughters arising from CBC cells. The Batlle group had shown in human CRC, the Lgr5 high population overlaps with the Ephrin B2 (EphB2) Receptor high population, which there are antibodies to, that allows FACs sorting and isolation of the Lgr5 high cells from human CRC (Batlle, Henderson et al. 2002; Merlos-Suarez, Barriga et al. 2011). Isolation of this population showed it enriched for tumour initiating capacity. Moreover tumours with high expression of these markers showed increased chances of relapse. This finding is somewhat controversial as the Medema group has shown that although colon cancer stem cells are defined by high Wnt activity, the tumours that carry the worse prognosis instead have the intestinal stem cell markers hypermethylated (de Sousa, Colak et al. 2011). It is perhaps unsurprising that in a complex situation of colorectal cancer where tumours carry many mutations that simple correlation between the intestinal stem cells and cancer has not been found. It is interesting to note that recently it has been suggested that a BRAf-like signature carries a poor prognosis in CRC and this is associated with lower levels of Wnt signalling and hence might be expected to have low levels of the stem cells markers (Popovici, Budinska et al. 2012).

Label-Retaining Stem cells

In parallel with the Cheng and Leblond studies another intestinal stem cell population was described by Potten et al (Potten, Kovacs et al. 1974). They labelled cells undergoing DNA replication by using ³H-Thymidine and showed that among the proliferative cells 15 to 20% were slowly dividing (hence their name: label-retaining cells (LRC)). These cells were described as located at the position +4 of the crypt just above the Paneth cells. B lymphoma Mo-MLV insertion region 1 homolog (Bmi1) is essential for the self-renewal of hematopoietic cells and its

role in other adult stem cell populations has been studied in a mouse model expressing a tamoxifen-inducible *Cre* from the *Bmi1* locus (Sangiorgi and Capecchi 2008). In a similar set of experiments to the ones I described above with *Lgr5-Cre^{ER}* these mice were then crossed to the Rosa 26 Lac-Z reporter and lineage tracing was observed. One slight caveat to these experiments is that both the Clevers laboratory and the recent work by the de Sauvage group have shown *Bmi1* expressed throughout the crypt (Sangiorgi and Capecchi 2008; Itzkovitz, Lyubimova et al. 2012; Munoz, Stange et al. 2012). This would therefore suggest that although the *Bmi1* positive cells would contain the label retaining cells, not every *Bmi1* positive cell would be a LRC. The existence of a 'back-up' population of cells which can replace the *Lgr5* positive is however not in doubt. Recent experiments have shown that targeting the *Lgr5* stem cells with diphtheria toxin does not kill the intestine and a non-*Lgr5* positive stem cell population repopulates the intestine (Tian, Biehs et al. 2011). This does not necessarily have to be a LRC as cells may fall back into the niche and then repopulate the intestine. Recent experiments by the Clevers and Fodde laboratories have suggested that there may be secretory/differentiated progenitor cells that repopulate the crypt post injury (van Es, Sato et al. 2012; Wang, Sacchetti et al. 2012). Given these cells have differentiated they could be thought also as LRC cells as differentiated cells would retain a BrdU or histone 2B-GFP (H2B-GFP) label. However this is rather a different concept to a specialized back up population of slowly dividing stem cells.

Other markers have been reported for the +4 stem cell population. Telomerase is a ribonucleoprotein complex that helps maintain the integrity of chromosome ends through numerous cell divisions. *Telomerase reverse transcriptase* (*Tert*) expression has been shown in the intestine. Moreover, a transgenic mouse model expressing *Tert* together with the GFP reporter demonstrated the presence of long label retaining single cells (Breault, Min et al. 2008) which are mostly in G₀ since they do not express the cell cycle marker Ki67 (Montgomery, Carlone et al. 2011). In addition, the *Tert* positive cells are distinct from the *Lgr5* positive cells, are also located at the +4 position of the crypt, are radioresistant and exert multipotency. Furthermore, *Tert* expression is also in a gradient decreasing from the bottom of the crypt towards the top of the crypt. Another

marker for the slow cycling stem cells has also been suggested: Leucine-rich repeats and immunoglobulin-like domains 1 (*Lrig1*). *Lrig1* is an inhibitor of the growth factor erythroblastic leukemia viral oncogene homolog 2 (*ErbB*) signalling. A lineage tracing experiment in transgenic mice expressing the Lac-Z reporter under the control of Tamoxifen injection in the *Lrig* positive cells (*Lrig-CreER-R26R/LacZ* mice) showed that a single injection of the inducer labels single cells located at the bottom of the intestinal crypts and that the labelling is spreading to the entire crypt villus structure within fourteen days (Powell, Wang et al. 2012). Also, *Lrig* cells are actively repopulating irradiation damaged crypts. Consistently with a slow cycling stem cell population, only 25% of the *Lrig* positive cells exhibit Ki67 whereas the rate of *Lgr5* positive cells is 75%. In addition *Lrig* and *Lgr5* rarely colocalise in cells. Interestingly *Apc* deletion in *Lrig* positive cells as well as *Lrig* deletion in adult intestinal cell resulted in large adenoma formation.

In conclusion, there are at least 2 distinct stem cell populations within the intestine which have been described to have different roles in intestinal epithelium maintenance. First, the rapid cycling population in charge of the constant turnover of cells during normal maintenance and secondly, quiescent, slow cycling or differentiated population which may act as a reservoir for the fast cycling population after specific injuries. Whether this back up population needs to have a specific identity is still unclear or whether this reflect cells that fall back into the niche upon killing of the *Lgr5* positive cells and then adopt a stem cell fate. These questions will no doubt be unravelled over the next few years in this rapidly evolving field. However for the purpose of my thesis there is little doubt that the *Lgr5* positive cells mark a population of intestinal stem cells that express a specific signature of genes.

1.2.3 Identifying different epithelial lineages within the intestinal epithelium

The intestinal epithelium is a highly organised structure. The visualisation of the different cell types, the migration of the cells and the area of proliferation is a powerful tool to distinguish the normal tissue from a diseased one. For each cell type, a specific histochemical or immunohistochemical stain has been developed in order to characterise them.

The Goblet cells produce acidic mucus. Therefore, it is possible to stain them using a basic dye, the alcian blue, targeting the acidic polysaccharides of the mucus colouring it in blue. Entero-endocrine cells are argyrophil which means that they can be impregnated with silver. A staining (grimelius staining) combining silver and a reducing agent turning it into visible metallic silver is used to visualise them. As previously mentioned, Paneth cells are secreting enzymes such as defensins and lysozyme therefore they can be visualised by lysozyme immunohistochemistry (IHC).

Bromodeoxyuridine (BrdU) is a synthetic analogue of thymidine and is incorporated during S-Phase of the cell cycle. In mouse tissues, an IHC for BrdU allows the visualisation of proliferative cells at a specific time. Cell migration can also be visualised using BrdU labelling. The BrdU is incorporated for approximately two hours after injection as it is bioavailable only for this amount of time. In the mouse normal epithelium, two hours after injection, the BrdU positive cells are located in the crypt compartment. At 48 hours after injection, the BrdU positive cells are now located only in the villi and not in the crypt, indicating the cell migration up the axis (Figure 4). When the intestinal epithelium is transformed such as in the case of a homozygous *Apc* mutation, an increase in proliferation is observed as highlighted by the higher BrdU incorporation.

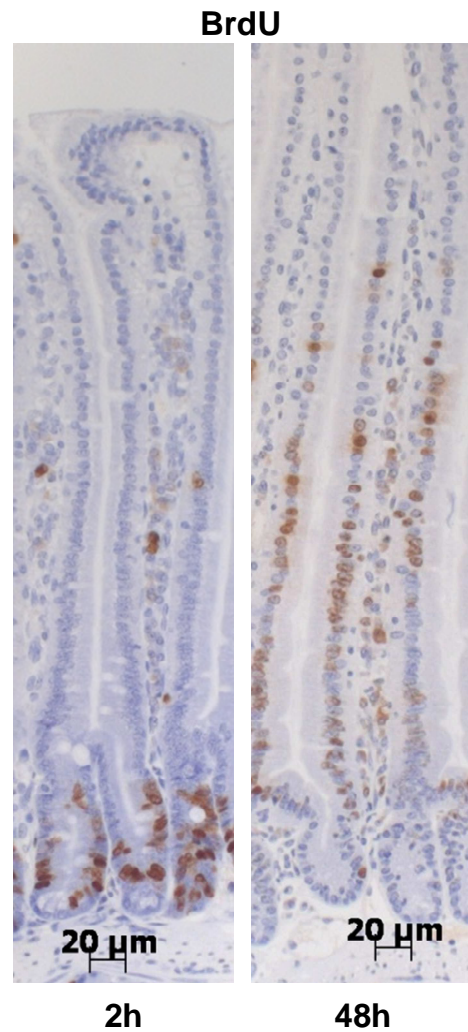


Figure 4: Cell migration in mouse intestinal epithelium

BrdU was injected in wild type mice. After two hours, the BrdU was incorporated in the cells in S-phase. Mice were sacrificed 2 hours (left panel) and 48 hours (right panel) after BrdU injection. An IHC for BrdU was performed. The BrdU positive cells appear in brown. At 2 hours after BrdU injection, the BrdU positive cells are located in the intestinal crypts. At 48 hours after injection, the positive cells are located in the villi illustrating the cell movement in the epithelium.

1.3 The WNT signalling cascade

There are three pathways associated with Wnt ligands: the Wnt/Ca²⁺ pathway, the non-canonical planar cell polarity pathway and the canonical pathway (Clevers 2006). In this thesis I will focus only on the canonical pathway. This pathway is active during embryogenesis and regulates the self-renewal of several tissues in adult. Consequently, a deregulation of this pathway is often seen in cancer and especially in CRC.

1.3.1 The canonical WNT pathway

The Wnt signalling pathway is widely conserved and consists in an activation cascade of several proteins starting by the binding of the Wnt ligand to its receptors. *Wnt* was first discovered in *Drosophila* where the *wingless* (*wg*) gene was showed to control segment polarity during development of the larva (Nusslein-Volhard and Wieschaus 1980). Not long after this discovery, the gene *Int1* was identified in mice as an oncogene in virus-induced mammary tumours (Nusse and Varmus 1982). Then, *wg* was showed to be the homologue of the murine *Int1* gene (Rijsewijk, Schuermann et al. 1987), the contraction of the two names giving its final designation *Wnt*. There are 19 *Wnt* genes conserved in mammals (<http://www.stanford.edu/group/nusselab/cgi-bin/Wnt/>). The first Wnt protein purified and biochemically characterized was the murine Wnt3a (Willert, Brown et al. 2003). Wnts are cysteine rich proteins of approximately 350-400 amino acids that contain an N-terminal signal peptide for secretion.

The Wnt cascade (Figure 5 A) starts with the binding of a Wnt ligand to a transmembrane frizzled receptor (Fz) associated with a transmembrane receptor low-density lipoprotein receptor-related protein 5/6 (LRP5/6). This results in the scaffold protein Axin to translocate to the membrane and bind the intracellular tail of the LRP5/6 receptor. The outcome of this interaction is the dissociation of the β -Catenin destruction complex consisting of Axin, Glycogen synthase kinase 3 β (GSK3 β), casein kinase 1 (CK1) and Apc (Reya and Clevers 2005; Clevers 2006). Simultaneously, the binding of Wnt ligand to its receptor results in the phosphorylation of dishevelled (Dsh) proteins which then inhibit the activity of GSK3 β . Therefore GSK3 β is unable to phosphorylate β -Catenin which

then will not be recognised by the E3 ubiquitin ligase containing the F-box β -transducin repeats-containing protein (β -TRCP) protein (Yanagawa, van Leeuwen et al. 1995; Mao, Wang et al. 2001; Cadigan and Liu 2006). The unphosphorylated β -catenin can accumulate in the cytoplasm of the cell and is free to translocate to the nucleus. As β -catenin does not have a NLS its mechanism of the nuclear translocation is still not fully described and has generated conflicting reports. It was first thought that the protein binds directly to the nuclear membrane and translocates through the nucleopore by a mechanism relying on GTPase activity (Fagotto, Gluck et al. 1998). However, a more recent paper showed that β -catenin does not need interaction with the nucleoporins to enter the nucleus suggesting another mechanism (Suh and Gumbiner 2003). This study also showed that β -catenin encompasses two regions which could target it to the nucleus. Finally, β -catenin could also translocate by binding other proteins containing a NLS as suggested by its binding to the protein Kank (Wang, Kakinuma et al. 2006). Once in the nucleus, it binds to the Lymphoid enhancer factor/T-Cell factor (LEF/TCF) transcription factors to activate the transcription of Wnt target genes such as *cMyc* and *cd44* (He, Sparks et al. 1998; Wielenga, Smits et al. 1999).

When there is no Wnt signalling, CK1 and GSK3 β are able to phosphorylate β -Catenin allowing it to be recognised and ubiquitinated by the β -TRCP protein. Therefore, β -Catenin will be degraded by the proteasome and will not activate the Wnt target genes transcription (Aberle, Bauer et al. 1997; Polakis 2000; Clevers 2006) (Figure 5 B).

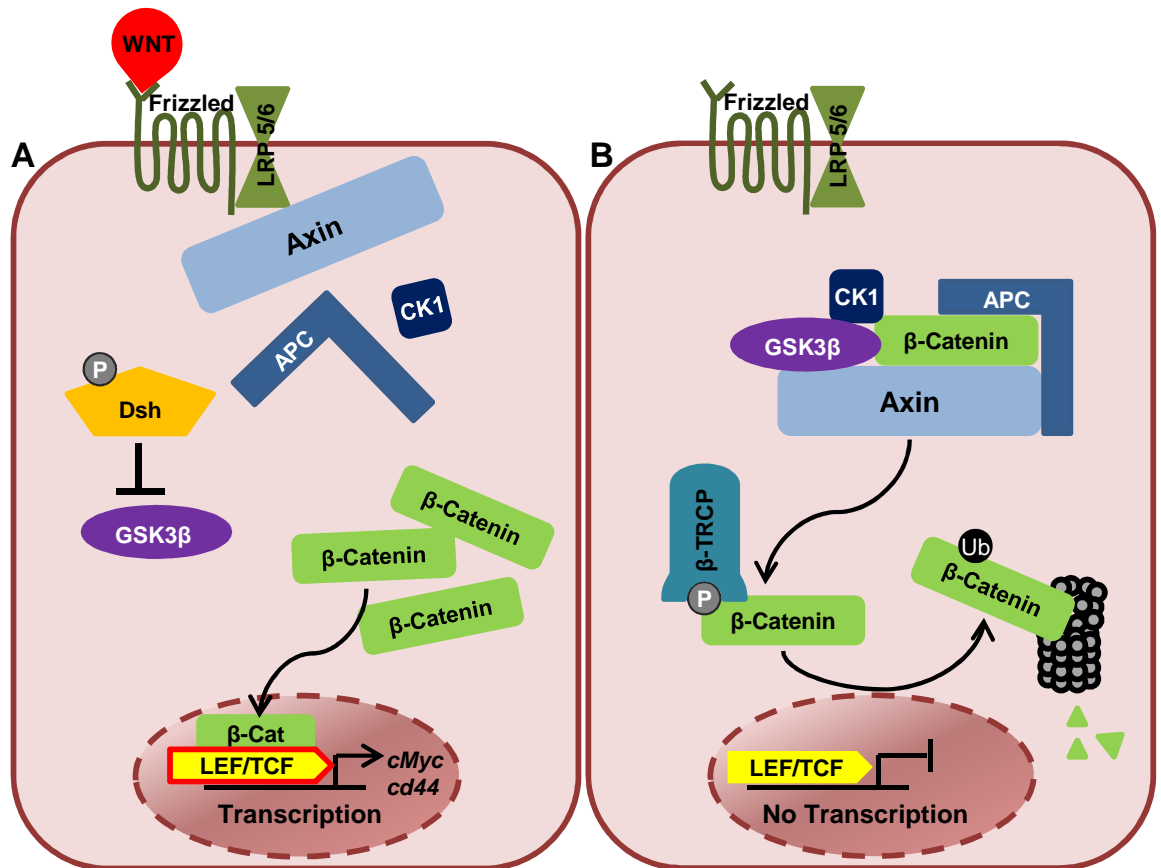


Figure 5: The Wnt pathway

A: Active Wnt pathway. B: Inactive Wnt pathway.

Adapted from Fodde et al., Nature Review, 2001

1.3.2 Adenomatous Polyposis Coli (APC)

The human *Apc* gene encodes for a 312 KDa scaffold protein (Grodin, Thliveris et al. 1991) which is a binding partner of β -Catenin (Rubinfeld, Souza et al. 1993; Su, Vogelstein et al. 1993) and is essential for the formation of the β -catenin destruction complex (Figure 6). The N-Terminal (N-Ter) part of the Apc protein has a coiled-coil domain predicting a possible oligomerisation (Day and Alber 2000). It also contains an armadillo repeats domain which allows Apc to interact with the regulatory unit of protein phosphatases 2A (PP2A) (Seeling, Miller et al. 1999) or the Apc-stimulated guanine nucleotide exchange factor for Rho family proteins (Asef) (Kawasaki, Senda et al. 2000). How these interactions

are regulated is not known. The centre of the protein contains two specific repeated amino acid sequences which are the β -Catenin binding sites (Rubinfeld, Souza et al. 1993; Su, Vogelstein et al. 1993; Rubinfeld, Albert et al. 1996). While the first 15-amino-acid repeat sequence is constitutively binding β -Catenin, the other one (20-amino-acid repeat sequence) is phosphorylation dependant. Within the second sequence, a Ser-Ala-Met-Pro (SAMP motif) amino acid sequence responsible for Axin binding is found (Hart, de los Santos et al. 1998; Fagotto, Jho et al. 1999). Several interaction motifs are found in the C-Terminal region of Apc notably one which allows binding to EB1, a microtubule binding protein (Askham, Moncur et al. 2000), which predicts also roles outside the Wnt cascade. Whereas the N-Terminal and the C-Terminal domains of Apc may vary between species, the centre of the protein is well conserved and is the site of most of the mutations leading to cancer (Nathke 2004).

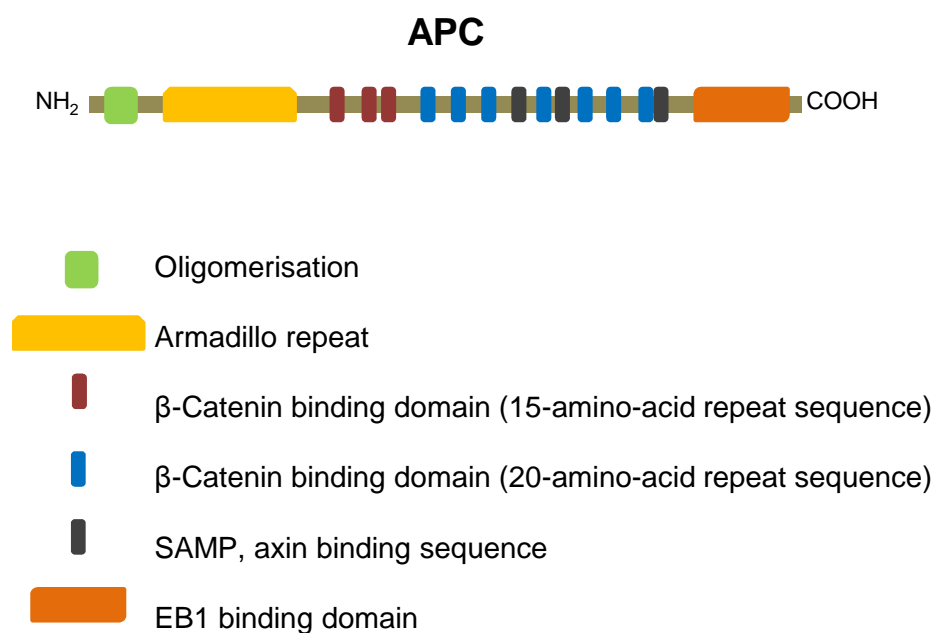


Figure 6: Structure of the Apc protein

Adapted from Fodde et al., Nature Review, 2001

Mutations in *Apc* are found in 80% of sporadic CRCs and disturb its ability to form the β -Catenin destruction complex. To initiate tumourigenesis by disturbing this particular protein, the mutation of both *Apc* alleles is necessary. This is the reason why a loss of heterozygosity (LOH) in the chromosome 5q where *Apc* is located is important to initiate the tumour formation (Vogelstein, Fearon et al. 1988; Vogelstein, Fearon et al. 1989). These characteristics of CRC are reproduced in our studies *in vivo* by the inducible mutation of *Apc* within the intestine of adult mice. In the work presented in this thesis I have investigated *Apc* loss in two ways. First, a mouse model where one copy of *Apc* is deleted from the adult intestine, the tumour formation depends on the sporadic loss of the other copy. These studies can last up to 400 days. Second, where the phenotype of *Apc* loss can be explored by acutely deleting both copies of *Apc* inducing the formation of a Crypt Progenitor-Like (CPL) phenotype which consists in altered crypt-villus architecture, a defect in migration of the cells along the crypt-villus axis and a nuclear localisation of β -Catenin in the gut epithelial cells (Sansom, Reed et al. 2004) (Figure 7).

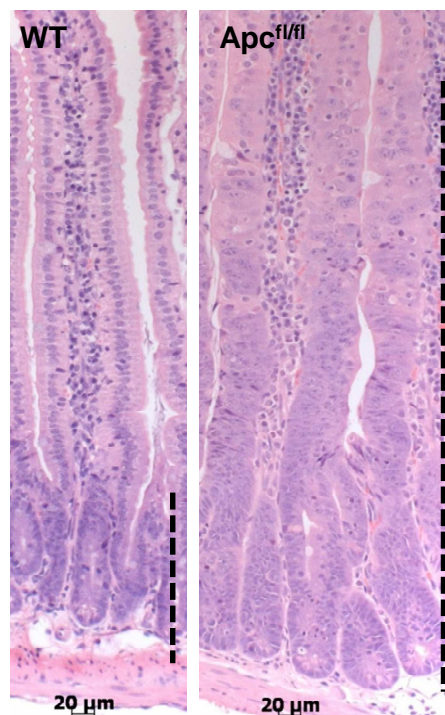


Figure 7: The CPL phenotype

H&E of wild type intestine (left panel) and *VilCre⁺ Apc^{fl/fl}* (right panel) taken at day 4 after *Cre* recombinase induction. The epithelium of the mouse which has lost the two copies of *Apc* is disorganised. The cells are no longer in a mono layer and the proliferative zone, indicated by the black dashed line, is drastically extended.

2 Introduction to pancreatic cancer

2.1 Pancreatic cancer

Pancreatic cancer (PC) represents less than 3% of diagnosed cancers in the UK (<http://www.cancerresearchuk.org/cancer-info/cancerstats/>). However, it is the fifth cause of death by cancer for both men and women (respectively 4.7% and 5.4% of cancer death) with an average survival of only 6 months. Over the years, the mortality due to this cancer has not decreased. Patients are often diagnosed late with aggressive and metastatic cancer making it particularly difficult to treat. For this reason, surgical resection is possible for only 20% of PC patients.

2.1.1 Biology of the pancreas

The pancreas is a mixed gland which can be divided into two components: the endocrine and the exocrine pancreas (Figure 8). The endocrine pancreas consists of the islets of Langerhans and some extra-islet endocrine cells. It has an essential role in the glycaemia control as the islets comprise the glucagon-producing α -cells and the insulin-producing β -cells. The exocrine pancreas is composed of the acini and the ducts and is important for digestion. The acinar cells secrete digestive enzymes which are channelled in the duct system to the gut. The ductal epithelium is composed of cuboidal cells placed in a single layer surrounding the lumen of the duct. Any modification of this structure can be an early sign of PC.

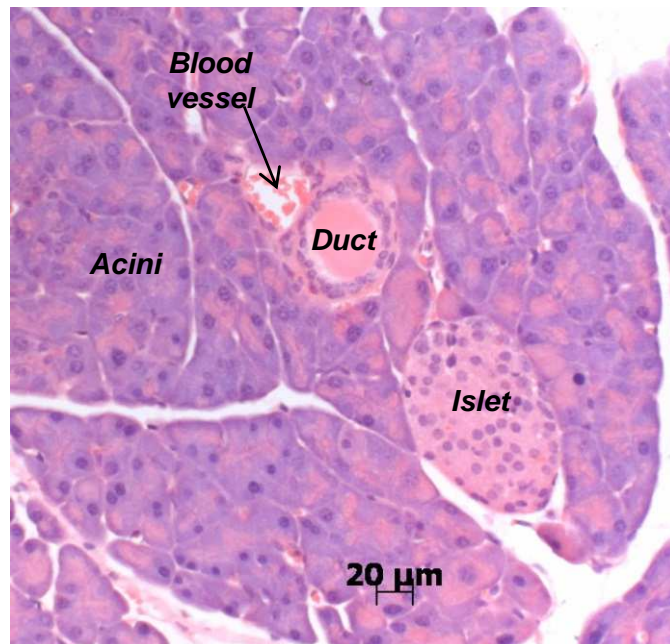


Figure 8: The mouse pancreas organisation

H&E of the pancreas of a wild type mouse. The three different structures can be observed: the acini, a duct and an islet of Langerhans.

2.1.2 Pancreatic cancer (PC)

There are several malignant PC forms, however, the most common and the most studied one is the Pancreatic Ductal Adenocarcinoma (PDAC). Most of the PDACs are sporadic but around 5% of cases occur in patients with increased risk factors such as *breast cancer type 2* (*brca2*) or *liver kinase B1* (*lkb1*) germline mutations (Jaffee, Hruban et al. 2002).

The early pancreatic lesions are called pancreatic intraepithelial neoplasia (PanIN). There are three stages defined by the degree of architectural and nuclear atypia (see http://pathology.jhu.edu/pancreas_panin/) (Hruban, Goggins et al. 2000; Hruban, Adsay et al. 2001; Kern, Hruban et al. 2001). At the PanIN1A stage, cells undergo a basal delocalisation of the nucleus and exhibit abundant mucin. The PanIN1B lesions are similar to the PanIN1A but have a papillary, micropapillary or basally pseudostratified architecture. At the PanIN2, the lesions show nuclear abnormalities such as loss of polarity, hyperchromatism and/or enlarged nucleus. Finally the PanIN3 lesions show a disorganisation of the

duct with cells placed in the lumen of the duct. There is abundant mucin production by dystrophic Goblet cells, increased and potentially abnormal mitoses and a loss of cell polarity. The PDAC presents severe dysplasia and is rapidly evolving to a metastatic stage (Figure 9).

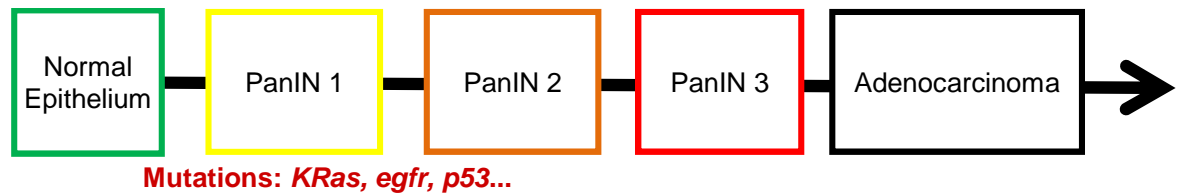


Figure 9: Overview of the evolution of PDAC

Initiating mutations allow formation of PanIN 1 gradually evolving to further stages of PanINs. Then accumulation of mutations allows the progression of adenomas to aggressive and invasive adenocarcinomas.

A genetic progression model has been proposed for PC (Hruban, Wilentz et al. 2000). *KRas* is mutated in over 90% of cases and genes such as *p16^{INK4A}* and *p53* are mutated in over 50% of cases. *KRas* mutation in mouse models of pancreatic cancer is capable of reproducing the entire PDAC evolution (Hingorani, Petricoin et al. 2003). The high MAPK pathway activation in these lesions induces senescence. Using mouse models, it has been shown that this senescence can be overcome by mutations in either *p16^{INK4A}* or *p53*, which are common in PDAC (Morton, Timpson et al. 2010). Therefore selection to overcome *KRas* induced senescence may drive progression and further mutation in PC.

2.2 The oncogene *Ras*

Ras genes encode for small GTP-binding proteins which are major elements of several signalling pathways. Ras has two states: off when it is bound to the nucleotide guanosine diphosphate (GDP) and on when it is bound to guanosine triphosphate (GTP). The switch between the two states is achieved by guanine nucleotide exchange factors (GEFs) and GTPase activating proteins (GAPs). However, Ras has an intrinsic GAP activity. Oncogenic forms of Ras have reduced Ras-GAP activity and therefore are constitutively active inducing a strong deregulation of signalling pathways affecting transformation, invasion and angiogenesis (Ellis and Clark 2000). The three forms of Ras namely Harvey Ras (HRas), Neuroblastoma Ras (NRas) and Kirsten Ras (KRas) are found to be mutated in various cancers. Oncogenic KRas is often found in CRC and PC while oncogenic NRas is found in melanoma.

2.2.1 KRas in CRC

The *Apc* mutation is considered to initiate CRC formation. However, in order for the cancer to progress, other mutations are necessary and the constitutive activation of *KRas* is another common mutation with 25% to 40% of CRCs having this mutation. Indeed it has been shown that a minimum of 25% of the CRC patients had an oncogenic *KRas* (Benhattar, Losi et al. 1993; Kressner, Bjorheim et al. 1998; Conlin, Smith et al. 2005; Winder, Mundlein et al. 2009). The hotspots for mutation in *KRas* are codons 12, 13 and 61. In a study of 342 patients diagnosed with colorectal cancer (Winder, Mundlein et al. 2009), most *KRas* mutations (21.7%) were found in codon 12. These reports highlight that the most frequent substitutions in codon 12 were glycine to aspartate (G12D) or valine (G12V). The prevalence of the mutations in codon 12 has been confirmed by other studies (Kressner, Bjorheim et al. 1998; Conlin, Smith et al. 2005; Winder, Mundlein et al. 2009). Therefore the mouse models I have used in this study carry the G12D (Jackson, Willis et al. 2001; Johnson, Mercer et al. 2001) or G12V mutations (Guerra, Mijimolle et al. 2003; Guerra, Schuhmacher et al. 2007). It is interesting to note that in humans the G12V mutation resulted in worse prognosis compared to the other mutations (Benhattar, Losi et al. 1993).

The effects of oncogenic *KRas* in the gut have been modelled *in vivo*. In mouse models, oncogenic *KRas* alone modifies the homeostasis of the colonic epithelium leading to hyperplasia and formation of aberrant crypt foci (ACF) (Calcagno, Li et al. 2008; Haigis, Kendall et al. 2008). However, the activation of *KRas* alone is not sufficient for tumour progression and the concomitant deletion of *Apc* is necessary for malignant tumourigenesis.

2.2.2 *KRas* in PC

KRas mutations have been found in over 90% of PC (Almoguera, Shibata et al. 1988; Smit, Boot et al. 1988; Hruban, van Mansfeld et al. 1993; van Es, Polak et al. 1995). This renders the mutation of *KRas* essential and presumably an initiating event in PCs. As in CRCs, the majority of the mutations occur in codon 12 and a small subset occurs in codons 13 and 61. Consequently, the effects of oncogenic *KRas* in PCs are studied *in vivo* using the G12D and G12V mutations as for the CRCs.

In vivo, the presence of oncogenic *KRas* targeted to the pancreas is sufficient to initiate PC. However there is a very long latency to develop PDAC suggesting other mutational events are required to drive tumour progression. Nevertheless, this model does recapitulate human pancreatic carcinogenesis with a reproduction of all stages of PC from the early PanIN lesions to the late PDAC (Hingorani, Petricoin et al. 2003). The mutation of *p53* cooperates with the oncogenic *KRas* and helps drive metastatic spread (Hingorani, Wang et al. 2005; Morton, Klimstra et al. 2008).

2.3 The MAPK pathway

The Mitogen-Activated Protein Kinase (MAPK) pathway results, after activation by growth factors or cytokines, in the serial activation of the following proteins: Ras, Raf, Mek and Erk (Figure 10).

After receptor activation by a ligand, a Src homology 2 domain-containing protein (Shc) interacts with the growth factor receptor and then recruits the GTP-exchange complex composed of growth factor receptor bound 2 (Grb2) and

Son of sevenless (Sos). Grb2/Sos complex recruits Ras-GTP which then recruits Raf from the membrane. Ras can also be activated by the Src Family Kinases (SFK) (Kim, Song et al. 2009; Matozaki, Murata et al. 2009). Raf activated by a tyrosine kinase, likely from the Src family, can then phosphorylate and therefore activate the mitogen-associated extracellular regulated kinase (Mek). Activated Mek phosphorylates specific threonine and tyrosine residues of extracellular regulated kinase (Erk) to activate it. Phosphorylated Erk has activating kinase functions in the cytoplasm and the nucleus where it can activate transcription factors such as ETS-like transcription factor 1 (Elk1) and Fos.

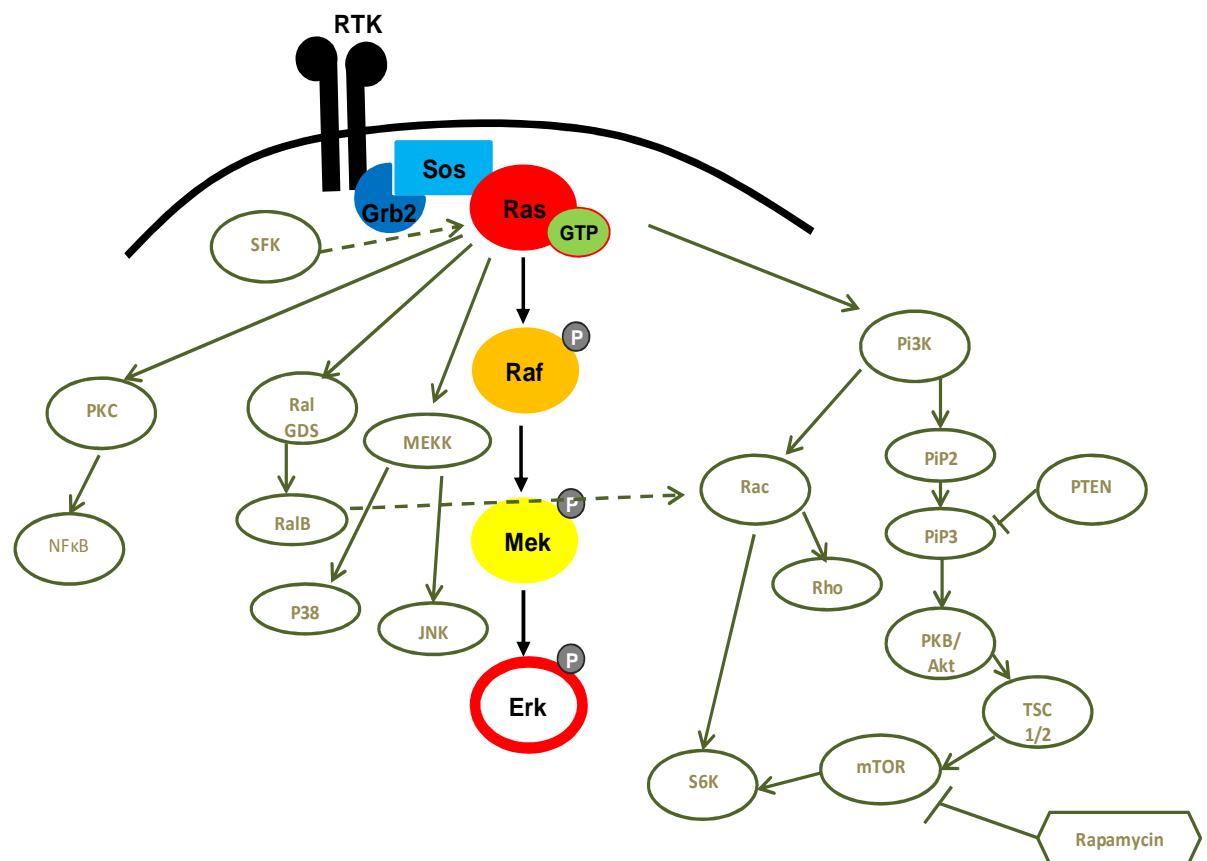


Figure 10: Overview of the MAPK pathway

The MAPK pathway activation is triggered by several mutations. At the membrane level, the receptor tyrosine kinases (RTKs) can be overexpressed and/or constitutively active by mutations (Grandis and Sok 2004). As already mentioned *Ras* is often mutated particularly in pancreatic cancer. *Raf* is also an oncogene: *V-raf murine sarcoma viral oncogene homolog B1* (BRaf) is frequently mutated in melanomas and CRCs (Davies, Bignell et al. 2002). However, no mutations in *Mek* and *Erk* have been reported so far.

2.3.1 The MAPKs

There are several MAPKs controlling different cellular functions after activation of the conventional MAPK pathway. In this thesis I will concentrate on MEK1/2 and ERK 1/2 as these are the best studied downstream effectors of Ras mutations. Other MAP kinases include the cJun NTerminal kinases (JNK) which is predominately activated by stress signals and regulates transcription factors such as cJun or p53 to modulate cell cycle control and apoptosis. P38 is also activated by stress signals and induces similar cell responses to JNK. Erk5 is a kinase similar to Erk 1/2 but is only phosphorylated by Mek5. Erk5 is activated by stress signals and specific growth factors such as nerve growth factor (NGF) and induces angiogenesis and neural differentiation (Regan, Li et al. 2002; Nishimoto, Kusakabe et al. 2005).

2.3.2 ERK 1/2

Erk 1/2 are the two predominant Erk isoforms (Erk1 is 44KDa and Erk2 is 42KDa) and are ubiquitously expressed. They are encoded by the genes *Erk1* and *Erk2* located on chromosome 16 in mice and chromosome 22 in human. They stimulate various and sometimes antagonistic cellular functions and the level of Erk 1/2 activation constitutes a balance which can control which cellular response is activated (Cagnol and Chambard 2010).

Erk 1/2 induces apoptosis following DNA-damage or by regulation of Tumour Necrosis Factor (TNF) related apoptosis-inducing ligand (TRAIL) (Tang, Wu et al. 2002; Drosopoulos, Roberts et al. 2005). Furthermore, Erk 1/2 can promote cell death by upregulation of *p53* (Persons, Yazlovitskaya et al. 2000; She, Chen et

al. 2000; Tang, Wu et al. 2002). Overactivation of Erk 1/2 is also associated with senescence (Mooi and Peeper 2006). In this case, genes involved in senescence such as *p53*, *p21* and *p19/Arf* are induced and there is an increased β -galactosidase activity (Bennecke, Kriegl et al. 2010). This senescence can be induced by oncogenic *KRas* (Tuveson, Shaw et al. 2004). Balancing with its cell growth arrest activity, Erk 1/2 induces cellular proliferation notably via activation of transcription factors *cMyc*, *fos*, *jun* and stimulates the transcription of *cyclin-dependent kinase 4* (*cdk4*) and *cyclin D*. Furthermore, Erk 1/2 can also stimulate cell survival by phosphorylating Forkhead box O3 (FOXO3A) and by repressing *Bim* expression (Yang, Zong et al. 2008). It is important to note that most of these functions of Erk 1/2 can be inhibited by the use of Mek inhibitors such as PD184352 (CI1040) PD0325901 or AZD6244 (Sebolt-Leopold, Dudley et al. 1999) (see result chapter). These drugs are currently in clinical trials (Rinehart, Adjei et al. 2004). However the antitumoural activity in human patients seems limited for the moment and an adjustment of the compound and/or the association with other drugs may be necessary.

There is a dynamic shuttling of the Erk 1/2 between the cytoplasm and the nucleus. The subcellular localisation of this protein is very important and has a significant impact on the cellular response following Erk 1/2 activation. During growth arrest, Erk 1/2 is mainly located in the cytoplasm. The translocation to the nucleus will allow Erk 1/2 to activate certain transcription factors and induce the transcription of its target genes, however the retention to the cytoplasm is sufficient to prevent this phenomenon (Brunet, Roux et al. 1999; Kim, Nose et al. 2000). The translocation to the nucleus is transient. Indeed a study performed using NIH-3T3 cells showed that following serum activation, Erk 1/2 is translocated and accumulates in the nuclei. This accumulation is lost six hours after stimulation (Pouyssegur, Volmat et al. 2002). The control of Erk 1/2 localisation is made by Mek activation (Lenormand, Brondello et al. 1998) and also anchoring proteins (Chuderland and Seger 2005) such as *Dusp6* in the cytoplasm (Karlsson, Mathers et al. 2004) or *Dusp5* in the nucleus (Mandl, Slack et al. 2005). Erk 1/2 also has a nuclear translocation signal (NTS) (Chuderland, Konson et al. 2008; Zehorai, Yao et al. 2010).

2.4 Other Ras effector pathways

In cells, signalling pathways are often overlapping. The MAPK pathway is no exception and whilst the direct pathway downstream of Ras activation is the Mek-Erk cascade, Ras also has impacts on many other signalling pathways (Figure 10). Of these, one of the pathways importantly affected by Ras activation is the Phosphatidylinositol 3-kinase/Akt (PI3K/Akt) cascade. Other cascades such as T lymphoma invasion and metastasis/RAS-related C3 botulinum substrate (Tiam/Rac) and Ras Related (Ral) A/B are also affected. These multiple effects of Ras activation have consequences when a particular signalling cascade is modified. Therefore, we can hypothesize that the blockade of one cascade can result in a compensatory over-activation of another cascade. Other pathways that have been shown to be activated by KRas in cell type specific manners include Wnt signalling, nuclear factor κ -light-chain-enhancer of activated B cells (NF κ B) and Signal Transducer and Activator of Transcription (STAT). In most cases the precise mechanism of this activation is unclear.

2.4.1 The PI3K/Akt pathway

The PI3K/Akt cascade starts with the activation of RTKs such as erythroblastic leukemia viral oncogene homolog 2 (ErbB2) or insulin growth factor receptor (IGFR). The activation of the RTK allows the activation of PI3K which then phosphorylates phosphatidylinositol biphosphate (PP2) to triphosphate (PP3). The Phosphatase and tensin homologue (PTEN) negatively regulates this pathway by removing a phosphate from PP3 reverting it back to its PP2 form. PP3 is an anchor protein for Akt (also called Protein Kinase B (PKB)) and phosphoinositide dependent protein kinase 1 (PDK1). This anchorage allows the phosphorylation of Akt by PDK1. Akt can then translocate to the membrane via PP3 or to the nucleus or remain in the cytosol where it can phosphorylate GSK3 β . Akt negatively regulates NF κ B by phosphorylating the inhibitor of kappa B (I κ B) kinase (IKK) which will phosphorylate the I κ B subunit to target it to the proteasome preventing NF κ B activation. The PI3K/Akt pathway also indirectly activates mammalian target of Rapamycin (mTOR) (For review:(Steelman, Abrams et al. 2008; Castellano and Downward 2011). It is important to note that PI3K contains a Ras binding domain. Indeed, Ras can bind the p110 α subunit of

PI3K and activate the downstream cascade. It has been shown that in mice expressing an oncogenic *KRas* (which results in lung tumourigenesis) (Johnson, Mercer et al. 2001), the inactivation of p110 α by two point mutations was sufficient to drastically reduce the number of tumours formed (due to higher apoptosis) (Gupta, Ramjaun et al. 2007).

2.4.2 The Tiam/Rac pathway

Rac is a rho family small GTPase and Tiam1 is one of its GEFs. Rac can be activated by Ras and has several outcomes. It has been mainly described as an important effector of actin reorganisation; however, it can also be involved in other signalling cascades such as the JNK pathway leading to the activation of transcription factors such as cJun and Elk1. Tiam1 has a Ras binding domain and Ras has been showed to be essential to Tiam1 activation and consequently Rac1 activation (Lambert, Lambert et al. 2002; Yamauchi, Miyamoto et al. 2005). Rac status has an impact on tumourigenesis. It has been shown to be upregulated in PDACs and its deletion in mouse models reduced tumourigenesis (Heid, Lubeseder-Martellato et al. 2011). Tiam1 is essential to tumour initiation in *Tiam1* deleted (*Tiam1*^{-/-}) mice. Indeed *Tiam1*^{-/-} mice treated with the skin tumour initiator 7,12-dimethylbenzanthracene / 12-O-tetradecanoylphorbol-13-acetate (DMBA/TPA) developed less tumours than wild type (wt) mice (Malliri, van der Kammen et al. 2002). Moreover the tumours from *Tiam1*^{-/-} mice had an increased apoptosis and grew much slower than the corresponding tumours in wt mice. Interestingly, in this model tumours from *Tiam1*^{-/-} mice were more advanced and a previous study suggested *Tiam1* to be involved in invasion (Habets, Scholtes et al. 1994).

3 The dusp family

In mammals, signal transduction is mostly controlled by phosphorylation and dephosphorylation. The MAPK signalling pathway is not an exception and phosphorylation represents a common mechanism to maintain the balance between kinase activation and negative regulatory controls. The Dual-Specificity Phosphatases (DUSPs) are a heterogeneous group of proteins which can dephosphorylate both threonine/serine and tyrosine residues in their substrates (hence their name “dual-specificity”).

There are 61 DUSPs grouped together by their highly conserved catalytic domain which has the following consensus sequence containing a histidine, a cysteine and an arginine: HCXXXXXR (Patterson, Brummer et al. 2009; Huang and Tan 2012). The consensus sequence (HCXXXXXR) creates a shallow catalytic site of 5.5 Å. The active residues cysteine and arginine of the signature motif are located in a loop near another loop containing a highly conserved aspartic acid; together the 2 loops form the enzymatic active site (Farooq and Zhou 2004).

The DUSPs are classified into seven subgroups (Figure 11). All these subgroups have very distinct targets. One of these DUSPs subgroup contains the preferred antagonist proteins of the MAPK pathway. These particular proteins are called the MAPK Phosphatases (MKPs). In this thesis we will only discuss this MKP subgroup due to their preferred targets the MAP Kinases. The proteins of the MKP subgroup of the DUSP family are defined based on the presence of the MAP kinase-binding (MKB) also named kinase-interaction motif (KIM) domain, an essential motif to MAP kinases interactions. The MKB/KIM domain interacts with the common domain of the MAPKs and is characterised by the conserved $\varphi\varphi\text{XRR}\varphi\text{XXG}$ motif where φ is a hydrophobic residue and X is any residue (Farooq and Zhou 2004). It is interesting to note that another DUSP subgroup, named atypical, presents some similarities with the MKP subgroup and has been sometimes been merged with this one.

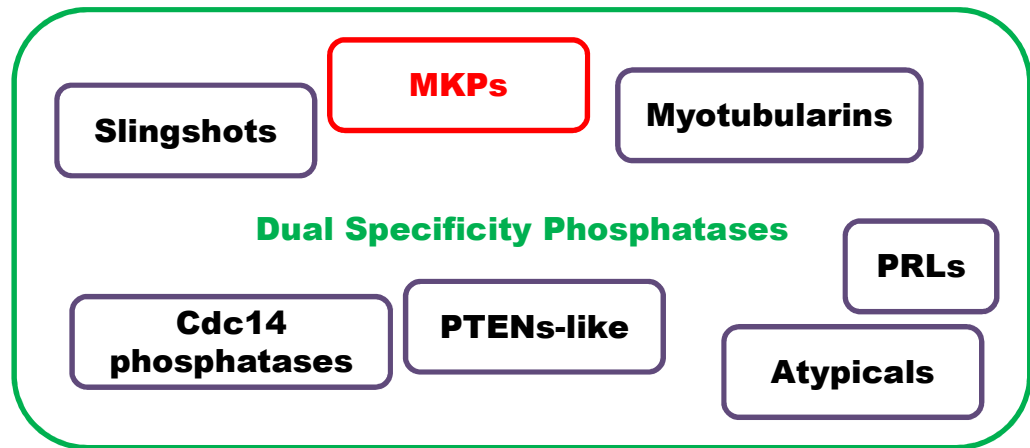


Figure 11: Dual Specificity Phosphatases classification:

The 61 Dusp proteins are classified into seven subgroups: Slingshots, MAP Kinase Phosphatases (MKPs), Myotubularins, Cdc14 phosphatases, Phosphatase of Regenerating Liver (PRLs), Phosphatase and Tensin homologue deleted on chromosome 10-like (PTENS-like) and Atypicals.

Adapted from Patterson et al, Biochem. J, 2009.

3.1 MKP proteins

The MAPK Phosphatases (MKPs), a subgroup of the DUSP family, are the preferred antagonist proteins of the MAPK pathway. There are ten catalytically active MKPs in mammals.

3.1.1 Structure

The MKPs can be subdivided into three groups according to their structure (Figure 12) (Farooq and Zhou 2004). The Type II MKPs have usually between 300 and 400 amino acids and contain a MKB/KIM domain and the consensus catalytic sequence HCXXXXXR. The Type III contains only Mkp5 (also known as Dusp10). Finally the Type IV MKPs have between 600 and 700 amino acids and contain a C-Terminal (C-Ter) sequence rich in prolines, glutamates, serines and threonines (sequence PEST). However, all MKPs have a similar structure which includes an N-Terminal (N-Ter) non catalytic domain and a C-Ter catalytic domain (Camps, Nichols et al. 2000; Theodosiou and Ashworth 2002; Owens and Keyse 2007; Patterson, Brummer et al. 2009).

The MKPs				
Gene	Other names	Ch.	Type	Cellular localisation
Dusp1	MKP1, CL100, hVH1	5q34	II	Nuclear
Dusp2	PAC1	2q11	II	Nuclear
Dusp4	MKP2, Sty8, hVH2, TYP1	8p12-p11	II	Nuclear
Dusp5	hVH3, B23	10q25	II	Nuclear
Dusp6	MKP3, PYST1, rVH6	12q22-q23	II	Cytoplasmic
Dusp7	PYST2, MKPX, B59	3p21	II	Cytoplasmic
Dusp8	HB5, hVH5, M3/6	11p15,5	IV	Both
Dusp9	MKP4, PYST3	Xq28	II	Cytoplasmic
Dusp10	MKP5	1q41	III	Both
Dusp16	MKP7	12p12	IV	Both

Figure 12: The MKPs classification and their human chromosome localisation

The MKPs are grouped according to their structure in type II, III or IV. Their chromosome localisation in the human genome is indicated in the column Ch.

Adapted from Keyse, *Cancer Metastasis Rev.*, 2008.

The C-Ter catalytic domain encompasses the conserved characteristic cysteine-dependent protein tyrosine phosphatase active site sequence I/VHCXAGXXR, where X is any residue (Camps, Nichols et al. 2000; Keyse 2000; Dickinson and Keyse 2006).

The N-Ter domain has a regulatory function. It contains a modular docking site determining the specificity to a given MAP kinase and a sequence determining the subcellular localisation of the MKP (Owens and Keyse 2007).

3.1.2 Subcellular localisation

There is a correlation between subcellular localisation and the specificity of the MKPs (Figure 13). Therefore they are subdivided in three categories: nuclear MKPs, cytoplasmic MKPs and shuttle MKPs (Camps, Nichols et al. 2000; Theodosiou and Ashworth 2002; Caunt and Keyse 2012).

The Nuclear mitogen and stress inducible MKPs are Dusp1, Dusp2, Dusp4 and Dusp5. These phosphatases have a nuclear localisation signal (NLS) in their N-Ter non catalytic domain (Mandl, Slack et al. 2005; Wu, Zhang et al. 2005). All these proteins can target Erk but they can also target p38 and/or JNK.

The Erk specific cytoplasmic MKPs are Dusp6, Dusp7 and Dusp9. They all share a nuclear export signal (NES) within their N-Terminal non catalytic domain determining their preferential localisation in the cytoplasm (Karlsson, Mathers et al. 2004).

Finally the JNK-p38 specific MKPs are Dusp8, Dusp10 and Dusp16. These phosphatases can be considered as shuttle proteins because of their dual subcellular localisation (Tanoue, Moriguchi et al. 1999; Masuda, Shima et al. 2001).

Gene	Specificity	Cellular localisation
Dusp1	JNK, p38 > ERK	Nuclear
Dusp2	ERK, p38	Nuclear
Dusp4	JNK, p38, ERK	Nuclear
Dusp5	ERK	Nuclear
Dusp6	ERK	Cytoplasmic
Dusp7	ERK	Cytoplasmic
Dusp9	ERK > p38, JNK	Cytoplasmic
Dusp8	JNK, p38	Both
Dusp10	JNK, p38	Both
Dusp16	JNK, p38	Both

Figure 13: The MKPs specific targets and their cellular localisation

Adapted from Keyse, Cancer Metastasis Rev., 2008.

3.2 MKPs and cancer

3.2.1 Dusp1

Most of the MKPs have been reported as modified in cancer. I will briefly mention Dusp1 as this MKP has been studied most extensively in relationship to cancer.

Dusp1 has been shown to be upregulated in various cancers such as colon, lung, prostate, ovarian, breast and bladder (Loda, Capodiceci et al. 1996; Magi-Galluzzi, Mishra et al. 1997; Zhang, Zhou et al. 1997; Denkert, Schmitt et al.

2002; Wang, Cheng et al. 2003; Chattopadhyay, Machado-Pinilla et al. 2006; Moncho-Amor, Ibanez de Caceres et al. 2011). Also, it is interesting to note a loss of *Dusp1* expression in more advanced stages of colon, prostate and bladder cancers (Loda, Capodieci et al. 1996; Zhang, Zhou et al. 1997). Due to these observations, *Dusp1* is believed to be a tumour suppressor gene. However, in lung and breast cancer, *Dusp1* overexpression has been reported to increase chemotherapy resistance (Wang, Xu et al. 2006; Small, Shi et al. 2007). This could be due to its high affinity to JNK-p38 (Camps, Nichols et al. 2000; Small, Shi et al. 2007).

Interestingly the inhibition of *Dusp1* has been showed to increase hypoxia (Laderoute, Mendonca et al. 1999; Liu, Shi et al. 2005; Jin, Calvert et al. 2010). Furthermore, a role in regulation of the immune function has been also reported in several studies using *Dusp1* null mice (Chi, Barry et al. 2006; Salojin, Owusu et al. 2006; Frazier, Wang et al. 2009). Notably, *Dusp1* plays a role in the regulation of the bacterial lipopolysaccharide (LPS) increasing the production of the inflammatory cytokines (Chi, Barry et al. 2006; Salojin, Owusu et al. 2006; Liu, Shepherd et al. 2007). Given the clear relationship between inflammation and cancer it is thus difficult to uncouple these functions of *Dusp1*.

3.2.2 Other MKPs

Several studies reported a significant impact on cancer by the nuclear MKPs subgroup. *Dusp2* has been shown to be downregulated in acute leukemia (Kim, Hahn et al. 1999). However, the overexpression of *Dusp2* in ovarian tumours was correlated with a poor prognosis in patients (Givant-Horwitz, Davidson et al. 2004). *Dusp4* overexpression is implicated in liver tumourigenesis (Yokoyama, Karasaki et al. 1997) and notably *KRas* activated cell lines exhibited high *Dusp4* expression (Yip-Schneider, Lin et al. 2001). *Dusp5*, the Erk specific phosphatase in the nucleus, has been suggested recently to be a p53 target as its transcription was activated by endogenous p53 after DNA damage in colon cancer cells (Ueda, Arakawa et al. 2003). Furthermore, we show in a microarray study that in a mouse model of intestinal tumourigenesis combining an *Apc* mutation and *KRas* activation resulted in *Dusp5* upregulation (see result chapter).

Dusp7 is highly expressed in myeloid leukemia cells in correlation with MAPK pathway activation (Levy-Nissenbaum, Sagi-Assif et al. 2003; Levy-Nissenbaum, Sagi-Assif et al. 2003; Levy-Nissenbaum, Sagi-Assif et al. 2003). *Dusp9* loss of expression is associated with advanced stages of epidermal carcinogenesis (Liu, Lagowski et al. 2007). The same study showed that the expression of *Dusp9* could induce tumour cell death, microtubule disruption and tumour regression *in vivo*. Furthermore, a low expression of *Dusp9* has been associated with bad prognosis in patients with clear cell renal carcinoma (Wu, Wang et al. 2011). *Dusp10* has been reported to have an anti-inflammatory activity (Zhang, Blattman et al. 2004) and it is thought to have a chemopreventive effect when activated by anti-cancer compounds such as resveratrol in prostate cancer cells (Nonn, Duong et al. 2007). An overexpression of *Dusp16* downregulates JNK activation and results in reduced transforming capacity of BCR-ABL transformed fibroblasts (Hoornaert, Marynen et al. 2003). Furthermore, a methylation-dependant silencing of *Dusp16* resulting in a modification of JNK signalling has been shown in Burkitt's lymphoma cells (Lee, Syed et al. 2010).

One of the weaknesses of most of these studies is that they were predominantly correlating expression of a specific DUSP in different cancers and few functional definitive experiments have been performed. This is one of the major reasons we decided to take a genetic approach to delete *Dusp6* and see if it modified tumourigenesis *in vivo*.

3.3 **Dusp6**

3.3.1 Structure of *dusp6*

Dusp6 (also named *Mkp3* or *Pyst1*) is located in human on chromosome 12 at band q22-q23 (Smith, Price et al. 1997). It has been cloned and characterised in 1996 using the characteristic extended active-site sequence motif VXXVHCXXGXRSXTXXXAYLM (where X is any amino acid) found in *Dusp1* (Groom, Sneddon et al. 1996; Muda, Boschert et al. 1996). Interestingly, *Dusp6* shares 73% sequence homology with *Dusp7* however their expression in tissues remains very different. While *Dusp6* shows a basal expression in most tissues, *Dusp7* seems to be limited to the liver and the muscle (Groom, Sneddon et al. 1996).

Mammalian Dusp6 has an N-Ter Cdc25 homology domain as well as an MKB/KIM domain (Figure 14). The MKB/KIM domain consists in open twisted five-stranded β sheets, each sheet being bordered by α helices (Farooq, Chaturvedi et al. 2001). The catalytic site is located in the C-Terminal. The catalytic site is 2.5 Å and is located in a shallow phosphate-binding loop of 5.5Å between the β 8 strand and the α 5 helix (Stewart, Dowd et al. 1999) (Figure 15). This rather small space allows the presence of both targeted residues (tyrosine and threonine) nearby the active site of Dusp6. The phosphatase possesses the three conserved residues of MKPs: Asp 262, Cys 293 and Arg 299. These amino acids have an important role in the modulation of the Dusp6 conformation during its activation.

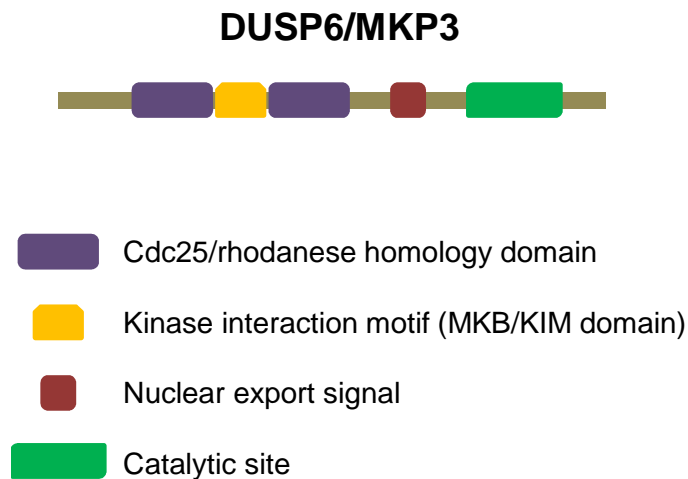


Figure 14: Structure of Dusp6/Mkp3

Adapted from Caunt and Keyse, FEBS, 2012.

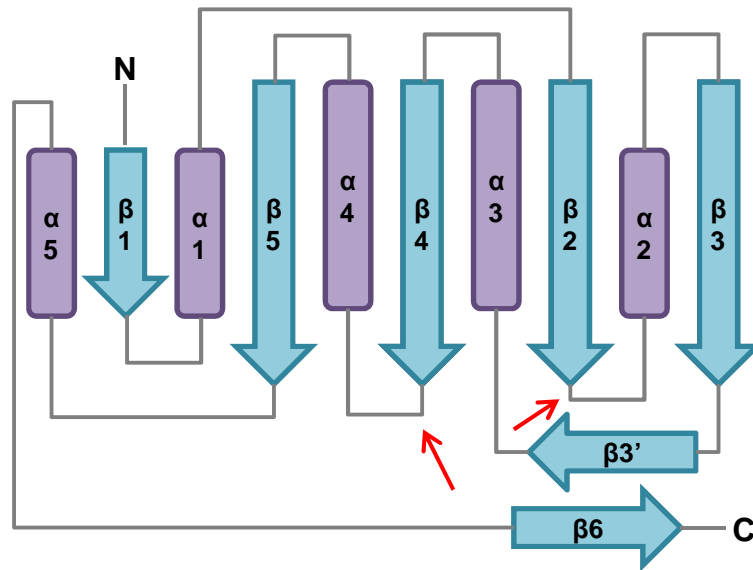


Figure 15: Representation of the MKB/KIM domain of Dusp6.

The strands are symbolised by blue arrows and helices are represented by purple cylinders. Switch points are indicated by red arrows.

Adapted from Farooq et al., *Molecular Cell*, 2001

3.3.2 Subcellular localisation

Dusp6 is only found in the cytosol, even following stimulation of the MAPK cascade (Groom, Sneddon et al. 1996), due to a NES sequence. This ensures a strong control of Erk 1/2 in the cytoplasm compartment.

3.3.3 Dusp6 targets specifically Erk

Several studies report the specificity of Dusp6 for Erk (Groom, Sneddon et al. 1996; Muda, Theodosiou et al. 1998; Bermudez, Jouandin et al. 2011). Indeed, Dusp6 efficiency to dephosphorylate JNK or p38 *in vitro* is 90 to 100 fold less; consequently the phosphatase is unable to block the activation of these proteins *in vivo*. Moreover, Dusp6 specifically binds and co-precipitates with Erk (Groom, Sneddon et al. 1996; Muda, Theodosiou et al. 1998). Furthermore, whereas the treatment with the Mek inhibitor CI1040/PD184352 induced a decrease in *Dusp6* mRNA levels in cancer cell lines, no change was observed with treatment with

the compounds LY294002, SP600125 and SB203580 respectively inhibiting PI3K, JNK and p38 (Bermudez, Jouandin et al. 2011).

3.3.4 Regulation of DUSP6

Dusp6 plays a key role in the control of the activation of the MAPK cascade. In return, Dusp6 has been found to be regulated by MAP kinases (Figure 16). In response to the activation of the MAPK cascade, *Dusp6* expression is activated in order to prevent an overactivation of Erk 1/2. Indeed, stimulation of the MAPK pathway by the fibroblast growth factor (FGF) or by platelet-derived growth factor (PDGF) results in Erk-dependant *Dusp6* mRNA upregulation (Eblaghie, Lunn et al. 2003; Jurek, Amagasaki et al. 2009). Dusp6 is also regulated at the post-transcriptional level. Whilst its normal mRNA half-life is between 20 to 40 minutes depending on the cell line, a Mek inhibitor treatment can reduce this period to only 8 minutes (Bermudez, Jouandin et al. 2011). This stabilisation through Mek/Erk signalling seems to be via the 3'UTR region of *Dusp6* mRNA since a construct enclosing the 3'UTR sequence of *Dusp6* presented an increased activity following Mek/Erk pathway stimulation. Moreover, in lung cancer cell lines, *Dusp6* expression seems regulated by the Erk-responsive transcription factor (ETS1) and is abrogated by Mek inhibition (Zhang, Kobayashi et al. 2010).

Simultaneously, there is a negative control of the Dusp6 protein in order to allow Erk 1/2 to play its role in signal transduction. For example, stimulation of cells by PDGF results in Dusp6 degradation (Jurek, Amagasaki et al. 2009). This is due to a MAPK pathway dependant phosphorylation of Ser 174 and Ser 159 of Dusp6 which induces the ubiquitinylation of the phosphatase and its degradation by the proteasome. Consequently, downregulation of Dusp6 enhanced Erk phosphorylation and therefore activation. Intriguingly, Dusp6 overexpression or stabilisation (by inhibition of the proteasome) enhanced Mek activation.

Dusp6 regulation can also be MAPK pathway independent. A redox regulation of Dusp6 has been reported. Indeed, a correlation was found between the increase of reactive oxygen species (ROS) in senescent cells and Dusp6 inactivation (Kim, Song et al. 2003). Additionally, Dusp6 is reversibly inactivated by oxidation *in vitro* (Seth and Rudolph 2006). Interestingly, the same study shows a protection

system within the protein: the multiple cysteine residues are capable of trapping the oxidative species and reactivate Dusp6.

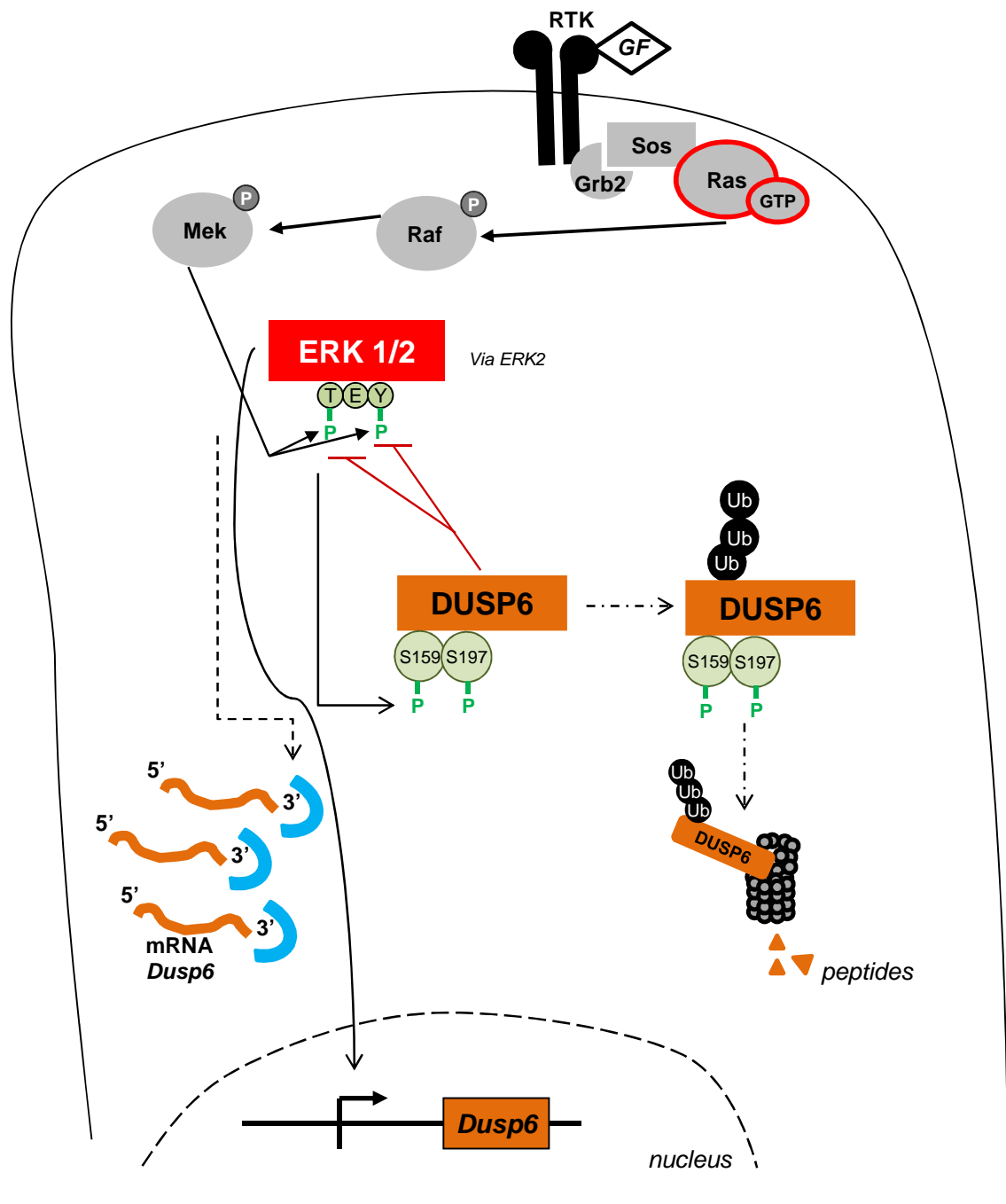


Figure 16: Overview of MAPK pathway and Dusp6 interactions

The activation of the MAPK pathway by growth factors (GF) induce *Dusp6* transcription and stabilisation of *Dusp6* mRNA via protection of its 3'UTR. The protein Dusp6 dephosphorylates Erk 1/2 to stop its activation. Simultaneously, the Erk phosphorylates Dusp6. Phospho-Dusp6 is then ubiquitinated and degraded via the proteasome.

3.3.5 Reciprocal activation and inactivation relationship between ERK and DUSP6

To understand the mutual regulation of Erk 1/2 and its negative regulator Dusp6, a number of studies have carefully analysed this precise interaction of Erk activation and Dusp6.

Erk 1/2, after being activated by Mek 1/2, is then able to bind specifically the N-terminal non catalytic domain of Dusp6 to activate the protein (Camps, Nichols et al. 1998; Farooq, Chaturvedi et al. 2001). Interestingly neither JNK/SAPK nor P38 can bind Dusp6 (Camps, Nichols et al. 1998). In the presence of Erk 1/2, there is an allosteric activation of Dusp6 by a structural reorganisation of the protein which leads to the closure of the flexible linker near the active site by the placement of the aspartic acid (Asp 262) near the residues Cys 293 and Arg 299 (Camps, Nichols et al. 1998; Stewart, Dowd et al. 1999; Fjeld, Rice et al. 2000; Farooq, Chaturvedi et al. 2001; Rigas, Hoff et al. 2001; Mark, Smith et al. 2007) (Figure 17). Then, the active Dusp6 can dephosphorylate Erk 1/2. In the absence of Erk 1/2, the Dusp6 phosphatase enters a conformation where the N-terminal domains bind the C-Terminal ones resulting in an inhibition of their catalytic domains (Mark, Aubin et al. 2008) (Figure 18).

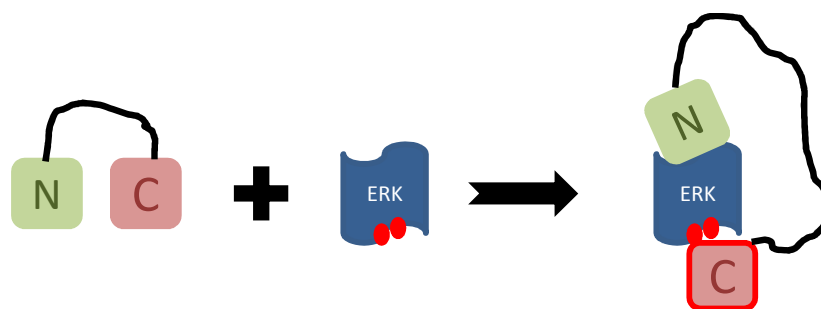


Figure 17: Erk-induced activation of Dusp6

Erk 1/2 binds to the N-terminal domain (green square) of Dusp6. Then the C-Terminal domain (pink square) of Dusp6 binds to Erk 1/2 leading to an allosteric activation of the C-Terminal domain of Dusp6 (pink square outlined in red). This activation leads to phosphorylation of the threonine and tyrosine of Erk 1/2 (red circles).

Adapted from Mark et al, J Biol Chem, 2008.

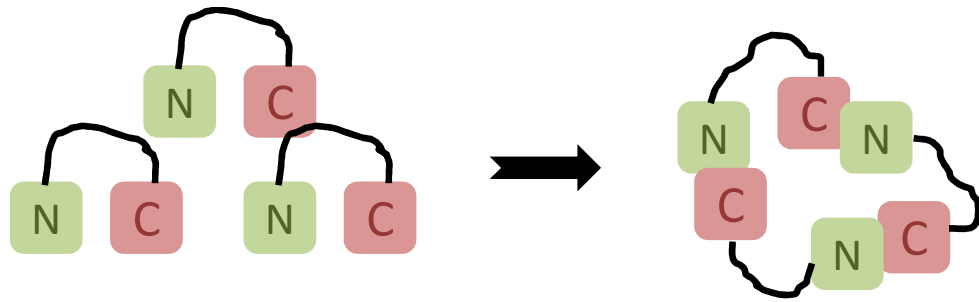


Figure 18: Autoinhibition of Dusp6

When Dusp6 is too abundant, oligomers are formed due to interdomain binding.

Adapted from Mark et al, J Biol Chem, 2008.

A regulation of Dusp6 by Erk 1/2 at a posttranslational level has also been reported (Marchetti, Gimond et al. 2005). Indeed, Erk 1/2 can phosphorylate the serines 159 and 197 of Dusp6 catalytic domain. This phosphorylation does not alter the catalytic activity of DUSP6 but leads to its instability since an inhibition of MAPK pathway by a Mek inhibitor protects Dusp6 from its degradation by the proteasome (Marchetti, Gimond et al. 2005).

3.3.6 Dusp6 and cancer

In human, Dusp6 is upregulated in pancreatic PanIN lesions (Furukawa, Fujisaki et al. 2005). Interestingly an abrogation of Dusp6 is reported in PDAC showing that the loss of Dusp6 is associated with the progression to aggressive pancreatic cancer. This abrogation could be due to hypermethylation (Xu, Furukawa et al. 2005). Furthermore, in ovarian cancer cell lines and human ovarian cancer samples, Dusp6 level is downregulated (Chan, Liu et al. 2008). Moreover, the expression of *Dusp6* in these ovarian cancer cell lines reduces tumourigenesis and cisplatin resistance. In primary lung tumours, the presence of Dusp6 is associated with a less growth (Okudela, Yazawa et al. 2009). Hypoxia is often associated with cancer and an effect of hypoxia on induction of *Dusp6* mRNA has been reported (Bermudez, Jouandin et al. 2011). This effect seems to be indirect as the *Dusp6* gene does not have a hypoxia responsive element (HRE). In cells expressing HIF1 α , the level of *Dusp6* mRNA was increased and this was

correlated with an activation of Mek/Erk pathway since treatment with CI1040/PD184352 reversed this upregulation. All of these studies are suggestive of the tumour suppressive potential of *Dusp6*.

However, there are conflicting reports in the literature concerning the role of *Dusp6* in tumorigenesis. In glioblastoma cell lines, *Dusp6* is upregulated and surprisingly its upregulation is associated with an increased resistance to Cisplatin (Messina, Frati et al. 2011). There is other evidence of an association between *Dusp6* overexpression and drug resistance. In Tamoxifen resistant primary breast tumours, there was a higher expression of *Dusp6* than in the Tamoxifen sensitive ones (Cui, Parra et al. 2006). However, in the breast carcinoma cell line MCF7, Tamoxifen treatment reduced *Dusp6* activity.

4 Fra1, a Ras pathways target

Fra1 (Fos related antigen 1), is a member of the Fos family proteins and is part of the transcription factor activator protein-1 (AP-1).

4.1 The AP-1 transcription factor

The Activator Protein 1 (AP-1) complex has been implicated as a driver of carcinogenesis because it regulates cellular processes such as proliferation, differentiation and apoptosis (Jochum, Passegue et al. 2001; Young and Colburn 2006). Furthermore due to the nature of its components, it can be activated by the MAPK pathway via Erk, JNK and p38 (Jochum, Passegue et al. 2001; Hasselblatt, Gresh et al. 2008) and it has been shown that mutations of *Apc* and *KRas* lead to elevated AP-1 activity (Park, Jeon et al. 2006).

AP-1 is composed of proteins of the Jun family (cJun, JunB and JunD) and of the Fos family (cFos, FosB, Fra1 and Fra2). It is classically a dimer consisting of Jun-Jun homodimers or Jun-Fos heterodimers (Young and Colburn 2006). However, recent *in vivo* studies on mouse models have shown that AP-1 components can form other complexes (Nateri, Spencer-Dene et al. 2005; Toualbi, Guller et al. 2007). After activation by JNK, cJun can interact with transcription factor 4

(TCF4) and β -Catenin (Nateri, Spencer-Dene et al. 2005). This complex increased tumourigenesis and therefore, the inhibition of JNK resulted in a reduction of colonic tumours. This finding illustrates the intricate overlap between pathways and suggests that the balance between the different complexes may be very important for homeostasis and tumourigenesis.

4.2 Fra1

Fra1 (also termed *Fosl1*) is a key component of the AP-1 complex and is essential during development of the placenta (Schreiber, Wang et al. 2000). The *Fra1* gene is located in man on chromosome 11 and encodes a 29KDa protein. The *Fra1* structure is similar to *Fos*. The protein contains a basic leucine-zipper domain essential for its interaction with other AP-1 partners and for DNA-binding.

Fra1 has been shown to be upregulated in a large variety of tumours including breast, lung, and colon carcinomas (Young and Colburn 2006). Its transcription is activated by the MAPK pathway but also by the Wnt pathway (Mann, Gelos et al. 1999; Young and Colburn 2006; Adisheshaiah, Li et al. 2008). Furthermore, its expression is up regulated following *Apc* loss. Most studies suggest that *Fra1* has a pro-tumourigenic role (Adisheshaiah, Li et al. 2008; Adisheshaiah, Vaz et al. 2008; Hamdi, Popeijus et al. 2008; Baan, Pardali et al. 2010). However, the balance between AP-1 complexes mentioned previously may impact on the outcome of *Fra1* deregulation (Mechta, Lallemand et al. 1997).

5 Murine models of cancer

To address the effects of the common mutations occurring in the main pathways involved in tumour initiation and progression, genetically modified mice are now routinely used.

In order to address the importance of *Dusp6* and *Fra1* in intestinal and pancreatic tumourigenesis, I used the bacterial Cre-LoxP system in three different models. The Cre-LoxP system leads to the expression of a site specific

bacteriophage recombinase (*Cre*) which promotes the recombination between two 34bp DNA sequences called LoxP sites (Abremski and Hoess 1984; Hoess and Abremski 1984). The *Cre* DNA recombinase expression is under the control of a tissue specific promoter namely either the Cytochrome p450 subfamily A1 (*Cyp1A1*) or the Villin gene (*Vil*) promoters in the intestine and *Pancreatic and duodenal homeobox 1* (*Pdx1*) promoter in the pancreas.

5.1 Cre Recombinase constructs:

5.1.1 Intestinal model: Vil-cre-ER system (VilCreER⁺)

In this system the *Cre* gene is fused to a mutated ligand binding domain of the human estrogen receptor (ER) and to a 9Kb regulatory region of the murine *Villin* gene promoter (el Marjou, Janssen et al. 2004). The injection of Tamoxifen, an estrogen receptor antagonist, will separate the Cre from the ER at the cell membrane and allow its translocation to the nucleus. This system yields up to 80% recombination in the differentiated enterocytes and the undifferentiated cells of the crypt in the intestine following the gradient of expression observed by the endogenous *Villin* namely increasing from the crypt to the differentiated cells of the villus (Muda, Boschert et al. 1996; Camps, Nichols et al. 1998; De Palma and Hanahan 2012). However it is important to note this transgene is expressed within intestinal stem cells and thus a brief pulse of Cre induced by Tamoxifen injection will induce heritable modifications within the crypt (el Marjou, Janssen et al. 2004).

5.1.2 Intestinal model: AH-Cre system (AhCre⁺)

Here the *Cre* recombinase expression is under the control of the *Cyp1A1* promoter. This promoter is usually transcriptionally silent but β -Naphthoflavone, a lipophilic xenobiotic, injected into the mice, will bind to the cytoplasmic aryl hydrocarbon receptor (hence the name AhCre) allowing it to translocate to the nucleus and specifically bind to the *Cyp1A1* promoter and initiate transcription. This system yields 80 to 100% recombination within the intestinal crypt (in both stem and transient amplifying populations) and the liver parenchyma (Ireland, Kemp et al. 2004). However this transgene also causes sporadic *Cre* expression,

even in the absence of the inducer, within the kidney, bladder, prostate, muscle and cerebellum.

5.1.3 Pancreatic model: Pdx-Cre system (PdxCre⁺)

This system allows the expression of the *Cre* recombinase under the control of the *Pancreatic and duodenal homeobox 1* gene (*Pdx1*). *Pdx1* is a gene coding for a protein involved in early embryonic development as well as in adult glucose-dependent regulation of insulin gene expression. Here a segment of 4.5Kb of *Pdx1* promoter has been inserted upstream the *Cre* recombinase gene and therefore drives a mosaic expression of the enzyme in both endocrine and exocrine pancreas as well as in the duodenal and gastric entero-endocrine cells (Gannon, Herrera et al. 2000). The recombination in this system is occurring during development between the embryonic stages E8.5 and E12.5 as well as in adult mice (Stanger, Tanaka et al. 2007). A mouse construct expressing GFP under the control of *Pdx1* allows us to visualise the extension of recombination in the pancreas as well as in the duodenum (Figure 19).

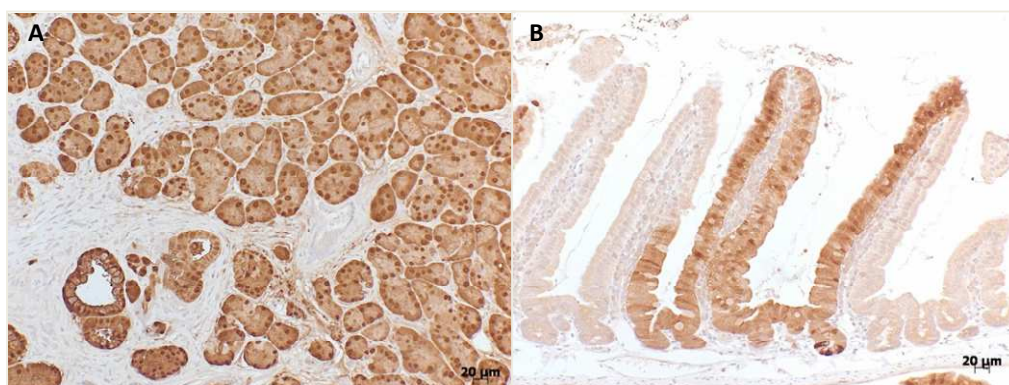


Figure 19: Recombination in the pancreatic model

Paraffin sections of a PdxCre⁺-GFP⁺ mice were stained for reporter GFP. The staining shows the extent of recombination in pancreatic (A) and duodenal (B) tissues.

5.2 Modified alleles:

5.2.1 Dusp6

The *Dusp6* constitutive knockout (*Dusp6*^{-/-}) mouse has been engineered and kindly provided by Professor Stephen M. Keyse [MRI/ Division of Cancer Research, Cancer Research UK Stress Response Laboratory, Division of Cancer Research] (unpublished) (Figure 20).

To construct the *Dusp6* null mouse, a Neomycin cassette has been inserted in the gene locus as well as three LoxP sequences resulting in the gene inactivation.

These mice are viable and have no overt phenotype in either the intestine or the pancreas (See result chapter).

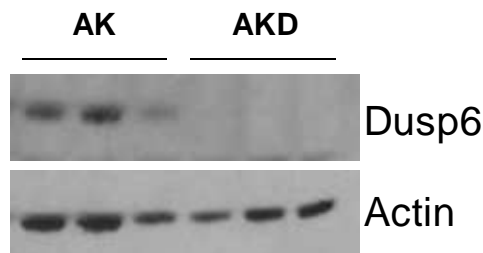


Figure 20: Dusp6 null allele

A western blot was performed on three different protein extracts from epithelial extracts of *VilCreER*⁺ *Apc*^{fl/+} *KRas*^{L^{SL}-G12D/+} (AK) and *VilCreER*⁺ *Apc*^{fl/+} *KRas*^{L^{SL}-G12D/+} *Dusp6*^{-/-} (AKD) mice. The absence of band in the AKD extracts confirm the absence of Dusp6 protein in the *Dusp6* null mice.

5.2.2 Fra1

Fra1 knockout is lethal during embryogenesis due to placental defects (Schreiber, Wang et al. 2000). Therefore, a conditional floxed allele of *Fra1* (*Fra*^{fl}) was generated in order to avoid lethality during embryogenesis (Eferl, Hoebertz et al. 2004). In this construct, the exons 3 and 4 containing the dimerisation and the DNA-binding domains of *Fra1* are flanked by two LoxP sites and a Green Fluorescent Protein (*gfp*) reporter gene is integrated into the N-Terminal part upon the flanked DNA sequences. The expression of the *Cre*

recombinase inactivates the *Fra1* gene and concomitantly allows the formation of a Fra1-GFP fusion protein (Eferl, Hoebertz et al. 2004). In order to highlight the recombination in the pancreas and the duodenum, we performed an immunohistochemistry for GFP on a *Pdx⁺ P53^{fl/+} Fra1^{fl/fl}* mouse. The staining showed an almost complete recombination in the pancreas and a high recombination rate in the duodenum.

The deletion of *Fra1* alone in both gut and pancreas does not seem to be associated with any overt phenotype (See result chapter).

5.2.3 Apc

The complete inactivation of *Apc* is lethal before day 6.5 of mouse embryonic gestation (Moser, Shoemaker et al. 1995). This is why we choose to delete *Apc* in the adult intestine using a conditional allele. The LoxP sites here are located in the introns 13 and 14 of the *Apc* gene. The action of the *Cre* recombinase results in the removal of exon 14 which causes a frameshift mutation (Shibata, Toyama et al. 1997). This silent mutant allele originally named *Apc580S* is called in this work *Apc^{fl}* because of its exon 14 deletion depending on the action of the *Cre* recombinase.

The deletion of *Apc* in the gut of adult mice has a profound effect on the crypt homeostasis and results in an altered crypt-villus architecture, a defect in migration of the cells along the crypt-villus axis and a nuclear localisation of β -Catenin in the gut epithelial cells (Sansom, Reed et al. 2004).

5.2.4 KRas

In humans, the hot spots for mutations in the *KRas* gene are located in codons 12, 13 and 61. At these codons, mutations result in decreased GTPase activity and constitutive signalling.

Mutations in codon 12 are frequent in both pancreatic and colon cancer, we therefore choose to use two oncogenic *KRas* alleles targeting this codon.

***KRas*^{LSL-G12D}**: This construct has a LoxP-STOP-LoxP (LSL) cassette knocked into the endogenous *KRas* locus (*KRas*^{LSL-G12D}). This construct leads to the inducible expression of a gain-of-function mutated *KRas* gene in the targeted organs whereby the *KRas* is constitutively active when the STOP codon is excised by the *Cre* recombinase (Jackson, Willis et al. 2001; Johnson, Mercer et al. 2001).

***KRas*^{LSL-G12V}**: In some experiments, we also used another oncogenic *K-Ras*^{LSL-G12V β geo} allele (referred in the thesis as *KRas*^{LSL-G12V}) in order to confirm our findings. In this model an internal ribosomal entry site (IRES) along with a β -geo cassette was introduced within the 3' UTR of the *KRas* allele. In this modified *KRas* allele, a STOP cassette flanked by two LoxP sites along with a sequence containing the codon 12 mutation was introduced in the first exon. In this system as well as in the *KRas*^{LSL-G12D}, the oncoprotein expression is depending on the removal of a floxed STOP cassette (Guerra, Mijimolle et al. 2003; Guerra, Schuhmacher et al. 2007). In these mice, expression of the β -geo marker allows the recombination events to be followed.

In the pancreas, the expression of both oncogenic *KRas* alleles induces the initiation of PanINs and, as the mice age, further stages of pancreatic lesions develop, up to the adenocarcinoma stage (Hingorani, Petricoin et al. 2003). These lesions present increased mucin production and can be senescent (Hingorani, Petricoin et al. 2003; Morton, Timpson et al. 2010).

The outcome of activating *KRas* in the intestine has generated conflicting reports. While the expression of *KRas*^{LSL-G12V} seems to have no phenotypical consequence on the gut epithelium (Sansom, Meniel et al. 2006), the expression of *KRas*^{LSL-G12D} induces hyperproliferation and tumour progression (Haigis, Kendall et al. 2008). However, and surprisingly, both models fail to induce an increase of Erk activation (Sansom, Meniel et al. 2006; Haigis, Kendall et al. 2008).

5.2.5 p53

There are several mouse constructs to inactivate *p53* which is an essential tumour suppressor gene. Here we choose to use the germline point mutant: *p53*^{LSL-R172H} (Olive, Tuveson et al. 2004). The point mutation leads to a structural

change of the protein which then can promote tumourigenesis independently of wt *p53* and allows metastasis formation. Moreover, in order to make the mutation inducible, the LoxP-STOP-LoxP cassette has been inserted into the intron 1 of the gene. The mutant protein accumulates in the cells and interferes with normal *p53* functions. Interestingly, in order to have disease progression in a mouse model of pancreatic cancer, a LOH of the wt *p53* allele is required (Hingorani, Wang et al. 2005).

6 Thesis aim

Despite the high frequency of oncogenic *KRas* mutations in cancer, the precise mechanistic consequences of these mutations are unclear. In pancreatic cancer *KRas* mutation is thought to initiate tumourigenesis. Understanding the precise outcome of *KRas* activation in cancer appears to be very important for the evolution of the therapeutic agents. In colorectal cancer *KRas* mutation causes tumour progression following an initiating *Apc* mutation. In this thesis, in these two distinct scenarios, I examined the functional importance of, two downstream transcription targets of *KRas* signalling: *Dusp6* and *Fra1*. *Dusp6* is predicted to be a tumour suppressor and on the other hand, *Fra1* is part of the AP-1 complex and is predicted to drive invasion and metastasis.

The aim of this work was first to determine the implication of the MAPK pathway in colorectal cancer. Then I intended to determine the functional significance of *Dusp6* and *Fra1* deletion in CRC and PC *in vivo* models as well as the mechanism of action of *Dusp6* and *Fra1* deletion.

MATERIALS AND METHODS

7 *In vivo* experiments

All experiments were performed following the UK Home Office guidelines.

All standard mice were maintained under non-barrier conditions and given a standard diet [CRM (E) expanded diet from Special Diets Services; Cat n° 801730] and water *ad libitum*.

Nude mice [Charles River Laboratories International, CD-1 nude mice] were housed in positively pressurised individually ventilated cages autoclaved prior to use. All animal handling was performed in a change station or category 2 hoods. The diet provided was irradiated and the drinking water was autoclaved.

7.1 Drug treatments

7.1.1 Induction reagents

Only the intestinal mouse models needed an injection of an inducer to activate the *Cre* recombinase.

- The recombinase of the *VilCreER⁺* model is induced by an intra-peritoneal (IP) injection of Tamoxifen at 80mg/Kg.

Preparation: 1g of Tamoxifen powder [Sigma; Cat n° T5648] was resuspended in 10ml of 100% ethanol [Sigma; Cat n° 34870]. Subsequently 90ml corn oil [Sigma; Cat n° C8267] was added to make a 10mg/ml solution. The drug was stored at -20°C.

- The recombinase of the *AhCre⁺* model is induced by an IP injection of β -Naphthoflavone at 80mg/Kg.

Preparation: 1g of β -Naphthoflavone powder [Sigma; Cat n° N3633] was resuspended in, 100ml corn oil [Sigma; Cat n° C8267] to make a 10mg/ml solution. The solution was heated with added stirring until the drug was completely dissolved. The aliquots were stored at -20°C .

7.1.2 MEK inhibitors

For both drugs the treatment regime was twice a day at 9AM and 5PM.

The inhibitor **CI-1040/PD184352** [SYNthesis med chem; Cat n° SYN-1031] was resuspended in DMSO and diluted in $\text{dH}_2\text{O}/10\%$ Cremophor [Sigma; Cat n° C5135] to obtain a solution at 10mg/mL. The solution was injected by IP route.

The inhibitor **AZD6244** [SYNthesis med chem; Cat n° SYN-1016] was resuspended in $\text{dH}_2\text{O}/0.5\%$ hydroxymethylpropylcellulose [Sigma; Cat n° 09963]/0.1% Tween 80 [Sigma; Cat n° P4780] to obtain a solution at 5mg/mL. The drug was administrated by oral gavage.

7.2 Mouse experiments

Two types of experiments were performed: survival or time point analysis. When the mice reached their end point, they were sacrificed using an approved schedule 1 procedure.

7.2.1 Time point experiments

The mice were sacrificed at a specific time point after induction of the *Cre* recombinase.

- For the experiments investigating the CPL phenotype, the mice were sacrificed 3 days after induction.
- For the intestinal Mek inhibitor treatment on established tumours experiment, the *VilCreER⁺ Apc^{fl/+} KRas^{LsL-G12D/+} Dusp6^{-/-}* mice were treated with CI1040 from day 10 and sacrificed at day 30 after *Cre* recombinase induction whereas the *VilCreER⁺ Apc^{fl/+} KRas^{LsL-G12D/+} Dusp6^{-/-}* mice were

treated with CI1040 from day 50 and sacrificed at day 80 after *Cre* recombinase induction.

- Finally, the β -Galactosidase staining on pancreatic mouse model were done on mice sacrificed at 40 days of age.

7.2.2 Survival experiments:

The mice were sacrificed when they displayed the following clinical signs: pale feet (only for the intestinal mouse model), hunched back and weight loss. Some mouse models developed skin papillomas. In this case if the papilloma reached 1.5cm in diameter, the mouse was sacrificed even in the absence of signs of ill health. Finally mice reaching the age of 500 days without clinical signs were sacrificed. These rules were all clearly mentioned in the licence of O. Sansom and fully accepted by the Home Office.

8 Mouse genotyping

Most of the mice in our laboratory are genotyped externally using the Transnetyx services (<http://www.transnetyx.com/>). The company uses a proprietary method based on real time PCR and DNA hybridisation to determine which alleles are present in the mice.

However, the assay for the *Dusp6* allele was not suitable for this method of genotyping, therefore I genotyped the mice for this allele.

8.1 DNA isolation:

Step 1: The lysis buffer [Puregen system from Flowgen; Cat n° FD-50K2] was mixed with proteinase K [Roche; Cat n° 03115844001] in a ratio of 10 μ L of proteinase K for 500 μ L of buffer. 500 μ L of this solution was added to an eppendorf containing 3mm of mouse tail and left for incubation overnight at 37°C with shaking.

Step 2: 200µL of Protein Precipitation solution [Flowgen; Cat n° FD-50K3] was added to each tube. After shaking, the tubes were centrifuged at maximum speed for 10 minutes.

Step 3: The resulting supernatants were placed in a new eppendorf and mixed with 500µL of isopropanol [Fisher; Cat n° P/7507/17] and then centrifuged at maximum speed for 15 minutes.

Step 4: The resulting pellets containing the DNA were left to dry and then resuspended in 100µL of nuclease free water [Sigma; Cat n° W4502].

8.2 Genotyping via Polymerase Chain Reaction (PCR)

8.2.1 Primers for the *Dusp6* construct

The primers sequences have been kindly given by Prof. Steve Keyse and have been synthesised by Integrated DNA Technologies.

Sequences: *Dusp6* Forward: 5' TGC GAG TAT GAG CGC CCA TTT GGT GGA TGC 3'

Dusp6 Reverse: 5' TTC AGA CCT CAT CTG AAA GAC ATG AGT AGT 3'

8.2.2 PCR reactions

The PCR reactions were performed using the GoTaq Flexi DNA Polymerase and its associated kit of polymerase buffer and 25mM MgCl₂ [Promega; Cat n° M8305]. The final volume of the PCR reaction was 50µl including 2.5µl of the tail DNA preparation (Figure 21).

PCR mix for 1 well	µL
5x Green GoTaq Flexi Buffer	10
MgCl ₂ (25nM)	5
dNTPs (10nM)	0.4
Primers (100µM)	0.2 (of each)
Go Taq	0.2
dH ₂ O	qsp 47.5
DNA sample	2.5

Figure 21: PCR mix

PCR Program:

Step 1: 95 °C for 3 minutes

Step 2: 95 °C for 30 seconds

Step 3: 55 °C for 30 seconds

Step 4: 72 °C for 1 minute

Step 5: Go to step 2, 30 times

Step 6: 72 °C for 5 minutes

Step 7: 15 °C forever

Finally the product of the PCR were run on a 4% agarose [Melford; Cat n° 9012-36-6] supplemented with ethidium bromide [Sigma; Cat n° E1510]. The products of this PCR gave the following bands: WT: 250bp and Null: 270bp.

9 Primary cell culture

9.1 Media for cell culture

Pancreatic medium: DMEM [Gibco; Cat n° 21969] with 10% of Fetal Bovine Serum [PAA; Cat n° A15-101], 1% of Penicillin-Streptomycin [Gibco; Cat n° 15070], and 2mM of L-Glutamine [Gibco; Cat n° 25030].

Gut medium: Advanced DMEM/F12 [Gibco; Cat n° 12634] with 10mM of HEPES [Gibco; Cat n° 15630], 1% of Penicillin-Streptomycin [Gibco; Cat n° 15070], 2mM of L-Glutamine [Gibco; Cat n° 15630], 0.1% BSA [Sigma; Cat n° A9647], 1% N2 [Invitrogen #17502-048], and 2% B27 [Invitrogen #12587-010].

Gut washing medium: Advanced DMEM/F12 [Gibco; Cat n° 12634] with 1% of Penicillin-Streptomycin [Gibco; Cat n° 15070].

9.2 Experiments on PDAC cell primary culture

9.2.1 PDAC culture

A piece of pancreatic tumour was harvested, mashed with a scalpel and then placed in 5mL of medium to shake for 30 seconds. The supernatant containing PDAC cells was harvested and placed in a 75cm flask [NUNC; Cat n° 153732] with an extra 10mL of medium. The cells were cultured at 37°C in 5% CO₂ humid atmosphere.

9.2.2 Organotypic collagen I Invasion Assay

Protocol adapted from: (Timpson, McGhee et al. 2011)

The 3D matrix made of skin fibroblasts and collagen from rat tails was prepared by Paul Timpson.

Step 1: Plating PDAC cells on top of the matrix

The prepared 3D matrix was moved to a 24-well dish using blunt forceps. Then 1mL of a 10⁴ PDAC cells suspension in pancreatic medium was plated on top of the matrix. The cells were allowed to grow to confluence on top of the matrix for 3-5 days.

Step 2: Transferring the matrix to a grid for invasion

A stainless steel sterile grid (provided by Paul Timpson) was placed in a 6 cm dish and pancreatic medium was added to a level above the grid. Then the matrix coated with PDAC cells was placed on the grid and the medium was adjusted so the bottom of the matrix was in contact with the pancreatic medium but not submerged. This is referred to as the air/liquid interface, which creates a nutrient gradient that promotes invasion. The pancreatic medium supplemented or not with CI1040 (500nM) was replaced every two days. The cells were left to invade for 2 weeks.

Step 3: Fixation

The matrix was placed onto a flat surface and cut in half with a scalpel and transferred to 4% formalin [Leica; Cat n° 3800600E] for overnight fixation. The matrix was then embedded and cut for IHC by the histology services.

9.3 Villi culture

The gut was isolated, flushed with PBS and cut open. The villi were scraped off with a glass cover slip, put into PBS and gently shaken in order to separate them. The enriched villi solution was then diluted to prevent an excess of mucus. After centrifugation at 600rpm at room temperature for 3 minutes, the villi were plated with matrigel [Growth Factor Reduced Matrigel, BD Biosciences Cat n° 356231] in 24 well tissue culture plate [Falcon; Cat n° 353047], covered with 500 μ L of gut medium supplemented with 50ng/mL EGF [Peprotech Cat n° AF-100-15], 100ng/mL Noggin [Peprotech Cat n° 250-38] and 500ng/mL mR-spondin1 [R & D Systems Cat n° 3474-RS] and placed at 37°C in 5% CO₂ atmosphere.

9.4 Crypt culture

The gut was isolated, flushed with PBS and cut open. The villi were scraped off with a glass cover slip and the remaining intestine tissue was placed in cold PBS. The intestine was then cut into small pieces and washed by pipetting up and down in cold PBS until the solution became clear. The clean intestine pieces were placed in 25mL of PBS with 5nM EDTA for 30 minutes with gentle shaking at 4°C. After aspiration of the cleaning solution the pieces were rinsed once in cold PBS. Then the crypts were detached with strong pipetting up and down with cold PBS. The supernatant obtained was supplemented with gut washing medium until reaching a volume of 50mL. The solution enriched in crypts was passed through a 70 μ M cell strainer [BD Falcon; Cat n° 352350] and centrifuged at 600rpm at room temperature for 5 minutes. The pellet was gently washed with gut washing medium and centrifuged 600rpm at room temperature for 3 minutes until the supernatant remained clear. The crypts were then plated with matrigel (Growth Factor Reduced Matrigel, BD Biosciences Cat n° 356231) in 24 wells

tissue culture plate [Falcon; Cat n° 353047], covered with gut medium supplemented with 50ng/mL EGF [Peprtech Cat n° AF-100-15] and 100ng/mL Noggin [Peprtech Cat n° 250-38] and placed at 37°C in 5% CO₂ atmosphere (Figure 22).

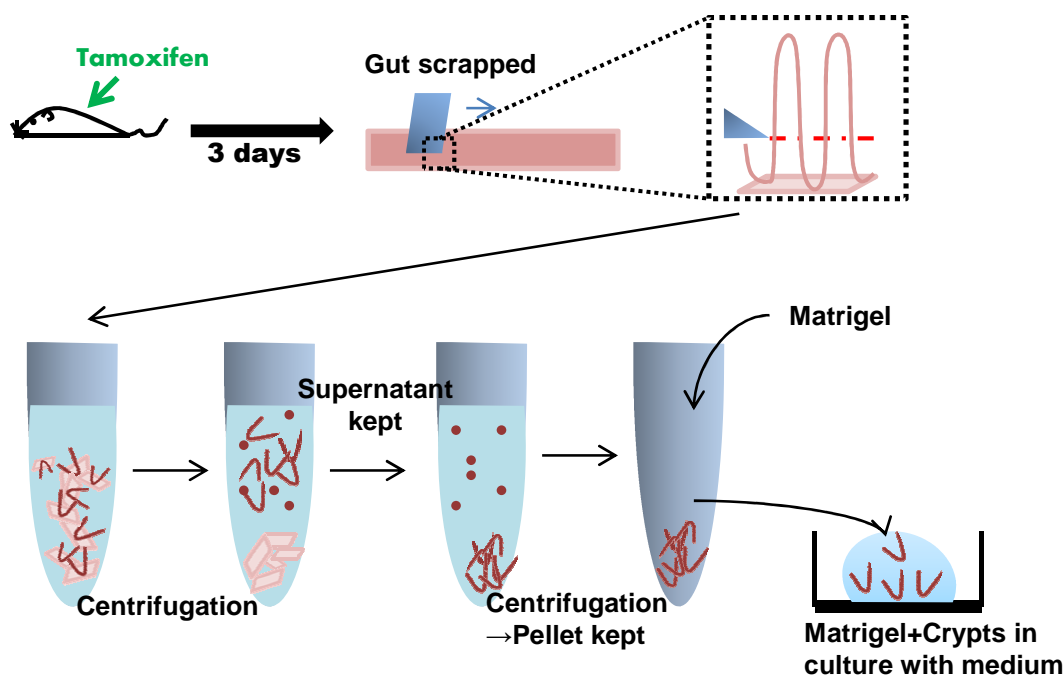


Figure 22: Crypt culture

10 Epithelial extraction

To obtain an extract enriched in epithelial cell from both crypt and villus, the following method has been used on freshly dissected intestine.

Step 1: A solution of HBSS [Gibco; Cat n° 14170-088] supplemented with EDTA to a final concentration of 10mM was prepared and 25mL of the solution were poured in 50mL Falcon tubes (2 tubes per mouse). The tubes were then placed in a water bath at 37°C.

Step 2: After flushing the gut with PBS, the intestines were placed inside out on a glass spiral.

Step 3: The intestines were incubated with shaking in the HBSS solution twice for 15 minutes. Two extracts were obtained: 0-15min classically used for RNA extraction and 15-30min classically used for protein extraction.

Step 4: The extracts were centrifuged at 4000 rpm at 4°C for 15 minutes.

Step 5: After supernatant removal, the pellets were resuspended in 1mL of cold PBS and centrifuged at maximum speed at 4°C for 15 minutes.

Step 6: The resulting clean pellets were snap frozen in liquid nitrogen and kept at -80°C.

11 Tissue isolation

Mice were sacrificed and organs (classically spleen, lungs, pancreas and liver) were harvested. When needed, the intestines were removed and flushed with either water or PBS. The tissues were then fixed in 3 different ways:

1- Quick Fixation

The tissues were incubated in 4% formalin [Leica; Cat n° 3800600E], overnight at 4°C for no more than 24 hours before processing and paraffin embedding.

2- Long Fixation

The tissues were incubated in 4% formalin [Leica; Cat n° 3800600E] for more than 24 hours before processing and paraffin embedding.

3- Methacarn Fixation

A solution of methanol (400mL) [Sigma; Cat n° 32213], chloroform (200mL) [Fisher Scientific; Cat n° C4960/PB17] and acetic acid (100mL) [Sigma; Cat n°

695092] was made fresh and used to incubate the intestines for no more than 24 hours. Then the intestines were moved to a 4% formalin [Leica; Cat n° 3800600E] solution overnight before being processed and paraffin embedded.

12 Immunohistochemistry on paraffin sections

Mouse tissues were embedded and cut by the Beatson Institute histology services.

Before antigen retrieval, all slides were dewaxed for a minimum of 5 minutes in xylene and rehydrated in decreasing concentrations of ethanol (100% - 95% - 70%) to end with a wash in water.

After counterstaining, all slides were dehydrated in increasing concentrations of ethanol (70%-95%-100%) and a final incubation in xylene for 5 minutes. The slides were then mounted.

12.1 Histochemistry

Most of the routine histochemistry and immunohistochemistry are performed by the Beatson Institute histology services. However, some IHCs were too complex to be done automatically. So I performed the IHCs for β -catenin, pSmad3, pErk, pMek and β -galactosidase.

12.2 Immunohistochemistries (IHCs)

12.2.1 β -Catenin IHC

Step 1: Peroxidase block

The slides were incubated 30 minutes in the following P-block supplemented with 2.5mL of 30% H₂O₂ [Fluka; Cat n° 95321] to a final concentration of 1.5% H₂O₂

Peroxidase block: 1L stock = 4.16g citric acid [Sigma; Cat n° 251275], 10.76g DiSodium Hydrogen Phosphate 2 hydrate [Sigma; Cat n° 71662].

Step 2: Antigen retrieval

The slides were boiled in a water bath for 50 minutes in 1X Tris EDTA solution (pH: 8.0). Then the slides were allowed to cool for 1 hour.

50X Tris EDTA solution: 1L stock = 242g Tris, 18.6g EDTA.

Step 3: Primary antibody

Endogenous staining was prevented by a prior incubation for 30 minutes in PBS/1% BSA. Then, the slides were incubated with β -catenin antibody (concentration 1:50) [BD Biosciences; Cat n° 610154] in 1%BSA/PBS for 2 hours at room temperature. Slides were then washed thoroughly in PBS.

Step 4: Secondary antibody

The slides were incubated with HRP-labelled polymer from Mouse Envision+ system [Dako; Kit: EnVision+ System- HRP Labelled Polymer; Cat n° K4000], for 1 hour at room temperature. Slides were then washed thoroughly in PBS.

Step 5: Visualisation of positivity and counterstaining using 3,3'-Diaminobenzidine (DAB).

The DAB solution [Kit: UltraVision Detection System; ThermoScientific; Cat n° TA-125-HDX] was prepared in a ratio 1mL: 1 drop and put on the sections until visualisation of positivity. Then the slides were rinsed in water and counterstain for 1 minute in Haematoxylin Z [CellPath; Cat n° RBA-4201-00A].

12.2.2 pErk and pMek IHCs

Step 1: Antigen retrieval

The slides were incubated in 0.01M citrate buffer for 4 minutes in pressure cooker at pressure (100°C). Then, they were allowed to cool for 30 minutes at room temperature in the solution.

Citrate Buffer: For 800mL: 14.4mL of Solution A and 65.6mL of Solution B.

Solution A: 10.5g Citric Acid [Sigma; Cat n° 251275] in 500mL H₂O and Solution B: 29.4g NaCitrate [Sigma; Cat n° W302600] in 1L H₂O.

Step 2: Prevention of endogenous staining

Endogenous staining was prevented by a prior incubation for 20 minutes in 3% H₂O₂ followed by an incubation for 1 hour in TBS/0.1% Tween/10% Normal goat serum [Dako; Cat n° X0907] at room temperature.

Step 3: Primary antibody

The slides were incubated with the primary antibody diluted in TBS/0.1% Tween/10% Normal goat serum overnight at 4°C.

pErk (1:100)[Cell Signalling; Cat n° 9101] ; pMek (1:125)[Cell Signalling; Cat n° 2338] ; pSmad3 (1:50) [Abcam; Cat n° ab52903].

Step 4: Secondary antibody

The slides were incubated with a biotinylated goat Anti-Rabbit secondary antibody (Vector labs; Kit: VECTASTAIN Elite ABC Kit (Rabbit IgG); Cat n° PK-6101), 1/200 in 10% Normal goat serum in TBS/T for 30 minutes at room temperature. The second step reagent was prepared 30 minutes prior use and kept at room temperature reagents (5ml TBS/T + 2 drops A + 2 drops B).

After the 30 minutes incubation with the secondary antibody, the slides were incubated with the second step reagent of the ABC kit for 30 minutes at room temperature.

Step 5: Visualisation of positivity and counterstaining using DAB

The solution was prepared in a ratio 1mL: 1 drop and put on the sections until visualisation of positivity. Then the slides were rinse in water and counterstain for 1 minute in Haematoxylin Z [CellPath; Cat n° RBA-4201-00A].

12.2.3 β -galactosidase IHC

Step 1: Solution preparation

- Fix solution: 500 μ L Glutaraldehyde (0.25%) [Sigma; Cat n° G5882], 1g paraformaldehyde (2%) [Fluka ; Cat n° 76240] in 49.5mL PBS.
- 20x Potassium cyanide stock solution (KC - solution) :

Dissolve in 100ml PBS (total volume): 3.28g of Potassium ferricyanide(III) ($K_3Fe(CN)_6$), [Sigma ; Cat n° 702587-50g] and 4.2g of Potassium hexacyanoferrate(II) Trihydrate, ($C_6FeK_4N_6 \cdot 3H_2O$), [Fluka; Cat n° 60279].

- X-Gal Staining solution: 9.3ml PBS 1mM $MgCl_2$ (pH5.5), 0.5ml 20x KC-solution and 0.25ml 40x X-Gal stock [Promega; Cat n° V394A].

Step 2: Thaw slides at RT and take care that the samples are not drying. Then fix the slides for 15 minutes in Fix solution at RT. Then wash samples with PBS 1mM $MgCl_2$.

Step 3: Cover samples with X-Gal staining solution and put into a “wet chamber” at 37°C overnight. Then wash the slides.

Step 4: Counterstain with nuclear fast red solution [Vector Laboratories; Cat n° H-3403].

13 Protein analysis

13.1 Protein extract preparation

A lysis buffer was prepared as follows: 1mL T-PER [ThermoScientific; Cat n° 78510] supplemented with 1µL of Aprotinin [Sigma; Cat n° A6279], 1µL of 1mM Sodium orthovanadate (Na_3VO_4) [Sigma; Cat n° S6508], 1µL Sodium Fluoride (NaF) [Sigma; Cat n° S7920] and 12.5µL Phenylmethanesulfonyl Fluoride Solution (PMSF) [Fluka; Cat n° 93482].

The adequate quantity of lysis buffer was added to the mouse tissue and left on ice for 10 minutes. Then the tissues were homogenized by pipetting up and down with decreasing size of needles and centrifuged at maximum speed for 10 minutes at 4°C. The supernatant containing the proteins was transferred into a new tube. This process was repeated until the extracts were clear.

13.2 Protein concentration measurement

The concentration of each protein extract were measured with the BCA Protein Assay kit [ThermoScientific; Cat n° 23225] and using the reader SPECTRAMaxPlus [Molecular Devices].

13.3 Western Blot

For Western analysis, proteins were run on a NuPAGE 10% or 12% Bis-Tris gel [Invitrogen; Cat n° NP0301BOX or n° NP0341BOX] using the tank XCell II Blot module [Invitrogen; Cat n° EI9051]

Protein samples were mixed with 2.5µL of NuPAGE LDS sample buffer [Invitrogen; Cat n° NP0007] supplemented with 2µL DTT and equalised with lysis buffer so that all samples were 40µg and of equal volume (20µl). They were then heated at 100°C for 5 minutes and loaded onto the gel.

Gels were run for 1 hour at 200V in NuPAGE MOPS SDS Running buffer [Invitrogen; Cat n° NP0001] or until the protein markers [Full Range Rainbow

recombinant, Invitrogen, Cat n° 2892534] had separated, on ice in order to preserve the phospho proteins.

Gels were then placed on a Hybond PVDF Transfer membrane [GE Healthcare; Cat n° RPN303F] previously incubated in methanol and between two layers of Whatman paper [Schleider & Schuell; Cat n° 3003-917]. The “sandwich” was then placed in transfer buffer (200mL SDS Blotting buffer, 400mL Methanol, 1400mL H₂O) and transferred for 1 hour at 30V on ice.

After transfer, the presence of proteins was checked by staining with a Ponceau red solution [Sigma; Cat n° P3504].

Blots were blocked in TBS/0.1% Tween/5% BSA for 30 minutes. Primary antibodies and conditions used to probe blots are listed below (Figure 23). Appropriate HRP-conjugated secondary anti-rabbit or anti-mouse antibodies were used [DAKO; Cat n° P0448 and P0447 respectively].

Blots were then washed in TBS/0.1% Tween and visualised using ECL plus (Amersham) on ECL film (Amersham).

Primary antibody	Cat. Number	Concentration	Secondary Antibody
MEK1/2	Cell Signalling; Cat n° 4694	1/1000	(α Mouse) Dako Cat n° P0447
pERK1/2	Cell Signalling; Cat n° 9101	1/1000	(α Rabbit) Dako Cat n° P0448
ERK1/2	Cell Signalling; Cat n° 9102	1/1000	(α Rabbit) Dako Cat n° P0448
pELK1	Abcam; Cat n° ab28818	1/1000	(α Rabbit) Dako Cat n° P0448
DUSP6	Abcam; Cat n° ab76310	1/500	(α Rabbit) Dako Cat n° P0448
TUBULIN	Sigma; Cat n° T6199	1/40000	(α Mouse) Dako Cat n° P0447

Figure 23: Immunoblot antibodies

14 Statistics:

In this work there are two major types of experiments: disease-free survival experiments and scoring experiments.

Scoring experiments:

I chose to use only three to five mice per group in order to comply with the rule of the three Rs: Refine - Reduce - Replace which promotes the ethical use of a minimum number of live animals for research. Due to this low number of mice per group it is not possible to test the distribution of the data. Therefore I assumed the data was not normally distributed and I used the non-parametric test Mann-Whitney which allowed the comparison of two groups of only three mice each. This test consist in comparing the medians of two sets of data assuming one set has larger values than the other one.

Disease-free survival test:

Disease-free survival experiments are routinely done in research and the data obtained are always considered not to have a normal distribution. Here I assumed that the data were not normally distributed and therefore I ran a non-parametric Log-rank test.

RESULTS

15 Oncogenic *KRas* phenotype in the CRC mouse model

Over 70% of colon cancers have a mutation in *Apc* and mouse models have shown that adenomas can be initiated by *Apc* mutation alone (Shibata, Toyama et al. 1997). To drive tumour progression in the mouse, other mutations are necessary. Oncogenic mutations in *KRas*, a key member of the MAPK superfamily, occur in 30% of cases of CRC. The association between Wnt pathway activation and *KRas* activation has been previously studied by Fodde's group in a mouse model carrying the mutated *Apc* allele *Apc*^{+/^{1638N} along with the oncogenic *KRas* allele *KRas*^{G12V}. They found evidences of synergetic effect of the two mutations on tumourigenesis (Janssen, Alberici et al. 2006; Alberici, de Pater et al. 2007). As *Dusp6* is thought to be upregulated following *KRas* activation, it was important to first analyse the phenotype associated with *KRas* mutation in the intestine.}

To test the effects of oncogenic *KRas* mutation in CRC, we used a transgenic mouse model where the VillinCre ER (*VilCreER*⁺) transgene is activated to drive an inducible *Cre* recombinase expression following an injection of Tamoxifen. These mice were crossed with models containing the conditional *Apc* mutant allele (Shibata, Toyama et al. 1997) and the knock-in *Lox-STOP-Lox KRas*^{G12D} (*KRas*^{LSL-G12D/+}) allele (Jackson, Willis et al. 2001; Johnson, Mercer et al. 2001).

15.1 Oncogenic *KRas* mutation increases proliferation rates of intestinal cells following *Apc* deletion.

15.1.1 Influence of *KRas* mutations on tumourigenesis

To address the influence of *KRas* mutation on tumourigenesis, we compared the tumour free survival of *VilCreER*⁺ (WT), *VilCreER*⁺ *Apc*^{fl/+} (*A*^{fl/+}) and *VilCreER*⁺ *Apc*^{fl/+} *KRas*^{LSL-G12D/+} (*A*^{fl/+}K) mice. In this model, tumours initiate when the wild type *Apc* allele is lost. The tumourigenesis will then be delayed or accelerated depending on other mutations within the transgenic model used.

As expected, the *VilCreER*⁺ mice did not develop cancer. Furthermore, it has been shown that *KRas* activation alone leads to intestinal hyperproliferation but does not promote intestinal tumourigenesis (Haigis, Kendall et al. 2008). Consistent with previous studies, the *VilCreER*⁺ *Apc*^{fl/+} mice developed multiple adenomas and showed a median survival of 290 days. The *VilCreER*⁺ *Apc*^{fl/+} *KRas*^{LsL-G12D/+} mice exhibited a drastic acceleration of tumourigenesis leading to a median survival of 100 days (Figure 24). This finding is consistent with the idea of multiple sequential mutations leading to invasive carcinoma in CRC.

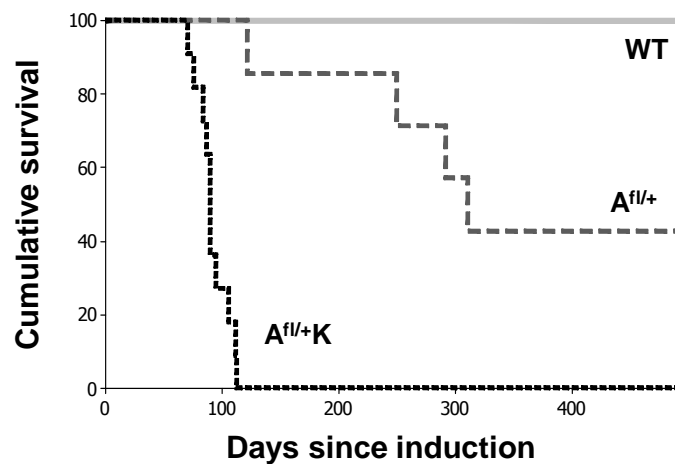


Figure 24: Effect of *KRas* activation on the tumour free survival

Kaplan-Meier curve showing the survival of *VilCreER*⁺ (WT) (light grey line ; n=10), *VilCreER*⁺*Apc*^{fl/+} (*A*^{fl/+}) (grey dashed line ; n=7) and *VilCreER*⁺*Apc*^{fl/+} *KRas*^{LsL-G12D/+} (*A*^{fl/+}*K*) (black dashed line ; n=13) mice.

Mice with intestinal tumours were sacrificed at the same point of illness or when they reached 500 days after induction of the *Cre* recombinase. The tumour free survival was significantly decreased between the *VilCreER*⁺ and the *VilCreER*⁺ *Apc*^{fl/+} groups (log rank p<0.001) as well as between the *VilCreER*⁺ *Apc*^{fl/+} and the *VilCreER*⁺ *Apc*^{fl/+} *KRas*^{LsL-G12D/+} groups (log rank p<0.001).

15.1.2 Influence of *KRas* mutation on the phenotype after an acute *Apc* deletion

To ascertain the mechanism by which *KRas* mutation cooperates with *Apc* loss we acutely deleted both copies of *Apc* (*Apc^{fl/fl}*) in the presence or absence of the oncogenic *KRas* allele within the intestinal epithelium. To investigate the effects on proliferation we focused on the crypts of the intestinal epithelium. The crypts contain a population of intestinal progenitors called the transient amplifying cells and their constant proliferation allows, in mice, the renewal of the epithelium every 72 hours. After deletion of both *Apc* alleles, the structure of the crypt expands into the villus giving a crypt-progenitor-like (CPL) phenotype. The CPL phenotype consists of increased proliferation, loss of migration and differentiation and increase of apoptosis (Sansom, Reed et al. 2004). Therefore the *Apc* deficient cells are blocked in a progenitor like state. Quantifying the CPL phenotype indicates the impact of different mutations on the epithelium. Proliferation was assessed using a 2 hours BrdU pulse-chase labelling which only marks cells in S-phase. In a normal epithelium, the proliferative cells are located in the crypt only whereas an acute deletion of *Apc* leads to an extension of the proliferative area. The quantification of the CPL phenotype is done by calculating the percentage as well as the total number of BrdU positive cells. Moreover an estimation of the size of the CPL area is given by the calculation of the position of the highest BrdU positive cell on the crypt-villus axis (Figure 25). The Wnt pathway activation is observed with the help of a β -catenin IHC: in a normal situation, β -catenin is located to the cell membranes and in some nuclei of cells at the bottom of the crypt. Nuclear staining is the sign of the activation of the pathway and all cells exhibit nuclear β -catenin following *Apc* loss in the intestinal epithelium.

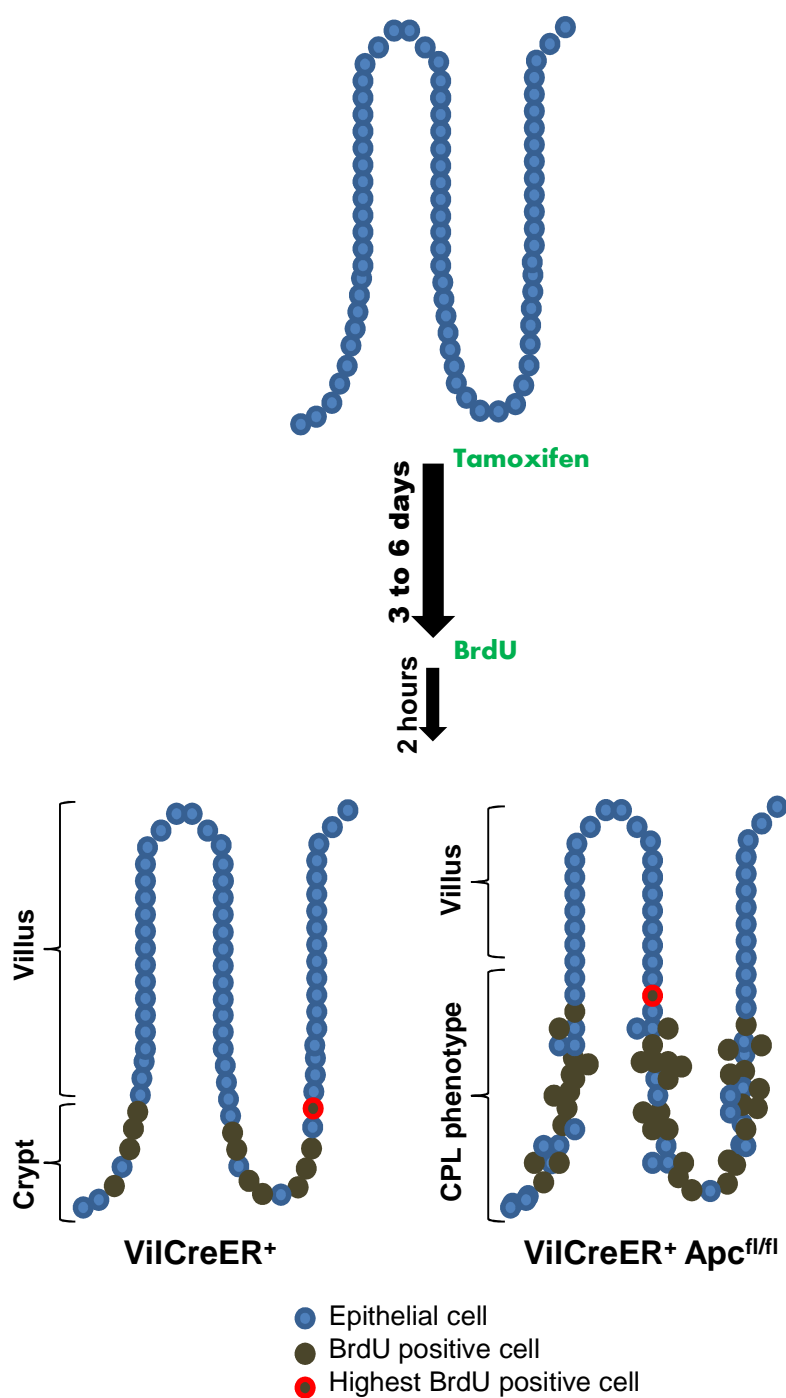


Figure 25: Quantification of proliferation

BrdU pulse-chase labelling experiments are performed on mice with an acute *Apc* deletion. At day 3 to 6 after *Cre* recombinase induction, the mice are injected with BrdU. During 2 hours, the BrdU will be incorporated in cells in S-phase. Then mice are sacrificed and an IHC for BrdU is performed.

Determining the position of the highest BrdU positive cell allows to estimate the CPL phenotype size.

At one day after induction of the *Cre* recombinase, no phenotypical differences were observed between *VilCreER⁺ Apc^{fl/fl}* (A) and *VilCreER⁺ Apc^{fl/fl} KRas^{LSL-G12D/+}* (AK) mice (Figure 26). The proliferative cells were located in the crypt and the nuclear β -catenin positive cells were observed at the bottom of the crypt. From day 2, phenotypical differences began to appear. The CPL phenotype was increased in the presence of the oncogenic *KRas* allele as underlined by the number of BrdU and nuclear β -catenin positive cells. At day 3 after induction, the difference between the two genotypes was even more pronounced with a drastic increase in proliferation in the presence of the oncogenic *KRas* allele highlighted by areas of proliferation with nuclear β -catenin positive cells in the crypt villus structure. The BrdU positive cell number was also highly increased in AK compared to A mice. This is in good agreement with the enhanced tumour progression observed in the *VilCreER⁺ Apc^{fl/+} KRas^{LSL-G12D/+}* mice of the survival experiment.

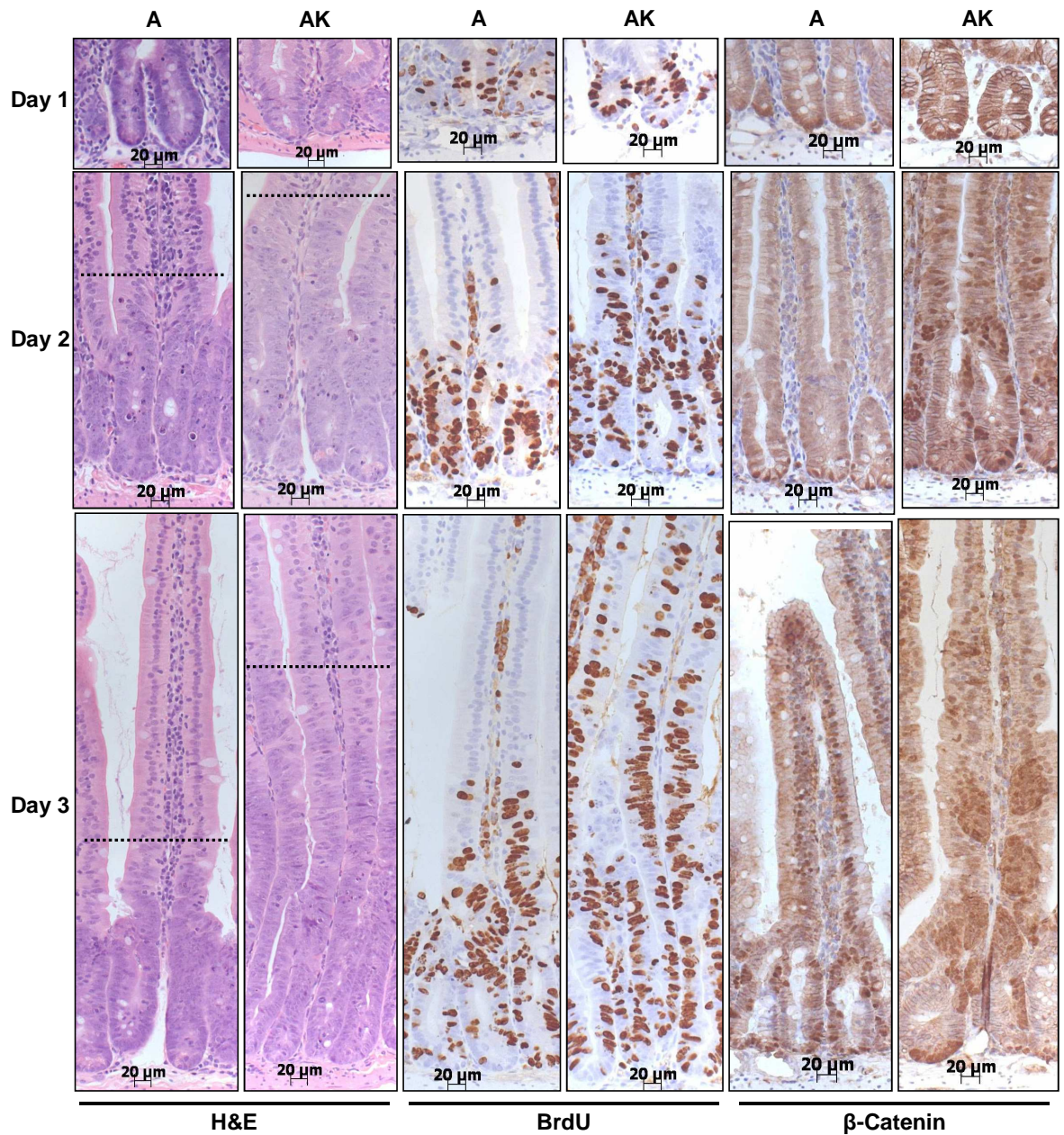


Figure 26: Effects of *KRas* activation on CPL phenotype following *Apc* deletion

H&E, BrdU and β -Catenin IHC were performed on paraffin sections of intestine of *VilCreER⁺Apc^{fl/fl}* (A) and *VilCreER⁺Apc^{fl/fl}KRas^{LSL-G12D/+}* (AK) mice at days 1, 2 or 3 after induction of the Cre Recombinase.

At day 1, no difference is observed between the two genotypes. From day 2, the AK mice have a larger CPL phenotype (CPL phenotype limit highlighted by a dashed line) with proliferative cells located higher on the crypt-villus axis and with an increased nuclear β -Catenin staining.

To determine the size of the CPL phenotype we then scored the position of the highest BrdU positive cells of 2 hours BrdU pulse labelling experiment (Figure 27). There were no differences noted at one day after induction, however, from day 2, the top BrdU positive cell was significantly higher on the crypt-villus axis in the AK compared to the A mice.

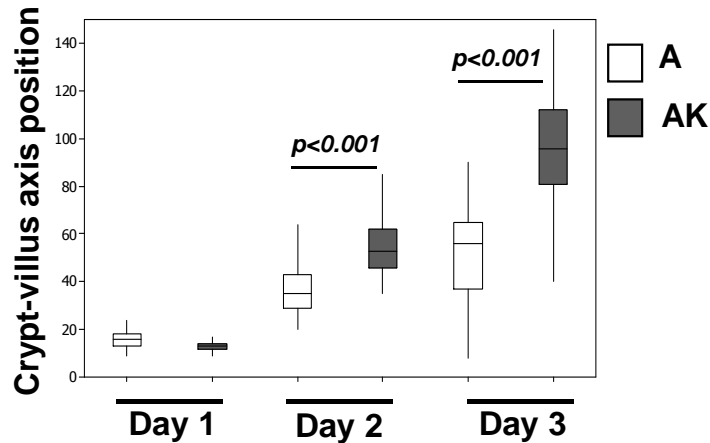


Figure 27: Effects of *KRas* activation on CPL phenotype area

The position of the last BrdU positive cell of 25 villi of *VilCreER⁺Apc^{fl/fl}* (A) (white), *VilCreER⁺Apc^{fl/fl}KRas^{LsL-G12D/+}* (AK) (grey) mice were scored and compared with a Mann-Whitney statistical test.

At day 1, no significant difference was observed between the two groups. At day 2 and day 3 there is a significant increase of the CPL phenotype area of *VilCreER⁺Apc^{fl/fl}KRas^{LsL-G12D/+}* ($p < 0.001$).

15.2 Oncogenic *KRas* allows an expansion of the cell of origin of the tumour

In our ageing mouse model described earlier, the *VilCreER⁺Apc^{fl/+}* mice always presented adenomas which seemed to arise from the crypt compartment (Figure 28, top panel). However, the lesions in the *VilCreER⁺Apc^{fl/+}KRas^{LsL-G12D/+}* mice seemed to arise separately from either the crypt or the villus compartment (Figure 28, bottom panel). This finding was consistent with the observation of proliferation areas in the villi of *VilCreER⁺Apc^{fl/fl}KRas^{LsL-G12D/+}* (AK) mice (Figures 26). Interestingly, in colon, the tumours were similar between the two

genotypes (Figure 29). However, it is important to note that whilst all of the $VilCreER^+ Apc^{fl/+} KRas^{LSL-G12D/+}$ mice developed colonic tumours only some $VilCreER^+ Apc^{fl/+}$ mice developed tumours in the colon resulting in an overall increased number of colonic tumours in $VilCreER^+ Apc^{fl/+} KRas^{LSL-G12D/+}$ mice (despite a much shorter latency).

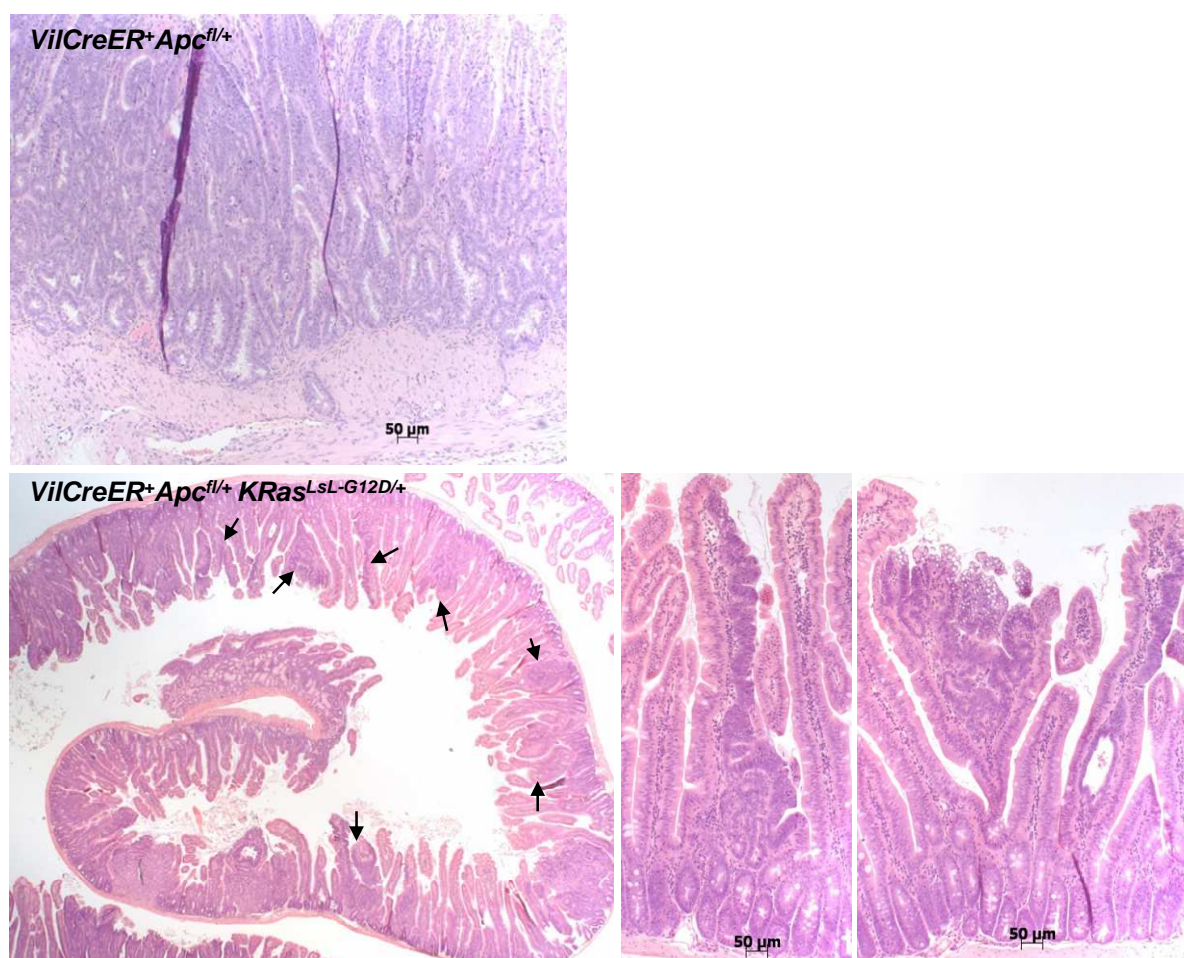


Figure 28: *KRas* activation allows tumours to form in the villus

H&E of $VilCreER^+ Apc^{fl/+}$ (top panel), $VilCreER^+ Apc^{fl/+} KRas^{LSL-G12D/+}$ (bottom panel) mice showing intestinal tumours.

$VilCreER^+ Apc^{fl/+} KRas^{LSL-G12D/+}$ mice developed several lesions (highlighted by black arrows) within the villi whereas the $VilCreER^+ Apc^{fl/+}$ did not.

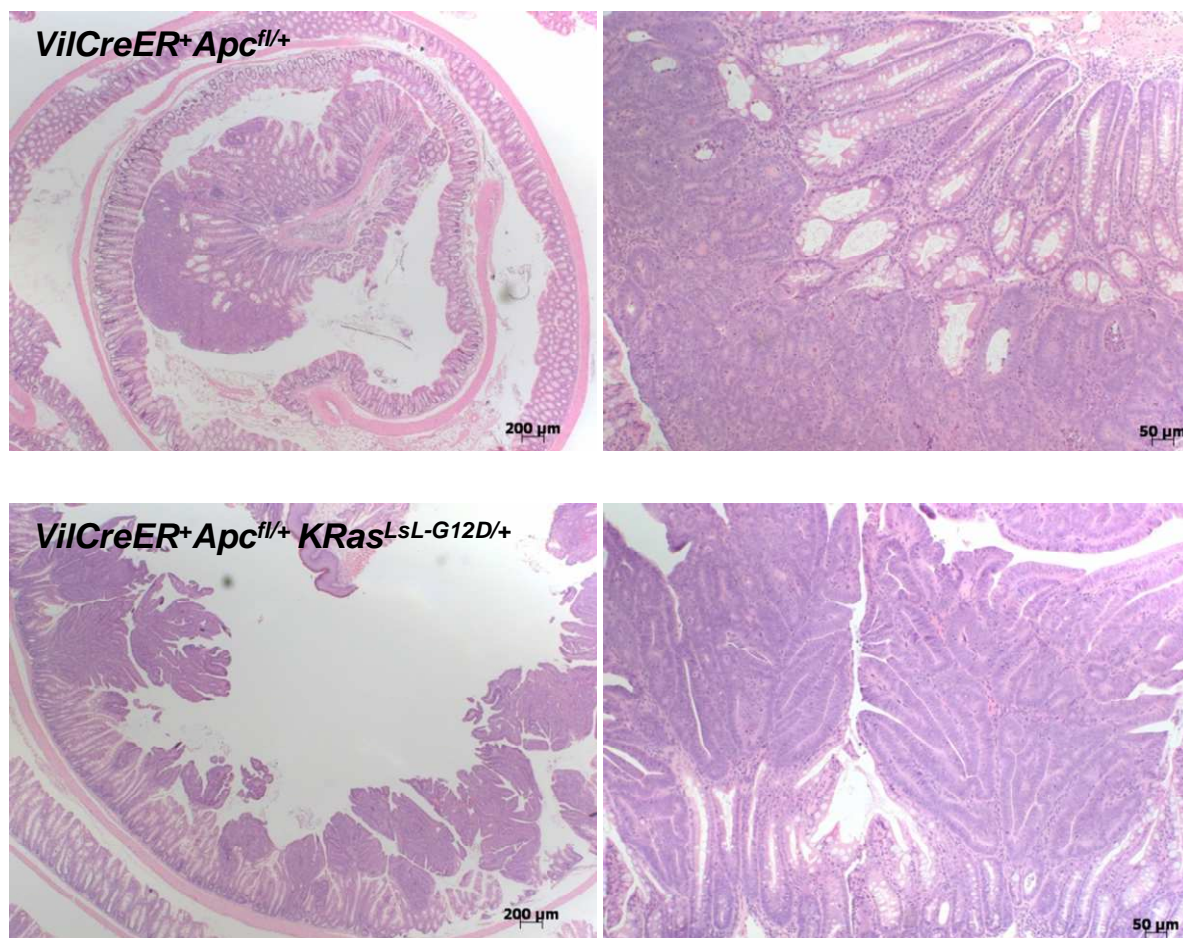


Figure 29: Tumour formation in the colon of *KRas* activated mice

H&E staining on paraffin sections of colon of *VilCreER⁺Apc^{fl/+}* (top panel), *VilCreER⁺Apc^{fl/+}KRas^{LSL-G12D/+}* (bottom panel) mice showing colonic tumours.

In order to investigate the possible expansion of cell of origin we decided to address the ability of the villus cells to form tumours. To do so, Patricia Cammareri performed an intestinal cell culture experiment where she specifically cultured villus cells from *VilCreER⁺* (WT), *VilCreER⁺Apc^{fl/fl}* (A) and *VilCreER⁺Apc^{fl/fl}KRas^{LSL-G12D/+}* (AK) mice. In this experiment, she quantified the percentage of adenoma structures (spheroids) formation in order to evaluate the ability of villus cells to initiate tumour formation. At both day 2 and day 3 after induction of the *Cre* recombinase, no spheroid formation was observed in WT mice (Figure 30). We observed an unexpected basal 0 to 2% rate of spheroid formation in A mice allowing us to conclude that the phenomenon can rarely occur without *KRas* activation. The dramatic increase of spheroid formation in

the AK mice, which presented a minimum of 20% of spheroid formation, indicates that the combination of *Apc* deletion and *KRas* activation may allow a different cell population to act as a tumour initiator. However it would be important to validate the origin and the cell type in order to confirm the dedifferentiation of villus cells.

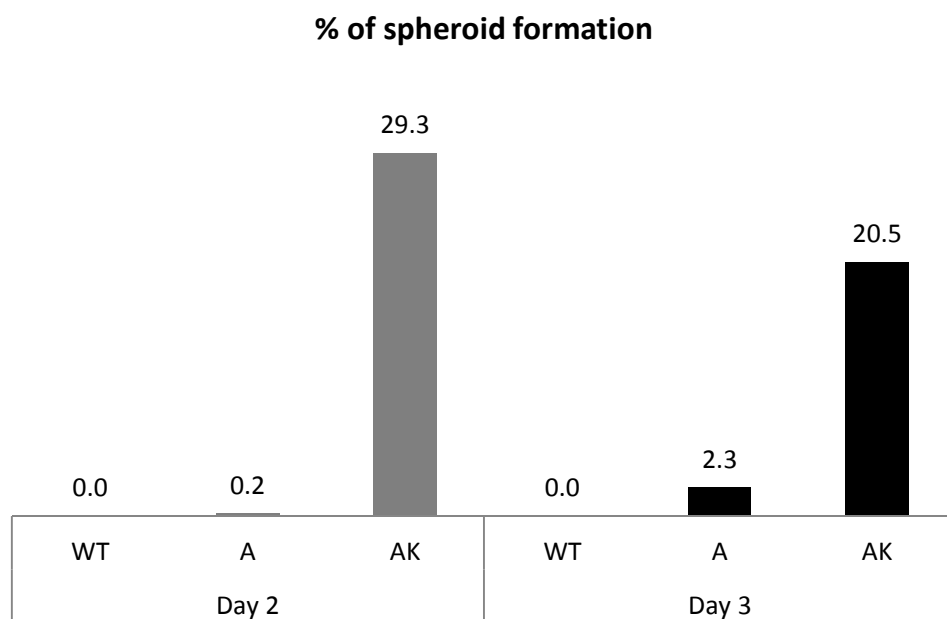


Figure 30: Effect of *KRas* activation on spheroid formation from the villus epithelium

The formation of spheroids in villi culture of *VilCreER*⁺ (WT), *VilCreER*⁺*Apc*^{*fl/fl*} (A), and *VilCreER*⁺*Apc*^{*fl/fl*} *KRas*^{*L^{SL}-G12D/+*} (AK) mice were scored and compared with a Mann-Whitney statistical test.

At both day 2 (grey) and day 3 (black) post-induction, there was a significant increase in the spheroid formation rate in AK mice compared to the two other mouse genotypes ($p < 0.001$).

Data provided by Patricia Cammareri

15.3 *KRas* activation signature

In order to study further the outcomes of *KRas* mutations on general gene expression and therefore signalling pathways expressions as MAPK, I sent whole intestine RNA samples of various cohorts of *VilCreER*⁺ mice taken at day 3 after *Cre* recombinase induction to be analysed in a microarray. We then analysed the fold change of each gene expression with an Anova statistical test performed by Gabriela Kalna. From the fold change value, the Log₂ expression value for each gene was calculated. It was this Log₂ expression value that Ann Hedley has been used to cluster mice and draw the following heatmaps. It is important to note that these microarray studies are indications for further investigation as the RNA is extracted from whole gut extract which includes not only the epithelium but also the stroma and the muscle layers. A quantification of the epithelial cells ratio could be used to normalise more accurately the results. However these studies are good primary read out of the consequences of the mutations of interest.

15.3.1 Wnt pathway signature

We first analysed the Wnt pathway signature of *VilCreER*⁺ (WT), *VilCreER*⁺ *Apc*^{fl/fl} (A) and *VilCreER*⁺ *Apc*^{fl/fl} *KRas*^{LSL-G12D/+} (AK) mice based on a list of upregulated genes in human colorectal lesions (Rigas, Hoff et al. 2001). To create this list of genes, H. Clevers' group analysed RNA obtained from biopsied tissues of normal mucosa, adenomas and carcinomas of patients (Rigas, Hoff et al. 2001). They studied the transcriptome of both adenomas and carcinomas compared with the normal mucosa and identified 208 genes upregulated in either one or both type of lesions.

We therefore compared the expression values of these genes in WT, A and AK mice taken at day 3 after induction of the *Cre* recombinase (Figures 31A and 31B). The expression on the heatmap is determined by the Z-score which is calculated for each row of data (gene). Then the data are centred and scaled by subtracting the mean of the row from every value and then dividing the resulting values by the standard deviation of the row. From this analysis it is clear that most of the WNT signature genes are upregulated after *Apc* loss as well as

following both *Apc* loss and *KRas* activation. Interestingly, some genes such as *cd44*, *ETS translocation variant 4* (*Etv4*) and *Myc* are gradually upregulated following *Apc* loss and both mutations. This confirms the Wnt pathway activation following the initiating *Apc* mutation and the importance of *KRas* activation in the upregulation of the Wnt pathway.

We then asked the software to compute the expression values and cluster the different samples. These clusters were determined by the mathematical Euclidean distance between each sample. The software is grouping samples which behave similarly among all their genes. Here, the three samples of each were grouped together confirming homogeneity between the samples of each genotype (Supplementary figure 1 - All the supplementary figures can be found in the Appendix).

Some of the results obtained were confirmed by qRT-PCR performed by Fatih Ceteci (Figure 32). He showed an upregulation following *Apc* loss of *Axin2*, *Lgr5*, *Lef1*, *cMyc*, *cd44* and *Sox9*. After the activation of *KRas*, he showed an enhanced upregulation of *cMyc*, *cd44* and *Sox9* but a downregulation of *Axin2*, *Lgr5* and *Lef1*. The surprising downregulation of *Lgr5* and *Axin2* could be linked to the downregulation of the transcription factor *Lef1*.

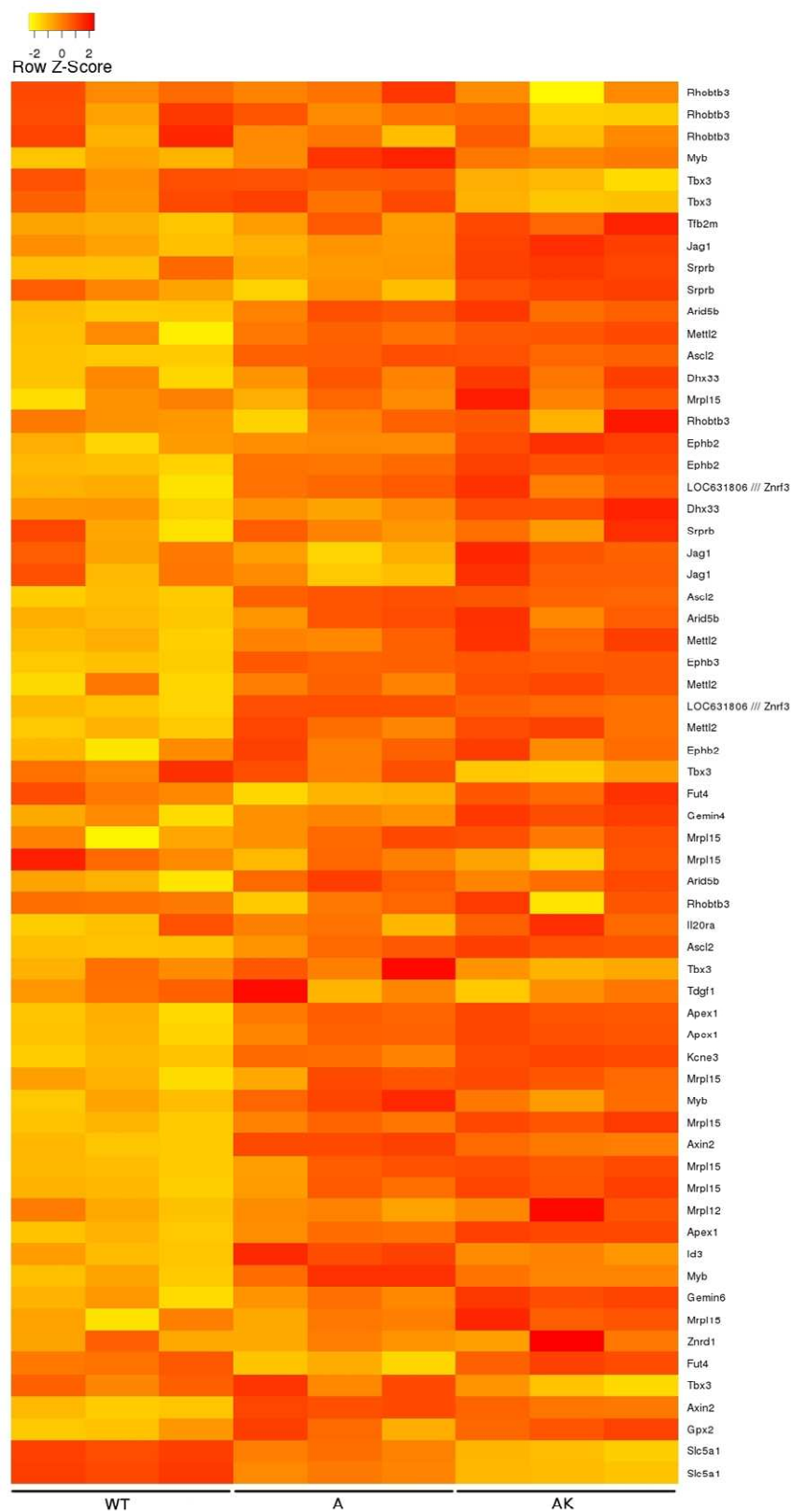
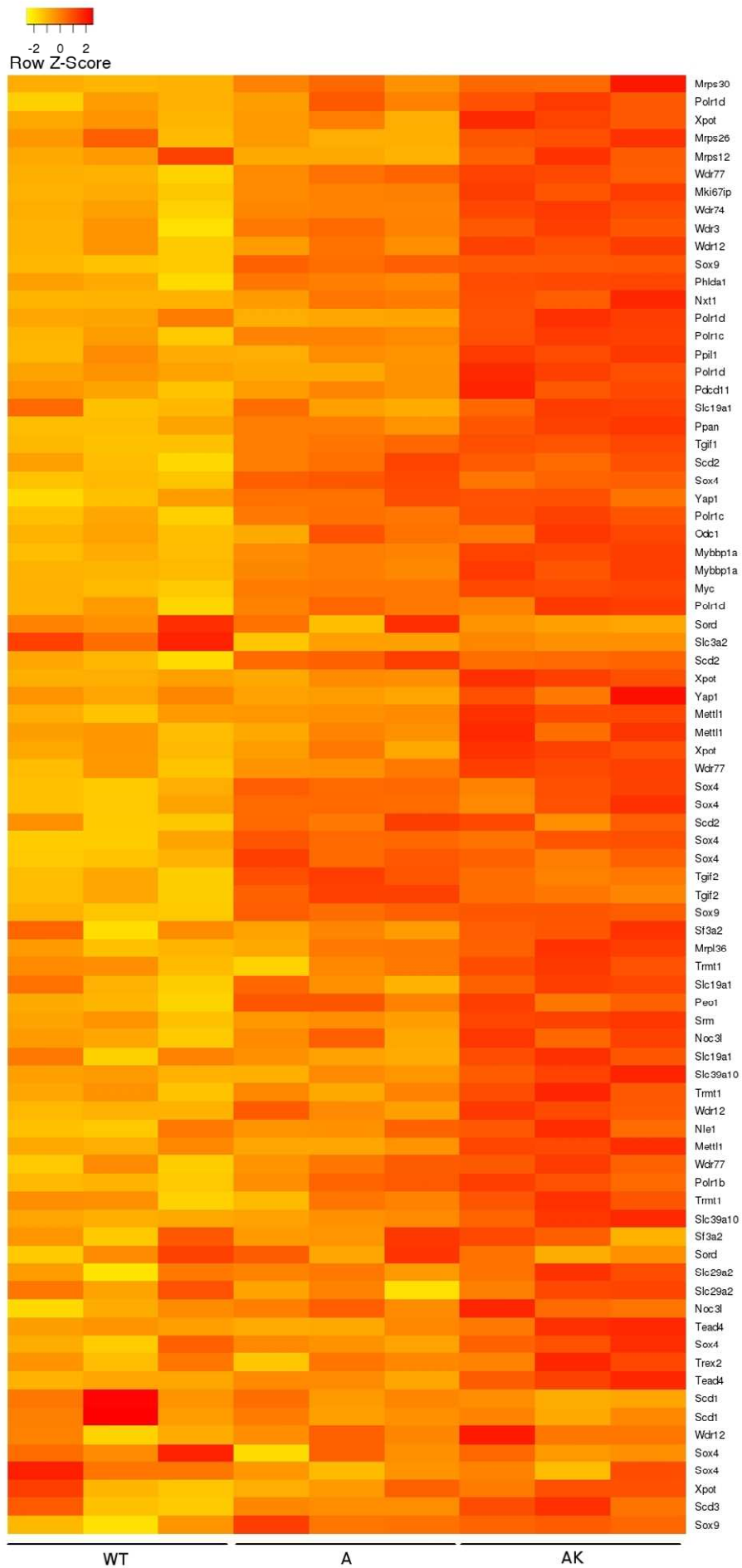


Figure 31A: WNT pathway signature

The genes found to be up-regulated in human colorectal adenomas were tested in whole gut extracts of *VilCreER⁺* (WT), *VilCreER⁺Apc^{fl/fl}* (A), and *VilCreER⁺Apc^{fl/fl} KRas^{LsL-G12D/+}* (AK) mice taken at day 3 after Cre recombinase induction. The Z-score is indicated by a range of colour from yellow (low expression) to red (high expression).



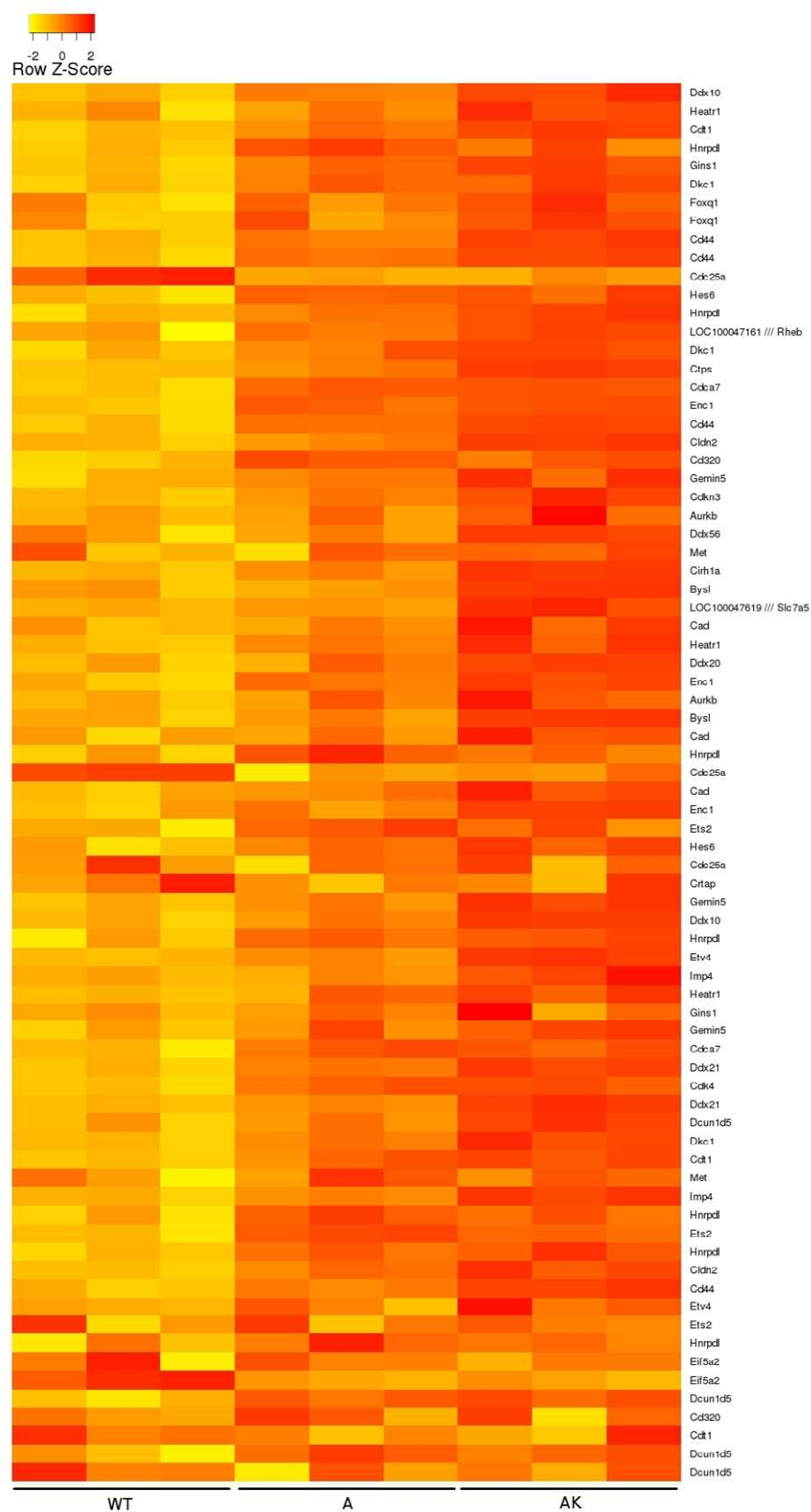


Figure 31B: WNT pathway signature

The genes found to be up-regulated in both human colorectal adenomas and human colorectal adenocarcinomas were tested in whole gut extracts of *VilCreER⁺* (WT), *VilCreER⁺Apc^{fl/fl}* (A), and *VilCreER⁺Apc^{fl/fl}KRas^{LSL-G12D/+}* (AK) mice taken at day 3 after Cre recombinase induction. The Z-score is indicated by a range of colour from yellow (low expression) to red (high expression).

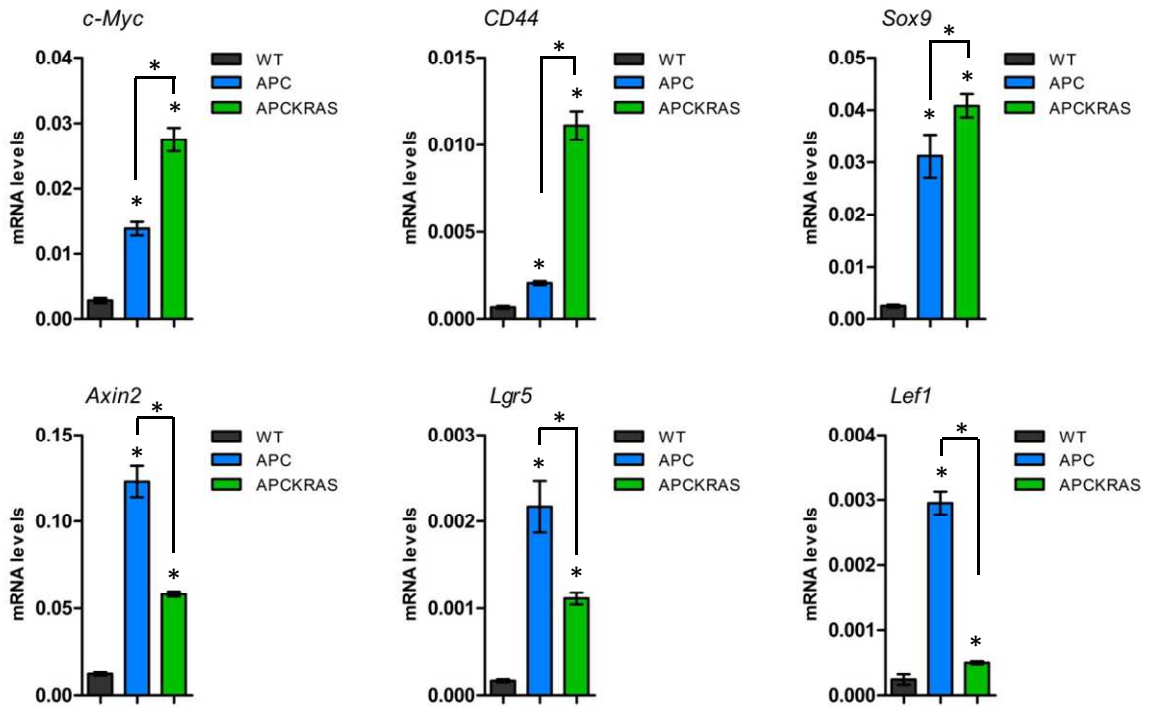


Figure 32: WNT pathway signature: confirmation of targets by qRT-PCR

Some Wnt/ β -Catenin target genes were tested in whole gut extracts of *VilCreER*⁺ (WT), *VilCreER*⁺ *Apc*^{fl/fl} (APC), and *VilCreER*⁺ *Apc*^{fl/fl} *KRas*^{L^{SL}-G12D/+} (APCKRAS) mice taken at day 3 after Cre recombinase induction. * indicates a p value p < 0.05 calculated with the Δ Ct method.

Data provided by Fatih Ceteci

15.3.2 Stem cell signature

We then analysed the expression of some intestinal stem cell markers in *VilCreER*⁺ (WT), *VilCreER*⁺ *Apc*^{fl/fl} (A) and *VilCreER*⁺ *Apc*^{fl/fl} *KRas*^{L^{SL}-G12D/+} (AK) mice. We observed an upregulation of stem cell markers after *Apc* loss (Figure 33). There were no clear enhanced upregulation following the addition of the oncogenic *KRas* allele. This shows the de-differentiation associated to tumourigenesis and the increased proliferation ability of the cells within the modified intestinal epithelium. Furthermore, the samples were clustered according to their genotype confirming their homogeneity (Supplementary figure 2). We noted an unexpected pattern of the *Olfm4* expression: the expression was similar in WT and A mice and was downregulated in AK mice. This is rather surprising as *Olfm4* has been shown to be upregulated in several CRC cells (van

der Flier, Haegebarth et al. 2009). However this marker appears to be Wnt independent which could explain the result observed here.

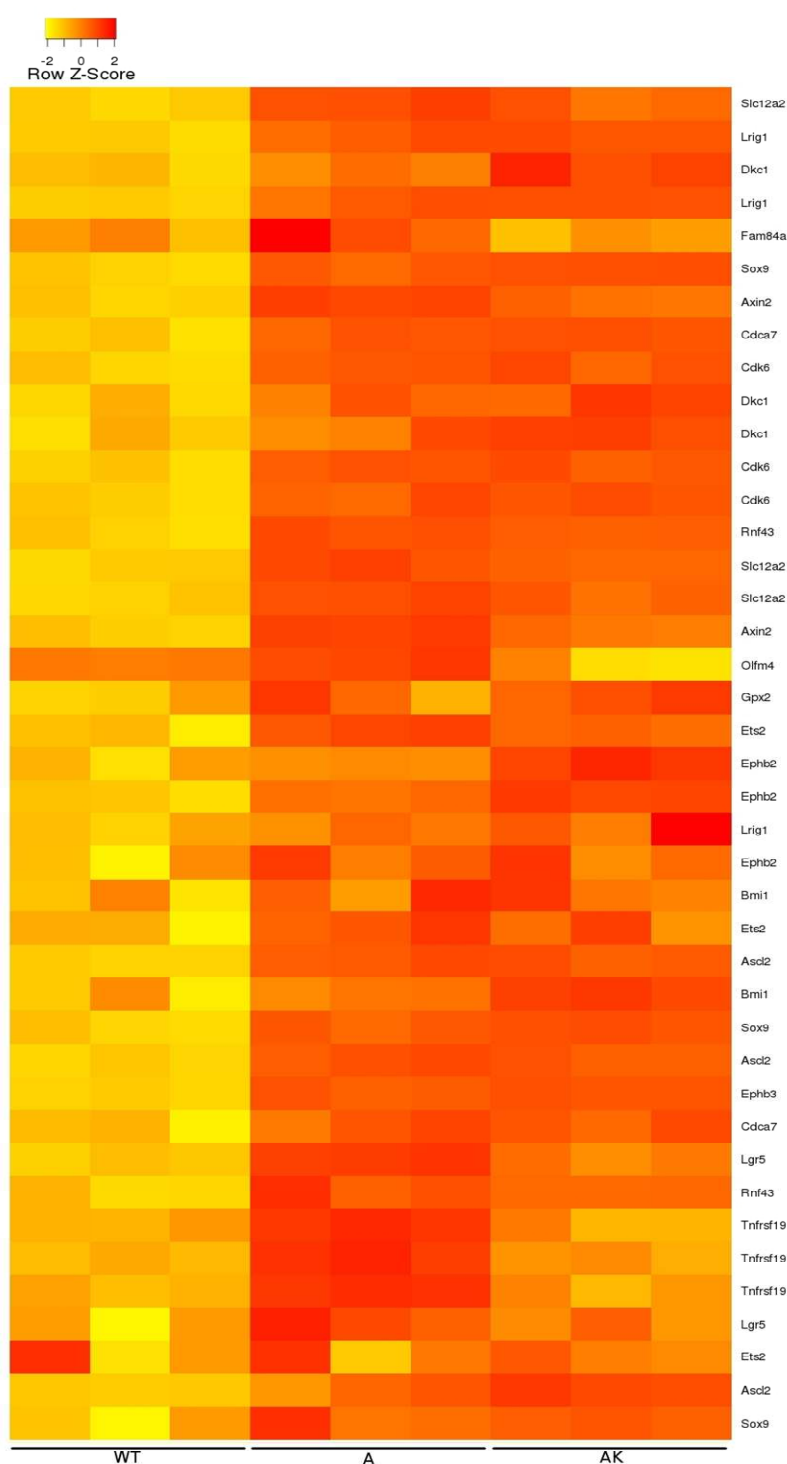


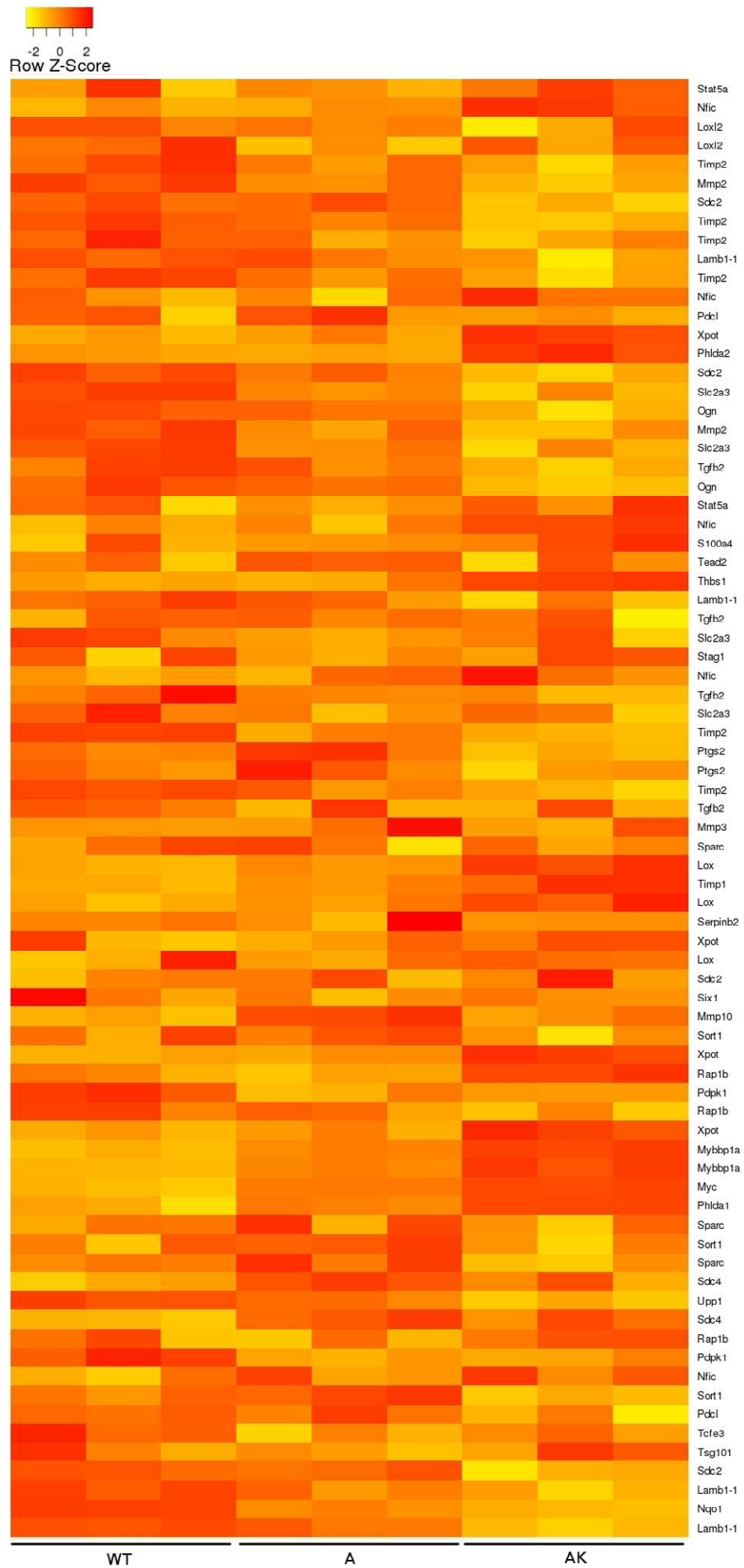
Figure 33: Stem cell signature

The expression of intestinal stem cell markers was tested in whole gut extracts of *VilCreER*⁺ (WT), *VilCreER*⁺*Apc*^{fl/fl} (A), and *VilCreER*⁺*Apc*^{fl/fl} *KRas*^{L^{SL}-G12D/+} (AK) mice taken at day 3 after *Cre* recombinase induction. The Z-score is indicated by a range of colour from yellow (low expression) to red (high expression).

15.3.3 MAPK pathway signature

Finally we analysed the effect of *Apc* loss and *KRas* activation on the MAPK pathway gene signature. We used a list of MAPK pathway targets identified by microarray-based transcriptome profiling (Stewart, Dowd et al. 1999; Mark, Aubin et al. 2008).

Once again, the software automatically clustered the samples according to their genotype confirming their homogeneity (Supplementary figure 3). However, the microarray shows that the expression of very few genes was changed following *Apc* deletion. These groups were then probably formed due to the presence of genes which are also part of the Wnt signature as *cd44* and *Myc*. The genes *cd44* and *Myc* are gradually increasing with mutations of *Apc* and then *KRas* illustrating the increase of Wnt pathway activation following *KRas* activation. Interestingly, *Ceacam1* (involved in angiogenesis) and *mmp10* (involved in tumourigenesis) were respectively downregulated and upregulated following *Apc* deletion but were back to a normal expression after *KRas* activation (Figure 34). Finally some genes were only upregulated following *KRas* activation: *Etv4*, *Dusp5*, *Fra1* (*Fosl1*) and in smaller extent *Dusp6*, all associated with tumourigenesis.



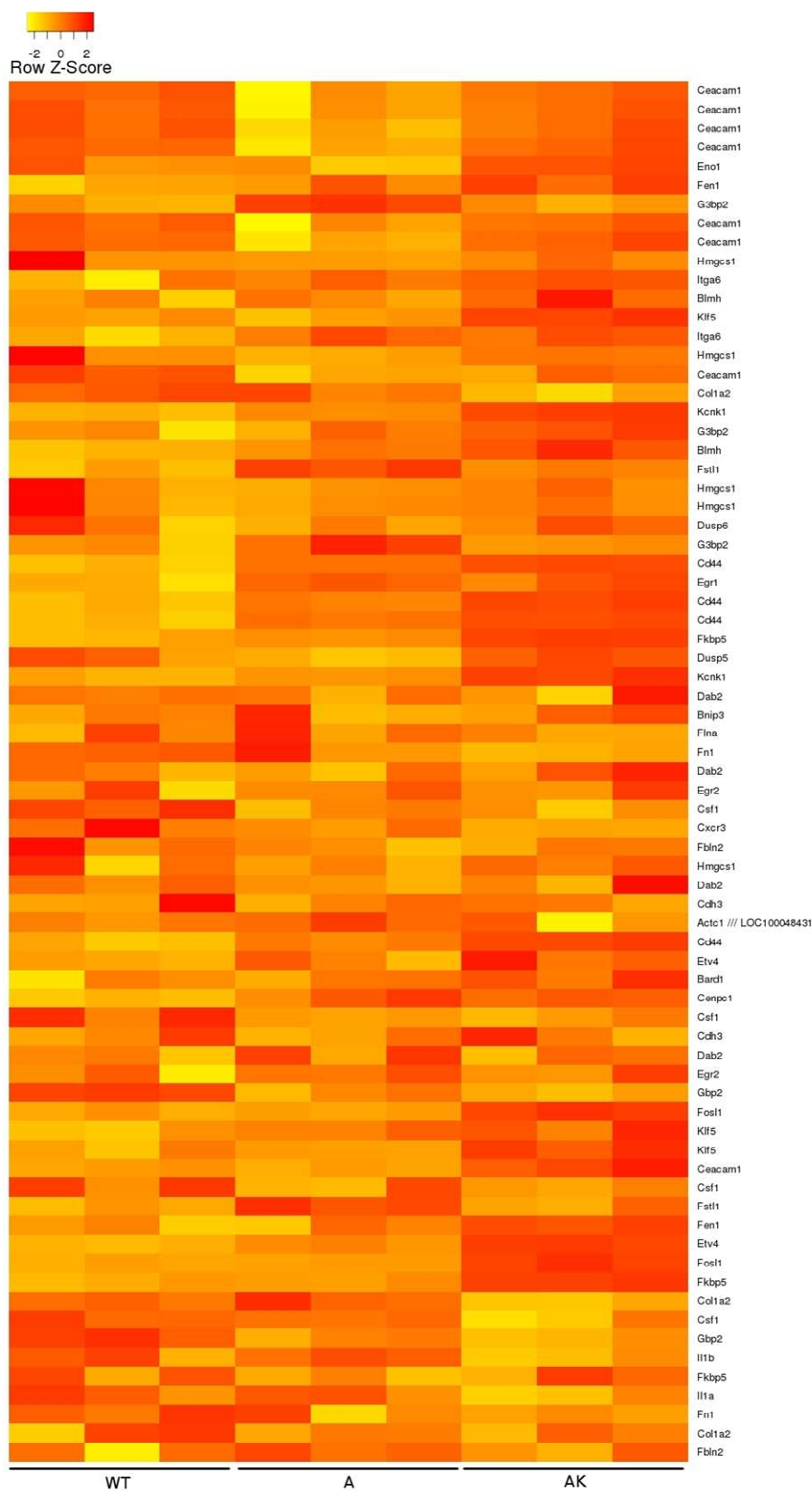


Figure 34: MAPK pathway signature

The MAPK pathway target genes identified by microarray based transcriptome profiling were tested in whole gut extracts of *VilCreER⁺* (WT), *VilCreER⁺Apc^{fl/fl}* (A), and *VilCreER⁺Apc^{fl/fl} KRas^{L^{SL}-G12D/+}* (AK) mice taken at day 3 after *Cre* recombinase induction. The Z-score is indicated by a range of colour from yellow (low expression) to red (high expression).

Given this lack of dramatic pathway activation we next examined the expression of putative negative feedback proteins of the MAPK pathway namely the MKPs: Dusp5 and Dusp6. The microarray suggested *Dusp5* to be upregulated. The redundancy between the MKPs, and particularly between Dusp6 and Dusp5 which are both very specific for Erk 1/2, can explain why Dusp5 is also upregulated following *KRas* activation. Our collaborator Prof. Stephen Keyse is currently investigating the outcome of *Dusp5* deletion in the context of *Apc* deletion in mouse model of colorectal cancer. Immunoblotting for Dusp6 performed on epithelial extracts of *VilCreER⁺* (WT), *VilCreER⁺ Apc^{fl/fl}* (A) and *VilCreER⁺ Apc^{fl/fl} KRas^{LsL-G12D/+}* (AK) mice showed the upregulation of Dusp6 in *KRas* activated mice (Figure 35). The specificity of the western blot was showed by the absence of the protein band in AK mice homozygous for the *Dusp6* null allele (AKD). Given, the very strong upregulation of Dusp6 following the MAPK pathway activation, we examined further its tumour suppressor capacity using a *Dusp6* knockout mouse provided by Prof. Stephen Keyse.

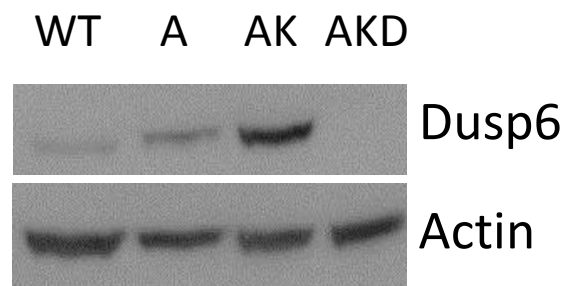


Figure 35: Levels of Dusp6 protein

Western Blot performed on epithelial extracts of intestine from *VilCreER⁺* (WT), *VilCreER⁺ Apc^{fl/fl}* (A), *VilCreER⁺ Apc^{fl/fl} KRas^{LsL-G12D/+}* (AK) and *VilCreER⁺ Apc^{fl/fl} KRas^{LsL-G12D/+} Dusp6^{-/-}* (AKD) mice taken at day 3 after induction of the *Cre* recombinase.

The protein Dusp6 was strongly upregulated following *KRas* activation while its expression was completely lost in *Dusp6* null mice.

16 *Dusp6* deletion effects in the context of *Apc* deletion driven tumourigenesis associated with *KRas* activation

To address the tumour suppressor effects of *Dusp6*, we first intercrossed the *VilCreER*⁺ mouse model with the *Dusp6* knockout mice (*Dusp6*^{-/-}). We aged *VilCreER*⁺ and *VilCreER*⁺ *Dusp6*^{-/-} mice and none of them developed tumours within 500 days (data not shown). This result showed that *Dusp6* deletion alone is not sufficient to initiate tumourigenesis in the mouse intestine. As *Dusp6* is deleted in the whole mice body, this also suggests that *Dusp6* loss on its own is not sufficient to start tumourigenesis in any tissue. This is probably due to the numerous MKPs and their redundancy. However, the specificity of *Dusp6* for Erk 1/2 we predict the tumour suppressor function of *Dusp6* may only be revealed if the gene was lost in the context of an oncogenic *KRas* mutation. Given the requirement of an *Apc* mutation to initiate intestinal tumourigenesis, we intercrossed *Dusp6* deficiency to mice that carried both *Apc* and *KRas* mutations.

16.1 *Dusp6* deletion effects during oncogenic *KRas* driven tumourigenesis

16.1.1 *Dusp6* loss effects in *VilCreER*⁺*Apc*^{fl/+} *KRas*^{L^{SL}-G12D/+} mice

We intercrossed the *VilCreER*⁺ mouse model carrying the *Apc* mutant allele (*Apc*^{fl/fl}) and the oncogenic *KRas* allele (*KRas*^{L^{SL}-G12D}) with the *Dusp6* knockout mice.

I aged *VilCreER*⁺ *Apc*^{fl/+} *KRas*^{L^{SL}-G12D/+} mice with or without *Dusp6* deletion until sickness or until they reached the age of 500 days. I observed that *VilCreER*⁺ *Apc*^{fl/+} *KRas*^{L^{SL}-G12D/+} *Dusp6*^{-/-} mice develop tumours much faster than *VilCreER*⁺ *Apc*^{fl/+} *KRas*^{L^{SL}-G12D/+} *Dusp6*^{+/-} or *VilCreER*⁺ *Apc*^{fl/+} *KRas*^{L^{SL}-G12D/+} mice. The median survival was 30 days for *Dusp6* null mice compared to 85 days for the *VilCreER*⁺ *Apc*^{fl/+} *KRas*^{L^{SL}-G12D/+} mice (Figure 36). The *VilCreER*⁺ *Apc*^{fl/+} *KRas*^{L^{SL}-G12D/+} *Dusp6*^{+/-} mice showed no difference in survival with the *VilCreER*⁺ *Apc*^{fl/+} *KRas*^{L^{SL}-G12D/+} mice. Furthermore, consistent with my previous observations of the phenotype associated with *KRas* activation I found several adenomas growing within the villi of the *VilCreER*⁺ *Apc*^{fl/+} *KRas*^{L^{SL}-G12D/+} *Dusp6*^{-/-} mice (Figure 37). Then, I performed

a β -Catenin IHC on tumours of the three mice genotypes. Nuclear β -Catenin accumulation was noted in intestinal and colonic tumours of the three mice cohorts indicating Wnt pathway activation in these lesions (Figure 38).

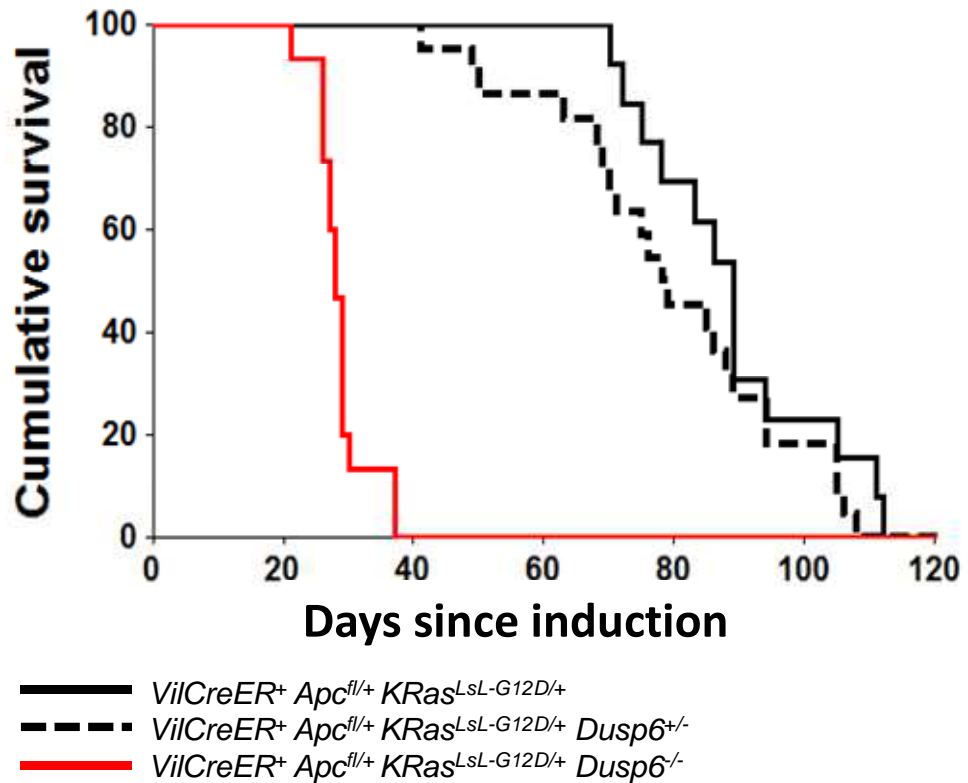


Figure 36: Effects of *Dusp6* deletion on tumour free survival

Kaplan-Meier curve showing the cumulative survival of $VilCreER^+ Apc^{fl/+} KRas^{LSL-G12D/+}$ (black solid line ; n=13), $VilCreER^+ Apc^{fl/+} KRas^{LSL-G12D/+} Dusp6^{+/-}$ (black dashed line ; n=22) and $VilCreER^+ Apc^{fl/+} KRas^{LSL-G12D/+} Dusp6^{-/-}$ (red solid line ; n=15) mice. Mice with intestinal tumours were sacrificed at the same point of illness or when they reached 500 days after induction.

The tumour free survival was significantly decreased between both $VilCreER^+ Apc^{fl/+} KRas^{LSL-G12D/+}$ and $VilCreER^+ Apc^{fl/+} KRas^{LSL-G12D/+} Dusp6^{+/-}$ and $VilCreER^+ Apc^{fl/+} KRas^{LSL-G12D/+} Dusp6^{-/-}$ mice (log rank: $p < 0.001$). No significant difference was found between $VilCreER^+ Apc^{fl/+} KRas^{LSL-G12D/+}$ and $VilCreER^+ Apc^{fl/+} KRas^{LSL-G12D/+} Dusp6^{+/-}$ mice.

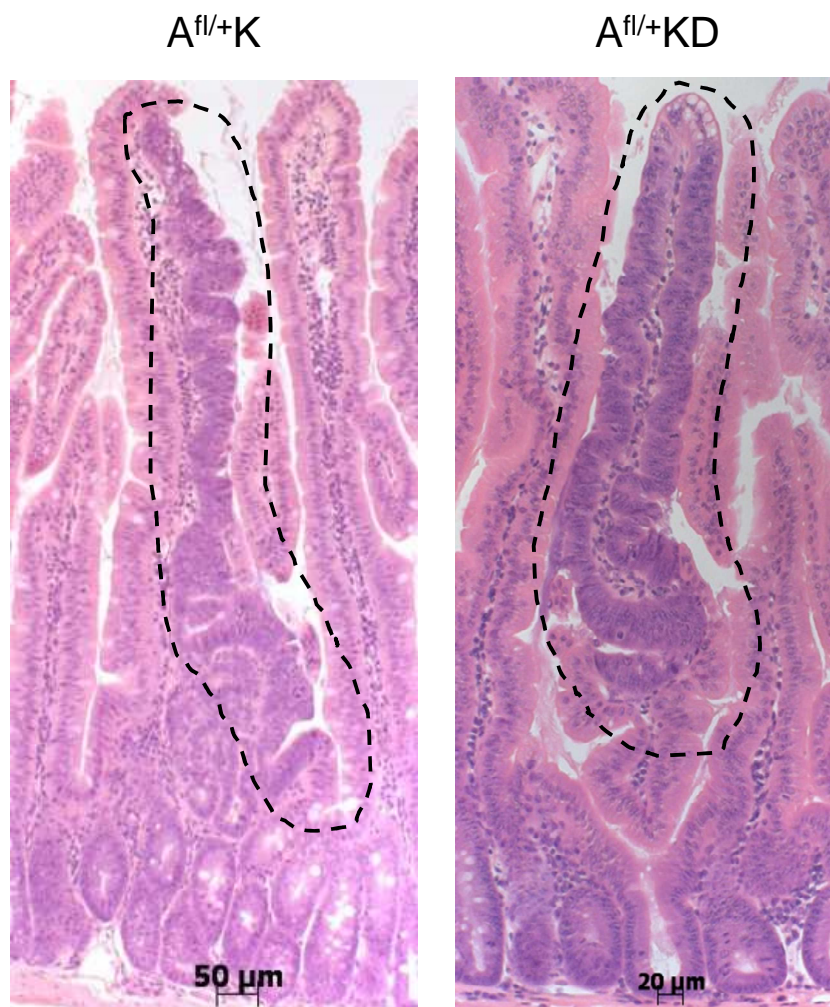


Figure 37: *KRas* activation allows tumours to form in the villus independently of *Dusp6* status

H&E staining was performed on paraffin intestinal sections of *VilCreER*⁺ *Apc*^{fl/+} *KRas*^{LSL-G12D/+} (*A*^{fl/+K}) and *VilCreER*⁺ *Apc*^{fl/+} *KRas*^{LSL-G12D/+} *Dusp6*^{-/-} (*A*^{fl/+KD}) mice at end point tumourigenesis.

Both genotypes developed several lesions within the villi.

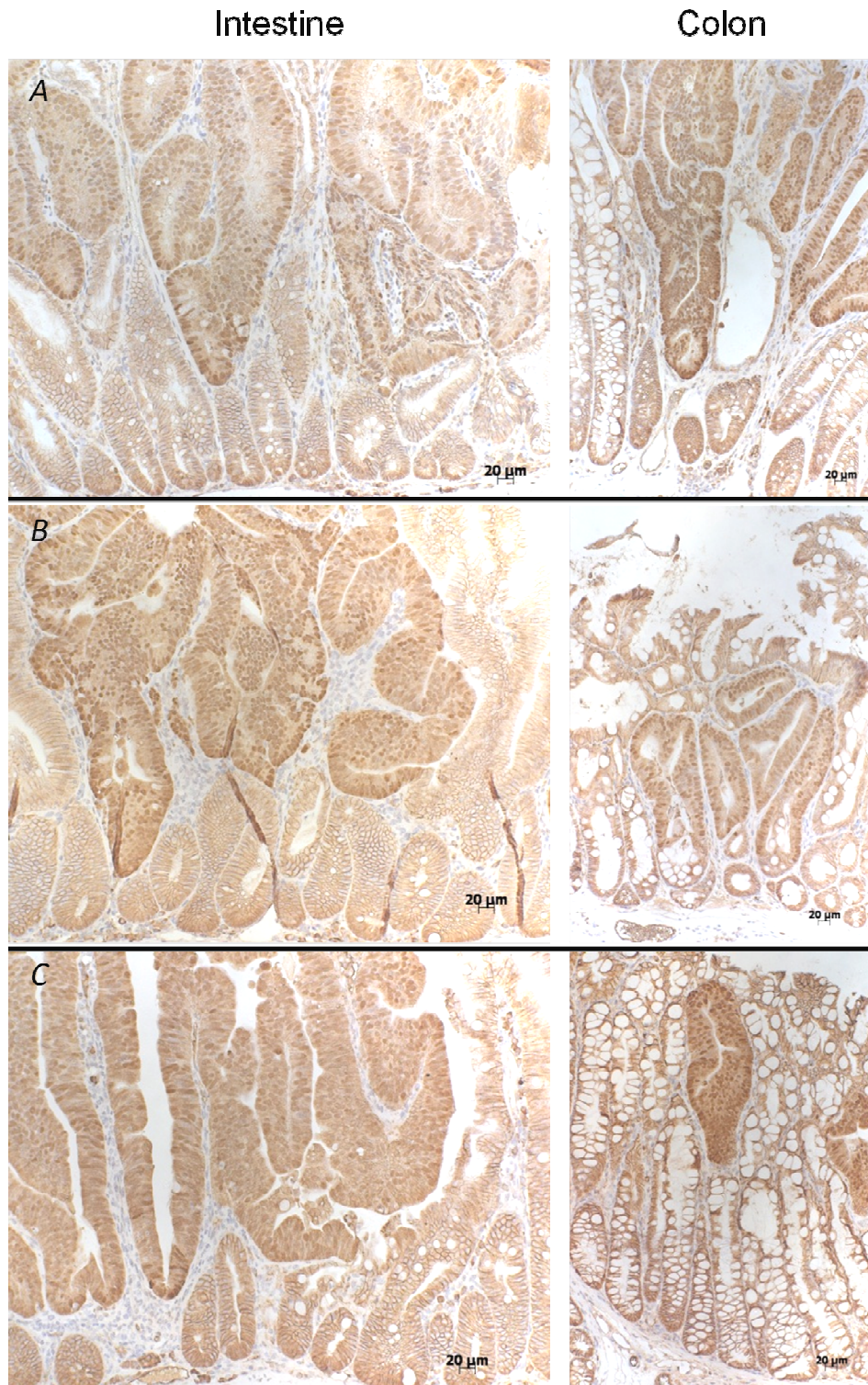


Figure 38: Wnt pathway activation following *Apc* deletion and *KRas* activation

IHC for β-Catenin was performed on paraffin sections of intestinal (left) and colonic (right) tumours of *VilCreER⁺ Apc^{fl/+} KRas^{L^SL-G12D/+}* (panel A), *VilCreER⁺ Apc^{fl/+} KRas^{L^SL-G12D/+} Dusp6^{+/-}* (panel B) and *VilCreER⁺ Apc^{fl/+} KRas^{L^SL-G12D/+} Dusp6^{-/-}* (panel C) mice.

In the three genotypes there is nuclear β-Catenin staining in tumour tissue showing the Wnt activation in these lesions.

Given the very rapid tumourigenesis and high tumour burden, I thought that this short latency would not allow metastasis formation. Indeed lesions were limited to the epithelium area and were not crossing the muscle wall. Therefore, I wanted to assess if these tumours would progress further if they had a longer time to evolve. To attempt this, I aged a cohort of mice with the same genotypes but used a lower concentration of the inducer: only 8mg/Kg of Tamoxifen instead of the full 80mg/Kg dose (Figure 39). This induction regime reduced tumour initiation and therefore prolonged the median survival time to 150 days instead of 30 days for $VilCreER^+ Apc^{fl/+} KRas^{LSL-G12D/+} Dusp6^{-/-}$ mice and to 380 days instead of 85 days for $VilCreER^+ Apc^{fl/+} KRas^{LSL-G12D/+}$ mice. In this model, as well as in the full induction one, the *Dusp6* deletion drastically decreased the survival.

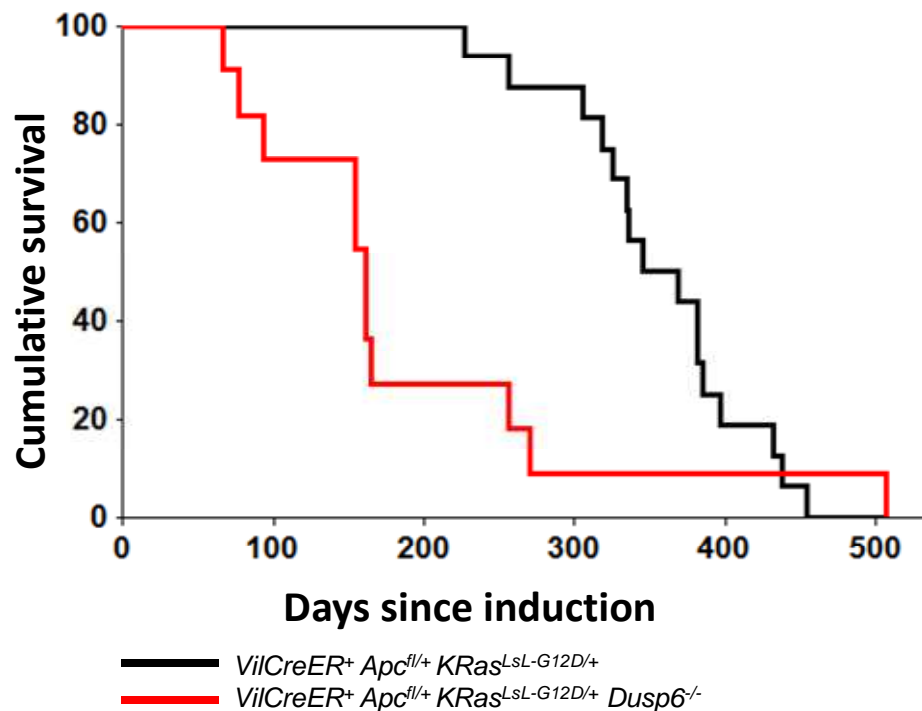


Figure 39: Effects of *Dusp6* deletion in the context of slower tumourigenesis

Kaplan-Meier curve showing the cumulative survival of $VilCreER^+ Apc^{fl/+} KRas^{LSL-G12D/+}$ (black line ; n=16) and $VilCreER^+ Apc^{fl/+} KRas^{LSL-G12D/+} Dusp6^{-/-}$ (red line ; n=10) mice. These mice were induced with 8mg/Kg tamoxifen injection instead of the usual 80mg/kg concentration. Mice with intestinal tumours were sacrificed at the same point of illness or when they reached 500 days after induction.

The tumour free survival was significantly decrease between both $VilCreER^+ Apc^{fl/+} KRas^{LSL-G12D/+}$ and $VilCreER^+ Apc^{fl/+} KRas^{LSL-G12D/+} Dusp6^{-/-}$ (log rank: $p=0.02$).

Surprisingly, very few lesions were found in the villi (Figure 40). This could be due to the induction regimen targeting and recombining less in the villi area. Furthermore, lesions invading through the intestinal muscle wall were observed (Figure 40A), indicating the ability of these genotypes to generate invasion. Indeed 75% of *VilCreER*⁺ *Apc*^{fl/+} *KRas*^{L^{SL}-G12D/+} and 40% of *VilCreER*⁺ *Apc*^{fl/+} *KRas*^{L^{SL}-G12D/+} *Dusp6*^{-/-} mice had invasive tumours. However, these conditions remained insufficient to allow metastasis formation. This could mean that other events, as for example *p53* mutation, are necessary to initiate the metastatic process more rapidly.

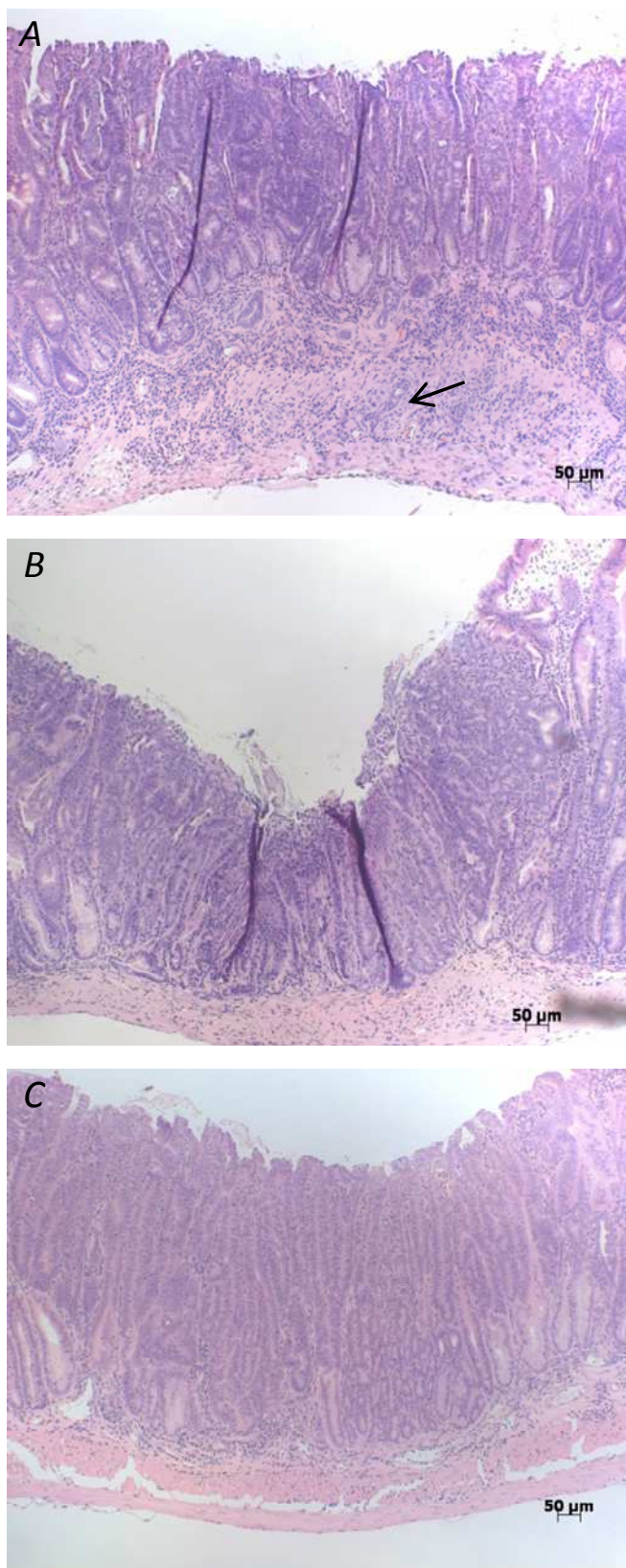


Figure 40: Effects of *Dusp6* deletion in the context of slower tumourigenesis

H&E staining was performed on paraffin sections of *VilCreER⁺ Apc^{fl/+} KRas^{LsL-G12D/+}* (A), *VilCreER⁺ Apc^{fl/+} KRas^{LsL-G12D/+} Dusp6^{+/-}* (B) and *VilCreER⁺ Apc^{fl/+} KRas^{LsL-G12D/+} Dusp6^{-/-}* (C) mice. An arrow indicates invasion.

16.1.2 *Dusp6* loss effects in *VilCreER⁺Apc^{fl/+} KRas^{LSL-G12V/+}* mice

As previously noted, there are conflicting reports regarding the outcome of a constitutively active *KRas* mutation (Sansom, Meniel et al. 2006; Haigis, Kendall et al. 2008). I therefore assessed the effects of the *KRas^{LSL-G12V}* allele in the same context as previously described. I aged a cohort of *VilCreER⁺ Apc^{fl/+} KRas^{LSL-G12V/+}* mice with or without *Dusp6* deletion until sickness or until they reached the age of 500 days. Here I observed similar results to the *KRas^{LSL-G12D}* allele when induced with 8mg/Kg of Tamoxifen: *VilCreER⁺ Apc^{fl/+} KRas^{LSL-G12V/+} Dusp6^{-/-}* mice developed tumours much faster than *VilCreER⁺ Apc^{fl/+} KRas^{LSL-G12V/+}* mice with a median survival reduced from 150 to 100 days (Figure 41). It is interesting to note that *KRas^{LSL-G12V}* allele had a slower tumourigenesis than the *KRas^{LSL-G12D}* allele allowing tumours to undergo invasion and preventing lesion formation in villi (Figure 42). However, no metastases were observed in this model either.

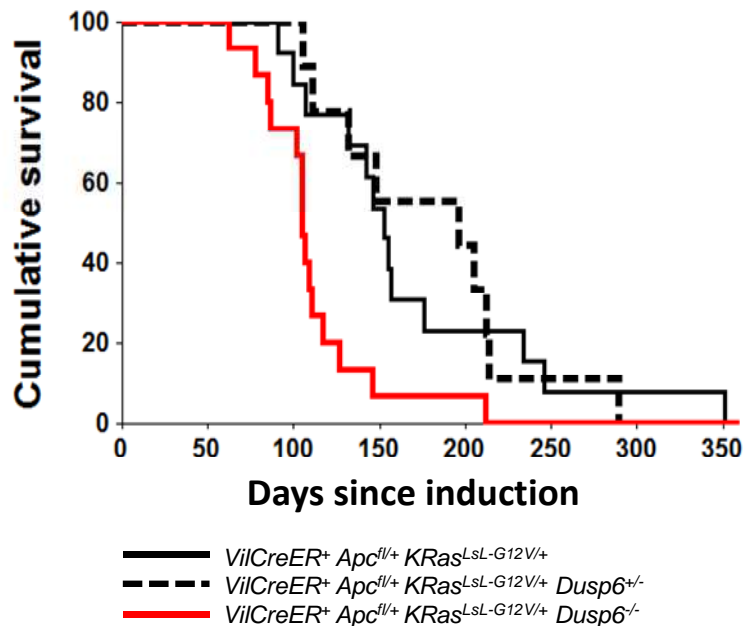


Figure 41: *Dusp6* deletion decreases survival following *KRas* activation (*KRas^{LSL-G12V}* allele).

Kaplan-Meier curve showing the cumulative survival of *VilCreER⁺ Apc^{fl/+} KRas^{LSL-G12V/+}* (black solid line ; n=13), *VilCreER⁺ Apc^{fl/+} KRas^{LSL-G12V/+} Dusp6^{+/-}* (black dashed line ; n=9) and *VilCreER⁺ Apc^{fl/+} KRas^{LSL-G12V/+} Dusp6^{-/-}* (red solid line ; n=15) mice. Mice with intestinal tumours were sacrificed at the same point of illness or when they reached 500 days after induction.

The tumour free survival was significantly decrease between both *VilCreER⁺ Apc^{fl/+} KRas^{LSL-G12V/+}* and *VilCreER⁺ Apc^{fl/+} KRas^{LSL-G12V/+} Dusp6^{+/-}* and *VilCreER⁺ Apc^{fl/+} KRas^{LSL-G12V/+} Dusp6^{-/-}* mice (log rank: p=0.004). No significant difference was found between *VilCreER⁺ Apc^{fl/+} KRas^{LSL-G12V/+}* and *VilCreER⁺ Apc^{fl/+} KRas^{LSL-G12V/+} Dusp6^{+/-}* mice.

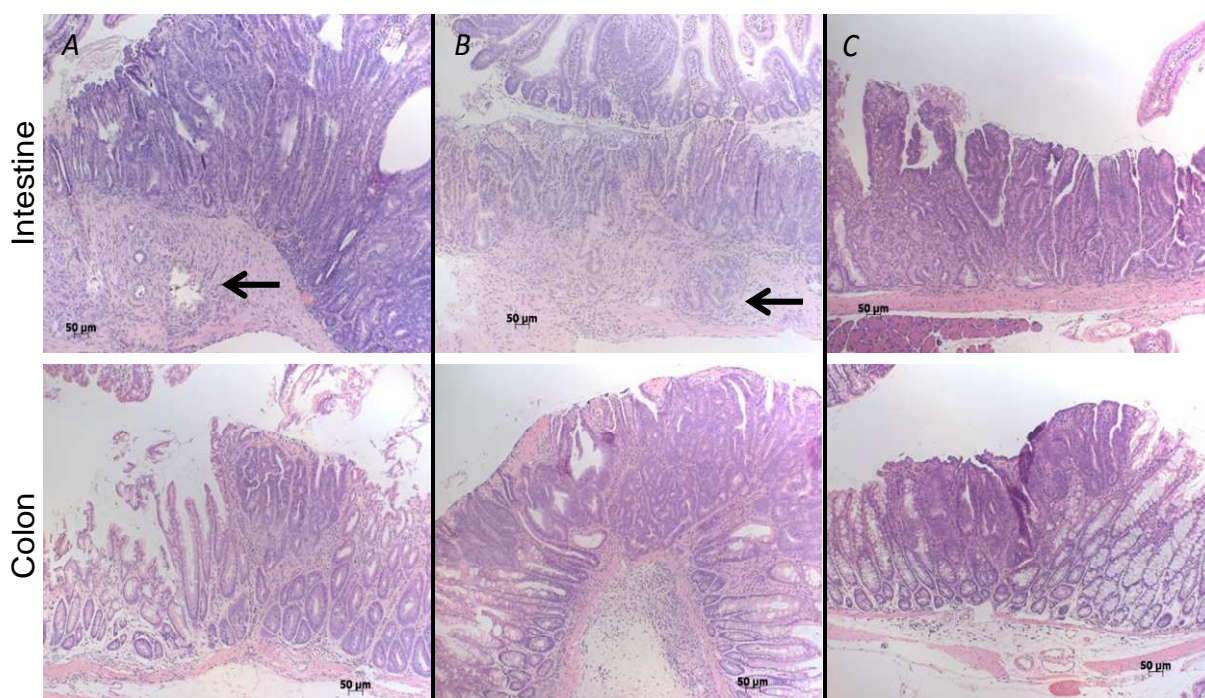


Figure 42: Tumour formation following *KRas* activation (*KRas*^{LsL-G12V} allele).

H&E staining of intestinal (top) and colonic (bottom) tumours from *VilCreER*⁺ *Apc*^{fl/+} *KRas*^{LsL-G12V/+} (panel A), *VilCreER*⁺ *Apc*^{fl/+} *KRas*^{LsL-G12V/+} *Dusp6*^{+/-} (panel B) and *VilCreER*⁺ *Apc*^{fl/+} *KRas*^{LsL-G12V/+} *Dusp6*^{-/-} (panel C) mice.

Invasion is indicated by arrows.

These findings taken together showed that the association of *Apc* deletion and *KRas* activation was able to initiate tumourigenesis and invasion. Moreover, in all models *Dusp6* deletion induced a drastic enhancement of the effects of the oncogenic *KRas* allele on tumourigenesis.

16.2 *Dusp6* deletion effects on CPL phenotype

16.2.1 *Dusp6* loss effects on proliferation

To investigate further the effects of *Dusp6* deletion on proliferation I used the acute *Apc* deletion model previously described where both *Apc* alleles are deleted after induction of the *Cre* recombinase. Proliferation was assessed using a 2 hours BrdU pulse-chase labelling. The proliferative cells, as highlighted in Figure 43A, are illustrating a larger CPL phenotype area. I scored the total number of proliferative cells as well as the position of the highest BrdU positive cell in the CPL structure. This scoring has shown a trend of increased total number of proliferative cells (p value = 0.08) (Figure 43B). The percentage of proliferation in CPL area (Figure 43D) did not change between the groups of mice. However, there was an increase of CPL phenotype area in the AKD mice compared with the AK ones as highlighted by the highest BrdU positive cell at a median position of 119 on the crypt villus axis instead of 91 (Figure 43C) (p value 0.02). These findings highlight an increase in proliferation zone but also demonstrate that the proliferation rate within the proliferation zone seems to remain unchanged between the different genotypes.

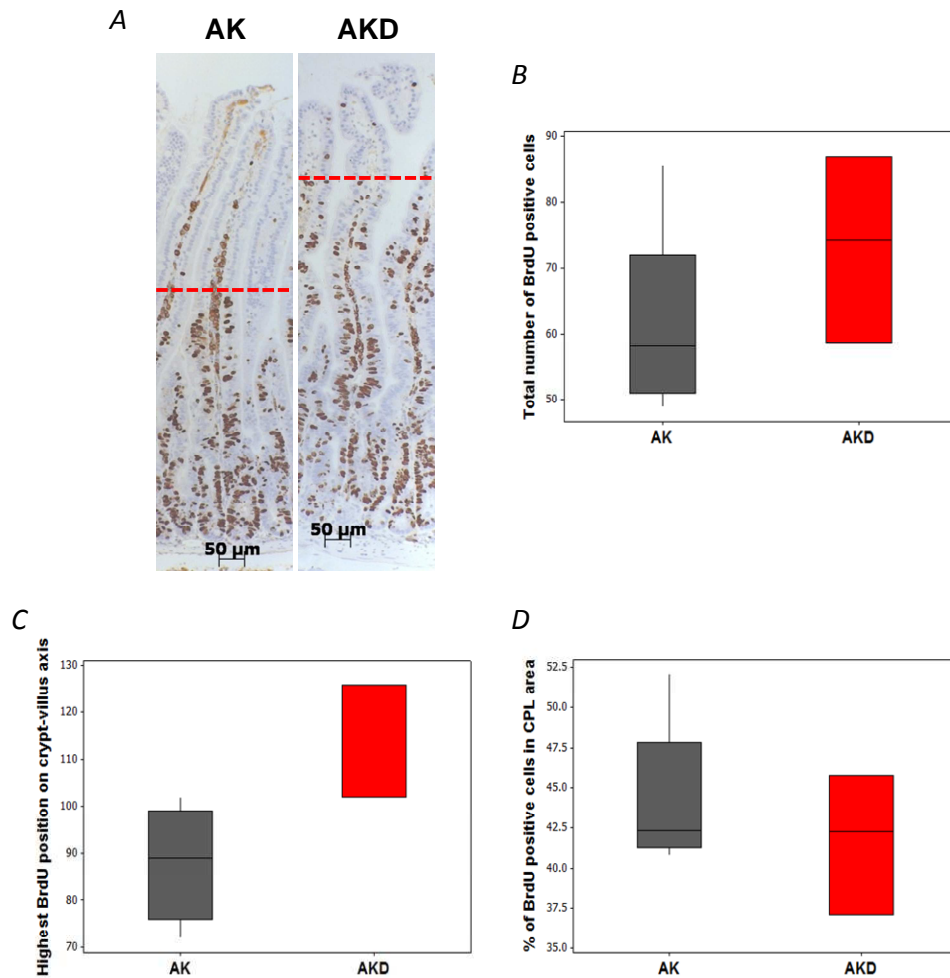


Figure 43: The effects of *Dusp6* deletion on the CPL phenotype

2 hours BrdU pulse-chase labelling experiment was performed on *VilCreER⁺ Apc^{fl/fl} KRas^{LsL-G12D/+} Dusp6^{+/+}* (AK) and *VilCreER⁺ Apc^{fl/fl} KRas^{LsL-G12D/+} Dusp6^{-/-}* (AKD) mice.

A: Immunohistochemistry for BrdU was performed on paraffin section of *VilCreER⁺ Apc^{fl/fl} KRas^{LsL-G12D/+} Dusp6^{+/+}* (AK) and *VilCreER⁺ Apc^{fl/fl} KRas^{LsL-G12D/+} Dusp6^{-/-}* (AKD) mice. The highest BrdU positive cells are highlighted by dashed lines showing an increase in CPL area following *Dusp6* deletion.

B,C,D: Box plots showing respectively the total number of BrdU positive cells, the position of the highest BrdU positive cell on the crypt-villus axis and the percentage of proliferation in CPL phenotype of AK (dark grey) (n=5) and AKD (red) (n=3) mice. Mann Whitney test p values: **B** p=0.08 ; **C** p=0.02 ; **D** p=0.76.

16.2.2 *Dusp6* loss effects on cell differentiation

Given tumours can form from villi compartment we hypothesised that the capacity of the villi cells to dedifferentiate following *KRas* activation might be expanded by *Dusp6* loss. In order to confirm the loss of differentiation and the strong proliferation, I performed several IHC (Figure 44). An H&E staining confirmed the CPL phenotype size difference between *VilCreER⁺ Apc^{fl/fl} KRas^{LsL-G12D/+}* (AK) and *VilCreER⁺ Apc^{fl/fl} KRas^{LsL-G12D/+} Dusp6^{-/-}* (AKD) mice as highlighted by the red (AKD) and the dashed black (AK) lines. In these epitheliums, Goblets cells did not seem altered as shown by the Alcian blue staining. I observed an upregulation of p21 and p53 in a subset of cells within the CPL phenotype of both mice cohort. This increase of p21 and p53 in the CPL phenotype has been shown to be the result of a high proliferation (Fjeld, Rice et al. 2000). Finally, the presence of Sox9 positive cells in the CPL phenotype areas shown a Wnt pathway activation associated with this hyperproliferation.

Apart from the clear proliferation increase in AKD mice compared to the AK ones, no other differences were observed suggesting *Dusp6* deletion to be mainly resulting in upregulation of cell proliferation.

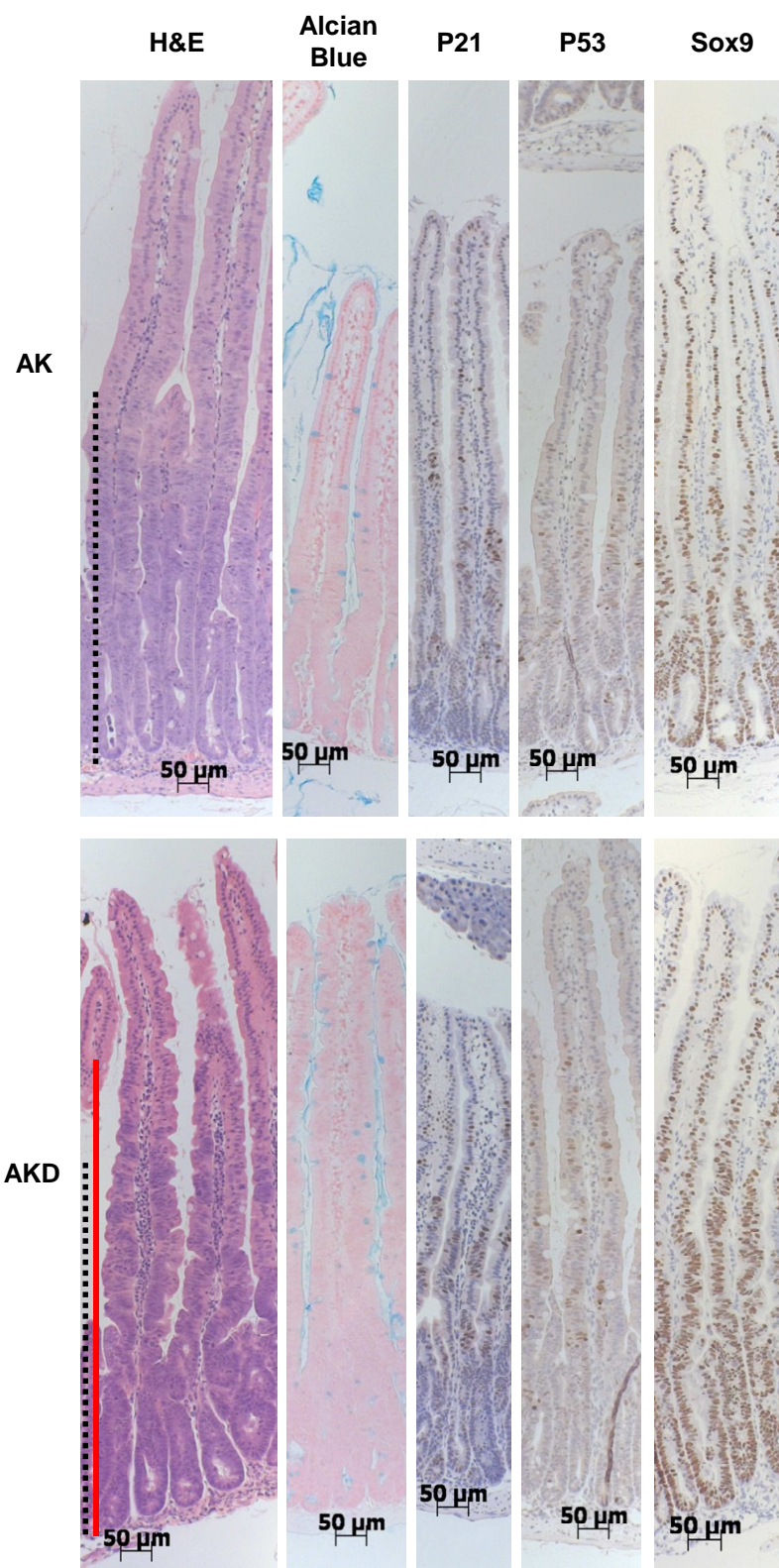


Figure 44: Comparison of the CPL phenotype of AK and AKD mice

H&E staining, Alcian blue (marking goblet cells) staining, p21 IHC, p53 IHC and Sox9 IHC of CPL phenotypes of *VilCreER⁺ Apc^{fl/fl} KRas^{L^{SL}-G12D/+}* (AK, top panel) and *VilCreER⁺ Apc^{fl/fl} KRas^{L^{SL}-G12D/+} Dusp6^{-/-}* (AKD, bottom panel) mice.

The length of the CPL phenotype is indicated by a dashed black line for AK mice and by a red line for AKD mice.

16.3 *Dusp6* loss signature

In order to study further the outcomes of *Dusp6* deletion associated with *KRas* mutation on general gene expression and therefore signalling pathway output, I sent whole intestine RNA samples of *VilCreER⁺ Apc^{fl/fl} KRas^{LsL-G12D/+}* (AK) and *VilCreER⁺ Apc^{fl/fl} KRas^{LsL-G12D/+} Dusp6^{-/-}* (AKD) mice taken at day 3 after *Cre* recombinase induction to be analysed in a microarray. The samples were analysed as previously described. It is interesting to note that one sample in the AKD group behave rather differently than the other ones. An increase in the number of mice in each cohort could reveal if this mouse is a unique case. However for the following analysis I excluded this particular mouse.

16.3.1 Wnt pathway signature

I analysed the Wnt pathway signature of *VilCreER⁺ Apc^{fl/fl} KRas^{LsL-G12D/+}* (AK) and *VilCreER⁺ Apc^{fl/fl} KRas^{LsL-G12D/+} Dusp6^{-/-}* (AKD) mice based on the previously described H. Clevers' group list of up-regulated genes in human colorectal adenomas (Rigas, Hoff et al. 2001) (Figures 45 A and B). There were no major changes brought by *Dusp6* loss except a downregulation of few genes as *Myb*, *Gemin5* and *Rhobtb3* and an upregulation of *Sox4*. This strong similarity between the two groups shows that *Dusp6* deletion does not affect much the WNT pathway signature in the context of oncogenic *KRas* driven tumourigenesis. However, these minor changes were enough to cluster the samples according to their genotype (Supplementary figure 4).

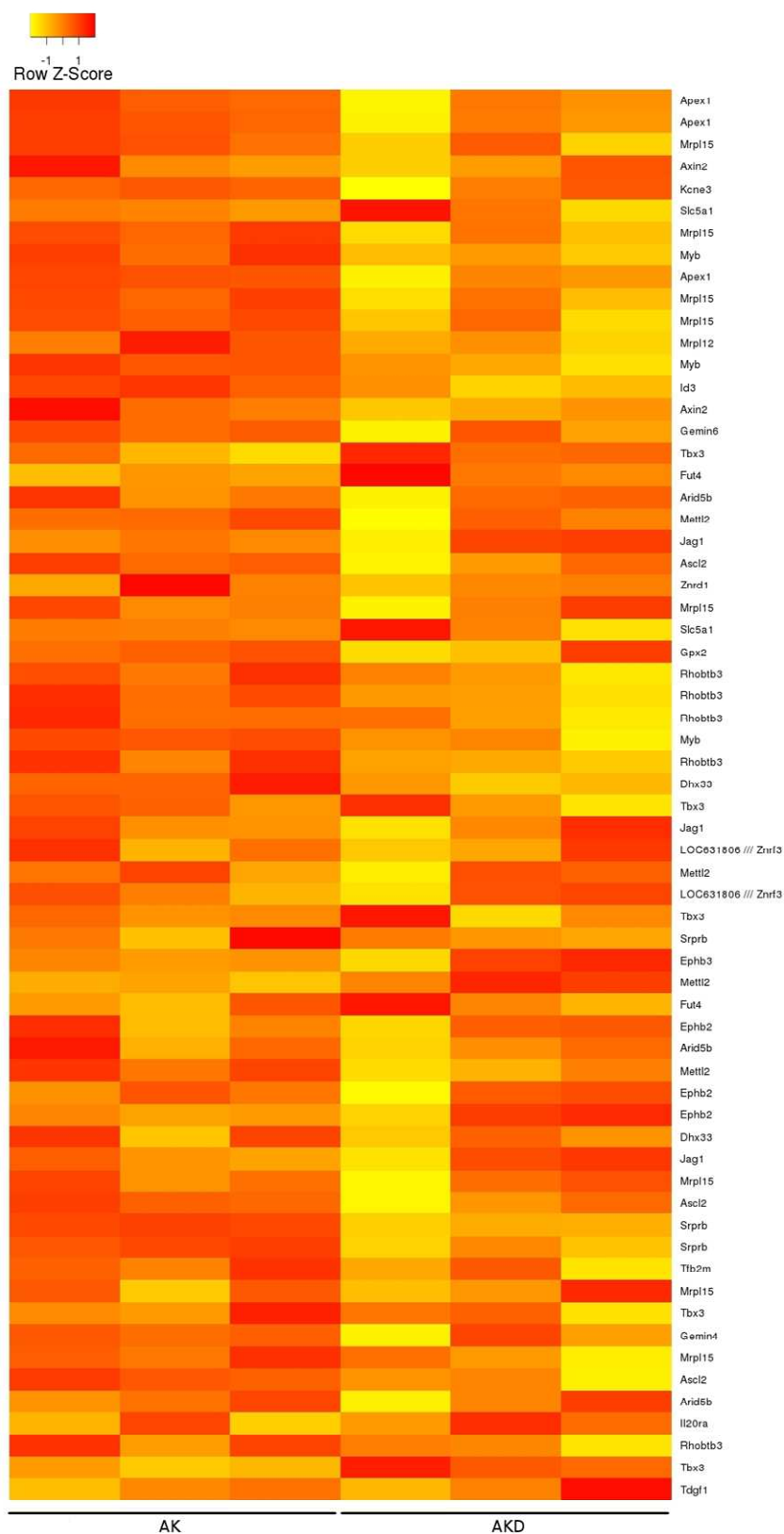
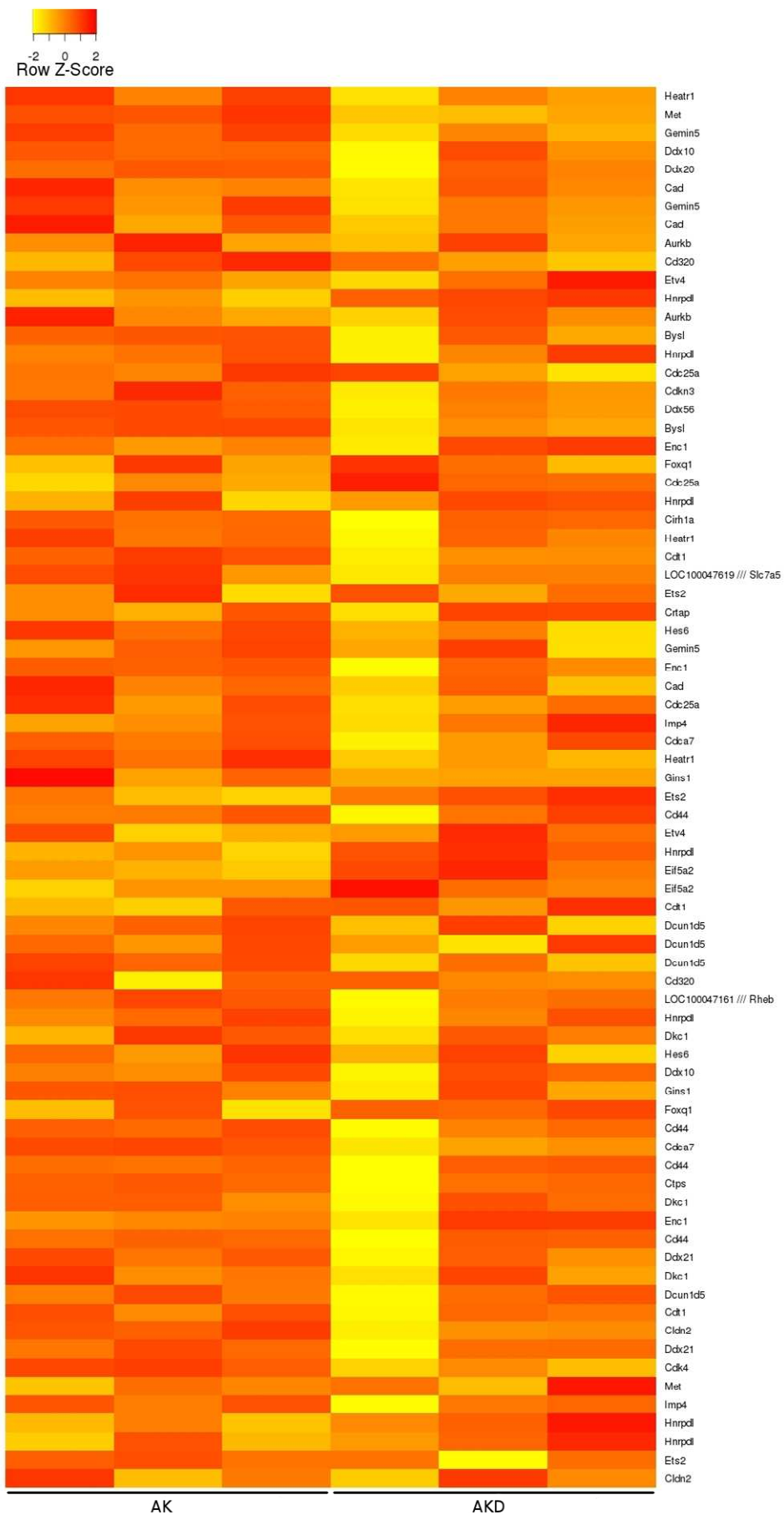


Figure 45A: WNT pathway signature

The genes found to be up-regulated in human colorectal adenomas were tested in whole gut extracts of *VilCreER⁺ Apc^{fl/fl} KRas^{L^{SL}-G12D/+}* (AK) and *VilCreER⁺ Apc^{fl/fl} KRas^{L^{SL}-G12D/+} Dusp6^{-/-}* (AKD) mice taken at day 3 after Cre recombinase induction. The Z-score is indicated by a range of colour from yellow (low expression) to red (high expression).



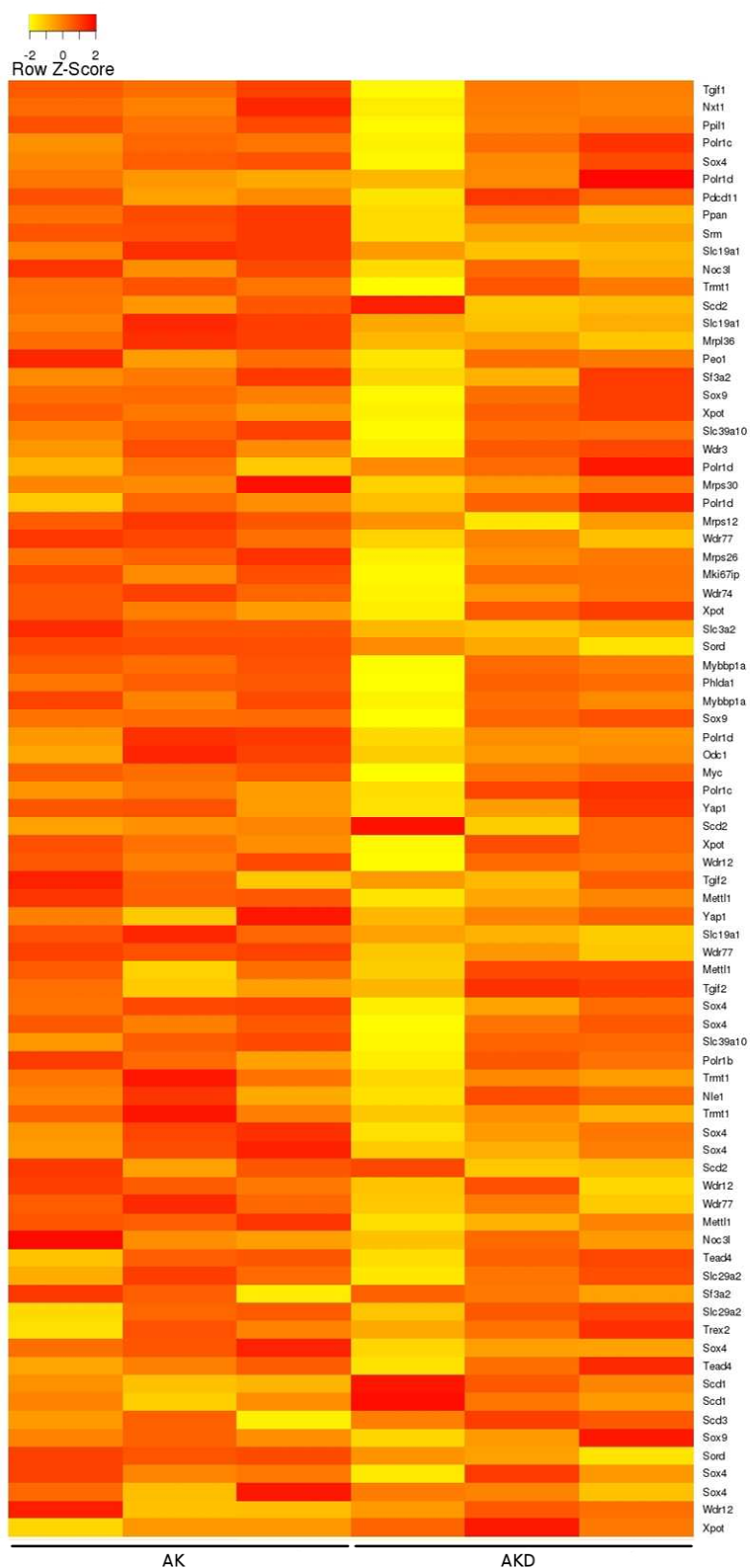


Figure 45B: WNT pathway signature

The genes found to be up-regulated in both human colorectal adenomas and human colorectal adenocarcinomas were tested in whole gut extracts of *VilCreER⁺ Apc^{fl/fl} KRas^{LsL-G12D/+}* (AK) and *VilCreER⁺ Apc^{fl/fl} KRas^{LsL-G12D/+} Dusp6^{-/-}* (AKD) mice taken at day 3 after Cre recombinase induction. The Z-score is indicated by a range of colour from yellow (low expression) to red (high expression).

16.3.2 Stem cell signature

I then analysed the expression of some intestinal stem cell markers in AK and AKD mice. I could not find any relevant difference between the two groups of mice (Figure 46). This is highlighting the absence of *Dusp6* deletion effects on the stem cell signature genes in this context. Moreover, the samples were clustered in groups of genotype highlighting the absence of effects of *Dusp6* loss on stem cell signature genes (Supplementary figure 5).

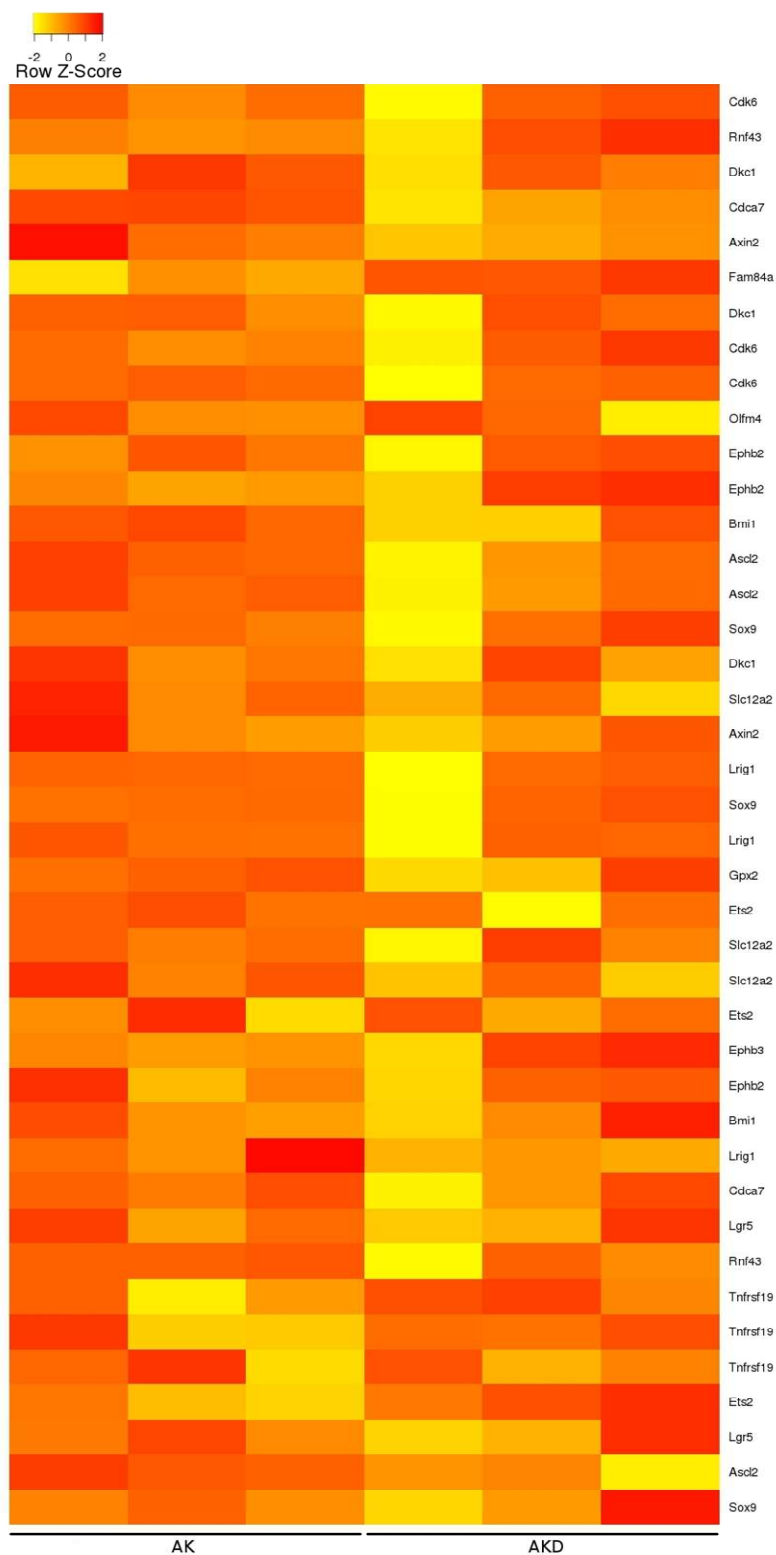


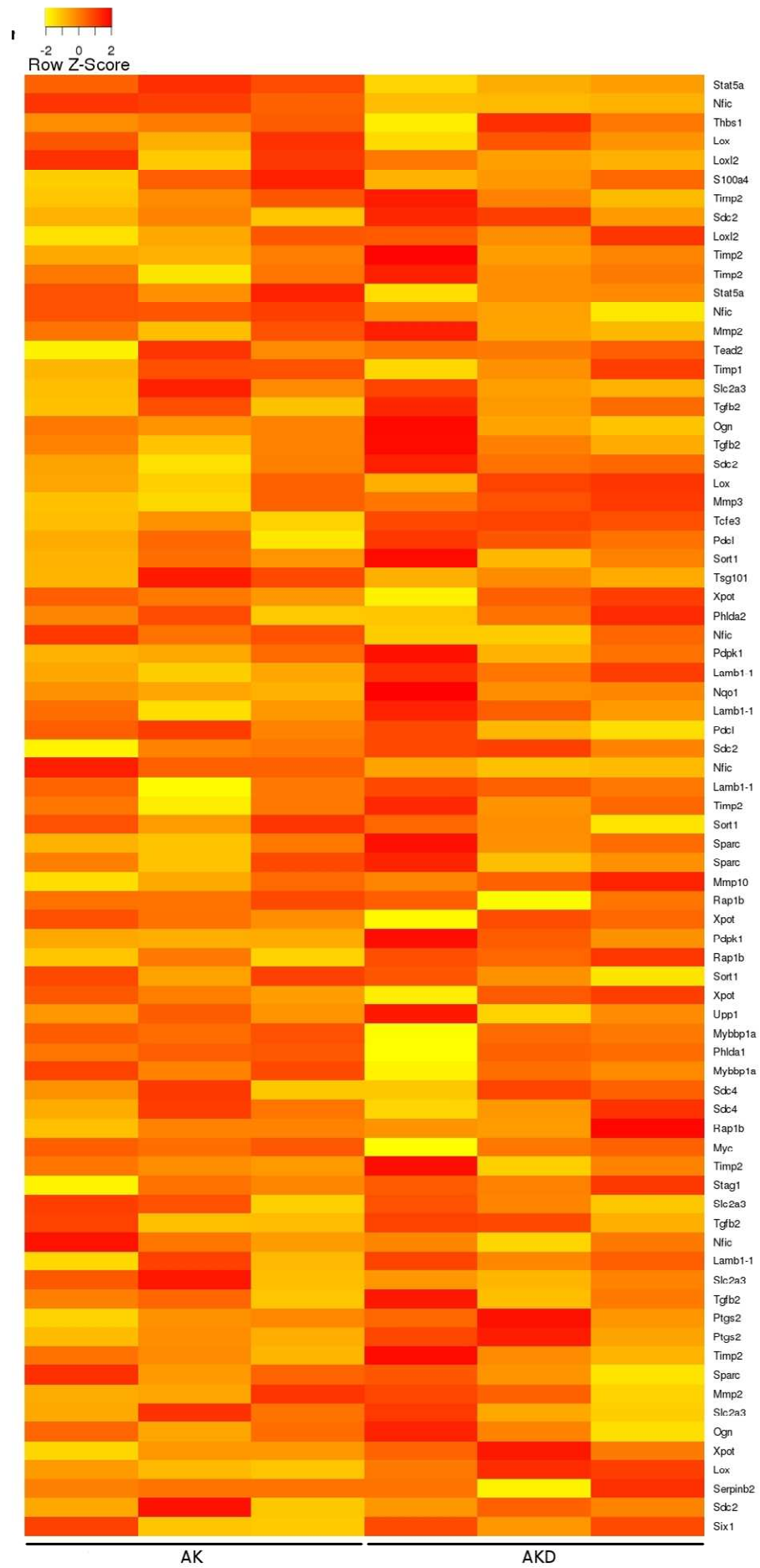
Figure 46: Stem cell signature

The expression of intestinal stem cell markers was tested in whole gut extracts of *VilCreER⁺ Apc^{fl/fl} KRas^{L^{SL}-G12D/+}* (AK) and *VilCreER⁺ Apc^{fl/fl} KRas^{L^{SL}-G12D/+} Dusp6^{-/-}* (AKD) mice taken at day 3 after Cre recombinase induction. The Z-score is indicated by a range of colour from yellow (low expression) to red (high expression).

16.3.3 MAPK pathway signature

Finally I analysed the effect of *Apc* loss and *KRas* activation on the MAPK pathway gene signature using the list of MAPK pathway targets identified by microarray-based transcriptome profiling (Stewart, Dowd et al. 1999; Mark, Aubin et al. 2008).

Unexpectedly, the pattern of gene expression remained rather unchanged after *Dusp6* loss (the remaining *Dusp6* expression seen in the hitmap is due to the probe for *Dusp6* which target the untruncated part of the RNA before the Neo cassette in the transgene construct) highlighting a minor effect of the gene deletion on MAPK pathway (Figure 47). However, this microarray analysis were done on whole gut samples and it would be interesting to analyse the outcome of the mutations in the cytoplasm and the nucleus separately as Erk is a shuttle protein between the two cell compartment and the balance in Erk concentration is strongly affecting cell signalling. Nevertheless, the samples were still grouped according to their genotype highlighting a constant gene expression pattern in samples of same genotypes (Supplementary figure 6). It is important to note the upregulation of *Dusp5*. *Dusp5*, as part of the MAPK phosphatases family, is the phosphatase specific for Erk 1/2 in the nucleus. This could be a compensatory upregulation limiting the impact of *Dusp6* loss on Erk 1/2 phosphorylation and therefore on MAPK pathway. However, the microarray was performed on whole gut samples in order to obtain good quality RNA. Therefore, the RNA includes not only the gut epithelial cells but also the muscle layers which could buffer the variations of expressions. This difficulty could be bypassed by studying the impact of *Dusp6* deletion on the Erk activation. Unfortunately, there is a lack of efficient antibodies detecting *Dusp6* and Erk 1/2 in the tissues we decided to study. Therefore, we decided to analyse the functional significance of *Dusp6* deletion by association with a Mek inhibitor treatment.



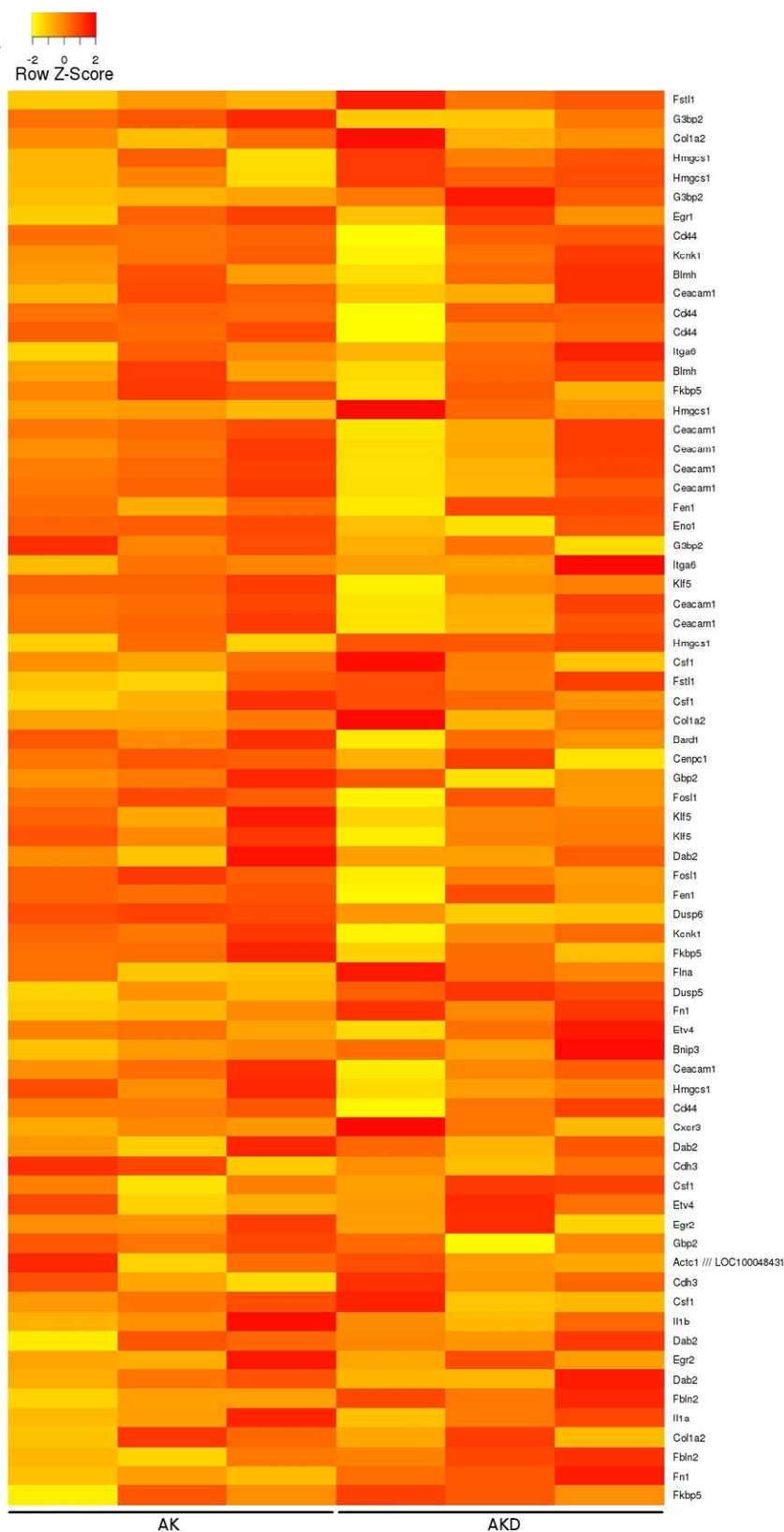


Figure 47: MAPK pathway signature

The MAPK pathway target genes identified by microarray based transcriptome profiling were tested in whole gut extracts of *VilCreER⁺ Apc^{fl/fl} KRas^{LsL-G12D/+}* (AK) and *VilCreER⁺ Apc^{fl/fl} KRas^{LsL-G12D/+} Dusp6^{-/-}* (AKD) mice taken at day 3 after Cre recombinase induction. The Z-score is indicated by a range of colour from yellow (low expression) to red (high expression).

17 The functional outcome of Mek inhibition following *Dusp6* loss

17.1 The chemoprevention effects of Mek inhibition are *Dusp6* loss dependent

To investigate whether *Dusp6* deletion was exacerbating the *VilCreER⁺ Apc^{fl/+} KRas^{L^{SL}-G12D/+}* mice phenotype via MAPK pathway activation, I performed a chemoprevention experiment using the pharmacological MEK inhibitor CI1040 (also named PD184352) (Sebolt-Leopold, Dudley et al. 1999) on the *VilCreER⁺ Apc^{fl/+} KRas^{L^{SL}-G12D/+}* and *VilCreER⁺ Apc^{fl/+} KRas^{L^{SL}-G12D/+} Dusp6^{-/-}* mice. In this case, inhibition of Mek1/2 should reduce the activation of Erk 1/2 and since *Dusp6* is an Erk 1/2 phosphatase if this is the mechanism by which *Dusp6* loss is accelerating tumourigenesis and/or tumour initiation then an inhibition of Mek should reverse *Dusp6* deletion effects.

The mice were treated with a 200mg/Kg daily dose of CI1040 or with vehicle from the first day after induction of the *Cre* recombinase and were sacrificed when showing signs of intestinal ill health (Figure 48). The *VilCreER⁺ Apc^{fl/+} KRas^{L^{SL}-G12D/+}* mice treated with the drug vehicle had the same median survival (90 days) as the untreated mice. However, the *VilCreER⁺ Apc^{fl/+} KRas^{L^{SL}-G12D/+} Dusp6^{-/-}* mice treated with CI1040 doubled their median survival to 62 days after induction. Surprisingly, the same drug treatment on *VilCreER⁺ Apc^{fl/+} KRas^{L^{SL}-G12D/+}* mice did not result in tumourigenesis regression: the median survival remained at 85 days after induction of the *Cre* recombinase. So the inhibition of the MAPK pathway at Mek level is reducing tumour initiation only when *Dusp6* is deleted. This finding is the first indication that *Dusp6* loss has an effect on the MAPK cascade depending on *KRas* activation but also different than the *KRas* activation alone.

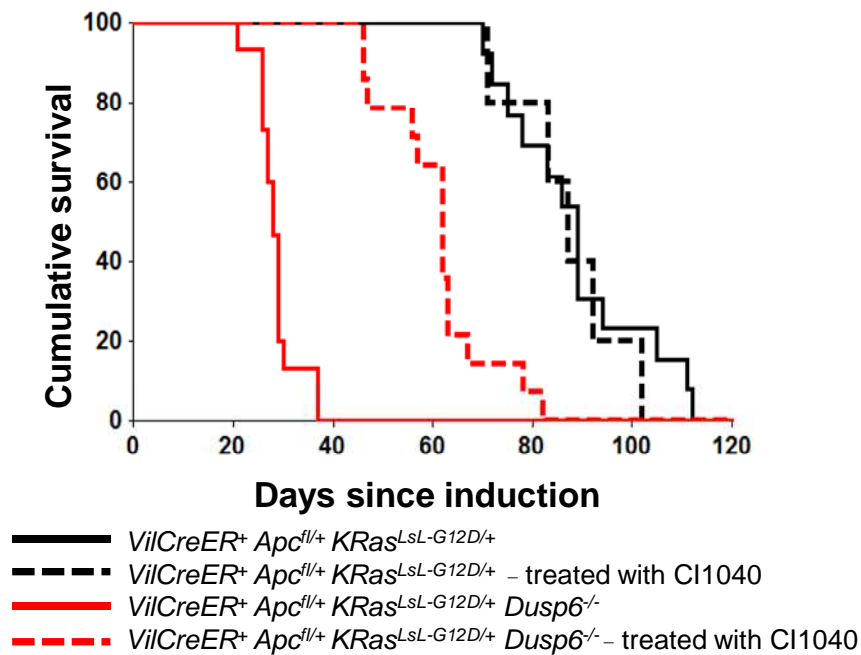


Figure 48: Effects of Mek inhibition on survival

Kaplan-Meier curve showing the survival of $VilCreER^+ Apc^{fl/+} KRas^{LsL-G12D/+}$ mice treated with CI1040 (black dashed line ; n=5) or untreated (black solid line ; n=13) and $VilCreER^+ Apc^{fl/+} KRas^{LsL-G12D/+} Dusp6^{-/-}$ mice treated with CI1040 (red dashed line ; n=14) or untreated (red solid line ; n=15). Mice with intestinal tumours were sacrificed at the same point of illness.

The treatment increases significantly the survival in $VilCreER^+ Apc^{fl/+} KRas^{LsL-G12D/+} Dusp6^{-/-}$ mice (log rank $p < 0.001$) but does not have an effect in $VilCreER^+ Apc^{fl/+} KRas^{LsL-G12D/+}$ mice (log rank: $p > 0.5$).

I then investigated the effect of the drug on tumour progression. I treated $VilCreER^+ Apc^{fl/+} KRas^{LsL-G12D/+} Dusp6^{-/-}$ mice with CI1040 from day 10 after induction, namely when tumours had already raised in the intestine. I then compared their tumour number with the vehicle ones sacrificed at day 30 after induction. The treated mice had a drastic reduction in tumour number compared to the untreated ones and the tumours remaining in these mice appeared to be a lot smaller than in the vehicle treated mice (Figure 49). A similar experiment was performed on $VilCreER^+ Apc^{fl/+} KRas^{LsL-G12D/+}$ mice. This time the mice were treated from day 50 after *Cre* recombinase induction namely when they had tumours developed. Here again the CI1040 treatment remained inefficient (Figure 50) bringing a second evidence of the particularity of the outcome of *Dusp6* loss.



Figure 49: Effects of Mek inhibition on tumourigenesis in *Dusp6* null mice

H&E staining as performed on paraffin sections of *VilCreER⁺ Apc^{fl/+} KRas^{LsL-G12D/+} Dusp6^{-/-}* mice treated with vehicle (right) or CI1040 (left) and sacrificed at 30 days after *Cre* recombinase induction.

Arrows are showing tumours in the intestine. CI1040 treated mice show a strong diminution in tumourigenesis.

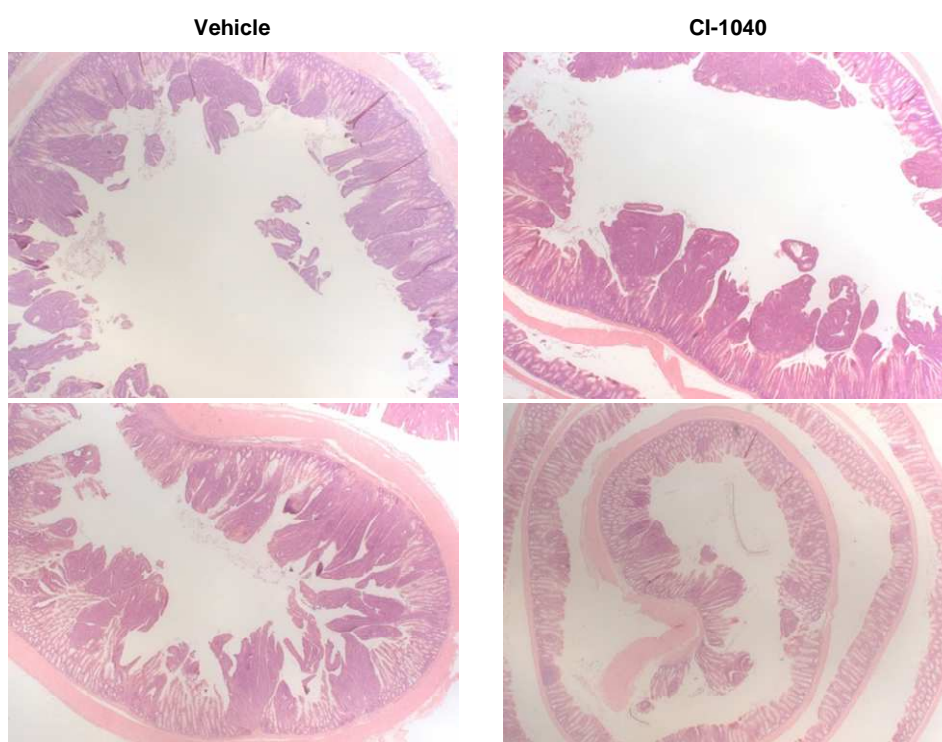


Figure 50: Effects of Mek inhibition on tumourigenesis

H&E staining was performed on paraffin sections of *VilCreER⁺ Apc^{fl/+} KRas^{LsL-G12D/+}* mice treated with vehicle (right) or CI1040 (left) and sacrificed at 80 days after *Cre* recombinase induction. No difference was observed between the two treatments.

17.2 Mek inhibition affects the CPL phenotype only when *Dusp6* is deleted

To investigate further the effect of Mek inhibition on *Dusp6* deleted mice, I used the acute *Apc* deletion model. I quantified the CPL phenotype of *VilCreER⁺ Apc^{fl/fl} KRas^{LSL-G12D/+}* (AK) and *VilCreER⁺ Apc^{fl/fl} KRas^{LSL-G12D/+} Dusp6^{-/-}* (AKD) mice treated with two different Mek inhibitors namely CI1040 and AZD6244. The drugs have an IC-50 of 300nM and 14nM respectively and were both shown to highly inhibit Mek 1/2 resulting in an inhibition of Erk 1/2 (Davies, Reddy et al. 2000; Yeh, Marsh et al. 2007). The drugs were given at a concentration of 100mg/Kg for CI1040 and 25mg/Kg for AZD6244 twice daily to ensure the presence of the drugs all day long. The results obtained with the two Mek inhibitors were similar despite their small specificity variations. Proliferation was assessed using a 2 hours BrdU pulse-chase labelling. In good agreement with the previous findings both CI1040 and AZD6244 drug treatments reduced significantly the CPL phenotype area in AKD mice (p-values = 0.02 and 0.03 respectively) (Figure 51). As expected, no downregulation of CPL phenotype were observed in AK mice following the treatment with CI1040 (Figure 52).

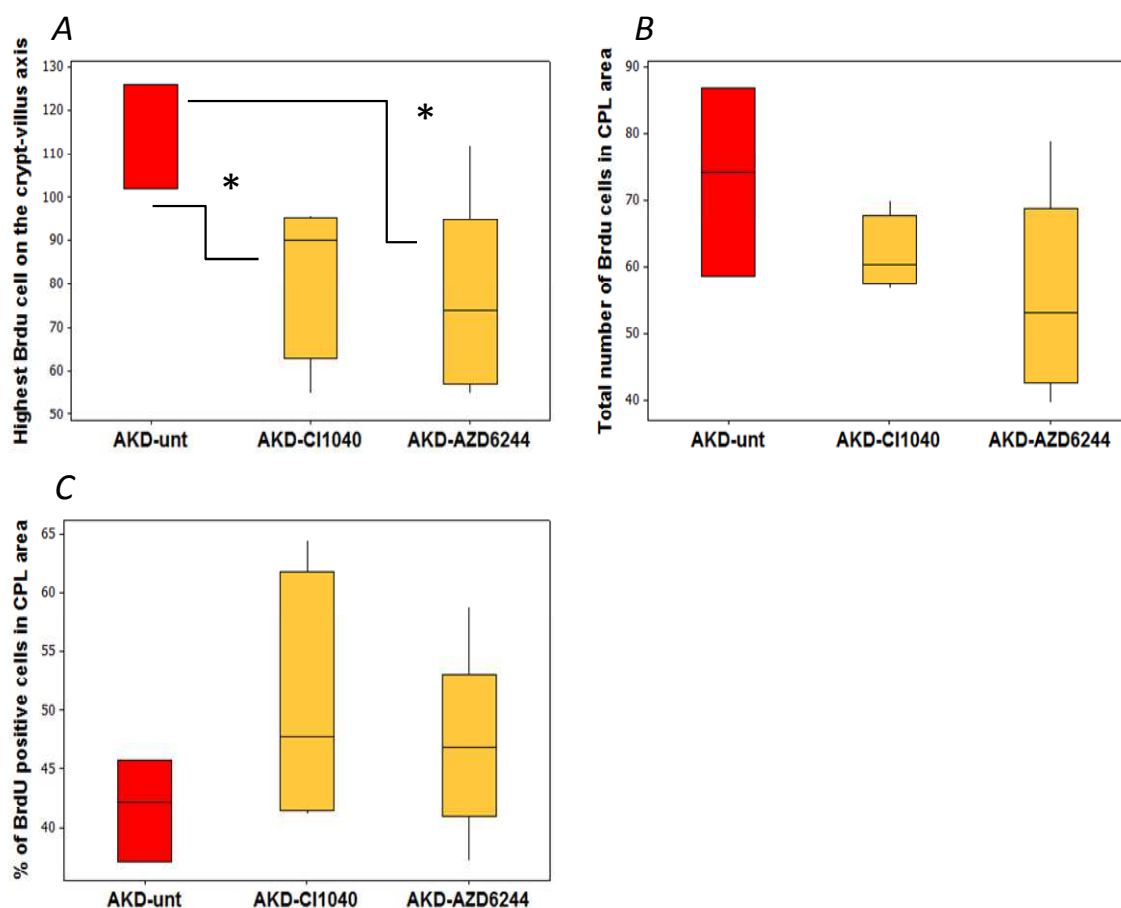


Figure 51: Effects of Mek inhibition on proliferation in the CPL phenotype of *Dusp6* null mice

CPL phenotype quantification by two hours BrdU pulse-chase labelling experiment. *VilCreER⁺Apc^{fl/fl}KRas^{LSL-G12D/+}Dusp6^{-/-}* mice (AKD) were sacrificed at day 3 after induction of *Cre* recombinase. The AKD mice were either untreated (red) (n=3), treated with CI1040 (n=4) or treated with AZD6244 (n=5) (both in yellow).

Box plots showing the position of the highest BrdU positive cell of AKD mice (A), the total number of BrdU positive cells per half crypt (B) and the percentage of BrdU positive cells in the CPL area (C) were drawn.

A Highest BrdU+ position - Mann Whitney test p-values	
AKD unt. Vs AKD CI1040	0.02
AKD unt. Vs AKD AZD6244	0.03
B Total of BrdU+ cells - Mann Whitney test p-values	
AKD unt. Vs AKD CI1040	0.18
AKD unt. Vs AKD AZD6244	0.08
C % of BrdU+ cells - Mann Whitney test p-values	
AKD unt. Vs AKD CI1040	0.29
AKD unt. Vs AKD AZD6244	0.11

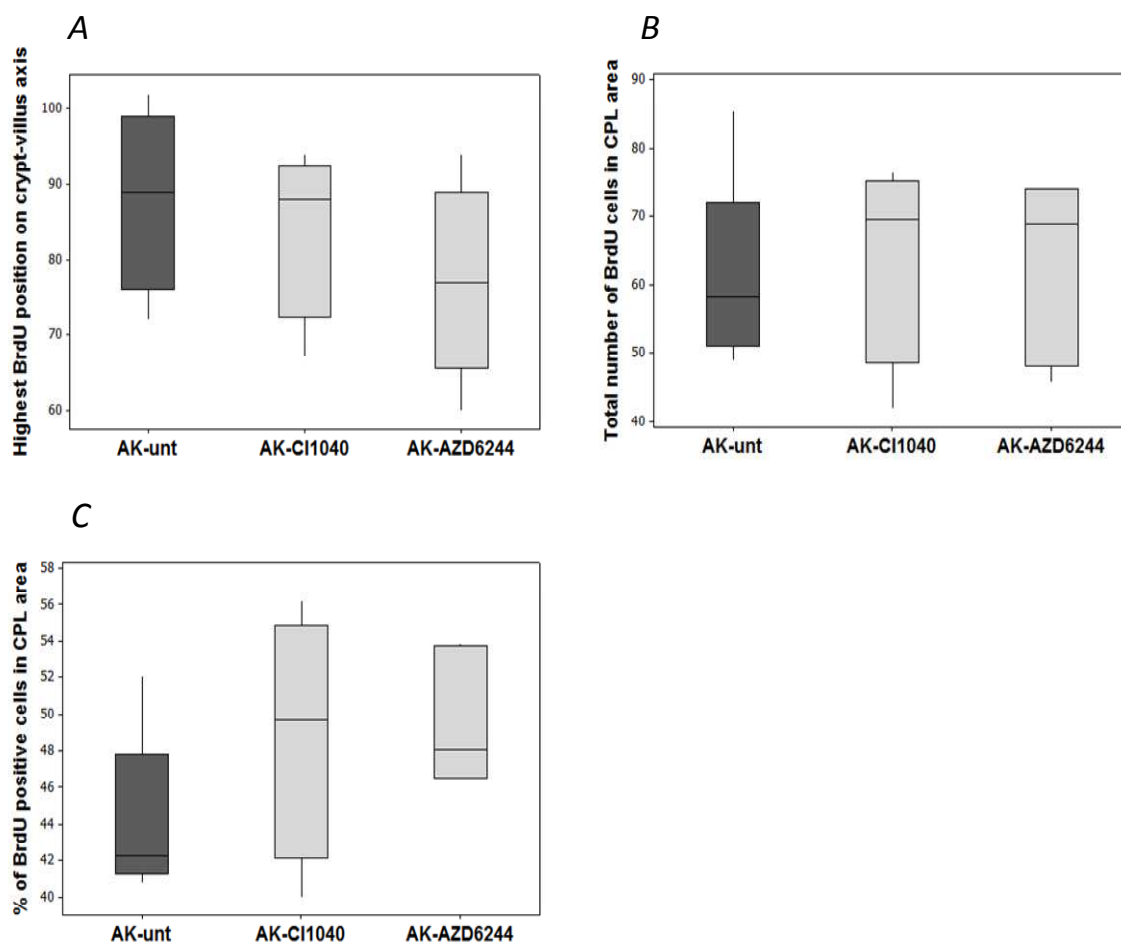


Figure 52: Effects of Mek inhibition on proliferation in the CPL phenotype of *KRas* activated mice

CPL phenotype quantification by two hours BrdU pulse-chase labelling experiment. *VilCreER⁺ Apc^{fl/fl} KRas^{LsL-G12D/+}* mice (AK) were sacrificed at day 3 after induction of Cre recombinase. The AK mice were either untreated (n=5) (dark grey) or treated with CI1040 (n=4) or AZD6244 (n=5) (light grey).

A, B and C: Box plot showing respectively the position of the highest BrdU positive cell, the total number of BrdU positive cells per half crypt and the percentage of BrdU positive cells in the CPL area of AK mice treated or not with CI1040.

A Highest BrdU+ position - Mann Whitney test p-values	
AK unt. Vs AK CI1040	0.27
AK unt. Vs AK AZD6244	0.1
B Total of BrdU+ cells - Mann Whitney test p-values	
AK unt. Vs AK CI1040	0.71
AK unt. Vs AK AZD6244	1
C % of BrdU+ cells - Mann Whitney test p-values	
AK unt. Vs AK CI1040	0.27
AK unt. Vs AK AZD6244	0.03

Taken together this data suggests that when *Apc* is lost and *KRas* is activated, the MAPK pathway may not be the main signalling cascade involved. This is perhaps not surprising as both the Wnt and *KRas* pathways have many downstream effectors and thus dependence on any single pathway would be unlikely. Therefore the inhibition of other pathways such as Pi3K/Akt or Rac along with the inhibition of MAPK pathway is currently investigated in the lab and will help clarify which pathway is mainly involved in the response to *Apc* deletion and *KRas* activation. Moreover given potential feedback loops it is also likely that if any effector pathway is downregulated another may be stimulated (Tenbaum, Ordonez-Moran et al. 2012). Our data however suggest that the one reason the MAPK pathway is not the preferred cascade is that *Dusp6* is already counteracting the activation of the MAPK pathway. When *Dusp6* is removed there is an increase in proliferation which is now completely reliant of MAPK pathway as shown with the sensitivity to the Mek inhibitors. Indeed it seems that *Dusp6* deletion channel the signal through the MAPK pathway by removing an important negative feedback loop. It is interesting to note *Dusp5* activity is also high suggesting that again other feedback mechanisms are also limiting MAPK activation. We could speculate that combined deletion of *Dusp5/6* might cause a dramatic activation of MAPK pathway. In this circumstance it may yield too high a level of pathway activity that may be deleterious for cancer cell proliferation. Indeed there are many reports that overexpression of *KRas* and/or high Erk pathway activation can lead to senescence.

We next wished to test the specificity of *Dusp6* deletion as our data would suggest *Dusp6* was only activated in the context of a *KRas* mutation and therefore we might expect *Dusp6* deletion to have some impact when *KRas* mutation is targeted to the intestine in the absence of an *Apc* mutation. Moreover we would expect, given the low expression of *Dusp6* following *Apc* loss, very little impact in tumours that have just lost *Apc* (in the absence of *KRas* mutation).

18 Dusp6 deletion effects on tumourigenesis

18.1 Dusp6 deletion effects in the context of Apc deletion alone

In order to confirm the necessity of *KRas* activation to induce *Dusp6* deletion effects on tumourigenesis, I aged *VilCreER⁺ Apc^{fl/+}* and *VilCreER⁺ Apc^{fl/+} Dusp6^{-/-}* mice after induction of the *Cre* recombinase. As expected, in this context *Dusp6* loss did not have an effect on tumourigenesis confirming the dependence to MAPK pathway activation (Figure 53).

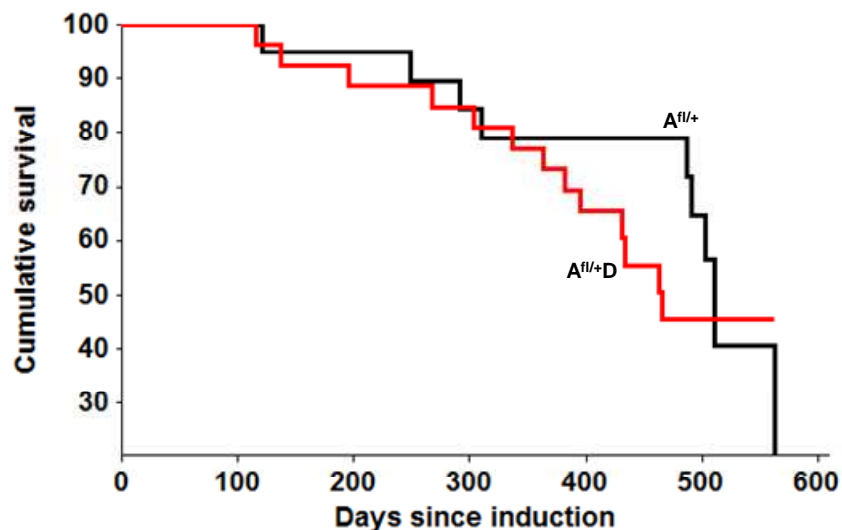


Figure 53: *Dusp6* deletion has no effect following *Apc* deletion alone

Kaplan-Meier curve showing the survival of *VilCreER⁺ Apc^{fl/+}* (*A^{fl/+}*) (black line ; n=19) and *VilCreER⁺ Apc^{fl/+} Dusp6^{-/-}* mice (*A^{fl/+}D*) (red line ; n=26). Mice with intestinal tumours were sacrificed at the same point of illness or until they reached 500 days after induction.

The survival was not different between the two genotypes: log rank p=0.2.

18.2 *Dusp6* deletion effects in the context of *KRas* activation alone

It has been shown that *KRas* activation alone could lead to intestinal hyperproliferation (Haigis, Kendall et al. 2008) but does not promote intestinal tumourigenesis. We therefore wanted to assess if *Dusp6* deletion had an impact on intestinal tumourigenesis in the context of *KRas* activation only.

To do so, I aged *VilCreER⁺ KRas^{LsL-G12D/+} Dusp6^{+/+}* along with *VilCreER⁺ KRas^{LsL-G12D/+} Dusp6^{-/-}* mice until they show intestinal sickness or until they reached the age of 500 days. In agreement with published data, *VilCreER⁺ KRas^{LsL-G12D/+}* mice did not develop intestinal tumours (Figures 54 and 56). The addition of *Dusp6* deletion resulted in tumour formation and a median survival of 250 days (Figure 54). This is another evidence of the strong effect of *Dusp6* loss lead by *KRas* activation on tumourigenesis. The tumours growing from these mice were not invasive but were highly proliferative as indicated by a 2 hours BrdU pulse-chase labelling (Figure 55).

Interestingly, in the tumours of *VilCreER⁺ KRas^{LsL-G12D/+} Dusp6^{-/-}* mice, a positive nuclear staining of β -Catenin as well as a positive Sox 9 staining showed Wnt pathway activation (Figure 56). However, the reason of this activation remains uncertain. On the other hand, the Sox 9 staining of *VilCreER⁺ KRas^{LsL-G12D/+}* mice remained restricted to the crypt and the pattern of β -Catenin staining remained normal, namely in the nucleus of cells of the bottom of the crypt and at the cells membrane.

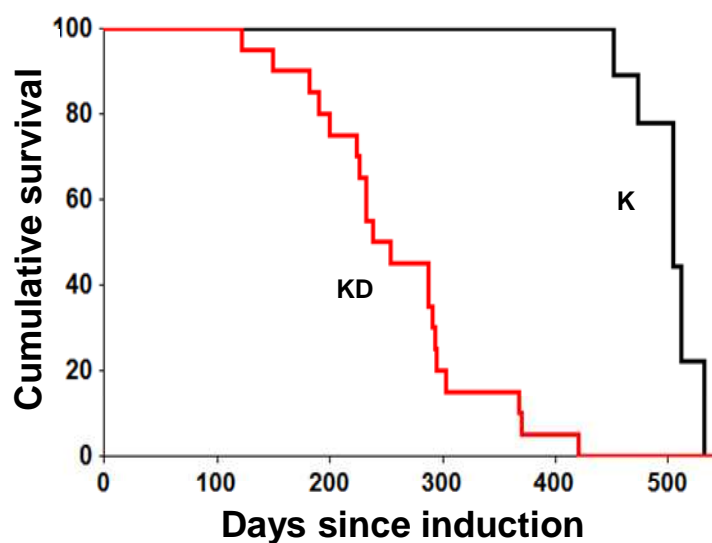


Figure 54: *Dusp6* deletion reduces the survival following *KRas* activation

Kaplan-Meier curve showing the survival of *VilCreER⁺ KRas^{LsL-G12D/+}* (K) (black line ; n=9) and *VilCreER⁺ KRas^{LsL-G12D/+} Dusp6^{-/-}* mice (KD) (red line ; n=20). Mice with intestinal tumours were sacrificed at the same point of illness or until they reached 500 days after induction.

The survival was significantly different between the two genotypes: log rank $p < 0.001$. *Dusp6* deletion decreases median survival from 500 days to 250 days.

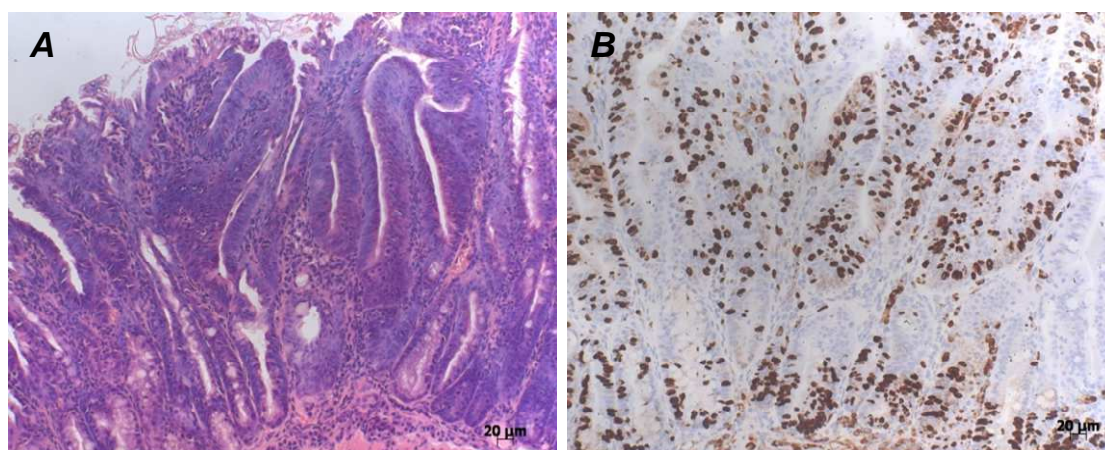


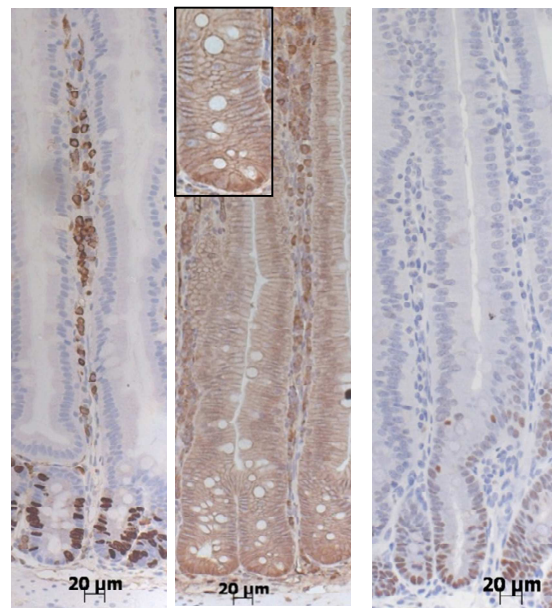
Figure 55: *Dusp6* deletion allows tumour formation following *KRas* activation

H&E staining and BrdU IHC were performed of paraffin sections of intestine of *VilCreER⁺ KRas^{LsL-G12D/+} Dusp6^{-/-}* mice.

A: H&E of an intestinal tumour of a *VilCreER⁺ KRas^{LsL-G12D/+} Dusp6^{-/-}* mouse.

B: BrdU staining in an intestinal tumour of a *VilCreER⁺ KRas^{LsL-G12D/+} Dusp6^{-/-}* mouse showing the high level of proliferation of these tumours.

K

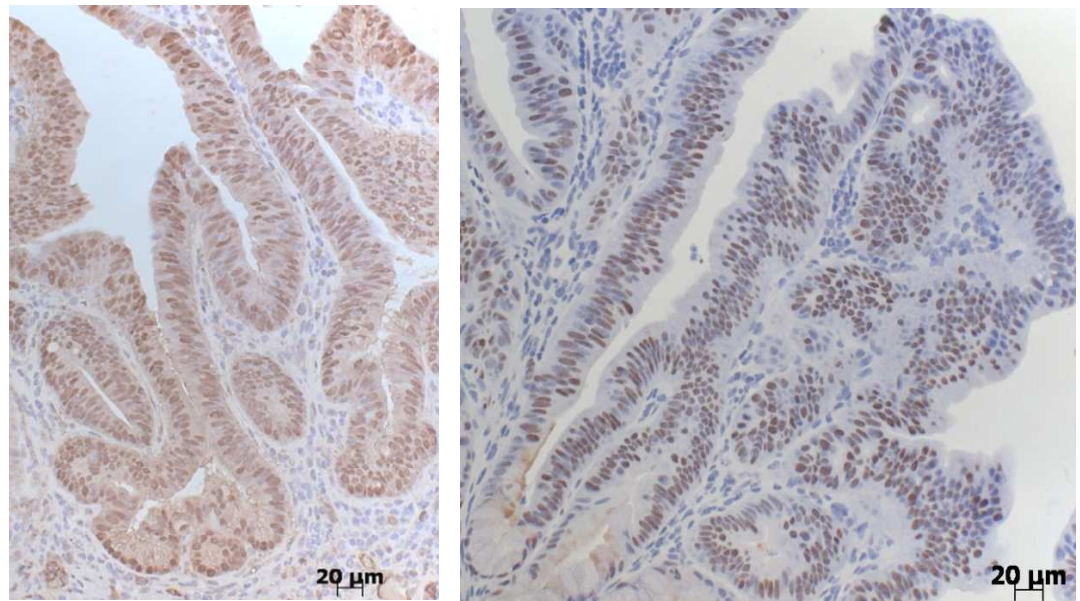


BrdU

 β -Catenin

Sox 9

KD

 β -Catenin

Sox 9

Figure 56: Activation of Wnt signalling in *KRas* activated mice

Immunohistochemistries for BrdU, β -Catenin and Sox9 were performed on paraffin sections of intestine from *VilCreER⁺ KRas^{LSL-G12D/+}* (K) and *VilCreER⁺ KRas^{LSL-G12D/+} Dusp6^{-/-}* mice (KD).

K: The BrdU staining shows proliferation is restricted to the crypt. The β -Catenin staining is located in the nuclei of cells at the bottom of the crypt and at the cell membrane and Sox 9 is also restricted to the bottom of the crypts.

KD: Nuclear β -Catenin and Sox 9 staining is located in the nuclei of most of the cells of the intestinal tumour showing a Wnt pathway activation in these lesions.

19 Effects of *Dusp6* deletion on MAPK pathway

I have proven previously that *Dusp6* deletion effects are dependent on *KRas* activation and are reversed by the inhibition of MAPK pathway at Mek level. It is now interesting to determine by which mechanism *Dusp6* deletion affect the MAPK pathway and, at a more global level, cell proliferation and tumourigenesis. *Dusp6* dephosphorylates Erk 1/2, so in order to assess the effects of *Dusp6* deletion on Erk activation I performed an IHC for pErk 1/2 and pMek 1/2 on *VilCreER⁺ Apc^{fl/+} KRas^{LsL-G12D/+}* and *VilCreER⁺ Apc^{fl/+} KRas^{LsL-G12D/+} Dusp6^{-/-}* mice (Figure 57).

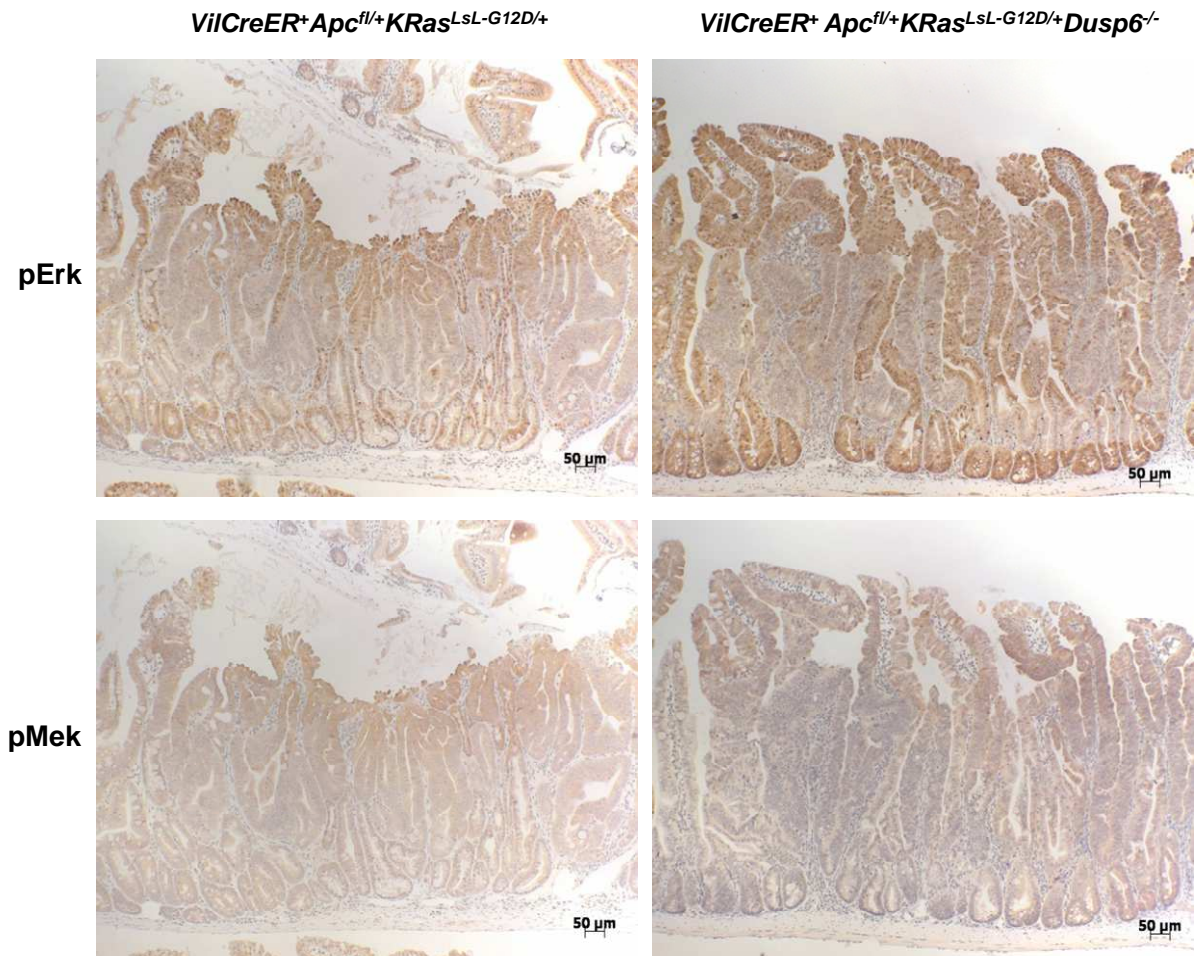


Figure 57: MAPK pathway activation following *Apc* deletion and *KRAS* activation

Immunohistochemistries for pErk and pMek were performed on paraffin sections of intestine from *VilCreER⁺Apc^{fl/+}KRAS^{LSL-G12D/+}* and *VilCreER⁺Apc^{fl/+}KRAS^{LSL-G12D/+}Dusp6^{-/-}* mice.

VilCreER⁺Apc^{fl/+}KRAS^{LSL-G12D/+} : The pErk staining is mainly restricted to the edge of the villi and the bottom of the crypts. The core of the tumour does not show an Erk activation. The pMek staining follow the pattern of pErk staining confirming the direct link between Erk and its specific kinase Mek.

VilCreER⁺Apc^{fl/+}KRAS^{LSL-G12D/+}Dusp6^{-/-} : The staining for both protein is similar to *VilCreER⁺Apc^{fl/+}KRAS^{LSL-G12D/+}* mice suggesting that *Dusp6* deletion does not affect the MAPK pathway activation in this model.

Erk activation (pErk) is restricted to the crypts forming a distinct line in the gut epithelium. There is also an Erk phosphorylation at the edge of the villi which could be caused by an activation of Erk by the bacteria found in the intestine (Sung Hee Lee 2010). The core of the tumours showed very little staining suggesting very little or no Erk activation in these intestinal tumours. The pMek pattern matched the pErk one in both normal and tumourigenic epithelium.

Nonetheless the IHC for both phospho-protein stayed rather unclear and if *Dusp6* deletion did not seem to have an effect on Mek and Erk activation in this context we could not conclude this was a real effect. Indeed the staining here does not allow the visualisation of subtle changes that might appear between the genotypes.

To study further the effect of *Dusp6* deletion, I then performed a western blot analysis on epithelial extracts of *VilCreER⁺* (WT), *VilCreER⁺ Apc^{fl/fl}* (A), *VilCreER⁺ Apc^{fl/fl} KRas^{LsL-G12D/+}* (AK) and *VilCreER⁺ Apc^{fl/fl} KRas^{LsL-G12D/+} Dusp6^{-/-}* (AKD) mice (Figure 58). Unexpectedly, I found a downregulation of active Erk following *KRas* activation while total Erk remained unchanged. This result were confirmed by the downregulation of pElk1 a direct target of Erk 1/2. This downregulation was not affected by the loss of *Dusp6*. However, a western blot analysis of protein samples from crypt culture of A and AK mice done by David Huels suggested that there were no difference in Erk activation between the samples. This result is not in agreement with the figure 58 and questions the conservation of the phospho-proteins in the protein samples from epithelial extracts. Further investigations are currently done on crypt culture samples with *Dusp6* deletion in order to confirm the finding. However, the MAPK cascade is regulated by numerous kinases and phosphatases and a complex network of negative feedback loops and the surprising effect of *KRas* activation in our model may be the outcome of these complex regulation mechanisms. Interestingly, I found total Mek upregulated following *KRas* activation (Figure 58). I was unable to obtain a good immunoblot for pMek and therefore it was impossible to ascertain the impact of total Mek increase on Mek activation. I performed an IHC for pErk 1/2 and pElk 1 on these mice gut epithelium (Figure 59). In these mice we found the pErk 1/2 staining restricted to the edge of the villi and to the crypt. The pElk 1 staining was restricted to highly proliferative areas within the villi of *VilCreER⁺ Apc^{fl/fl} KRas^{LsL-G12D/+}* (AK) and *VilCreER⁺ Apc^{fl/fl} KRas^{LsL-G12D/+} Dusp6^{-/-}* (AKD) mice. Here the activation of Elk 1 reveals the MAPK pathway activation in the CPL phenotype of these mice. However no differences were observed between AK and AKD mice.

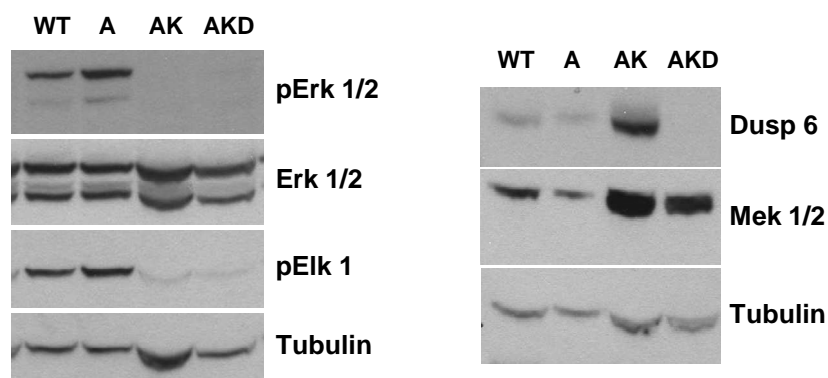


Figure 58: MAPK pathway activation in the intestinal epithelium

Western Blot performed on protein from epithelial extracts of intestine from *VilCreER*⁺ (WT), *VilCreER*⁺*Apc*^{fl/fl} (A), *VilCreER*⁺*Apc*^{fl/fl}*KRas*^{L^SL-G12D/+} (AK) and *VilCreER*⁺*Apc*^{fl/+}*KRas*^{L^SL-G12D/+}*Dusp6*^{-/-} (AKD) mice.

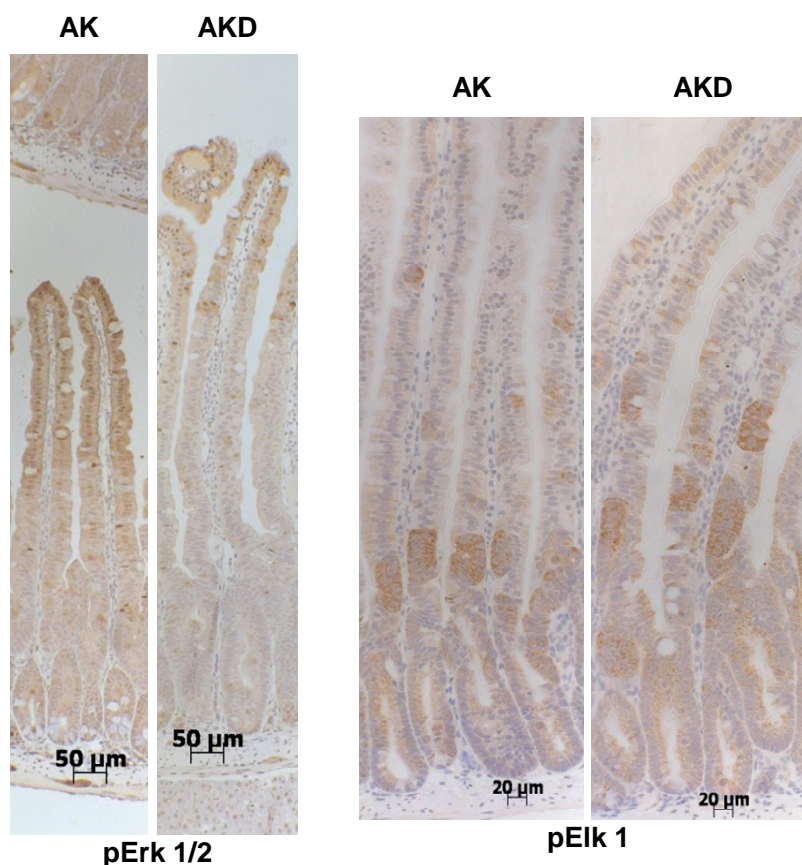


Figure 59: MAPK pathway activation in CPL phenotype

Immunohistochemistry for pErk 1/2 (left panel) and pElk 1 (right panel) were performed on paraffin sections of intestine from *VilCreER*⁺*Apc*^{fl/fl}*KRas*^{L^SL-G12D/+} (AK) and *VilCreER*⁺*Apc*^{fl/+}*KRas*^{L^SL-G12D/+}*Dusp6*^{-/-} mice (AKD).

AK and AKD: pElk 1 staining is increased in the proliferative zones of the CPL phenotype suggesting an upregulation of the MAPK pathway in the CPL phenotype however pErk staining is restricted to the edge of the villi.

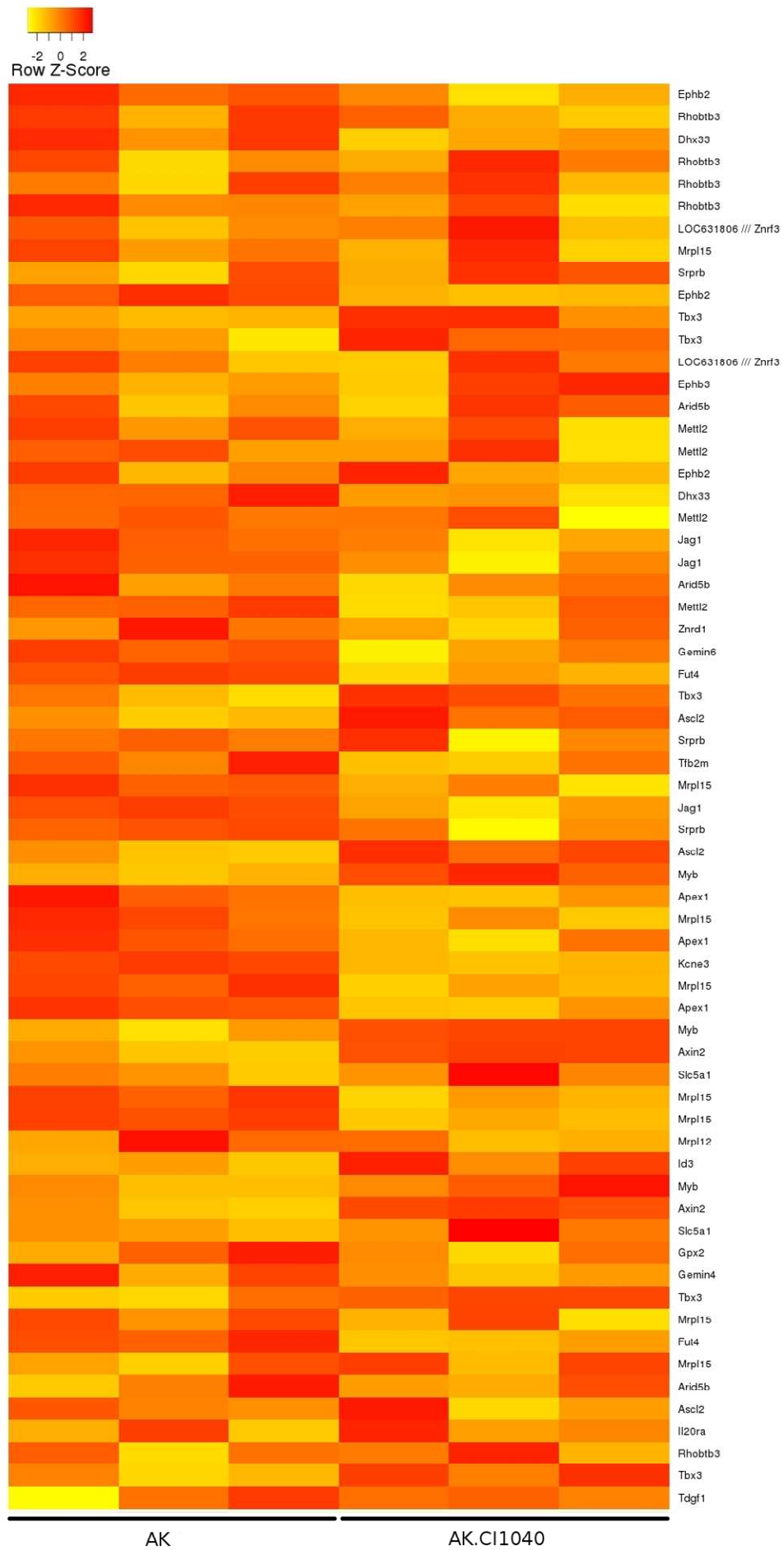
These rather contradictory results taken together do not allowed having a clear answer regarding the outcome of *Dusp6* deletion but also of *KRas* activation in this context. Here the lack of powerful tools to ascertain Erk activation is highlighted and the use of more advanced technics or better readout will be necessary to determine the impact of these two mutations on MAPK cascade activation.

20 Impact of Mek inhibition on gene signature

Given the conflicting results obtained by immunoblot and IHC, we decided to investigate alteration in genes expression signature using microarray analysis performed on whole gut RNA from *VilCreER⁺ Apc^{fl/fl} KRas^{LsL-G12D/+}* (AK) and *VilCreER⁺ Apc^{fl/fl} KRas^{LsL-G12D/+} Dusp6^{-/-}* (AKD) mice treated or not with the MEK inhibitor CI1040.

20.1 Wnt pathway signature

I analysed the Wnt pathway signature of AK and AKD mice treated or not with the Mek inhibitor CI1040 based on the previously described H. Clevers' group list of upregulated genes in human CRCs (Rigas, Hoff et al. 2001) (Figures 60 A and B). Globally the CI1040 treatment has similar outcomes in both AK and AKD mice. There were however a small number of genes such as *Rhobtb3* which were upregulated after CI1040 treatment only in AKD mice. This is confirmed by the clusters formed separating in two groups the untreated samples and the treated ones (if we exclude the already mentioned AKD sample with the very unique behaviour) (Supplementary figure 7). Interestingly, a number of genes were downregulated in both genotypes namely *EphB2*, *Jag1*, *Etv4*, *Sox9*, *cd44* and *Myc*. Given the CI1040 was unable to stop the proliferation of the AK mice it suggests that reduction of these proteins is not sufficient to stop the efficient proliferation of AK cells. Interestingly *Sox4* is upregulated after treatment in both AK and AKD mice. But overall, there were no major changes brought by the inhibition of Mek in the two genotypes.



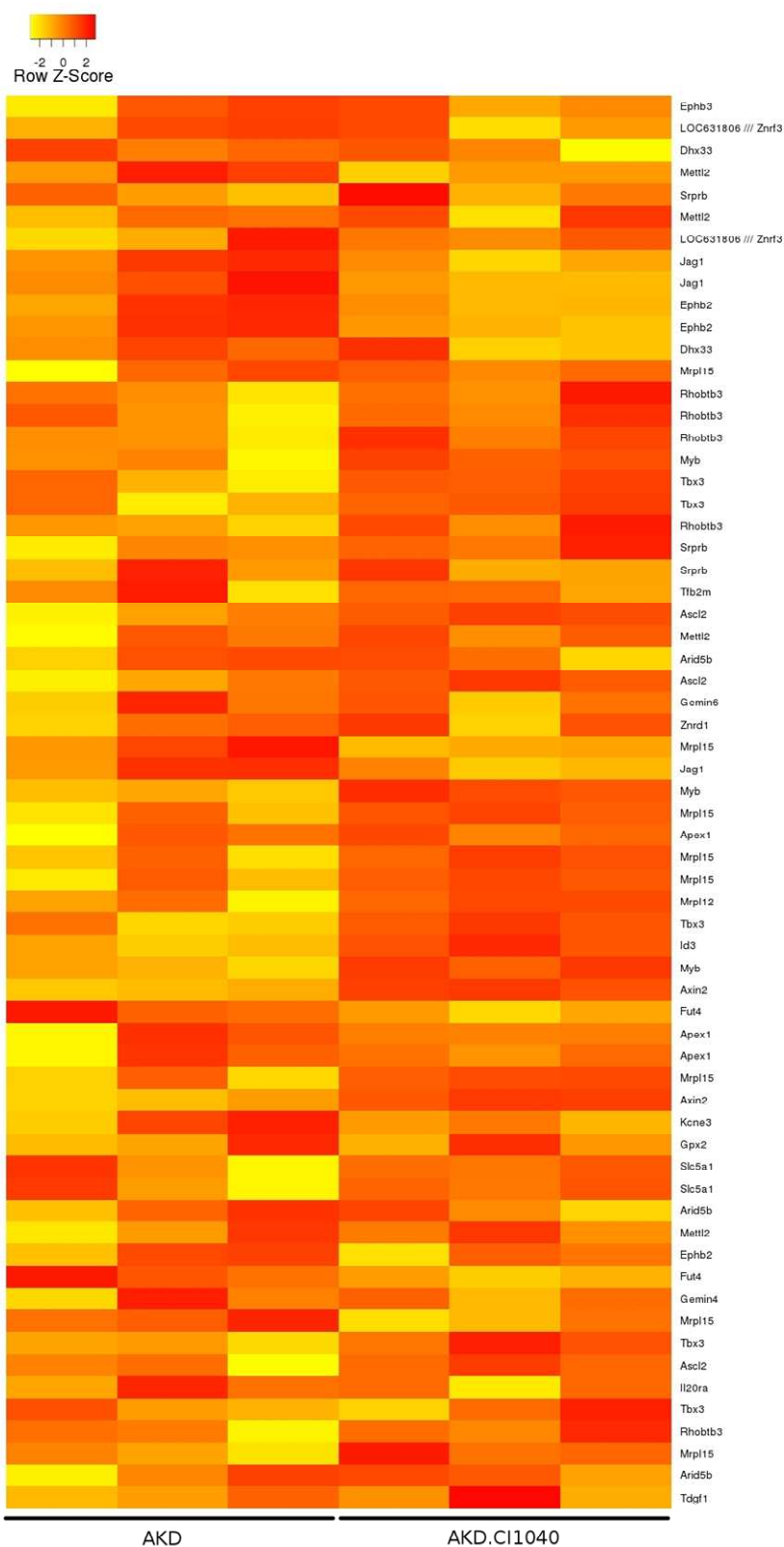
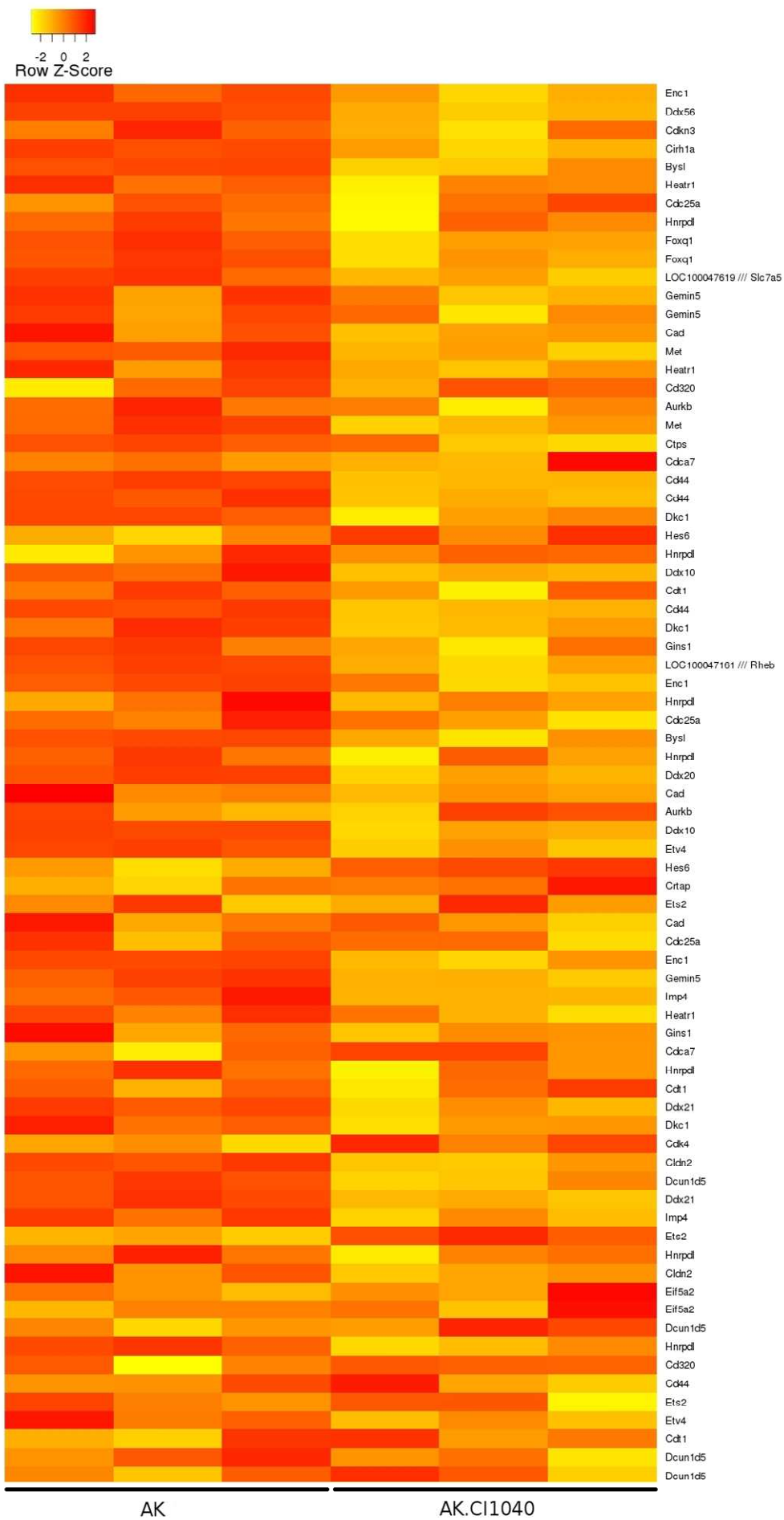
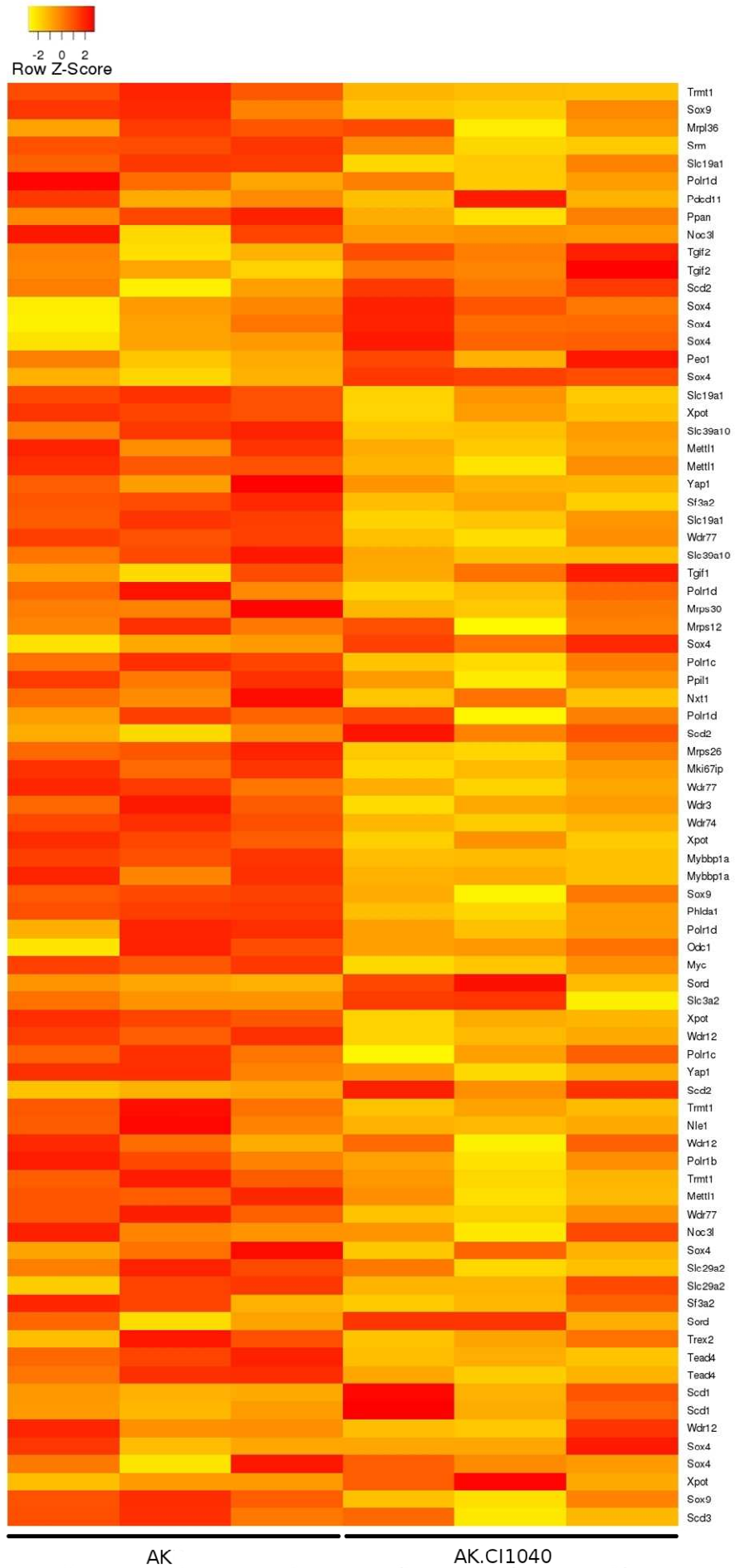
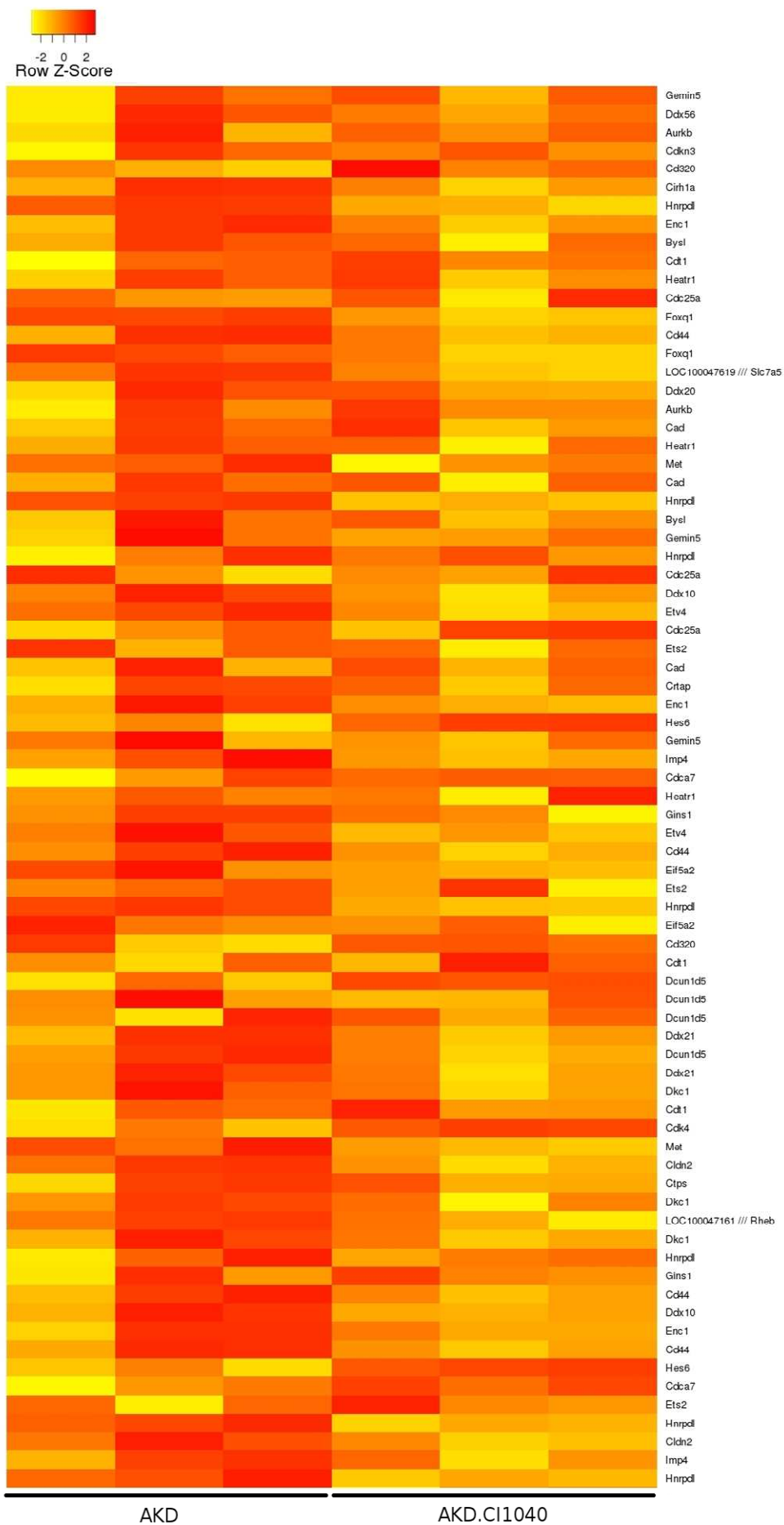


Figure 60A: WNT pathway signature

The genes found to be up-regulated in human colorectal adenomas were tested in whole gut extracts of *VilCreER⁺ Apc^{fl/fl} KRas^{L^{SL}-G12D/+}* untreated (AK) or treated with Mek inhibitor (AK CI1040) and *VilCreER⁺ Apc^{fl/fl} KRas^{L^{SL}-G12D/+} Dusp6^{-/-}* untreated (AKD) or treated (AKD CI1040) mice taken at day 3 after Cre recombinase induction. The Z-score is indicated by a range of colour from yellow (low expression) to red (high expression).







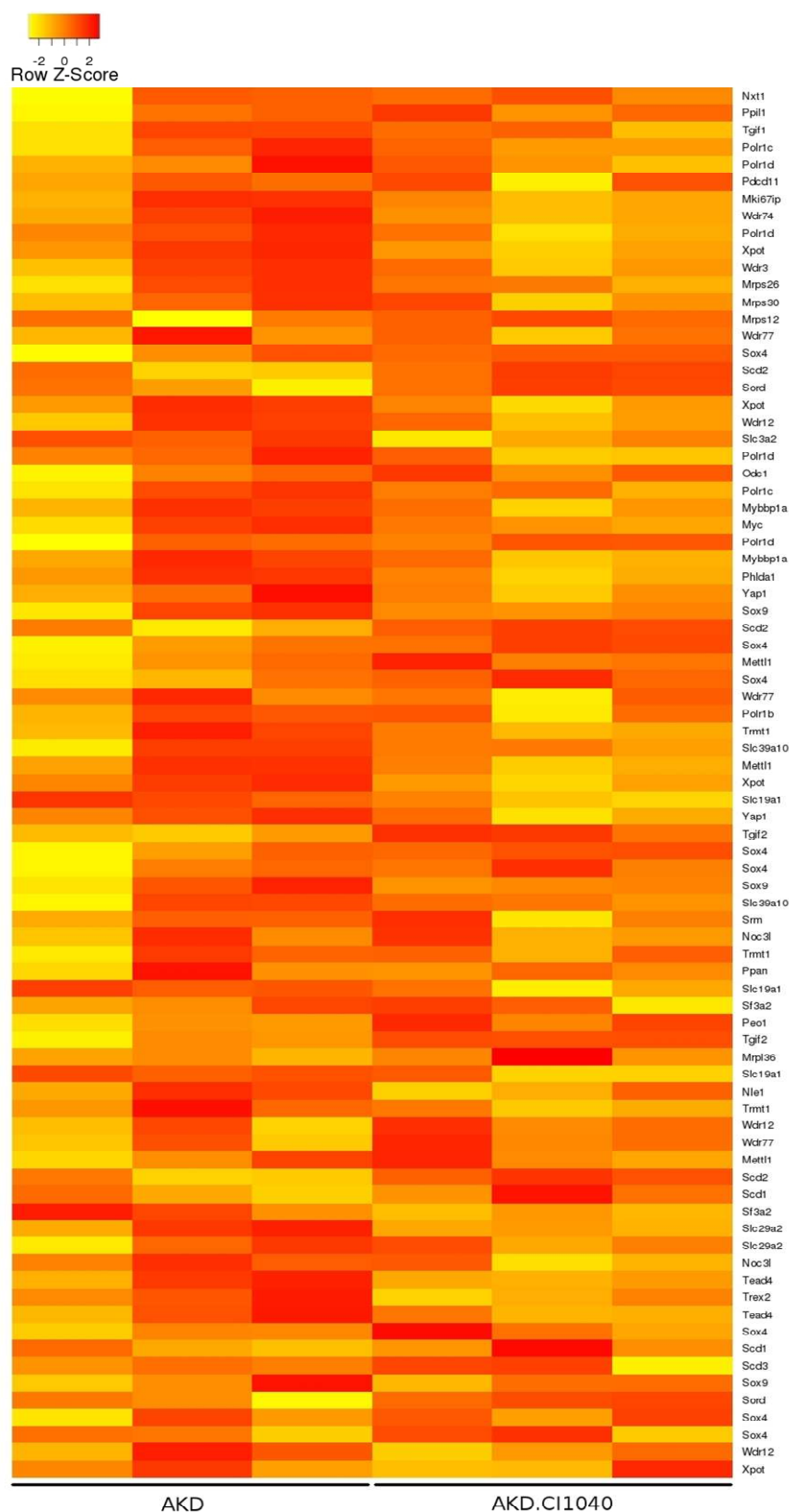
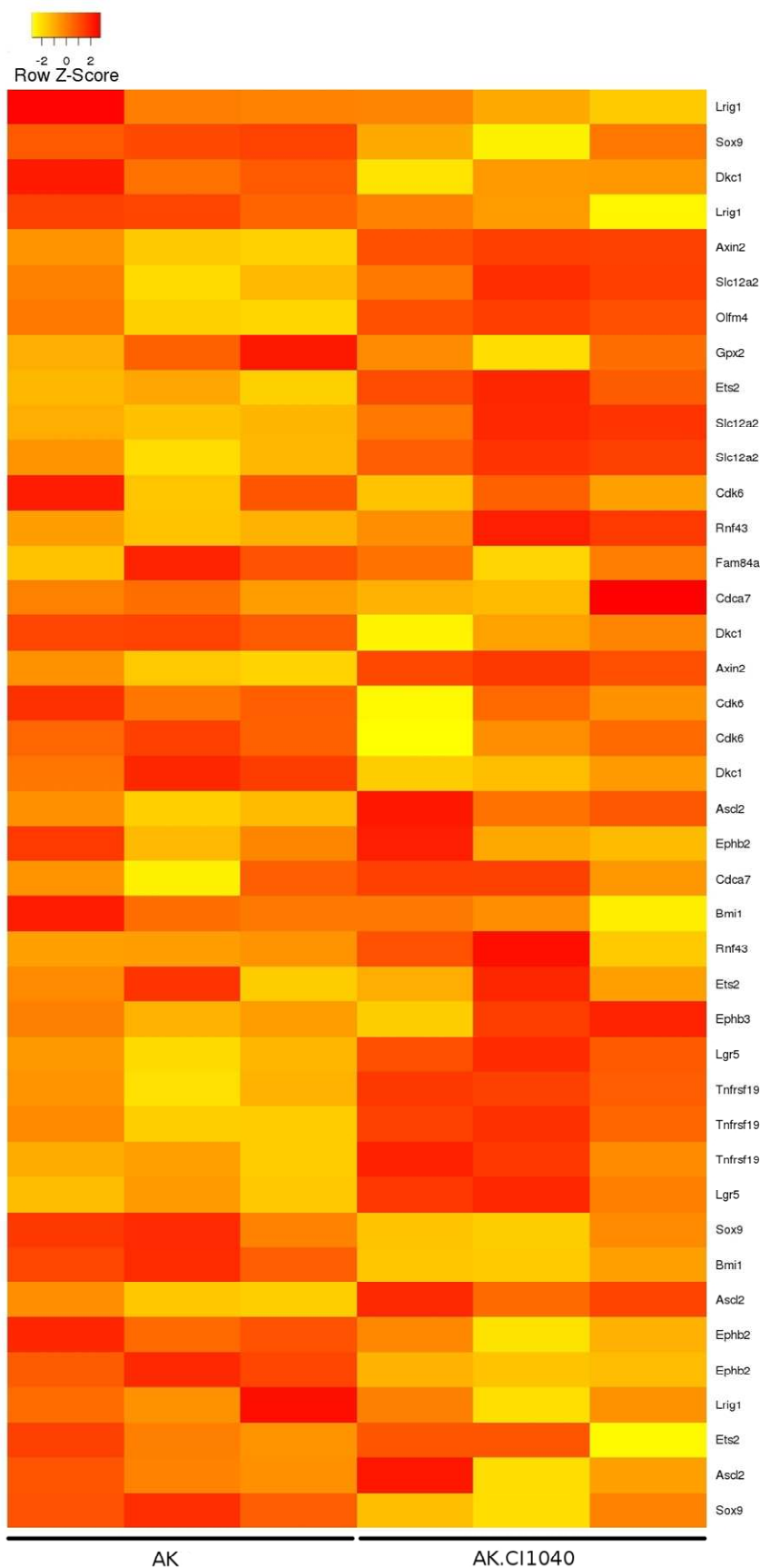


Figure 60B: WNT pathway signature

The genes found to be up-regulated in both human colorectal adenomas and human colorectal adenocarcinomas were tested in whole gut extracts of *VilCreER⁺ Apc^{fl/fl} KRas^{L5L-G12D/+}* untreated (AK) or treated with Mek inhibitor (AK CI1040) and *VilCreER⁺ Apc^{fl/fl} KRas^{L5L-G12D/+} Dusp6^{-/-}* untreated (AKD) or treated (AKD CI1040) mice taken at day 3 after *Cre* recombinase induction. The Z-score is indicated by a range of colour from yellow (low expression) to red (high expression).

20.2 Stem cell signature

I then analysed the expression of intestinal stem cell markers in AK and AKD mice treated or not with the Mek inhibitor CI1040 (Figure 61). Here again, both genotypes reacted in the same way to the treatment and the samples were clustered in two distinct groups according to their treatment (Supplementary figure 8). No clear impact on the intestinal stem cells was observed with Mek inhibition: some genes such as *Ascl2*, *Lgr5* and *Olfm4* were upregulated following the treatment whereas genes such as *Bmi1* and *Lrig* were downregulated. These rather conflicting effects did not allow us to establish a clear effect of Mek inhibition on stem cells.



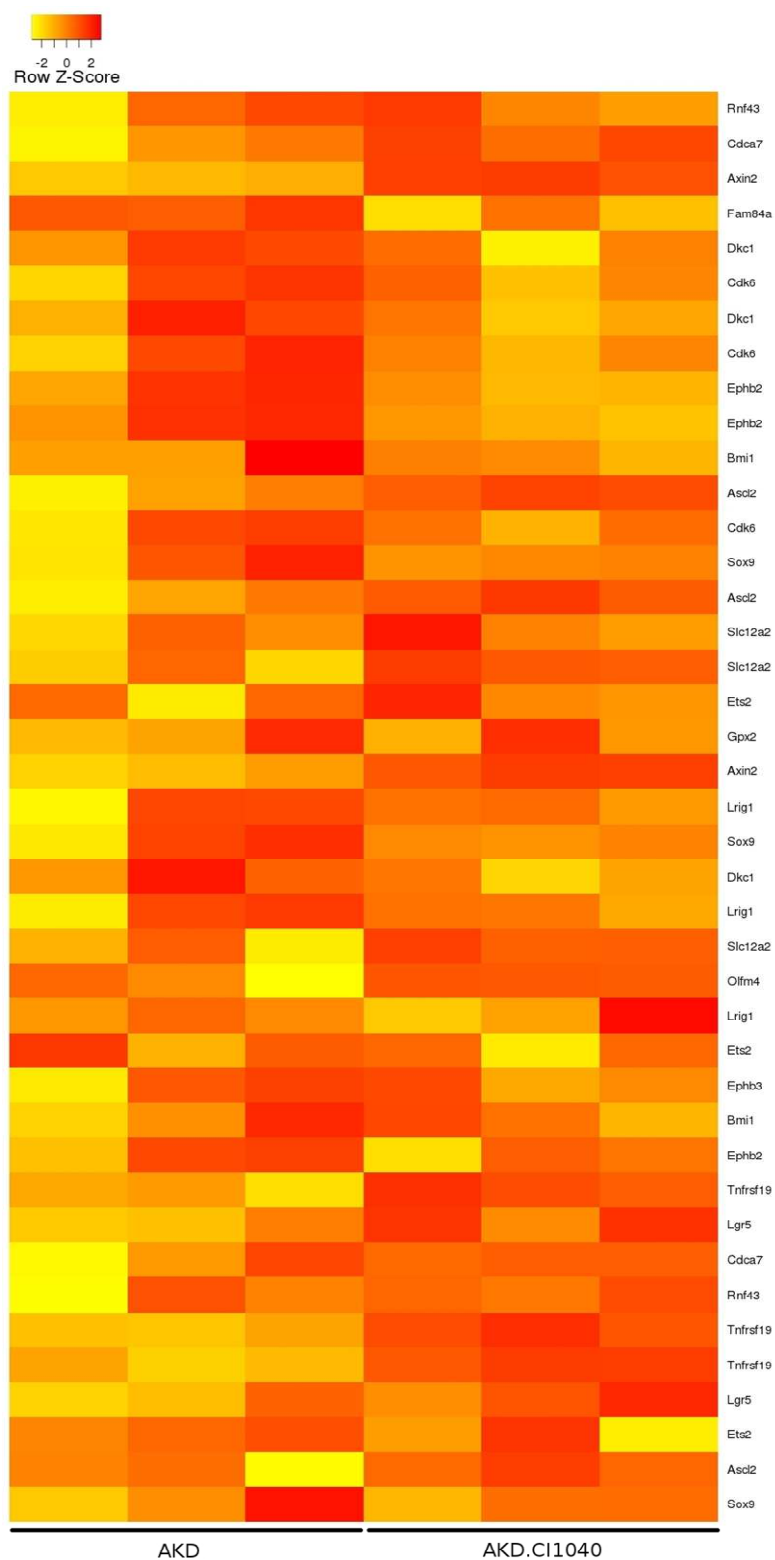
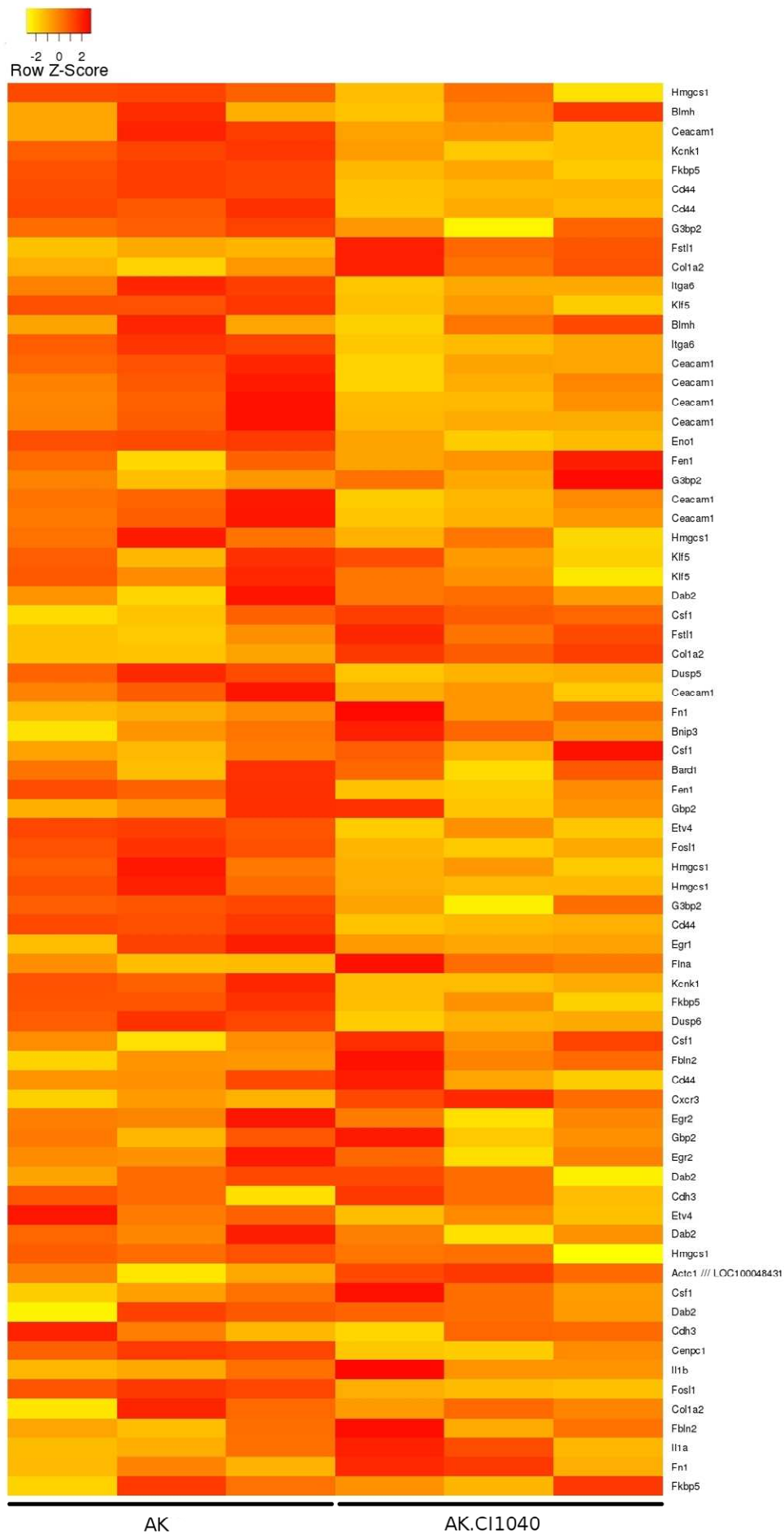


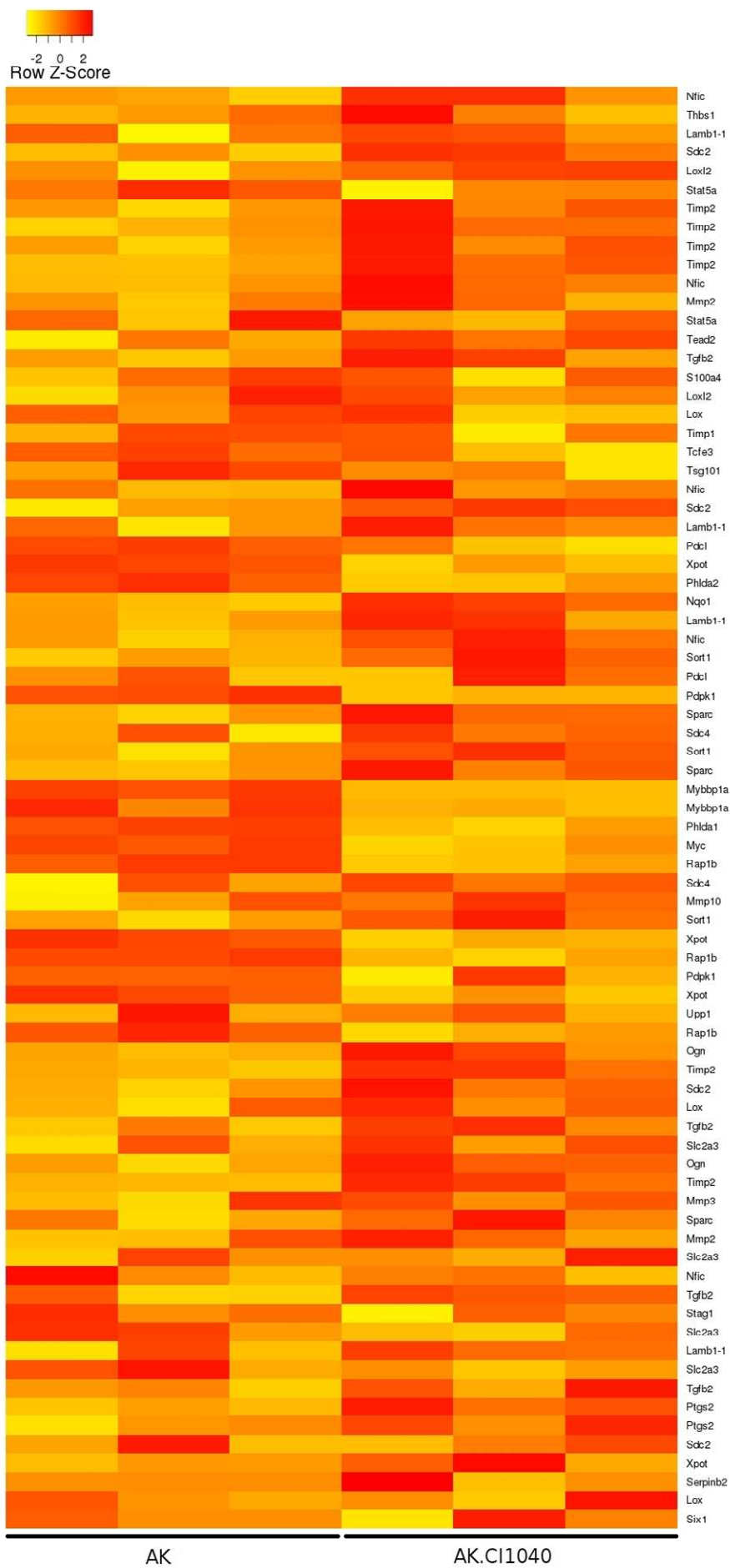
Figure 61: Stem cell signature

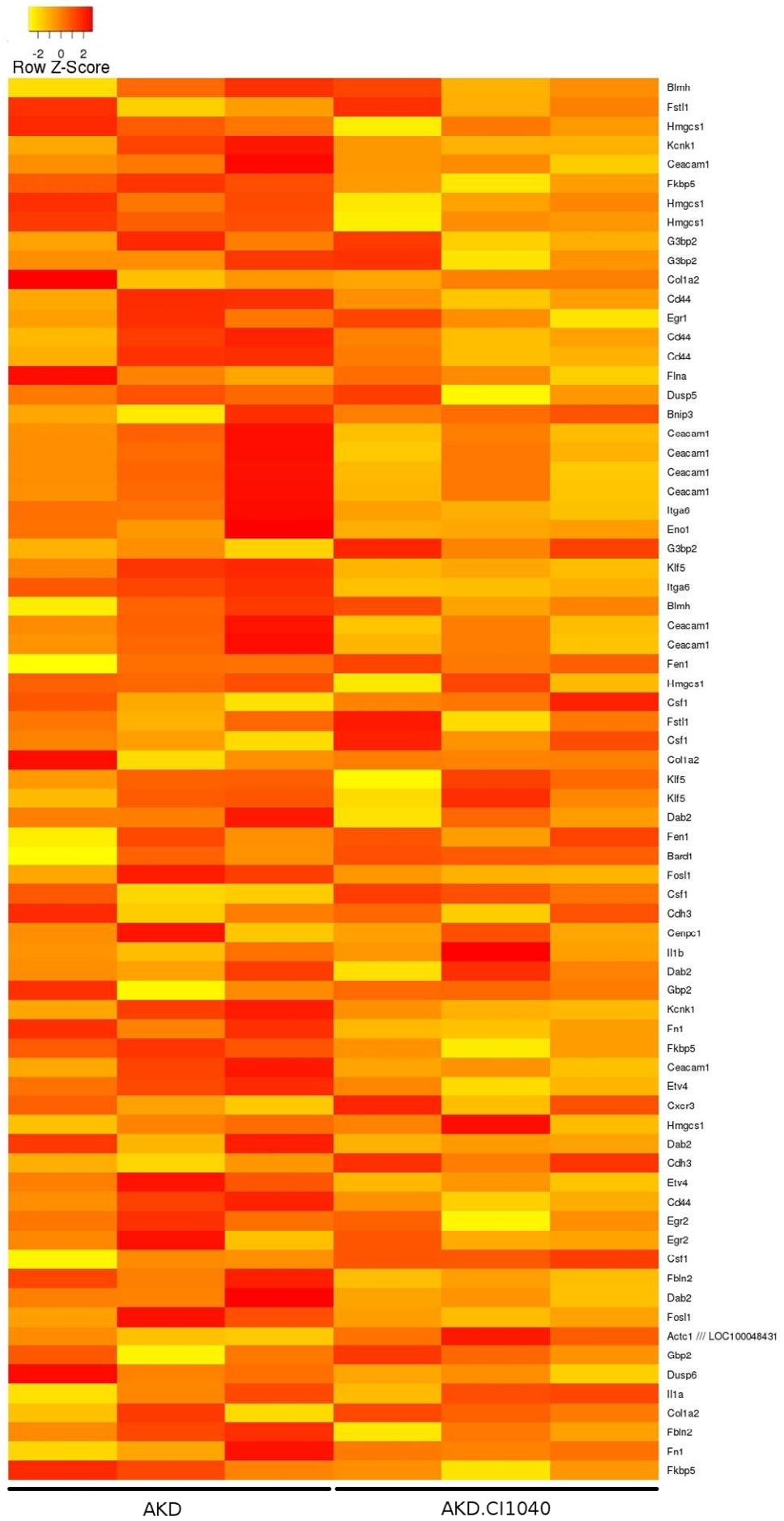
The expression of intestinal stem cell markers was tested in whole gut extracts of *VilCreER⁺ Apc^{fl/fl} KRas^{LsL-G12D/+}* untreated (AK) or treated with Mek inhibitor (AK CI1040) and *VilCreER⁺ Apc^{fl/fl} KRas^{LsL-G12D/+} Dusp6^{-/-}* untreated (AKD) or treated (AKD CI1040) mice taken at day 3 after *Cre* recombinase induction. The Z-score is indicated by a range of colour from yellow (low expression) to red (high expression).

20.3 MAPK pathway signature

Finally I analysed the effect of Mek inhibition on the MAPK pathway gene signature. As expected both genotypes behave in similar way and the samples were clustered according to their treatment (except the one AKD sample) (Supplementary figure 9). Among the changes observed we can note a downregulation of *Fra1* and *Dusp5* following CI1040 treatment (Figure 62). Interestingly *Dusp6* was also downregulated in AK mice treated. This data highlights that the Mek inhibition was able to inhibit the MAPK pathway in AK intestines; however this was not sufficient to stop proliferation.







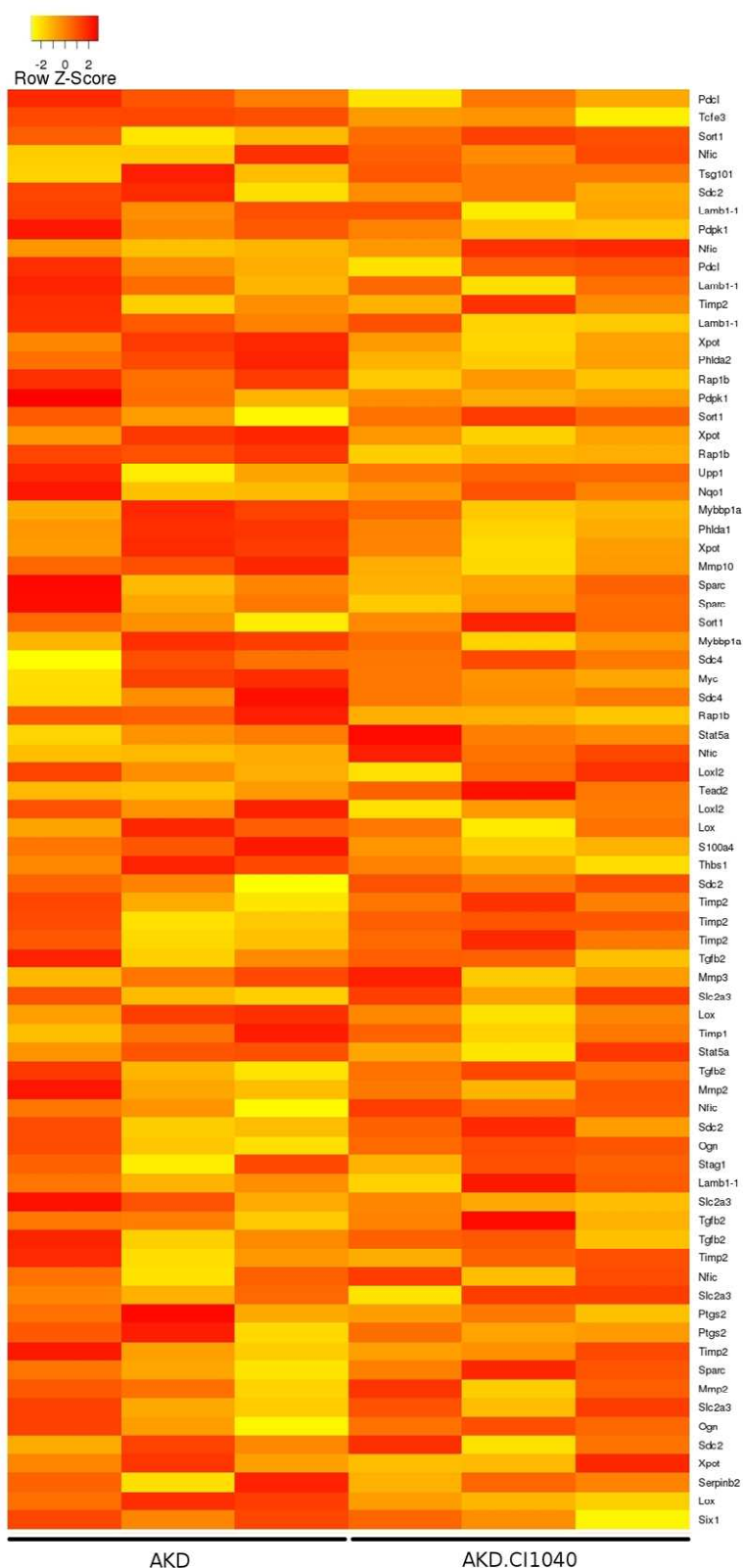


Figure 62: MAPK pathway signature

The MAPK pathway target genes identified by microarray based transcriptome profiling were tested in whole gut extracts of *VilCreER⁺ Apc^{fl/fl} KRas^{LSL-G12D/+}* untreated (AK) or treated with Mek inhibitor (AK CI1040) and *VilCreER⁺ Apc^{fl/fl} KRas^{LSL-G12D/+} Dusp6^{-/-}* untreated (AKD) or treated (AKD CI1040) mice taken at day 3 after Cre recombinase induction. The Z-score is indicated by a range of colour from yellow (low expression) to red (high expression).

An analysis of 195 colon and rectum adenocarcinoma (TCGA, Nature 2012) on the website <http://www.cbioportal.org/public-portal> showed that 10% of tumours had a modification in *Dusp6*. Interestingly only 50% of these tumours were correlated with *KRas* activation suggesting that *Dusp6* could have a wider spectrum of action. Given our failure to see an impact on *Apc* deletion, it is possible that *Dusp6* loss could modify those tumours that carry *BRaf* mutation. I am currently testing this hypothesis *in vivo* by intercrossing mice that carry a *BRaf*^{L^{SL}-V600E} allele to the *Dusp6* KO mice.

Despite difficulties in assessing the MAPK pathways *in vivo*, I have shown that *Dusp6* deletion clearly increased cell proliferation and tumour initiation in CRC via a positive effect on the MAPK pathway. It would be interesting to investigate the effects of *Dusp6* deletion followed by Mek inhibition on long term established tumours in order to see if a blockage of the MAPK pathway could induce tumour regression.

Microarray analysis can be analysed in different ways. In this thesis I chose to use the fold change and the resulting Log 2 expression ratio. Given the limited impact of Mek inhibition on *KRas* activated mice, I investigated other ways to analyse microarray data in order to potentially highlight the unexpected effect of *KRas* mutation. Therefore I did another type of analysis called rank product analysis which ranks the genes according to their importance between two groups. I analysed the data of A and AK mice in order to investigate pathways importantly deregulated. The selection of the 1000 most deregulated genes between the two sets of samples established a link between *KRas* activation and metabolism. Indeed the gene selection entered into the IPA network analyser (<https://analysis.ingenuity.com/>) highlighted the importance of drug and amino acid metabolism pathways. The *KRas* activation impact on metabolism is currently investigated by Fatih Ceteci.

21 Dusp6 in Pancreatic tumourigenesis

In the previous chapter I have shown that the effects of *Dusp6* loss were dependent on *KRas* activation. Given that *KRas* activation alone does not initiate colorectal cancer, this suggests that in CRC, *Dusp6* downregulation may occur at late stages in tumourigenesis. I therefore decided to test the role of *Dusp6* in Pancreatic Cancer (PCs) as *KRas* mutations are the initiating event in nearly all PCs (Smit, Boot et al. 1988; Hingorani, Petricoin et al. 2003). Moreover *Dusp6* expression appears to be upregulated in dysplastic cells of the pancreatic ducts which are thought to be precursor lesions of the invasive pancreatic ductal adenocarcinoma (PDAC). Importantly, *Dusp6* expression is reduced or abolished in the PDAC suggesting that its downregulation may drive tumour progression (Furukawa, Fujisaki et al. 2005).

The mouse pancreatic model I used combines a pancreatic specific *Cre* recombinase (*PdxCre*) (Gannon, Herrera et al. 2000), with the previously described oncogenic *KRas* allele (*KRas^{LSL-G12D}*). These mice were intercrossed with the *Dusp6* knockout mice (*Dusp6^{-/-}*) provided by Stephen Keyse.

21.1 *Dusp6* loss increases tumourigenesis following *KRas* activation

I generated cohorts of *PdxCre⁺ KRas^{LSL-G12D/+}* mice with or without *Dusp6* and aged them until they developed signs of ill health. The mice predominantly developed pancreatic cancer but also occasionally papillomas, due to the sporadic *Cre* recombinase expression in the skin. At the same time *Cre* expression in the caecum led to intussusceptions, particularly in *PdxCre⁺ KRas^{LSL-G12D/+} Dusp6^{-/-}* mice, due to an increase in goblet cells in the colon as seen in the CRC mouse model.

In this model, in good agreement with the results in the intestinal model, *Dusp6* loss dramatically shortened the disease free survival of the mice developing PC (Figure 63). With the deletion of *Dusp6* the median survival was reduced from 220 days (in *PdxCre⁺ KRas^{LSL-G12D/+}* mice) to 120 days. No significant difference

was observed between $PdxCre^+ KRas^{LSL-G12D/+}$ and $PdxCre^+ KRas^{LSL-G12D/+} Dusp6^{+/-}$ mice.

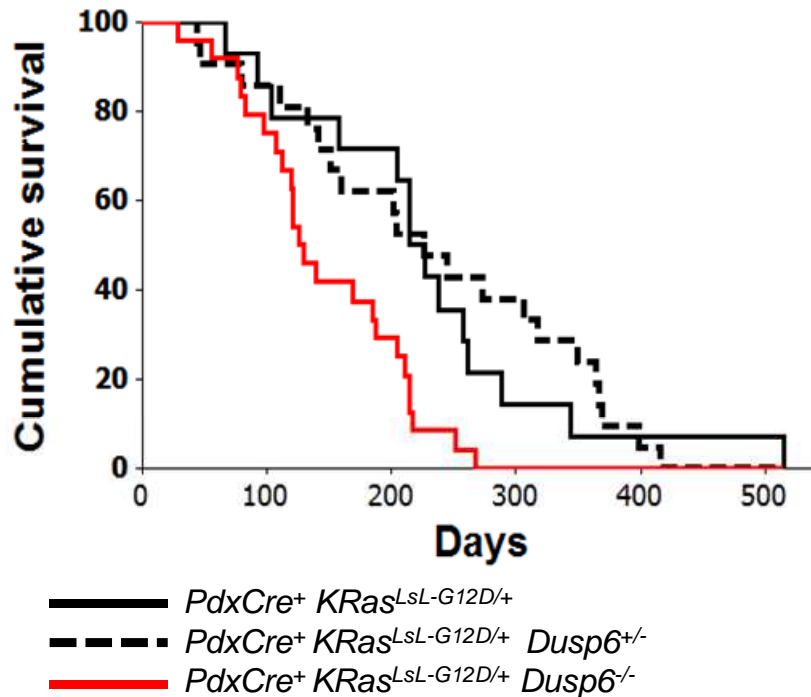


Figure 63: Effects of *Dusp6* deletion on survival in the context of tumourigenesis driven by the $KRas^{LSL-G12D/+}$ allele

Kaplan-Meier curve showing the cumulative survival of $PdxCre^+ KRas^{LSL-G12D/+}$ (black solid line ; n=14), $PdxCre^+ KRas^{LSL-G12D/+} Dusp6^{+/-}$ (black dashed line ; n=21) and $PdxCre^+ KRas^{LSL-G12D/+} Dusp6^{-/-}$ (red solid line ; n=24) mice. Mice with pancreatic tumours were sacrificed at the same point of illness or when they reached 500 days.

The tumour free survival was significantly decrease between both $PdxCre^+ KRas^{LSL-G12D/+}$ and $PdxCre^+ KRas^{LSL-G12D/+} Dusp6^{+/-}$ and $PdxCre^+ KRas^{LSL-G12D/+} Dusp6^{-/-}$ mice (log rank: respectively p=0.006 and p=0.001). No significant difference was found between $PdxCre^+ KRas^{LSL-G12D/+}$ and $PdxCre^+ KRas^{LSL-G12D/+} Dusp6^{+/-}$ mice (log rank: p=0.7).

Within the intestine I showed that *Dusp6* deletion could expand the cell of origin in a MAPK dependent manner. Within PDAC there is discussion whether PDAC originates in the duct or occurs via acini to ductal metaplasia. Interestingly, in our pancreatic cancer model, lesions seemed to be initiated from 2 different cell populations: from the ducts but also from acini which here present a phenotype similar to the panINs, with an accumulation of mucine showed by alcian blue staining (Figure 64). This might indicate that PDACs could be derived from

multiple cells of origin in the background of *Dusp6* deletion. A more careful characterisation of this would be of interest as several contradictory reports have been written regarding the cell of origin of PDAC.

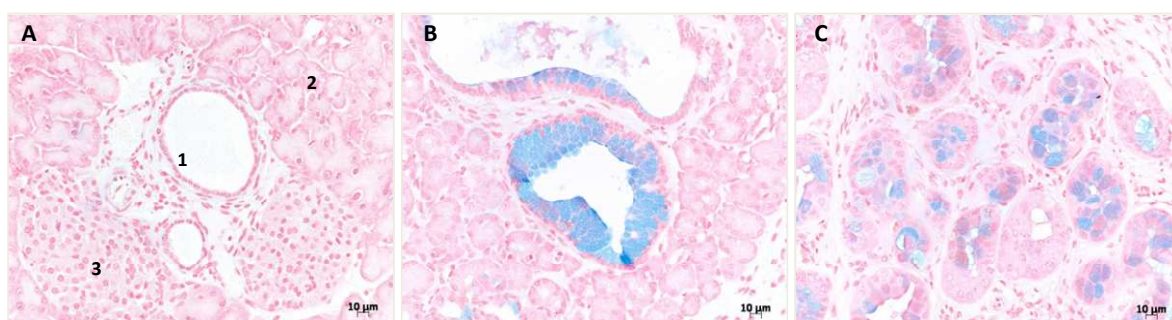


Figure 64: Multiple cells of origin for pancreatic lesions

Paraffin sections of *PdxCre⁺ KRas^{LSL-G12D/+} Dusp6^{-/-}* mouse pancreas representative of all genotypes were stained for alcian blue.

A: Normal pancreatic tissue. 1: Duct, 2: Acini and 3: Islet. **B:** panIN type I (ductal dysplastic pancreatic lesion). An accumulation of mucin in the cells of the duct can be observed. **C:** PanIN like acini lesions with an accumulation of mucin in the cytoplasm.

It has been shown that early panIN lesions undergo senescence in the context of *KRas* activation (Morton, Timpson et al. 2010). *Dusp6* deletion had no effect on the senescence response. IHC for β -galactosidase on pancreas from *PdxCre⁺ KRas^{LSL-G12D/+} Dusp6^{+/+}* and *PdxCre⁺ KRas^{LSL-G12D/+} Dusp6^{-/-}* mice taken at 50 days of age shows that in both genotypes some panIN lesions were senescent (Figure 65). Therefore *Dusp6* deletion is strongly accelerating tumourigenesis in PC and allows lesions to grow from not only the ducts but also the acini. However, it has no effect on the senescence of the PanIN lesions.

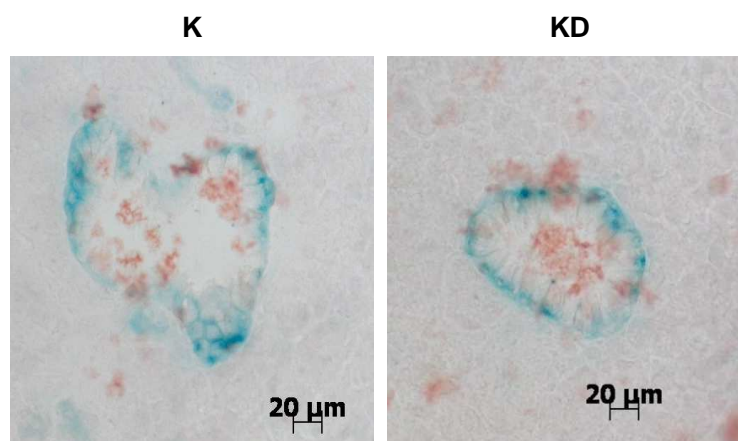


Figure 65: Senescence

Frozen sections of pancreas of *PdxCre*⁺ *KRas*^{LSL-G12D/+} (K) and *PdxCre*⁺ *KRas*^{LSL-G12D/+} *Dusp6*^{-/-} (KD) mouse were stained for β-Galactosidase. No difference was noticed between the two genotypes.

Given the fact that the *KRas*^{LSL-G12V} allele induced tumourigenesis with a longer latency in both the intestine and the pancreas, we wondered if *Dusp6* loss would accelerate a slightly more rapid model of PDAC driven by the *KRas*^{LSL-G12V} allele. The mutation of *p53* occurs in 50% of human PCs. In order to renders the model more aggressive, I choose to add the *p53* mutant allele (*p53*^{LSL-R172H}) to the *PdxCre*⁺ *KRas*^{LSL-G12V/+} mice due to its faculty to mimic the *p53* mutant accumulation in PCs and because of its high metastatic outcome (Olive, Tuveson et al. 2004; Morton, Timpson et al. 2010). In this case *Dusp6* loss results in acceleration of tumourigenesis with *PdxCre*⁺ *KRas*^{LSL-G12D/+} *p53*^{LSL-R172H/+} *Dusp6*^{-/-} mice having a median survival of 170 days compared to 240 days in *PdxCre*⁺ *KRas*^{LSL-G12V/+} *p53*^{LSL-R172H/+} mice (Figure 66).

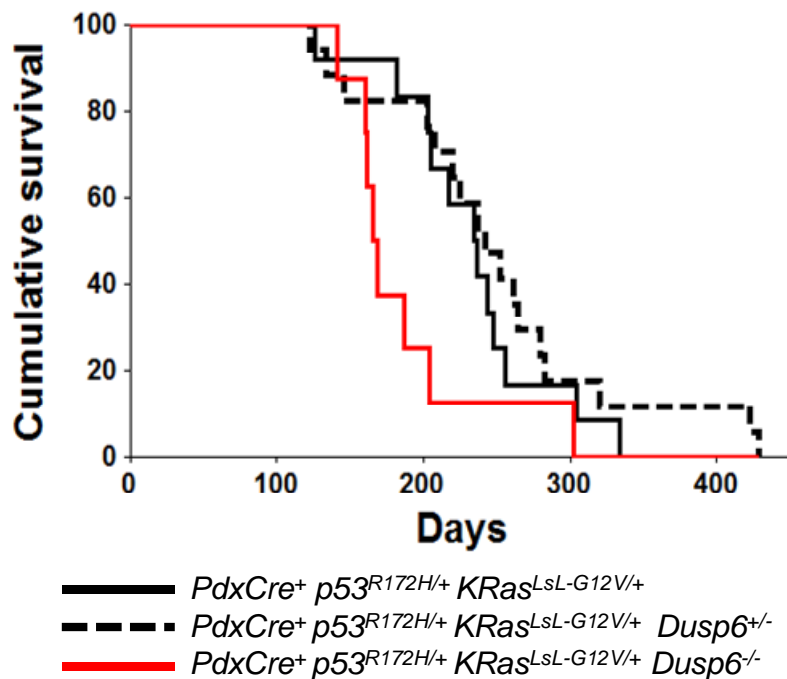


Figure 66: Effects of *Dusp6* loss on survival in the context of tumourigenesis driven by the *KRas^{LSL-G12V/+}* allele

Kaplan-Meier curve showing the cumulative survival of *PdxCre⁺ p53^{R172H/+} KRas^{LSL-G12V/+}* (black solid line ; n=12), *PdxCre⁺ p53^{R172H/+} KRas^{LSL-G12V/+} Dusp6^{+/-}* (black dashed line ; n=17) and *PdxCre⁺ p53^{R172H/+} KRas^{LSL-G12V/+} Dusp6^{-/-}* (red solid line ; n=8) mice. Mice with pancreatic tumours were sacrificed at the same point of illness or when they reached 500 days. The tumour free survival was significantly decrease between both *PdxCre⁺ p53^{R172H/+} KRas^{LSL-G12V/+}* and *PdxCre⁺ p53^{R172H/+} KRas^{LSL-G12V/+} Dusp6^{+/-}* and *PdxCre⁺ p53^{R172H/+} KRas^{LSL-G12V/+} Dusp6^{-/-}* mice (log rank: p=0.04). No significant difference was found between *PdxCre⁺ p53^{R172H/+} KRas^{LSL-G12V/+}* and *PdxCre⁺ p53^{R172H/+} KRas^{LSL-G12V/+} Dusp6^{+/-}* mice (log rank: p=0.4).

21.2 *Dusp6* heterozygosity allows the formation of metastases

Although I did not observe a difference in survival between *PdxCre⁺ KRas^{LSL-G12D/+}* and *PdxCre⁺ KRas^{LSL-G12D/+} Dusp6^{+/-}* mice, there was a significant increase in liver metastasis in *PdxCre⁺ KRas^{LSL-G12D/+} Dusp6^{+/-}* mice (Figure 68-Table). Indeed almost 35% of the *Dusp6* heterozygote mice developed liver metastases while only 18% of the *PdxCre⁺ KRas^{LSL-G12D/+}* and 9.5% of *PdxCre⁺ KRas^{LSL-G12D/+} Dusp6^{-/-}* mice did. Here the loss of one copy of *Dusp6* clearly contributes to invasion. Intriguingly the mice which had lost both copies of *Dusp6* developed very few metastatic tumours. This phenomenon could be explained by the rapid

tumourigenesis exhibited by the *PdxCre*⁺ *KRas*^{LSL-G12D/+} *Dusp6*^{-/-} mice which result in large primary tumours often blocking the intestine and therefore showing quickly signs of ill health. This shorter latency may have not allowed enough time to develop invasive tumours. TGF β signalling has been reported in several studies to be involved in tumour progression and invasion in late stages of tumourigenesis (for review : Millet and Zhang 2007; Tarasewicz and Jeruss 2012). Interestingly a positive staining for phospho-mothers against decapentaplegic homolog 3 (pSmad3) in lesions of the three genotypes suggested the activation of the TGF β signalling pathway (Figure 67). However the TGF β signalling status needs more investigation to determine if there was a pSmad3 increase in the *PdxCre*⁺ *KRas*^{LSL-G12D/+} *Dusp6*^{+/-} mice and if it was linked to the increase seen in invasion.

The liver metastases found in *PdxCre*⁺ *KRas*^{LSL-G12D/+} *Dusp6*^{+/-} mice were confirmed to originate from the pancreatic tumour by a positive Pdx-1 staining. An IHC for Mcm2 (a protein essential to the replication process) showed that these lesions were highly proliferative (Figure 68-IHCs). Finally these metastases had an increase in MAPK pathway activation as showed by pErk positive staining (Figure 68). This finding was the first evidence of MAPK cascade activation following *Dusp6* deletion.

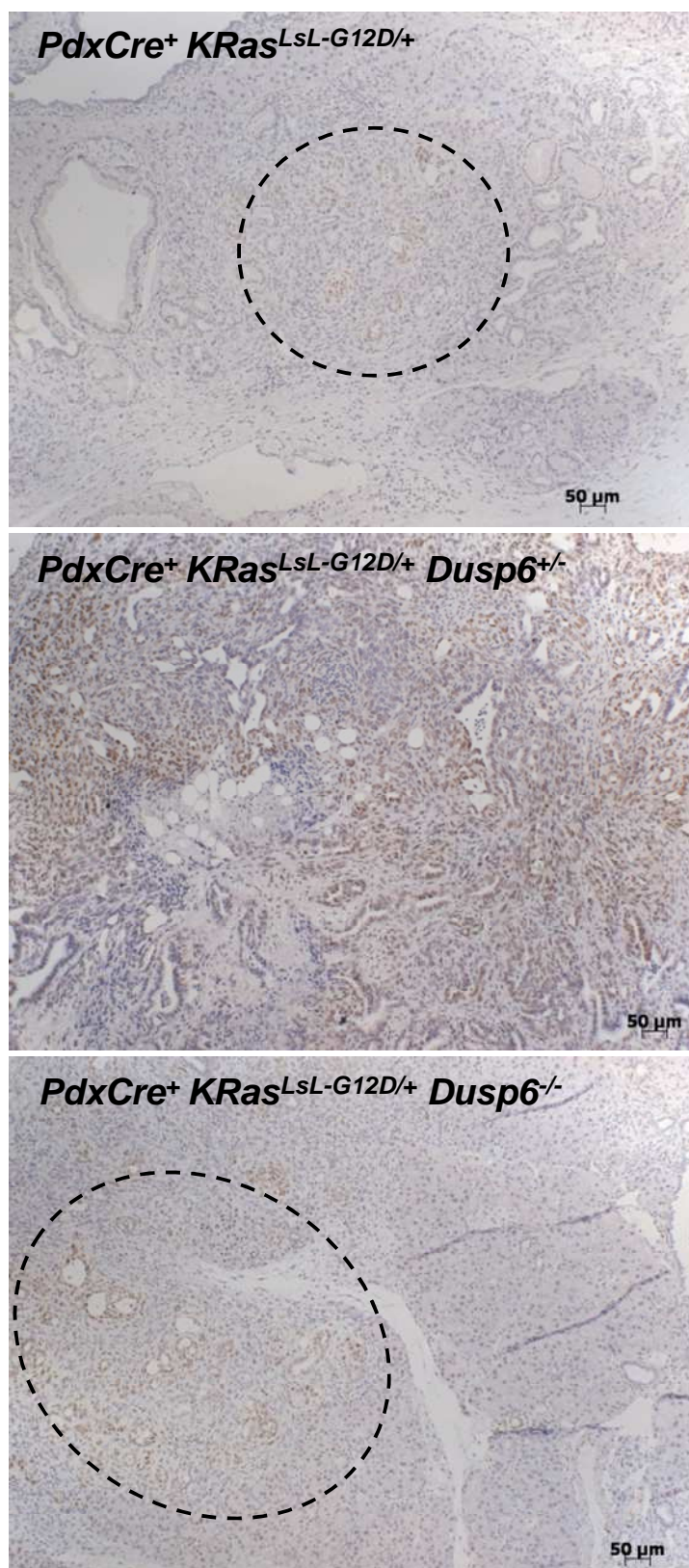


Figure 67: Activation of the TGFβ pathway

Paraffin sections of pancreas were stained for pSmad3.

In the three genotypes, a positive staining for pSmad3 were observed in pancreatic lesions.

	Dusp6 +/+	Dusp6 +/-	Dusp6 -/-
Mice with liver mets. / total mice	3/17	8/23	2/21
Percentage of mice developping mets.	17.60%	34.80%	9.50%
Age at death with mets. (days)	227 to 500	151 to 399	215 to 307

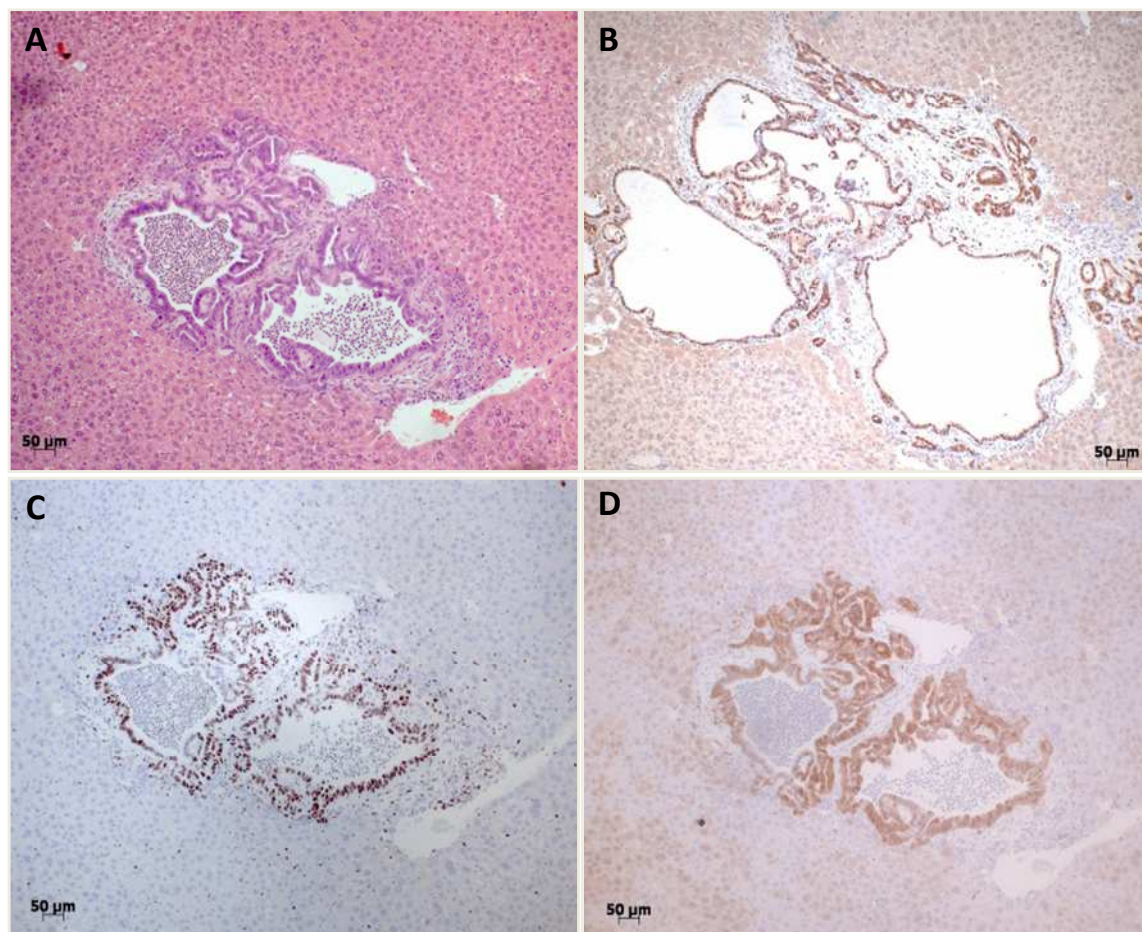


Figure 68: Liver metastasis

Table: H&E stained liver from mice sacrificed due to pancreatic cancer were analysed and the mice presenting liver metastasis was scored.

There is an increase in formation of metastasis in the liver in *PdxCre*⁺ *KRas*^{LSL-G12D/+} *Dusp6*^{+/-} mice compared to the two other genotypes.

IHCs: Paraffin sections of liver from a *PdxCre*⁺ *KRas*^{LSL-G12D/+} *Dusp6*^{+/-} mouse were stained for H&E (A), Pdx-1 (B), MCM2 (C) and pErk (D).

The lesion seen on H&E is confirmed to come from a primary tumour in the pancreas with its positive staining for Pdx-1 (B). This lesion is positive for MCM2 (part of the DNA replication helicase complex) showing hyper proliferation (C) and has an activation of Erk (D). Taken together these data allow us to confirm the presence of metastases in the liver in *PdxCre*⁺ *KRas*^{LSL-G12D/+} *Dusp6*^{+/-} mice.

In order to assess the capacity of 3D invasion of PDAC cells from *PdxCre*⁺ *KRas*^{LSL-G12D/+} and *PdxCre*⁺ *KRas*^{LSL-G12D/+} *Dusp6*^{+/-} mice I performed with the help of Paul Timpson, an organotypic assay. To do so I first cultured cells from PDACs, then placed the cells on a 3D matrix of fibroblasts imbedded in rat collagen which was in turn placed on a stainless steel grid. This grid was then placed in a plate with enough medium to touch the bottom of the matrix but not submerging it creating a gradient of nutrients. The cells attracted by the nutrient gradient and in capability to invade are then starting to move towards the bottom of the 3D matrix. Invading cells were visualised with a pan-cytokeratin AE1/AE3 staining specific for epithelial cells. Surprisingly both genotypes were able to invade through the matrix (Figure 69). However it is interesting to note the phenotypical difference between the invasion of cells derived from lesions from *PdxCre*⁺ *KRas*^{LSL-G12D/+} and *PdxCre*⁺ *KRas*^{LSL-G12D/+} *Dusp6*^{+/-} mice. Indeed, the cells with wild-type *Dusp6* showed a collective invasion forming cell clusters in a shape of a duct. In cells from *Dusp6* heterozygote mice the invasion was similar to a mesenchymal migration with elongated cells invading further in the 3D matrix. This observation may indicate that the linear invasion exhibited by the *Dusp6* haploinsufficient cells may be more efficient for metastasis formation than cluster invasion. Interestingly, treatment with a Mek inhibitor (CI1040 500nM) changed the invasion mechanism from linear to collective cluster in *PdxCre*⁺ *KRas*^{LSL-G12D/+} *Dusp6*^{+/-} mice.

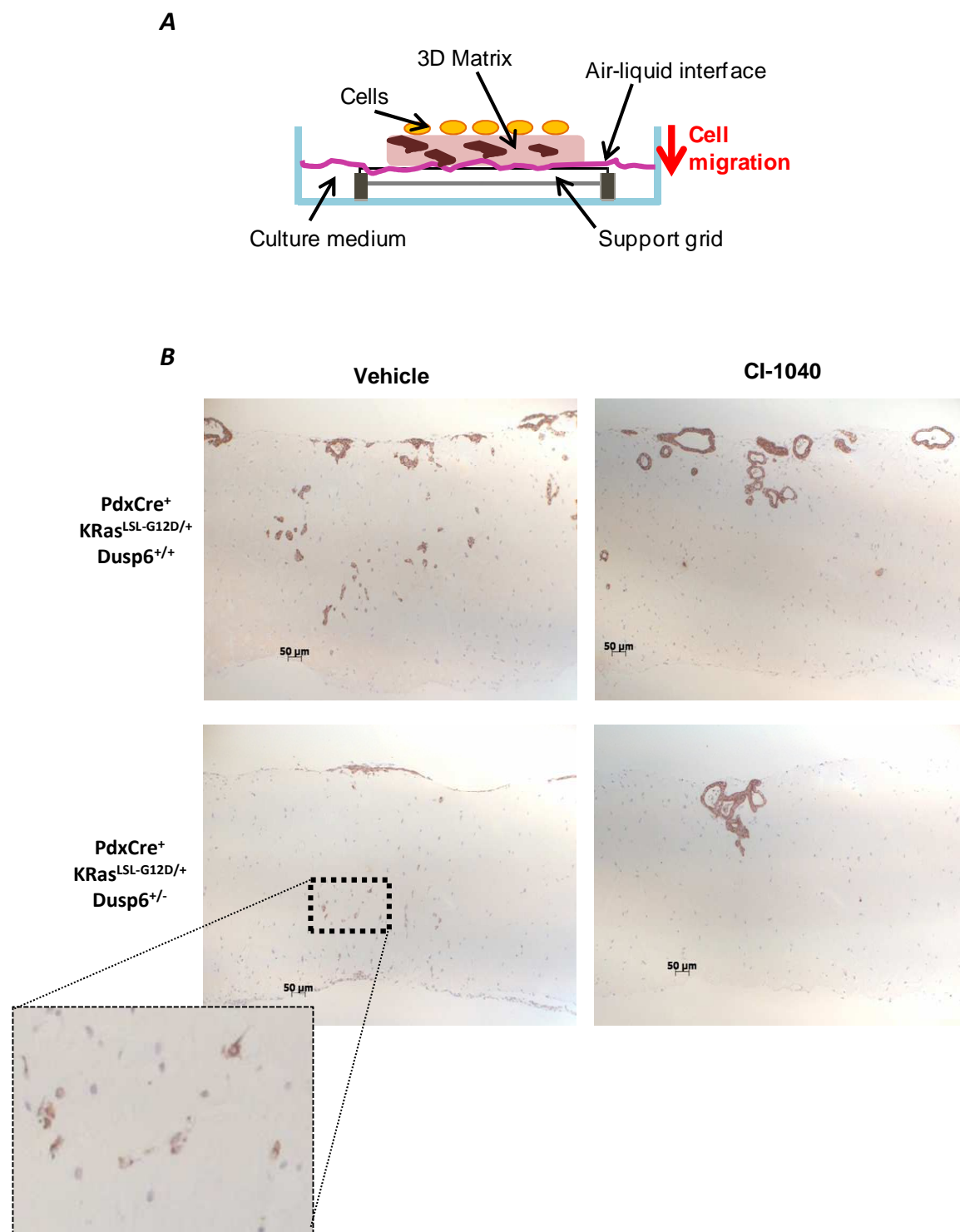


Figure 69: Organotypic assay

A: The organotypic assay system

B: Cultured PDAC cells from *PdxCre⁺ KRas^{LSL-G12D/+}* (top panel) and *PdxCre⁺ KRas^{LSL-G12D/+} Dusp6^{+/-}* (bottom panel) were put on top of a fibroblast matrix placed on a grid. Only the bottom of the matrix touched the culture medium creating a nutrient gradient. The cells were culture with a CI1040 treatment or its vehicle.

The fibroblast 3D matrix was embedded in paraffin and then sections were stained for pan-cytokeratin AE1/AE3.

21.3 Effects of *Dusp6* deletion on MAPK pathway

21.3.1 Erk activation is independent of *Dusp6* status

Activation of Erk is a key event in tumourigenesis and the loss of *Dusp6* could be one of the mediators of this activation. In order to prove this hypothesis, I have stained sections for pErk and pMek from mice with premalignant lesions at day 35 and day 60 (Figure 70), as well as mice with pancreatic cancer (Figure 71). Interestingly, there seems to be an activation of Erk in both the early lesions and PDAC irrespective of *Dusp6* status. However, this finding will need further investigation as, as previously mentioned, these IHC are not powerful enough to highlight possible subtle differences.

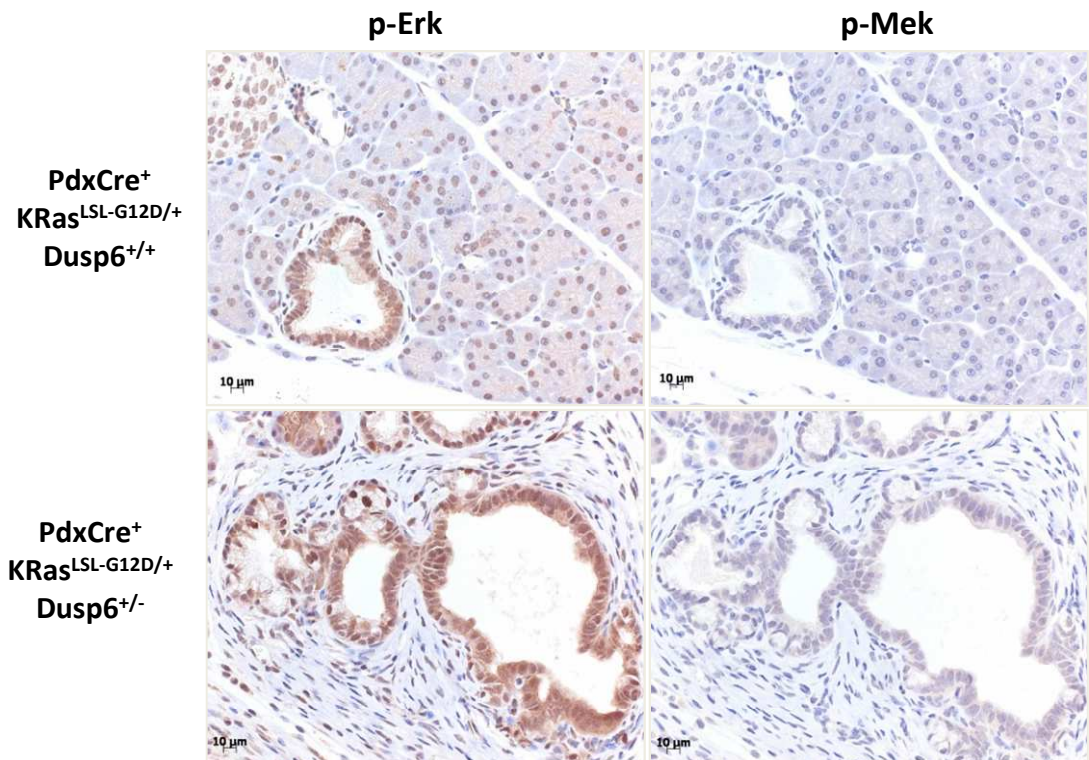


Figure 70: Activation of Erk in early pancreatic lesions

Paraffin sections of pancreas from *PdxCre⁺ KRas^{LSL-G12D/+}* (upper panel) and *PdxCre⁺ KRas^{LSL-G12D/+} Dusp6^{-/-}* mice (bottom panel). Mice taken at 35 days of age were stained for pErk (left panel) and pMek (right panel).

An activation of Erk but no activation of Mek can be observed in the lesions from the two genotypes.

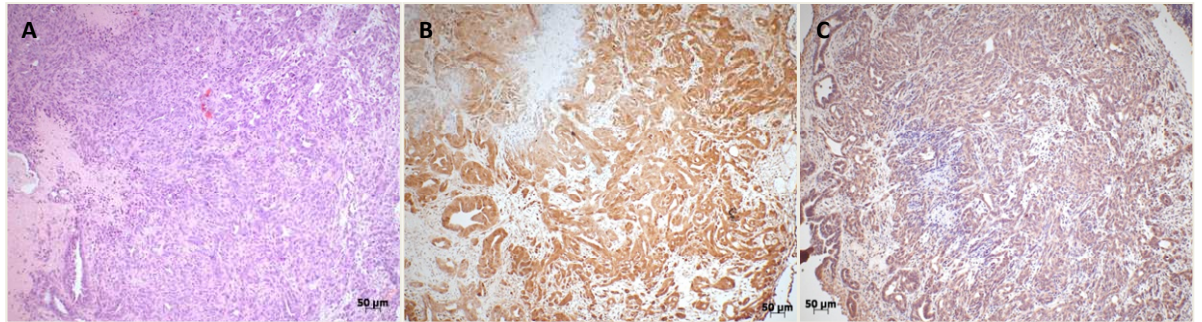


Figure 71: PDAC characteristics

Paraffin sections of a representative PDAC from *PdxCre⁺ KRas^{LSL-G12D/+} Dusp6^{+/-}* mice were stained for H&E (A), pErk (B), pMek (C).

21.3.2 Effect of Mek inhibition on tumourigenesis

Finally I assessed the impact of Mek inhibition on tumourigenesis. To do so I performed an allograft experiment on CD1-nude mice where cultured PDAC cells from *PdxCre⁺ KRas^{LSL-G12D/+}*, *PdxCre⁺ KRas^{LSL-G12D/+} Dusp6^{+/-}* and *PdxCre⁺ KRas^{LSL-G12D/+} Dusp6^{-/-}* mice were implanted subcutaneously. At day 3 after cell implantation, we started the treatment with 200mg/Kg CI1040 or vehicle daily. The PDAC cells from *PdxCre⁺ KRas^{LSL-G12D/+} Dusp6^{-/-}* mice grow faster than cells from *PdxCre⁺ KRas^{LSL-G12D/+}* or *PdxCre⁺ KRas^{LSL-G12D/+} Dusp6^{+/-}*. Treatment with the Mek inhibitor resulted in an important tumour growth reduction especially in the *Dusp6* deleted mice (Figure 72). This confirmed the MAPK pathway activation within these pancreatic cancer models. However none of the nude mice presented liver or other organ metastasis.

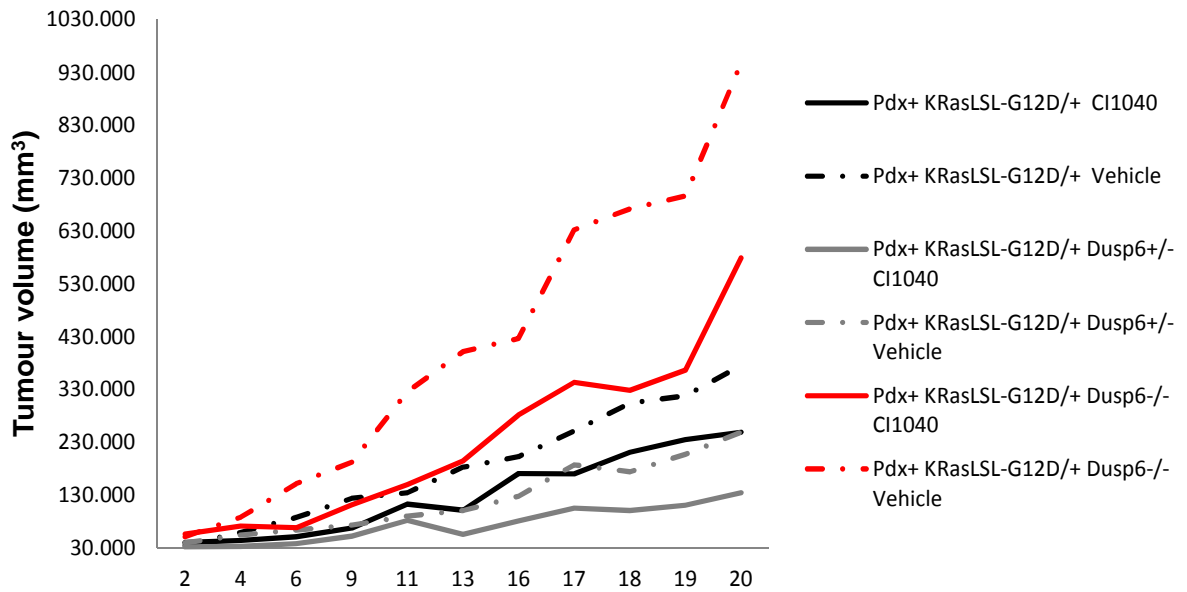


Figure 72: Allograft experiment

Nude mice were injected subcutaneously with cultured PDAC cells from *PdxCre⁺ KRas^{LSL-G12D/+}*, *PdxCre⁺ KRas^{LSL-G12D/+} Dusp6^{+/-}* and *PdxCre⁺ KRas^{LSL-G12D/+} Dusp6^{-/-}* mice. The tumours were measured every other day and the mice were sacrificed when the tumour reached 1.5cm or when they ulcerated.

Statistics were calculated with the help of a method created by Russell Thompson and Gordon Smyth using the T-Test to determine the p-values between two curves: <http://bioinf.wehi.edu.au/software/compareCurves/>.

p-values obtained after 10000 random sampling steps	
<i>PdxCre⁺ KRas^{LSL-G12D/+} unt.</i> vs CI1040	0.003
<i>PdxCre⁺ KRas^{LSL-G12D/+} Dusp6^{+/-} unt.</i> vs CI1040	< 0.0001
<i>PdxCre⁺ KRas^{LSL-G12D/+} Dusp6^{-/-} unt.</i> vs CI1040	0.0001
<i>PdxCre⁺ KRas^{LSL-G12D/+}</i> vs <i>PdxCre⁺ KRas^{LSL-G12D/+} Dusp6^{+/-}</i>	< 0.0001
<i>PdxCre⁺ KRas^{LSL-G12D/+}</i> vs <i>PdxCre⁺ KRas^{LSL-G12D/+} Dusp6^{-/-}</i>	0.0004
<i>PdxCre⁺ KRas^{LSL-G12D/+} Dusp6^{+/-}</i> vs <i>PdxCre⁺ KRas^{LSL-G12D/+} Dusp6^{-/-}</i>	< 0.0001

These results taken together showed an activation of the MAPK cascade as well as a potential TGF β pathway in the pancreatic cancer model independently of the *Dusp6* status. However, *Dusp6* deletion is strongly accelerating tumorigenesis. Furthermore, the loss of one copy of *Dusp6* is contributing to invasion. This implies that *Dusp6* loss exacerbate the effects of *KRas* deletion in the pancreas. Our finding that tumours are responsive to Mek inhibition could suggest that it is the activation of Wnt signalling in combination with *KRas* mutation that leads to a resistance of Mek inhibition. This is suggested by a

recent paper by the Barbacid group (Navas, Hernandez-Porrás et al. 2012). They showed that loss of EGFR protected the pancreas from *KRas* driven carcinogenesis but not the intestine from *Apc* and *KRas* driven tumorigenesis. However as established PC only poorly responds to EGFR mediated therapy it suggests other mutations occur during pancreatic carcinogenesis that removes the dependency on the MAPK pathway.

22 The role of *Fra1* in two *in vivo* cancer models – a paradox

Fos related antigen 1 (*Fra1*) also named Fos-l 1, is a member of the Fos family of proteins and is part of the transcription factor activator protein-1 (AP-1). The AP-1 complex has been implicated as a driver of carcinogenesis given that it regulates cellular processes such as proliferation, differentiation and apoptosis (Jochum, Passegue et al. 2001; Young and Colburn 2006). It is a dimer consisting of Jun-Jun homodimers or Jun-Fos heterodimers (Young and Colburn 2006). AP-1 can be activated by the MAPK pathway via ERK, Jun N-terminal Kinase (JNK) and p38 (Jochum, Passegue et al. 2001; Hasselblatt, Gresh et al. 2008). It has been shown that mutations of *Apc* and *KRas* lead to elevated AP-1 activity (Park, Jeon et al. 2006).

Fra1 has been showed to be upregulated in a large variety of tumours including breast, lung, and colon carcinomas (Vial, Sahai et al. 2003; Pollock, Shirasawa et al. 2005; Zhang, Hart et al. 2005; Young and Colburn 2006) . Its transcription is activated by the MAPK pathway but also by the WNT pathway (Mann, Gelos et al. 1999; Young and Colburn 2006; Adisheshaiah, Li et al. 2008). *Fra1* has also been suggested to be essential for invasion (Adisheshaiah, Vaz et al. 2008) and to be a major transcriptional target following *KRas* activation (Mark, Aubin et al. 2008). Furthermore, we confirmed the upregulation of its expression following *Apc* loss and *KRas* activation (Figure 34). All of these studies suggested that *Fra1* should provide an advantage in tumourigenesis following *Apc* loss. We therefore hypothesized that its deletion would decrease tumourigenesis in our *in vivo* models.

22.1 *Fra1* deletion impacts on intestinal homeostasis

To address the effects of *Fra1* deletion in the intestine the *AhCre*⁺ mouse model was intercrossed with the conditional floxed allele of *Fra1* (*Fra1*^{fl}). I then investigated the effects of *Fra1* deletion on cell differentiation scoring the total number of entero-endocrine and Goblet cells and examining the position of Paneth cells (Figure 73). For the three cell types, no changes were observed following *Fra1* loss.

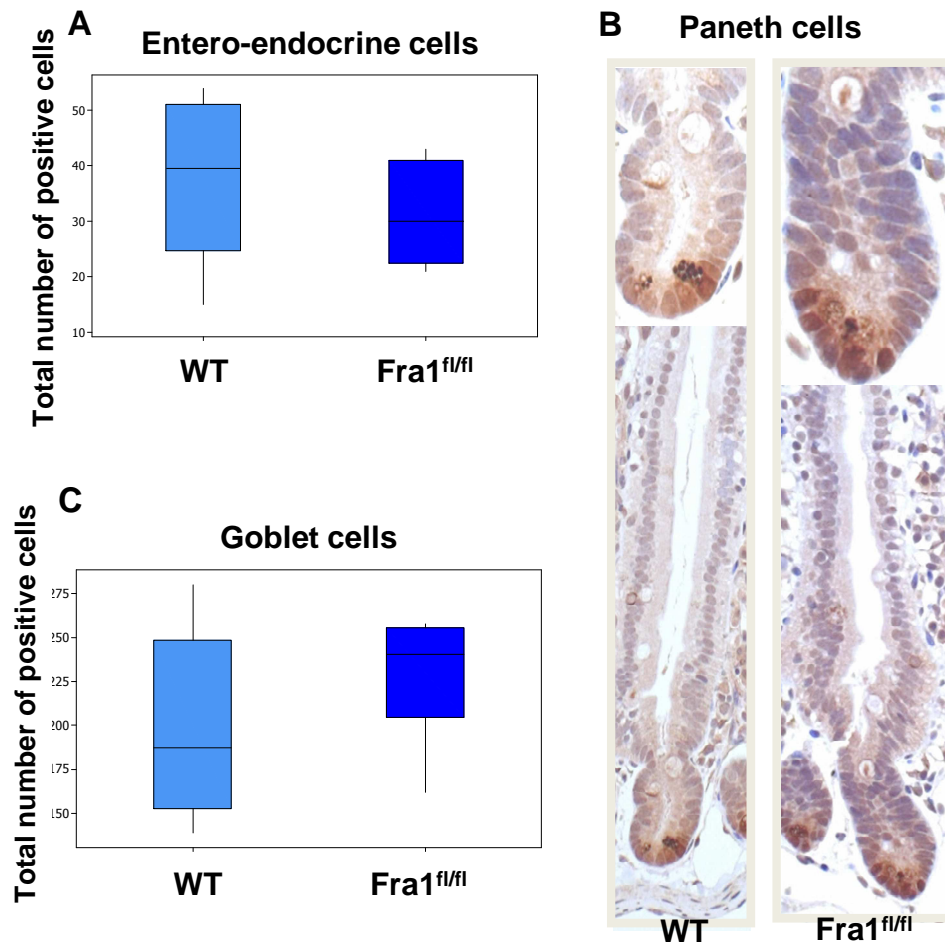


Figure 73: *Fra1* deletion does not affect differentiation

AhCre⁺ (WT) and *AhCre*⁺ *Fra1*^{fl/fl} (*Fra1*^{fl/fl}) mice were taken at day 4 after *Cre* recombinase induction. Histochemistry specific for entero-endocrine cells, Paneth cells, and goblet cells were performed and total number of entero-endocrine (A) and Goblet cells (C) were scored. Pictures of Paneth cells were taken to assess cells position (B). No difference was observed between the two genotypes (*p* value > 0.05 calculated with a Mann Whitney test).

To investigate the effects of *Fra1* deletion on proliferation, I performed a 24 hours and 48 hours BrdU labeling experiment on mice at day four after *Cre* recombinase induction. Whilst *Fra1* deletion had no impact on differentiation, it significantly increased the number of BrdU positive cells observed at days 5 and 6 post *Cre* recombinase induction following 24 and 48 hours BrdU labelling (Figure 74). Therefore this increase in proliferation following *Fra1* deletion was in contradiction with the expected *Fra1* role. In order to quantify mitosis in the gut epithelium, I performed a phospho histone H3 (pH3) IHC, a mitotic marker, on *AhCre*⁺ *Fra1*^{fl/fl} mice taken at day four after *Cre* recombinase induction. I

observed an upregulation of the mitosis following *Fra1* loss (Figure 75). The upregulation of BrdU staining together with the upregulation of pH3 suggests an increase in cell proliferation following *Fra1* loss alone.

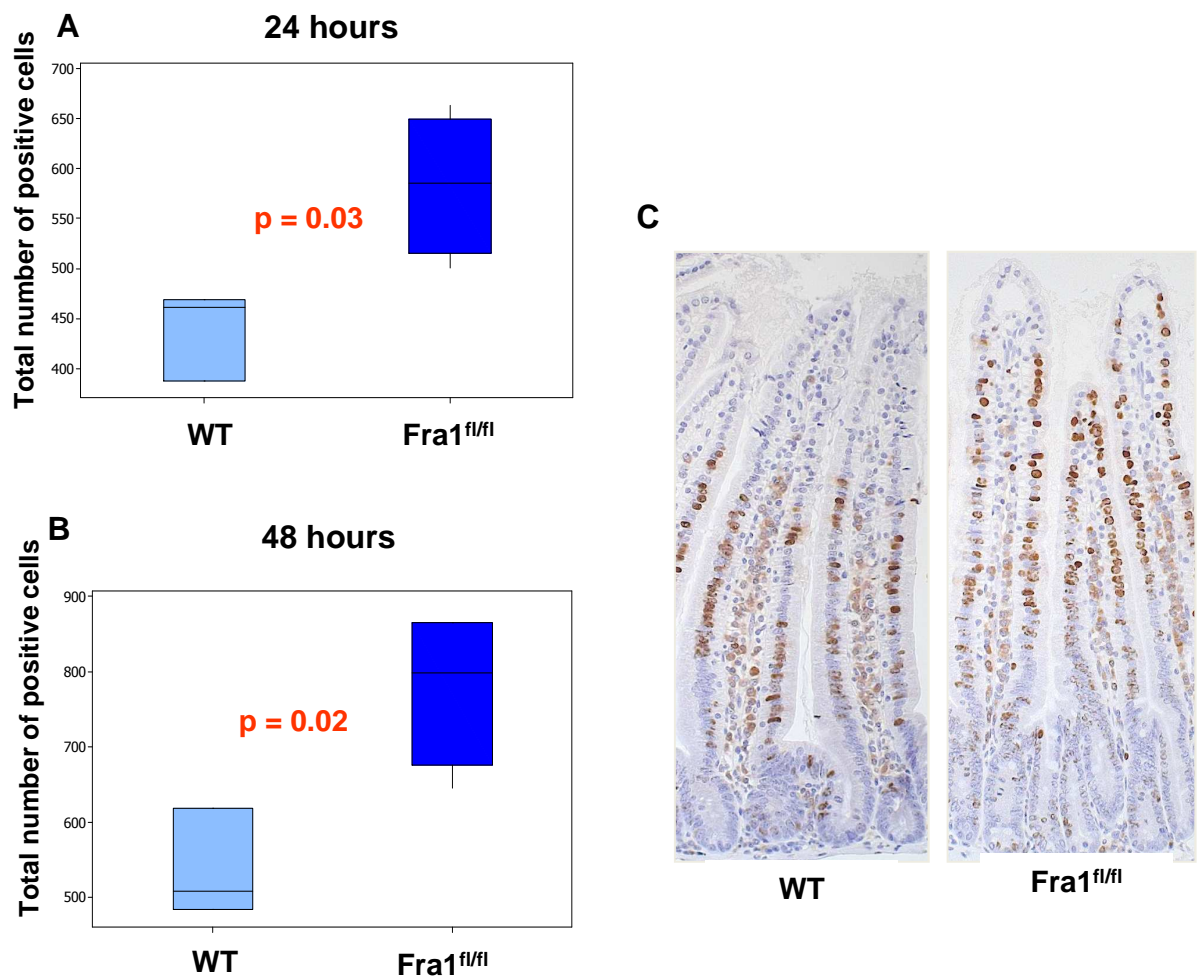


Figure 74: *Fra1* deletion affects proliferation

AhCre⁺ (WT) and *AhCre*⁺ *Fra1*^{fl/fl} (*Fra1*^{fl/fl}) mice were taken at day 5 and 6 after Cre recombinase induction and a BrdU labelling of 24 hours (A) or 48 hours (B and C).

IHC for BrdU was performed in order to highlight cells in S phase of the cell cycle. There were significantly more cells in S phase after *Fra1* deletion (p values = 0.03 (A) and 0.02 (B) calculated with a Mann Whitney test). This difference is illustrated by the IHC for BrdU of mice labelled for 48 hours (C).

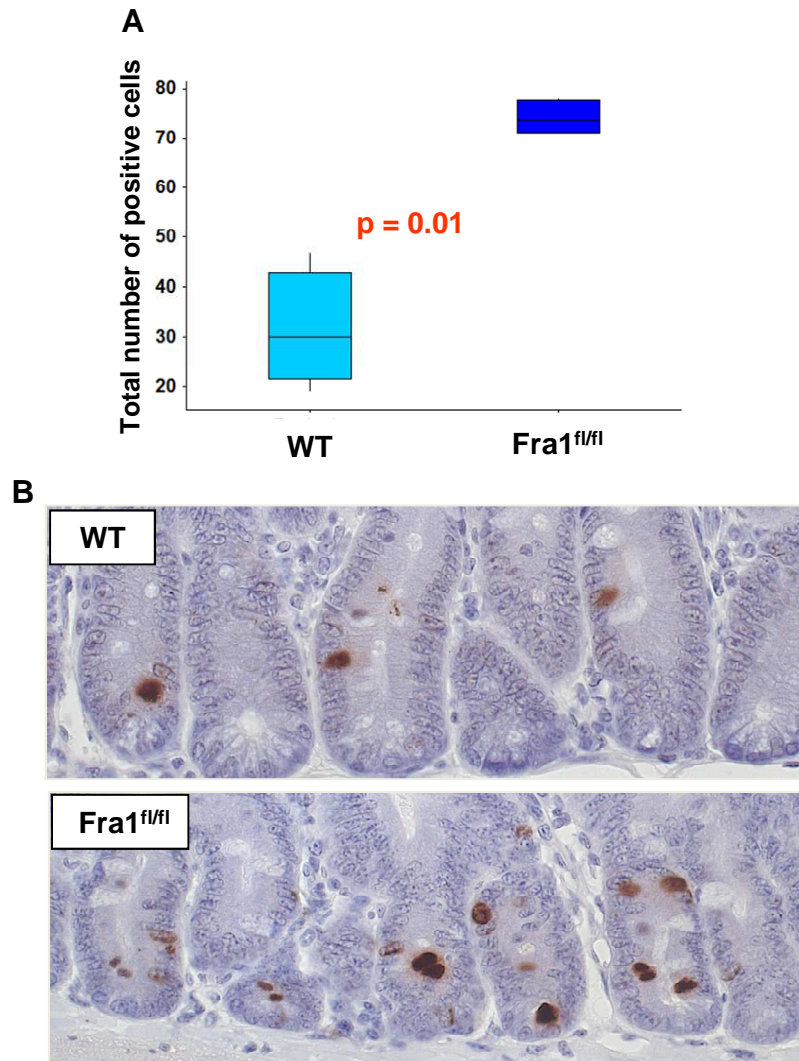


Figure 75: *Fra1* deletion affects mitosis

AhCre⁺ (WT) and *AhCre*⁺ *Fra1^{fl/fl}* (*Fra1^{fl/fl}*) mice were taken at day 4 after *Cre* recombinase induction. IHC for the mitotic marker phospho histone H3 (pH3) was performed in order to highlight cells in mitosis.

A: I quantified the total number of pH3 positive cells. There were significantly more mitotic cells after *Fra1* deletion (p values = 0.02) (calculated with a Mann Whitney test).

B: The IHC for pH3 on WT (upper panel) and *Fra1* deleted mice illustrated the increase in mitosis following *Fra1* loss.

22.2 Fra1 deletion can accelerate tumourigenesis

22.2.1 The effect of Fra1 deletion following *Apc* deletion

In order to investigate the impact of *Fra1* deletion on the mitotic index in the context of acute *Apc* deletion, I performed a pH3 IHC on *AhCre*⁺ *Apc*^{fl/fl} *Fra1*^{fl/fl} mice taken at day four after *Cre* recombinase induction. I observed a similar increase in mitosis as previously described in the wildtype mice which had lost *Fra1* (Figure 76).

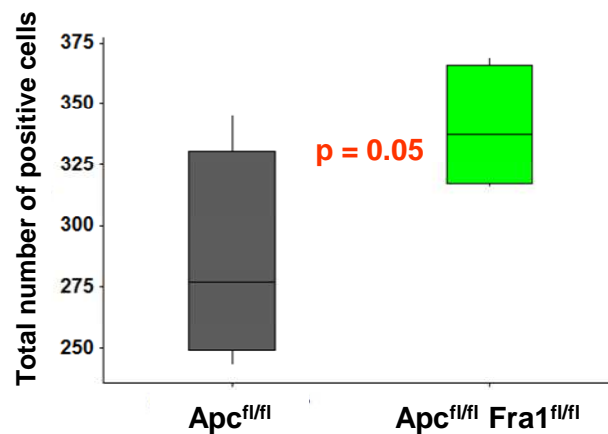


Figure 76: *Fra1* deletion affects mitosis

AhCre⁺ *Apc*^{fl/fl} (*Apc*^{fl/fl}) and *AhCre*⁺ *Apc*^{fl/fl} *Fra1*^{fl/fl} (*Apc*^{fl/fl} *Fra1*^{fl/fl}) mice were sacrificed at day 4 after *Cre* recombinase induction. An IHC for the mitotic marker phospho histone H3 (pH3) was performed in order to highlight cells in mitosis.

The total number of pH3 positive cells was quantified. Following *Apc* deletion *Fra1* loss increased the number of cells in mitosis (Mann Whitney: p value = 0.05).

In order to confirm the surprising positive impact on proliferation and possibly on tumourigenesis, we decided to investigate the impact of *Fra1* deletion on tumourigenesis. This work has been done by Rachel Ridgway. It is important to note that at this time, the *Villin Cre* system was not available in the laboratory hence the use of the alternative intestinal *Cre* system namely *AhCre*. *AhCre*⁺ *Apc*^{fl/+} and *AhCre*⁺ *Apc*^{fl/+} *Fra1*^{fl/fl} mice were aged until they showed signs of

intestinal illness. This experiment confirmed the results previously found in the acute *Apc* deletion model: following the loss of one copy of *Apc*, *Fra1* deletion decreased significantly the tumour free survival from a median of 180 in the presence of *Fra1* to 150 days without *Fra1* (Figure 77).

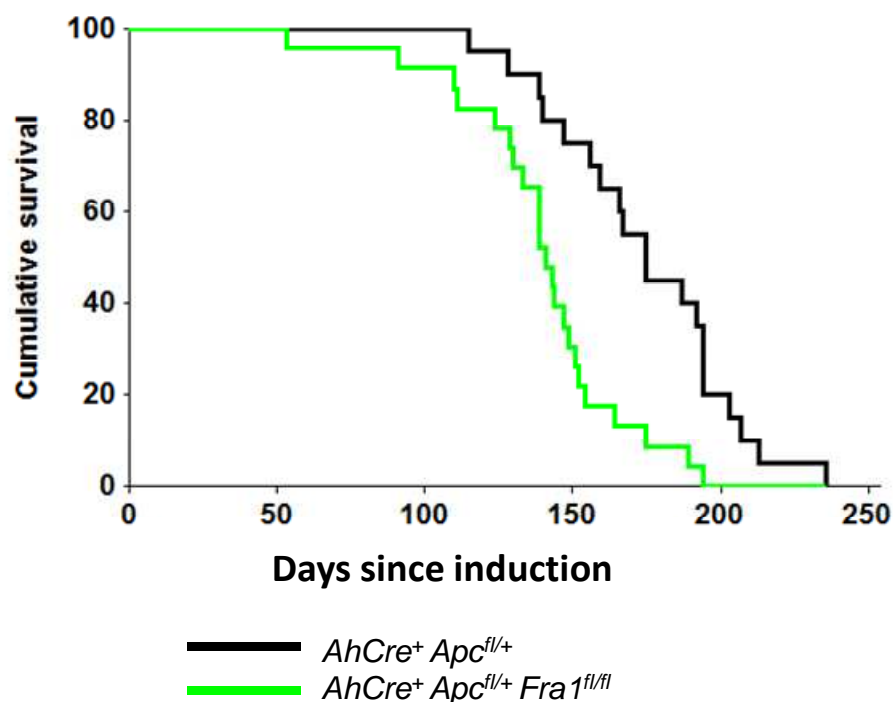


Figure 77: *Fra1* deletion decreases survival

Kaplan-Meier curve showing the cumulative survival of *AhCre⁺ Apc^{fl/+}* (black line) (n=20) and *AhCre⁺ Apc^{fl/+} Fra1^{fl/fl}* mice (green line) (n=23). Mice with intestinal tumours were sacrificed at the same point of illness.

The loss of the two copies of *Fra1* resulted in a reduction of the tumour free survival compared to *AhCre⁺ Apc^{fl/+}* mice (log rank: $p < 0.001$).

In good agreement with the results found on gut homeostasis after *Fra1* deletion and the increased proliferation due to *Fra1* in the acute *Apc* deletion model, *Fra1* seems to act as a tumour suppressor gene as its deletion reduces the tumour free survival in the aging model.

22.2.2 *Fra1* deletion in the context of *KRas* activation

Given the finding of my previous chapter where the mutation of *KRas* revealed the strong phenotypes of *Dusp6* deletion, I predicted that *KRas* mutation might alter the role plays into tumourigenesis switching it from a tumour suppressive role to the expected tumour promoter. Thus I decided to additionally examine the impact of *KRas* mutation on the phenotype of *Fra1* deletion.

Therefore in collaboration with Rachel Ridgway, we aged *AhCre*⁺ *Apc*^{fl/+} *KRas*^{LSL-G12V/+}, *AhCre*⁺ *Apc*^{fl/+} *KRas*^{LSL-G12V/+} *Fra1*^{fl/+} and *AhCre*⁺ *Apc*^{fl/+} *KRas*^{LSL-G12V/+} *Fra1*^{fl/fl} mice. The *AhCre* system induces recombination in the epithelium but also in kidney therefore, it is not compatible with the *KRas*^{LSL-G12D} allele as this particular allele results in kidney failure leading to death soon after birth; this is why we crossed the *KRas*^{LSL-G12V} allele to these mice. In this model, *KRas* activation did not alter the effect of *Fra1* loss on tumourigenesis in the context of *Apc* loss. Indeed, the *Fra1* deleted mice had a reduction in their median tumour free survival from 100 to 70 days compared with mice retaining *Fra1* (Figure 78). It is important to note that the loss of one copy of *Fra1* was sufficient to induce this tumour free survival reduction.

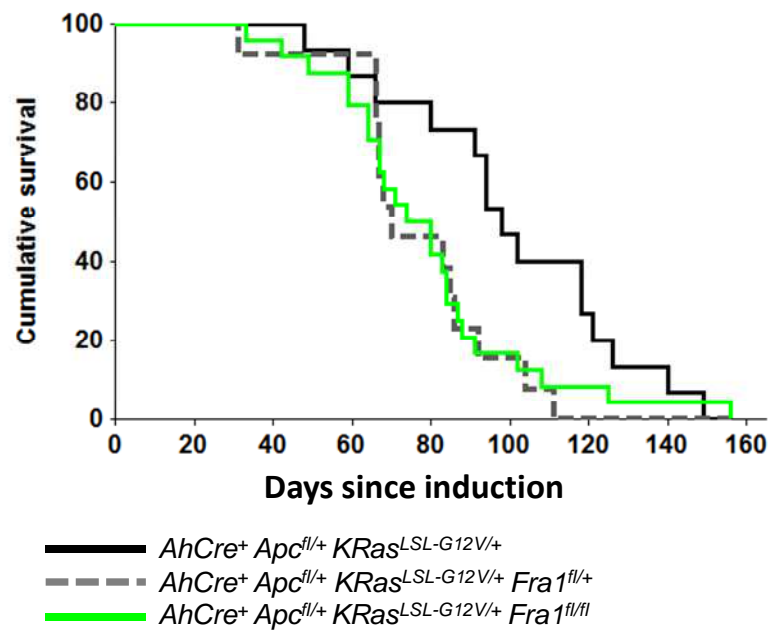


Figure 78: *Fra1* deletion decreases survival

Kaplan-Meier curve showing the cumulative survival of AhCre⁺ Apc^{fl/+} KRas^{LSL-G12V/+} (black line) (n=15), AhCre⁺ Apc^{fl/+} KRas^{LSL-G12V/+} Fra1^{fl/+} (grey dashed line) (n=13), AhCre⁺ Apc^{fl/+} KRas^{LSL-G12V/+} Fra1^{fl/fl} mice (green line) (n=24). Mice with intestinal tumours were sacrificed at the same point of illness.

The loss of one and two copy of *Fra1* resulted in a reduction of the tumour free survival compared to AhCre⁺ Apc^{fl/+} KRas^{LSL-G12V/+} mice (log rank: p=0.008 and p=0.05 respectively). There was no significant difference between the mice which have lost one or two copies of *Fra1* (log rank: p=0.8).

As explained in the introduction, the AhCre model delivers recombination not only in the intestine but also in the liver and constitutive cre expression to kidneys and other tissues. Therefore, as the Villin Cre system is specific to the gut and the KRas^{LSL-G12D} allele is viable when intercrossed to the VillinCreER I next decided to intercross this mouse to the *Fra1* deletion. Once again I obtained similar results to the AhCre system confirming the putative tumour suppressor role of *Fra1* in the intestine (Figure 79). Indeed the loss of both copies of *Fra1* reduced the median tumour free survival from 90 to 60 days. Interestingly, in this model the loss of only one copy of *Fra1* was not sufficient to reduce the tumour free survival. This could be due to the choice of KRas allele. It should be noted the KRas^{LSL-G12D} allele has a stronger impact on tumourigenesis

than the $KRas^{LSL-G12V}$ allele and therefore could mask the potential effect of the loss of one copy of *Fra1*.

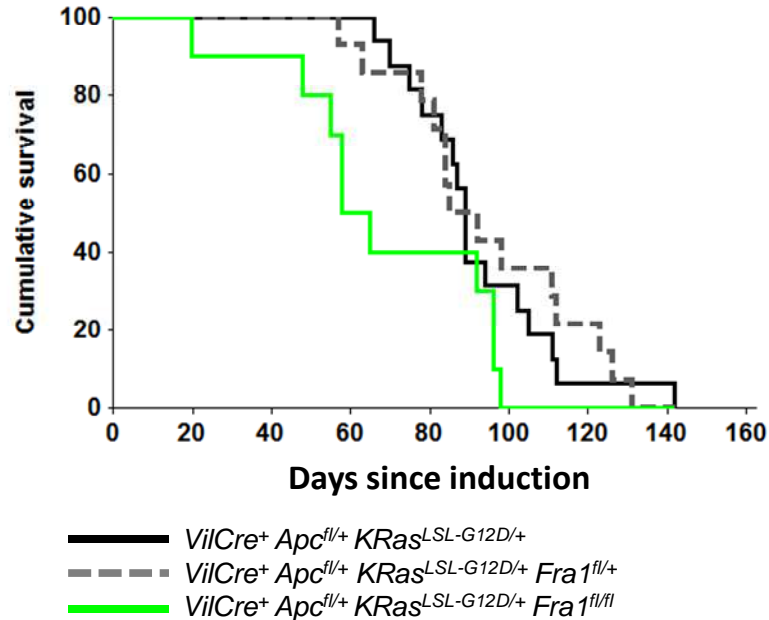


Figure 79: *Fra1* deletion decreases survival

Kaplan-Meier curve showing the cumulative survival of $VilCre^+ Apc^{fl/+} KRas^{LSL-G12D/+}$ (black line) (n=16), $VilCre^+ Apc^{fl/+} KRas^{LSL-G12D/+} Fra1^{fl/+}$ (grey dashed line) (n=14), $VilCre^+ Apc^{fl/+} KRas^{LSL-G12D/+} Fra1^{fl/fl}$ mice (green line) (n=10). Mice with intestinal tumours were sacrificed at the same point of illness.

The loss of the two copy of *Fra1* resulted in a reduction of the tumour free survival compared to both $VilCre^+ Apc^{fl/+} KRas^{LSL-G12D/+} Fra1^{fl/+}$ and $VilCre^+ Apc^{fl/+} KRas^{LSL-G12D/+} Fra1^{fl/fl}$ mice (log rank: p=0.05 and p=0.03 respectively). There was no significant difference with AK mice when only one copy of *Fra1* was lost (log rank: p=0.7).

22.3 *Fra1* deletion can increase tumour free survival

Given these very surprising findings in the intestine, namely that *Fra1* loss accelerated tumourigenesis, I next wished to examine the role of *Fra1* in another *KRas* driven cancer that had been shown to have upregulation of AP-1 complex. Within pancreatic cancer there was good evidence that the AP-1 complex is upregulated (Shin, Asano et al. 2009) and thus, we decided to investigate the impact of *Fra1* deletion in the pancreatic cancer *in vivo* model. To do so we intercrossed mice with the pancreatic specific *Cre* recombinase $PdxCre^+$ with the

oncogenic *KRas* allele, the mutant *p53* allele ($p53^{LSL-R172H}$) and *Fra1*^{fl/fl} mice. In the intestinal mouse model, we investigated the impact of *Fra1* loss in the context of activated *KRas* testing both oncogenic alleles. Therefore we generated two mouse colonies one with with $KRas^{LSL-G12V}$ and another with the $KRas^{LSL-G12D}$ allele. The mice were aged until they showed signs of ill health.

Whereas *Fra1* deletion promoted tumourigenesis in the intestinal model, *Fra1* loss increased the tumour free survival in this model of PDAC (Figure 80). $PdxCre^+ KRas^{LSL-G12V/+} p53^{LSL-R172H/+} Fra1^{fl/fl}$ mice showed signs of pancreatic illness at a latency of around roughly 100 days more than $PdxCre^+ KRas^{LSL-G12V/+} p53^{LSL-R172H/+}$ mice. As in the CRC model, the loss of one or both copies of *Fra1* had the same outcome (median survival of 300 days). A similar reduction in tumour onset was observed in $PdxCre^+ KRas^{LSL-G12D/+} p53^{LSL-R172H/+}$ when *Fra1* was lost (median survival increased from 150 to 220 days). However in this model the loss of one copy of *Fra1* were not sufficient to increase tumour free survival (Figure 81). Once again the use of the $KRas^{LSL-G12D}$ allele induced tumour onset a much faster latency than the $KRas^{LSL-G12V}$ allele.

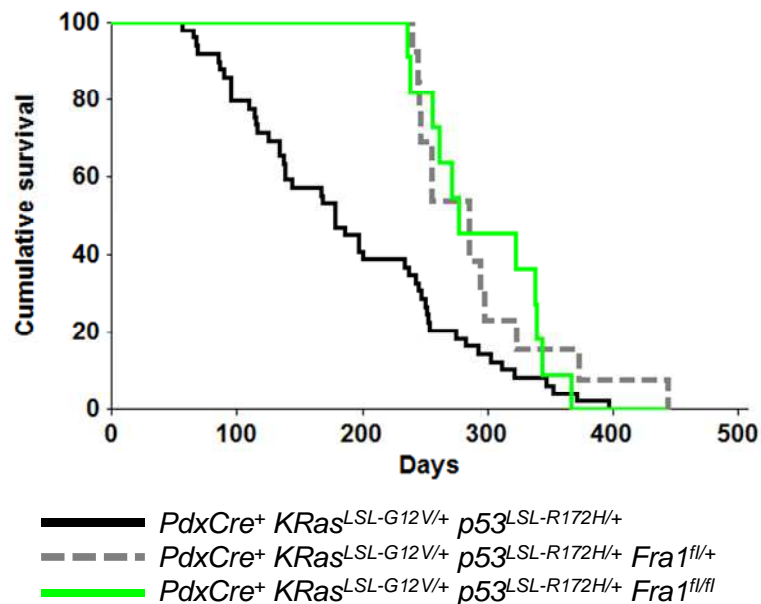


Figure 80: *Fra1* deletion increases survival in a pancreatic cancer model

Kaplan-Meier curve showing the cumulative survival of $PdxCre^+ KRas^{LSL-G12V/+} p53^{LSL-R172H/+}$ (black line) (n=49), $PdxCre^+ KRas^{LSL-G12V/+} p53^{LSL-R172H/+} Fra1^{fl/+}$ (dashed grey line) (n=13) and $PdxCre^+ KRas^{LSL-G12V/+} p53^{LSL-R172H/+} Fra1^{fl/fl}$ mice (green line) (n=11). Mice with pancreatic tumours were sacrificed at the same point of illness or when they reached 500 days after induction.

The loss of one and two copy of *Fra1* resulted in an extension of the tumour free survival compared to *PdxCre⁺ KRas^{LSL-G12V/+} p53^{LSL-R172H/+}* mice (log rank: $p=0.009$ and $p=0.03$ respectively). There was no significant difference between *PdxCre⁺ KRas^{LSL-G12V/+} p53^{LSL-R172H/+} Fra1^{fl/+}* and *PdxCre⁺ KRas^{LSL-G12V/+} p53^{LSL-R172H/+} Fra1^{fl/fl}* mice (log rank: $p=0.9$).

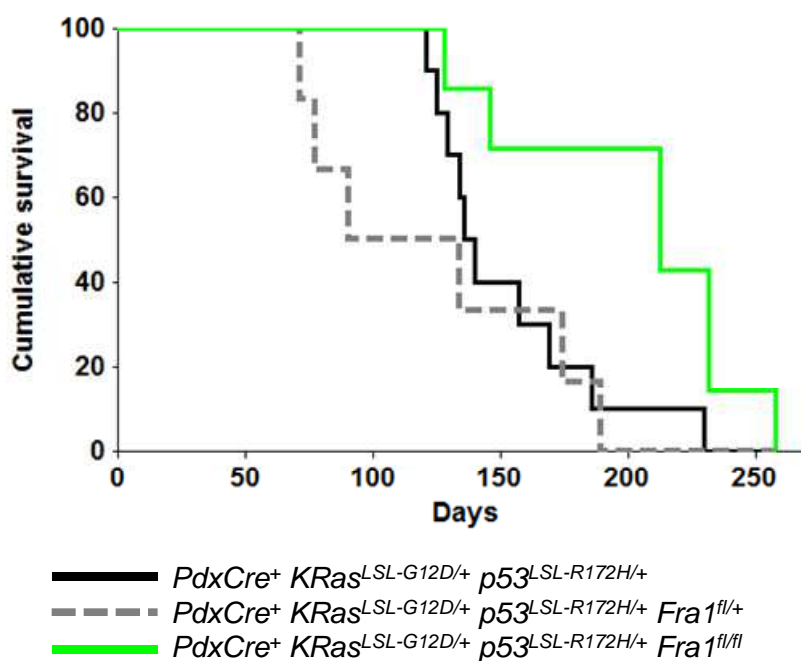


Figure 81: *Fra1* deletion increases survival in a pancreatic cancer model

Kaplan-Meier curve showing the cumulative survival of *PdxCre⁺ KRas^{LSL-G12D/+} p53^{LSL-R172H/+}* (black line) ($n=10$), *PdxCre⁺ KRas^{LSL-G12D/+} p53^{LSL-R172H/+} Fra1^{fl/+}* (dashed grey line) ($n=6$) and *PdxCre⁺ KRas^{LSL-G12D/+} p53^{LSL-R172H/+} Fra1^{fl/fl}* mice (green line) ($n=7$). Mice with pancreatic tumours were sacrificed at the same point of illness.

The loss of both copies of *Fra1* resulted in a increase in the tumour free survival compared to *PdxCre⁺ KRas^{LSL-G12D/+} p53^{LSL-R172H/+}* and *PdxCre⁺ KRas^{LSL-G12D/+} p53^{LSL-R172H/+} Fra1^{fl/+}* mice (log rank: $p=0.01$ and $p=0.08$ respectively). There was no significant difference between *PdxCre⁺ KRas^{LSL-G12D/+} p53^{LSL-R172H/+} Fra1^{fl/+}* and *PdxCre⁺ KRas^{LSL-G12D/+} p53^{LSL-R172H/+}* mice (log rank: $p=0.5$).

The AP-1 complex and *Fra1* has previously been suggested to be key in driver of invasion and metastasis. Given the PDAC model is an excellent model of invasion and metastasis I examined both gross and histological micrometastasis in the *PdxCre⁺ KRas^{LSL-G12D/+} p53^{LSL-R172H/+}* mice with and without *Fra1* deletion. Surprisingly given *Fra1* putative role in the metastatic process, *Fra1* deficient tumours were still able to metastasise. Moreover, the *Fra1* deleted mice had macrometastases.

Given this surprising result we went back to the intestinal model. We have previously shown that mice where *p53* is additionally mutated in context of *Apc* and *KRas* mutation can develop invasive tumourigenesis. In a manner similar to our previous studies *Fra1* deficient *VilCre⁺ Apc^{fl/+} KRas^{LSL-G12D/+} p53^{LSL-R172H/+}* mice still showed a trend toward accelerated tumourigenesis (but this was not quite statistically significant) (Figure 82). Analysis of intestines from these mice showed that 77% and 75% of mice which have lost respectively one or two copies of *Fra1* developed invasive intestinal or colon tumours. Interestingly the tumours developed in either intestine or colon but never in both at the same time.

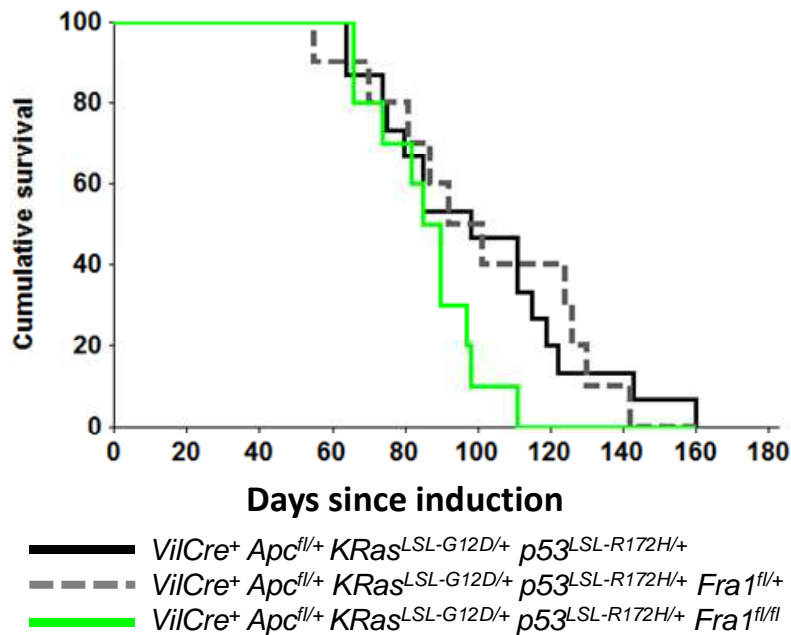


Figure 82: The effects of *Fra1* deletion are partially rescued by a *p53* mutation

Kaplan-Meier curve showing the cumulative survival of *VilCre⁺ Apc^{fl/+} KRas^{LSL-G12D/+} p53^{LSL-R172H/+}* (black line; n=15), *VilCre⁺ Apc^{fl/+} KRas^{LSL-G12D/+} p53^{LSL-R172H/+} Fra1^{fl/+}* (grey dashed line; n=10), *VilCre⁺ Apc^{fl/+} KRas^{LSL-G12D/+} p53^{LSL-R172H/+} Fra1^{fl/fl}* mice (green line; n=10). Mice with intestinal tumours were sacrificed at the same point of illness.

The loss of the two copy of *Fra1* resulted in a reduction (but not quite significant) of the tumour free survival compared to the two other types of mice (in both cases log rank: p=0.07). There was no significant difference between *VilCre⁺ Apc^{fl/+} KRas^{LSL-G12D/+} p53^{LSL-R172H/+}* (black line; n=15), *VilCre⁺ Apc^{fl/+} KRas^{LSL-G12D/+} p53^{LSL-R172H/+} Fra1^{fl/+}* mice (log rank: p=0.9).

22.4 Conclusion and discussion

I investigated the impact of *Fra1* deletion in two distinct *in vivo* cancer models. Surprisingly, the outcomes of this deletion were different in each model. In the CRC model, *Fra1* loss resulted in an accelerated tumourigenesis whilst in the pancreatic cancer model it resulted in slower tumourigenesis. Further studies will allow us to investigate the potential mechanisms of how *Fra1* loss could increase tumourigenesis in the intestine.

I showed that the loss of *Fra1* alone was able to modify gut homeostasis by increasing the cell proliferation. In the ageing CRC model, tumourigenesis is initiated when the remaining copy of *Apc* is lost. Therefore the increase of proliferation induced *Fra1* deletion could aid tumour initiation or the formation of tumours outwith the stem cell zone.

The main role of *Fra1* is as part of the AP-1 complex. However, recent studies have showed that AP-1 members can also binds other proteins and participate in other cell functions. A study done on a breast cancer cell line showed that *Fra1* can interact with *Smad2/3* in response to transforming growth factor β (TGF β) (Sundqvist, Zieba et al. 2012). This complex promotes invasion by facilitating the interaction of *Smad2/3* with the promoter of *mmp10*. More importantly, AP-1 members have been shown to interact with members of the WNT pathway. *TCF4*, *cJun* and β -Catenin are significantly upregulated in human colorectal cancer (Takeda, Kinoshita et al. 2008). It has been shown recently that *cJun* interacts with *TCF4* and β -Catenin to form a ternary complex. This complex activity seems dependent on β -Catenin since its siRNA-mediated knockdown reduces the activation of the complex target genes (Nateri, Spencer-Dene et al. 2005). Furthermore, in the *Apc*^{MIN} model (a mouse model with a nonsense mutation in codon 850 in one allele of the *Apc* gene) the inactivation of *cJun* reduces tumour number and size (Nateri, Spencer-Dene et al. 2005; Toualbi, Guller et al. 2007). The precise activity and role of each AP-1 complexes as well as the complexes formed with other partners is still to be fully understood. Bryan Miller in our laboratory is currently investigating the role of some of these complexes. Concerning the unexpected outcome that I found in the CRC model, we can hypothesise that changes in the levels of *Fra1* might liberate *cJun* from the AP-1

complex, allowing it to interact with β -Catenin. In this regard Bryan Miller has preliminary information to suggest that this may be occurring, with more β -catenin/Jun complex in the absence of *Fra1*. Thus investigating the nature of the AP-1 complexes in intestinal epithelium from *AhCre⁺ Apc^{fl/+}*, *AhCre⁺ Apc^{fl/+} Fra1^{fl/fl}* mice could define the mechanism of how *Fra1* deletion accelerates tumourigenesis in the context of activated Wnt signalling.

Within pancreatic cancer, as the activation of Wnt signalling is a much rarer event, then this might help explain why *Fra1* deletion is having a much more predicted role namely slowing tumourigenesis. It is interesting to note that other differences between the two tissues might also aid our understanding of context specific impact on tumourigenesis. Recently a link between *KRas*-activation induced downregulation of reactive oxygen species (ROS) via upregulation of its regulator nuclear factor erythroid-derived 2-like 2 (Nfe2l2 or Nrf2) has been shown (DeNicola, Karreth et al. 2011). Importantly the loss of *Nrf2* slows PanIN formation following *KRas* mutation in the pancreas. Importantly, in this study on *KRas* activated mouse embryonic fibroblasts (MEFs) it was observed that the effects of *KRas* activation on ROS production were partially rescued by the knockdown of *Fra1* as well as other AP-1 members. Interestingly in the intestine, our laboratory has shown that the activation of ROS stimulates proliferation following *Apc* loss and thus if in this situation *Fra1* deletion increases ROS we would again expect this might lead increased tumourigenesis. Future studies within the laboratory will specifically address this question.

Finally in both the intestinal and the pancreatic model we showed that *Fra1* loss does not protect against invasion and metastasis. From the literature this would have been the most expected phenotype. This might reflect in part that *in vitro* assays on migration do not fully recapitulate the invasion and metastasis process *in vivo* or that other family member might compensate to drive these functions. Moreover it should be noted particularly in pancreatic cancer studies as tumours are delayed those that grow have evolved to grow in the absence of *Fra1* and thus the tumour may have already compensated for *Fra1* absence.

DISCUSSION

23 Colorectal cancer and the MAPK cascade

Of all cancers, CRC is associated with activation of Wnt pathway as an early event. In this cancer, *KRas* activation occurs in more than 40% of cases during progression and confers a poor prognosis. Thus, it is crucial to work out the mechanism by which *KRas* activation increase tumourigenesis following *Apc* mutation and whether blocking the MAPK pathway at Mek level would be a good strategy to slow or reverse tumour progression. If so, several targets upregulated following *Apc* deletion and *KRas* activation, such as *Dusp6* and *Fra1*, could be interesting potential diagnosis tools.

Currently, there are several treatment options available to colon cancer patients once the cancer has been diagnosed and the cancer stage determined. Depending on the stage of the cancer, the patient can be treated by surgery, radiotherapy and/or chemotherapy. Research in these three fields is constantly improving the treatment options. Therefore detailed knowledge of the intrinsic molecular modifications leading to CRC is critical to improvement of chemotherapy treatments.

23.1 Current CRC chemotherapy treatments

Treating patients with CRC remains complicated despite the advance in diagnosis and treatment of the last years. Patients diagnosed with late stage CRC which has spread outside the colon are very difficult to treat and the various treatment regimens given are only giving small benefits in survival times. Patients with early stage carcinomas which have not spread beyond the wall of the colon have more treatment options (and are often cured by surgery) but a subset of these CRC's at stage2 or Dukes B still have a poor prognosis with a low response to treatments. Therefore in these early stage malignancies as only a small subset recur (20%) treating all patients with chemotherapy would not be beneficial and

thus it's a very important clinical question to know which patients to treat or find new therapies that have very few side effects.

In the majority, tumour resection is the preferred therapy. However, a treatment following resection can be given to prevent relapse and sometimes or when the tumour is not operable. Two major categories of drugs are used: compounds directed against key proteins of signalling pathways involved in tumour progression and drugs targeting RNA and DNA metabolism. It is striking that none of the current treatments are specifically directed against the major pathways disturbed in CRC namely Wnt and MAPK pathway. (<http://www.cancer.gov/cancertopics/pdq/treatment/colon/Patient/page4>)

Bevacizumab is an antibody directed against the vascular endothelial growth factor (VEGF) an important pro-angiogenic growth factor. The antibody binds to VEGF and prevents its ligation to the VEGF receptor. *Cetuximab* and *Panitumumab* are antibodies targeting the epidermal growth factor receptor (EGFR) preventing the activation of several pathways involved in tumour progression. *Regorafenib* is a small molecule which binds to and inhibits several targets such as VEGF receptor (VEGFR), platelet-derived growth factor receptor (PDGFR) and Raf kinases, which may result in the inhibition of tumor angiogenesis and tumor cell proliferation. *Ziv-aflibercept* is a protein made of segments of VEGF fused to the constant region of human immunoglobuline G1 (IgG1). It binds to VEGF and prevents the binding to the VEGF receptors.

Irinotecan hydrochloride is an alkaloid that converts into a metabolite inhibiting topoisomerase I activity. It stabilises the cleavable complex between topoisomerase I and DNA, resulting in DNA double stranded breaks during DNA replication. *Oxaliplatin* is an organoplatinum complex resulting in DNA crosslinks. *Capecitabine* metabolites inhibit DNA synthesis by reducing normal thymidine production and RNA and protein synthesis by competing with uridine triphosphate. *Fluorouracil* is an analogue of the nucleoside pyrimidine. When administrated to patients, fluorouracil is converted to different active metabolites and can be incorporated into RNA and /or DNA obstructing RNA and DNA processing. These drugs are given in advanced stage CRC, if the patient relapses or if no other chemotherapies are effective.

23.2 Finding new chemotherapy agents

The identification of the signalling pathways involved in CRC is crucial to the development of novel therapies. Indeed, the characterisation of the genetic profile of individual tumours in each patient is essential to determine which treatment is best. However sequencing the tumour of each patient is currently not a realistic option as the cost of the tests could never be covered. Nevertheless it is reasonable to reduce the numbers of mutations screened to the frequently mutated genes in CRC such as *Apc*, *KRas*, *BRaf* and *p53*. Indeed the study of 195 human CRC tumours (<http://www.cbioportal.org/public-portal>) indicated that the sequencing of these four genes would cover 95.4% of CRCs. Interestingly the study shows that *BRaf* (mutated in 13% of CRCs) and the three other mutations are mutually exclusive highlighting two distinct pools of patients. As predicted from the microarray analysis of this thesis *Dusp6* (mutated in 10% of CRCs analysed), *Fra1* (mutated in 2% of CRCs analysed) and *KRas* have a co-occurrence tendency. Furthermore, the study confirms a trend of co-occurrence between *Apc* and *KRas* mutations. It has been showed that patients with mutations in *KRas* are resistant to EGFR inhibitors (Lievre, Bachet et al. 2006; Lievre, Bachet et al. 2008; Allegra, Jessup et al. 2009; Normanno, Tejpar et al. 2009; De Roock, Claes et al. 2010). Indeed, in a study on 1022 tumour DNA samples, amongst tumours resistant to Cetuximab, 97.1% were exhibiting *KRas* mutations (De Roock, Claes et al. 2010). Moreover, the treatment of *KRas* mutated tumours with cetuximab is suggested to drive disease progression (Bokemeyer, Bondarenko et al. 2009). In addition, amongst the tumours with wild-type *KRas*, up to 65% are resistant to Cetuximab. These tumours have other mutations in *NRas*, *BRaf* and *PI3K* genes (De Roock, Claes et al. 2010). The gene *KRas* is mutated in more than 40% of CRCs and patients are routinely tested for their *KRas* status to decide which treatment is adequate to treat their tumour. Therefore it is crucial to find other treatments aimed at different targets as an alternative to EGFR inhibitors.

The one expected direct consequence of oncogenic mutation within *Kras* is that the MAPK cascade (Ras-Raf-Mek-Erk) should be upregulated in these CRCs. However, my experiments have shown that upregulation of pErk is hard to detect following *KRas* mutation in adenomas and critically, the treatment with

the Mek inhibitor CI1040 had no effect on either tumour free survival of *VilCreER⁺ Apc^{fl/+} KRas^{LsL-G12D/+}* mice or tumourigenesis of *VilCreER⁺ Apc^{fl/fl} KRas^{LsL-G12D/+}* mice. These findings are in good agreement with the results obtained by J. Yeh and colleagues showing that elevated Erk activation depends on *BRaf* but not *KRas* mutation in human CRC samples (Yeh, Routh et al. 2009). Indeed, a phase 2 study on patients with CRC showed no significant antitumour activity of CI1040 (Rinehart, Adjei et al. 2004). It is of interest that this study did not indicate the *KRas* status of the patients. In our laboratory, Ee Hong Tan has shown in a murine model of invasive CRC, that an upregulation of pErk is seen at the invasive edge of the tumour, however not throughout the tumour bulk. In this case it will be of interest to see if the use of Mek inhibitor such as CI1040 seems might suppress invasion and metastasis within this model.

These results suggest the signalling output and the functional importance of *KRas* mutations may be independent of the Mek-Erk cascade. *KRas* mutations could be therefore involved in the activation of other signalling cascades such as of PI3K pathway. Interestingly, a recent study on patient liver metastasis from *KRas* mutated primary CRC tumour transplanted in NOD/SCID mice reported a growth arrest effect of the Mek inhibitor AZD6244 as a monotherapy (Migliardi, Sassi et al. 2012). They observed a synergistic association of the Mek inhibitor AZD6244, the PI3K inhibitor BEZ235 and cetuximab. Yet the association of these chemotherapies did not lead to tumour regression as there was a reduction of the mitotic index but not an increase in apoptosis. This would be in favour of a cytostatic effect instead of a cytotoxic one explaining the rather weak effect on persisting tumours. They also noted similar results on samples from tumours presenting *NRas*, *BRaf* and/or *PI3K* mutations. These results suggest that such drug combination could have an effect on CRC patients with *KRas* mutations within their tumours. However preliminary data from our laboratory has shown little effects of combined Mek and mTOR inhibitor suggesting a more complex signalling in CRC. Nevertheless extra confidence would be gained if preclinical models showed a tumour regression as this is a much simpler model to treat than a human patient. Indeed when drugs have worked in the clinic, for example the *BRaf* inhibitor in tumours with *BRaf* mutation, preclinical models have shown tumour regression.

Another way to bypass the difficulty of targeting MAPK pathway in CRC would be to develop more drugs targeting the major deregulated pathway in CRC namely the WNT pathway. First the secretion of Wnt could be targeted. The *Porcupine* gene is required for the secretion of wingless and other Wnt protein in drosophila and mutation on its human ortholog is the cause of diseases. The conditional deletion of porcupine in mice impaired Wnt secretion and had drastic consequences in embryogenesis (Matozaki, Murata et al. 2009). The Frizzled (Fz) receptors are currently investigated as new drug targets. Notably, the use of secreted frizzled-related proteins (SFRPs) seems very promising. SFRPs are decoy receptors containing a cysteine-rich domain similar to the Fz Wnt binding domain. When the Wnt ligand binds these soluble receptors it does not reach its proper Fz/LRP5/6 receptor and therefore does not activate the Wnt pathway. Interestingly, *Sfrp* genes are often silenced by hypermethylation in CRC tumours inducing Wnt pathway activation (Suzuki, Watkins et al. 2004). The transfection of SFRPs in HCT116 (a CRC cell line with a β -Catenin mutation preventing its phosphorylation by the Apc/Axin/GSK3 complex) results in the decrease of β -Catenin level and then brought back Wnt signalling back to its basal level (Suzuki, Watkins et al. 2004). Furthermore collagen-derived SFRP-like polypeptide (such as V3Nter) reduces the expression of Cyclin D1 and c-Myc in CRC cell lines with a β -Catenin mutation (Quelard, Lavergne et al. 2008; Lavergne, Hendaoui et al. 2011). Moreover this polypeptide has been showed to reduce and delay the growth of tumours derived from HCT116 cells implanted in nude mice by binding Wnt3a (Lavergne, Hendaoui et al. 2011). Nevertheless, it is important to note that V3Nter had no effects on the SW480 cell line (containing an *Apc* mutation) limiting its effects to the β -Catenin mutant cell lines. Another soluble Wnt receptor has been generated by Polakis laboratory (Tenbaum, Ordonez-Moran et al. 2012). Their receptor coupling the frizzled8 cysteine-rich domain and the human Fc domain of immunoglobulin (F8CRDhFc) has been shown to inhibit the growth of mammary tumours allografts and of human teratoma xenografts in athymic nude mice. Furthermore an antibody targeted against LRP6 could be used to limit Wnt pathway activation. LRP6 antibodies targeting the LRP6 binding sites for Wnt1 and Wnt3a have been created (DeAlmeida, Miao et al. 2007). The treatment with these antibodies on xenograft of mammary tumours exhibiting high Wnt pathway activation implanted on nude

mice resulted in tumour regression. Another way to suppress the effects of an overactive Wnt pathway is to render more available the components of the β -Catenin degradation complex. Axin is part of this degradation complex. As tankyrase targets Axin to program its degradation via the proteasome, tankyrase inhibitors (TNKi) are stabilising Axin by preventing its degradation (Huang, Mishina et al. 2009; Waaler, Machon et al. 2012). A TNKi has been already proven to reduce tumour initiation *in vivo* in a CRC model of *Lgr5-Cre^{ERT2}* mice with an induced *Apc* mutation (Waaler, Machon et al. 2012). Liam Faller in our laboratory has started to evaluate the effects of dual treatment *in vivo* combining TNKi and a PI3K inhibitor as well as TNKi and rapamycin. *VilCreER⁺ Apc^{fl/fl} KRas^{LSL-G12D/+}* mice treated with both drug combinations have their CPL phenotype reduced. Moreover, a 5 day treatment with TNKi and rapamycin reduces proliferation in established tumours. Intriguingly, Resveratrol (3,40,5-trihydroxystilbene), a natural compound found in several plants such as grapes, has been established to have anti-cancer effects. Recently, a link between Resveratrol effects and inhibition of WNT pathway has been found. Indeed, treatment with Resveratrol abolished the β -catenin/TCF-mediated transcriptional activity in cells stimulated with Wnt ligand (Chen, Hsu et al. 2012). Resveratrol is believed to dissociate the complex β -catenin/TCF preventing the transcription of Wnt target genes. A summary of ways to target Wnt pathway can be found in Figure 83. As mentioned previously, *KRas* activation in CRC can dysregulate several signalling pathways. Interestingly aspirin has been reported to have a positive effect on survival of CRC patients (Janssen, Alberici et al. 2006; Alberici, de Pater et al. 2007; Kim, Song et al. 2009). If the precise mechanism of action is still not fully understood, it seems that aspirin can act as an inhibitor of the phosphorylation, hence activation, of S6 kinase 1 (S6K1) and 4E binding protein 1 (4EBP1) two important effectors of the mTOR pathway as shown in CRC cell lines (Davies, Reddy et al. 2000). Furthermore aspirin activates adenosine monophosphate-activated protein kinase (AMPK), a key protein in cellular energy homeostasis, leading to tumour growth arrest and induces autophagy. These examples of possible treatments show the wide spectrum of targets that can be investigated to increase the range of chemotherapies and improve patient survival.

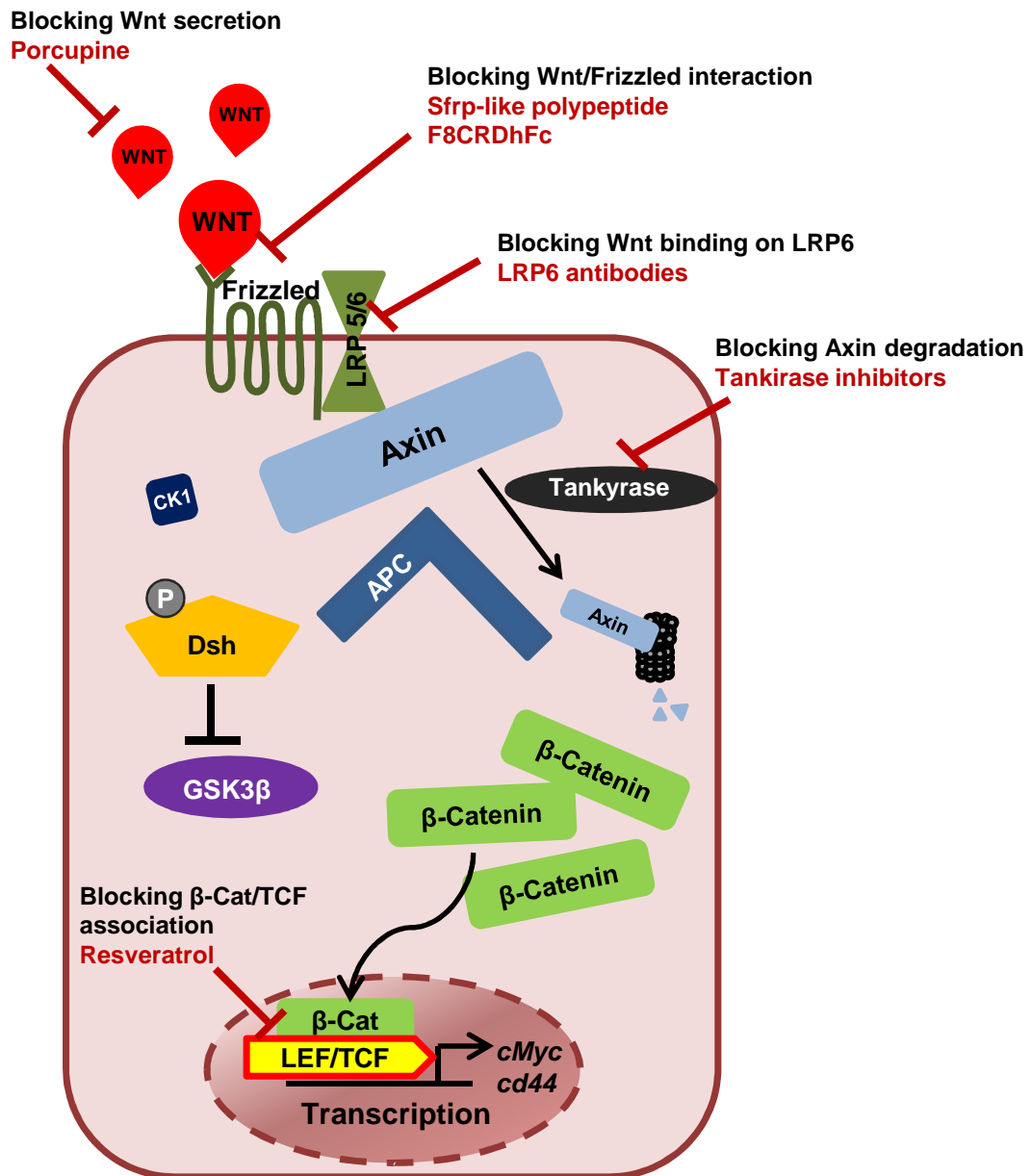


Figure 83: Targeting Wnt pathway

A recent study on a mouse model of *KRas* dependent PDAC showed that *KRas* is involved in the regulation of glucose metabolism (Ying, Kimmelman et al. 2012). In good agreement with this study, we found that a *KRas* mutation results in a change in the transcription of metabolism genes in the intestine. A microarray performed on samples of *VilCreER⁺ Apc^{fl/fl} KRas^{LsL-G12D/+}* mice showed perturbations in genes associated with metabolism. This could indicate that *KRas* mutations in CRC are mainly disturbing metabolism independently of the MAPK pathway activation. Interestingly, in the reported pancreatic cancer model used for these experiments, the expression of glycolytic genes such as *Glut1*, *Hk1*,

Eno1 and *Ldha* was reduced following Mek inhibition or oncogenic *KRas* inactivation. However, in the pancreatic cancer mouse model I have used Mek inhibition had an impact on tumour growth of PDAC cells from *PdxCre⁺ KRas^{LSL-G12D/+}* mice implanted subcutaneously into nude mice. In contrast, in the *VilCreER⁺* mice model for CRC, there was no impact of Mek inhibition on tumourigenesis. The effects of Mek inhibition seem to be limited to the PCs models. We could argue that the Mek inhibition has no impact on CRC models as CRC seems to be driven mostly by WNT pathway activation whereas PC can be initiated by *KRas* mutations alone. Further studies are now ongoing within the laboratory to carefully characterise the metabolic differences driven by additional *KRas* mutation and the functional significance of these alterations.

24 Is *Dusp6* a tumour suppressor gene?

Several lines of evidence indicate that *Dusp6* may be a potential tumour suppressor. First, *Dusp6* specifically dephosphorylates Erk, a key effector of the MAPK pathway involved in tumour progression. Secondly, *Dusp6* expression is regulated by Erk in a negative feedback loop. However, there are conflicting reports in the literature leading to the question of its tumour suppressor role *in vivo*.

24.1 *Dusp6* can act as a tumour suppressor

The results described in the *in vivo* models of PC and CRC of this thesis are arguing for a tumour suppressor effect of *Dusp6*. Indeed, in the CRC model following the acute *Apc* deletion, *Dusp6* loss increased strongly the CPL phenotype. In addition, in both PC and CRC aging models, the deletion of *Dusp6* drastically reduced the tumour free survival of the animals. Moreover, the loss of one copy of *Dusp6* in PC rendered the tumour more aggressive and allowed rapid formation of liver metastasis.

The results reported for the PC mouse model are in good agreement with the observations made on human pancreatic tumours that *Dusp6* is upregulated in PanIN lesions and lost in PDACs (Furukawa, Fujisaki et al. 2005). This suggests

that *Dusp6* is upregulated in response to early *KRas* activation and then finally lost as part of the several mutations necessary for tumour progression. This observed silencing of *Dusp6* in late PC stages is proposed to be mediated by hypermethylation of CpG sites in the promoter area (Xu, Furukawa et al. 2005). Consistent with observations made in pancreatic cancer, *Dusp6* expression was described as low in immortalised lung cancer cell lines and more importantly in human lung tumours (Okudela, Yazawa et al. 2009). In fact *Dusp6* expression was found inversely correlated with the tumour proliferation as indicated by Ki67 staining. Finally, an experiment showed that *Dusp6* expression could be recovered in cell lines by treatment with azacitidine which impairs DNA methylation and histone deacetylase suggesting, in good agreement with the observation made in human PC, that *Dusp6* silencing is due to hypermethylation and/or histone acetylation (Okudela, Yazawa et al. 2009). Another study reported similar results on oesophageal squamous cell carcinoma (ESCC) and nasopharyngeal carcinoma (NPC) (Wong, Chen et al. 2012). Low expression of *Dusp6* was observed in a large percentage of tumour tissues and cell lines and this downregulation was associated with hypermethylation of the *Dusp6* promoter. Interestingly, *Dusp6* loss was suggested to be involved in the epithelial-mesenchymal transition. Surprisingly, a tissue microarray (TMA) of ESCC human tissues analysis revealed that *Dusp6* expression was high in metastatic stages and was suggested to be a negative feedback loop response to oncogenic signalling of cancer cells. This upregulation is rather in contradiction with their previous observation and the results I found in the pancreatic cancer mouse model. One limitation of this study was that the matched primary tumour was not stained and thus it was unclear whether these tumours grew with high level of *Dusp6* or whether there was reactivation of *Dusp6* within the metastatic sample. As only 40% of ESCC analysed had low *Dusp6* expression it is possible that changes in *Dusp6* expression could be related to the mutation of different oncogenic and tumorigenic pathways during tumour progression ie *KRas* mutation. In ovarian cancer cell lines and primary cancer tissue, *Dusp6* expression was described as downregulated compared to normal tissue (Chan, Liu et al. 2008). Furthermore, the inhibition of *Dusp6* in ovarian cancer cell lines accelerated cell proliferation whereas the transfection of *Dusp6* in *Dusp6*-depleted cells suppressed proliferation. More importantly, *Dusp6* expression

restored cisplatin sensitivity in resistant cell lines suggesting that the loss of *Dusp6* in ovarian cancer is a sign of aggressive and chemoresistant cancer evolution. The putative tumour suppressor role of *Dusp6* in *Ras* activated tumours has also been suggested in a study on keratinocytes expressing activated HRas (Warmka, Mauro et al. 2004). In this study, the authors have used the tumour promoter drug Palytoxin to investigate signalling mechanisms which can be modulated during carcinogenesis. The Palytoxin treatment was inducing Erk activation by drastically reducing *Dusp6* protein levels. In addition, despite the presence of Palytoxin, the sustained exogenous *Dusp6* expression was able to reverse the Erk activating effects of the drug. All these experiments are confirming the hypothesis of a tumour suppressor role of *Dusp6*. However, there are some conflicting reports in the literature.

24.2 *Dusp6* can promote tumourigenesis

Intriguingly, and in contradiction with its role as an Erk activation regulator, *Dusp6* has been suggested to promote tumourigenesis in several models. Importantly, breast cancer models argue strongly in favour of a tumour promoting role of *Dusp6*. In cancer cell lines with induced growth arrest by phorbol 12-myristate 13-acetate (PMA) the silencing of *Dusp6* was promoting filopodia formation and accelerated the growth arrest process (Nunes-Xavier, Tarrega et al. 2010). Moreover, ectopic expression of *Dusp6* was able to stop the effects of PMA on cell lines and could also promote cell proliferation. Another study demonstrated a correlation between *Dusp6* expression and Tamoxifen resistance in breast cancer cell lines (Cui, Parra et al. 2006), *Dusp6* expression has also been associated with tumour promotion in glioblastoma cell lines (Messina, Frati et al. 2011). Indeed, *Dusp6* overexpression in cell lines was stimulating cell proliferation. Moreover, the *Dusp6* overexpressing cell lines implanted in nude mice produced tumours with rapid growth and cisplatin resistance.

One study on melanocytes is a good example of the difficulties intrinsic to assessing a tumour role for *Dusp6*. In this study, the authors showed an opposite effect of *Dusp6* expression in human melanocyte and mouse melanocyte cell

lines (Li, Song et al. 2012). Indeed *Dusp6* was acting as a tumour suppressor in human melanocytes but had pro-tumourigenic effects in their mouse counterparts. Furthermore, a human primary melanoma TMA analysis showed a correlation between high *Dusp6* and poor prognosis. This study illustrates the context dependant effects of *Dusp6* expression and the importance to connect *Dusp6* status to other mutations and tissue specificity in order to understand the role of *Dusp6* in different cancer types.

Therefore I believe my data has provided very important novel insights about the capacity of *Dusp6* to act as a tumour suppressor. My functional studies have shown that *Dusp6* loss can drive tumourigenesis in the presence of *KRas* mutation. One of the key questions is that although its loss can drive tumour progression, is this an important pathway in human carcinogenesis? As I mentioned in PDAC the data on human tumours does support this model: an early upregulation following *KRas* mutation and then a loss which could drive tumour progression. Functionally inhibition of Mek then affected tumour growth. Although mouse data in colon also gives a definitive answer that *Dusp6* loss can accelerate tumourigenesis one key question that remains is whether there is selection for *Dusp6* loss during tumourigenesis? The reason for this is that mutation of *Apc* and *KRas* together rapidly induces tumourigenesis and thus is there a strong selective pressure to lose *Dusp6*? It is important however to mention the lack of powerful tools to detect *Dusp6* at the protein level. Indeed, the lack of *Dusp6* antibodies is holding back the *in situ* analysis that could highlight the impact of *Dusp6* level in tumours/normal tissues. Certainly in our mouse models *Dusp6* expression is retained in tumours from *VilCreER⁺ Apc^{fl/+} KRas^{L^{SL}-G12D/+}* mice and these tumours are resistant to Mek inhibition. Moreover investigation of RNA expression in human cancers suggests that *Dusp6* may remain high in *KRas* mediated CRC (though extra data is required to support this).

One other important implication from our work is that MAPK inhibition in CRC, will only affect proliferation once *Dusp6* and perhaps other negative regulators of the MAPK pathway are lost. It is of interest to note that *Dusp6* has previously been suggested to be a predictor on MAPK responsiveness in human CRC cell

lines (Yeh, Marsh et al. 2007). Moreover my studies have shown that *Dusp5* is also upregulated following joint *Apc* loss and *KRas* mutation. Currently *Dusp5* knockout animals are being crossed in both the PDAC and CRC models. If *Dusp5* loss also has the same impact as *Dusp6* deletion then it may be that before a prediction upon the efficacy of Mek inhibition can be made a number of pathway components will need to be examined.

This raises another very important finding of my thesis, the difficulty in assessing MAPK pathway activation *in vivo*. My work with Mek inhibition in the *Dusp6* deleted animal clearly showed that MAPK activation was functionally important however an upregulation was hard to observe either in levels of pMek and pErk or in target gene activation. This somewhat reflects the lack of robust target genes for the MAPK pathway and difficulty of phospho-antibody staining *in vivo*. In order to investigate further the signalling pathways implicated following *Apc* and *KRas* mutation, we could propose the use of optical proteomics technologies namely fluorescence lifetime imaging microscopy (FLIM) and Forster resonance energy transfer (FRET) (For review: (Tarasewicz and Jeruss 2012)). The use of the FLIM/FRET technique has highlighted a new level of regulation of MAPK pathway. Indeed it has been shown in cells that have a mutated FGF receptor remains longer at the cell membrane instead of undergoing endocytosis and therefore prolongs FGF binding and increases MAPK pathway activation (Millet and Zhang 2007). This finding suggests a possible more complicated regulation of signalling pathways both upstream and downstream *KRas* activation in our models. This technique could help ascertain the major direct target of activated *KRas* in the complex CRC. Finally, this technique could be use to establish the different AP-1 complexes formed following *KRas* and *Fra1* mutations in order to determine a clearer role of *Fra1*: tumour promoter or suppressor.

Overall my data have confirmed a tumour suppressor role for *Dusp6* in both PC and CRC dependent on the MAPK pathway activation. However, the impact on Erk activation needs to be explored further. Importantly I showed that *KRas* activation oncogenic effects were not mainly driven by the direct downstream cascade namely the MAPK pathway and therefore, the investigation of the outcome of *KRas* activation is currently ongoing in the laboratory. Last but not

least, my data have highlighted a possible tissue-dependent outcome of *Fra1* expression which can act as tumour suppressor in CRC or as a tumour promoter in PC.

APPENDIX

Supplementary Figures: Clusters of the microarray samples

Microarray samples were analysed and their log₂ expression values were calculated. Then, they were clustered based on the Euclidean distance between the rows of a data matrix. The samples clustered together have similar gene expression behaviour. The values on the height axis are an indication of how similar samples are. The shorter the line is, the more similar the samples are. Therefore long lines are indicating very different samples.

Legend:

WT: *VilCreER*⁺

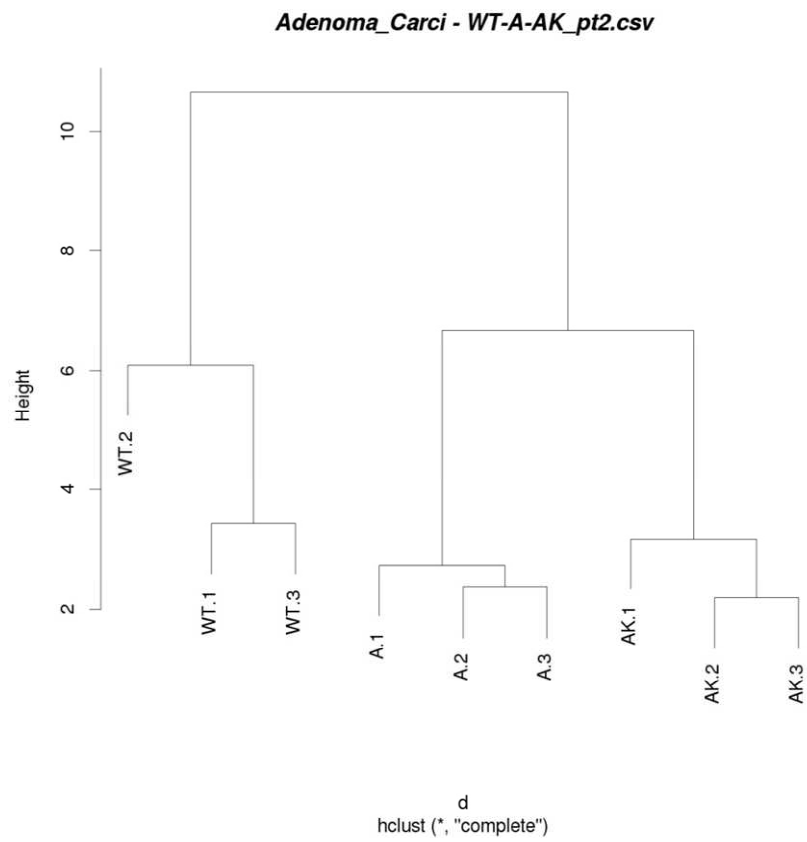
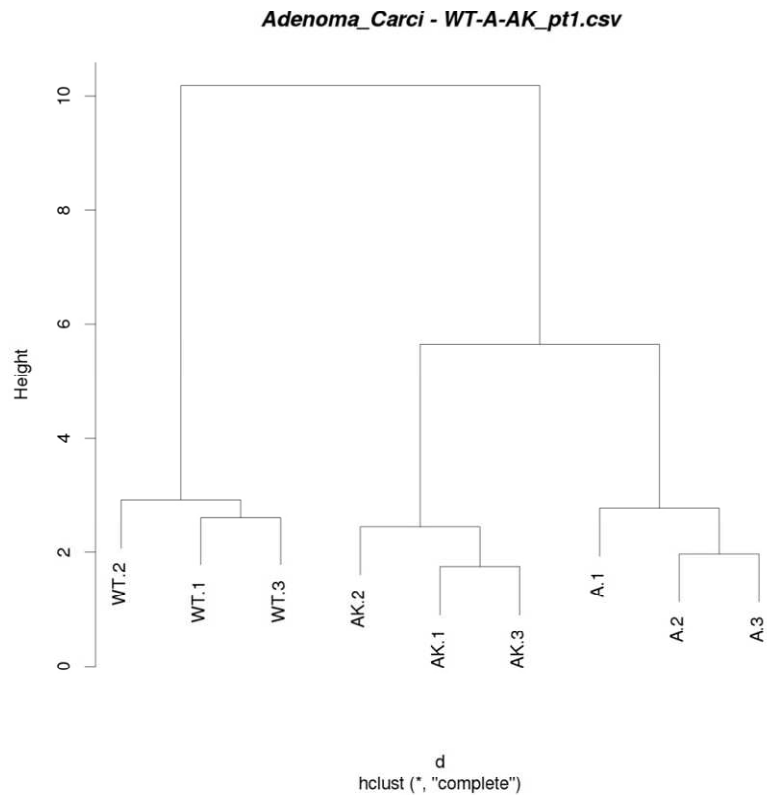
A: *VilCreER*⁺ *Apc*^{fl/fl}

AK: *VilCreER*⁺ *Apc*^{fl/fl} *KRas*^{LsL-G12D/+}

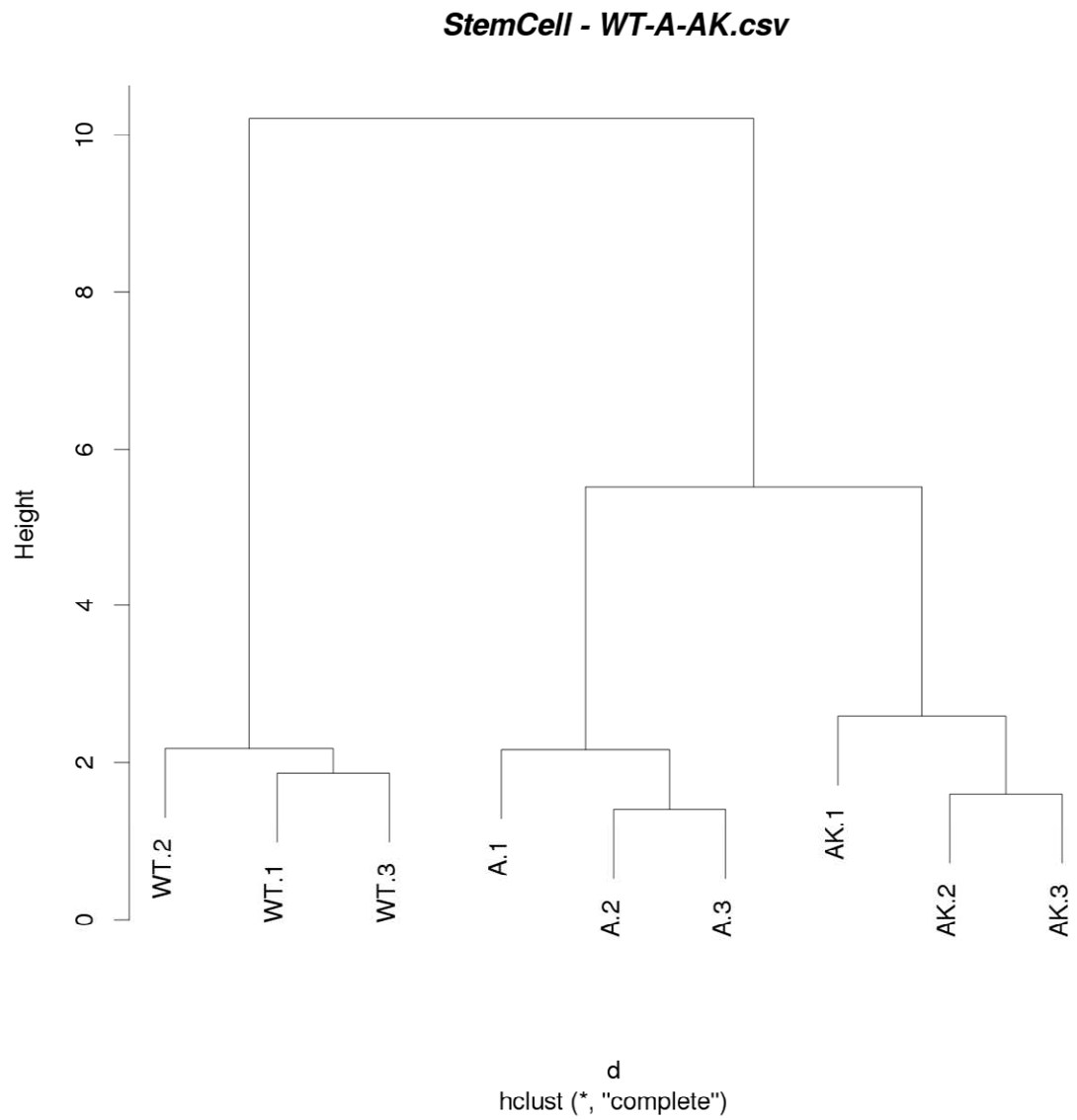
AKD: *VilCreER*⁺ *Apc*^{fl/fl} *KRas*^{LsL-G12D/+} *Dusp6*^{-/-}

AKC11040: *VilCreER*⁺ *Apc*^{fl/fl} *KRas*^{LsL-G12D/+} treated with C11040

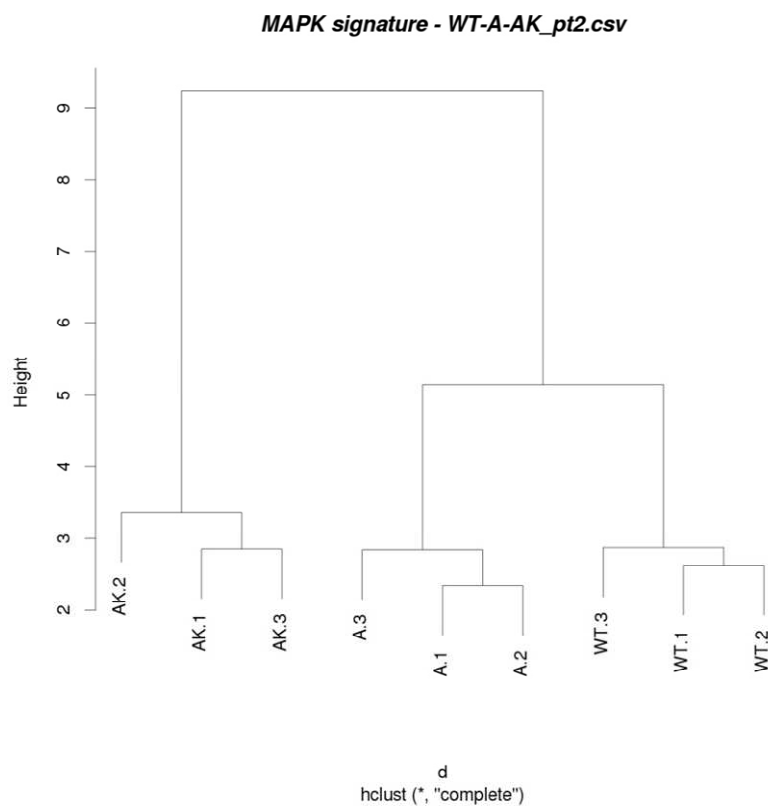
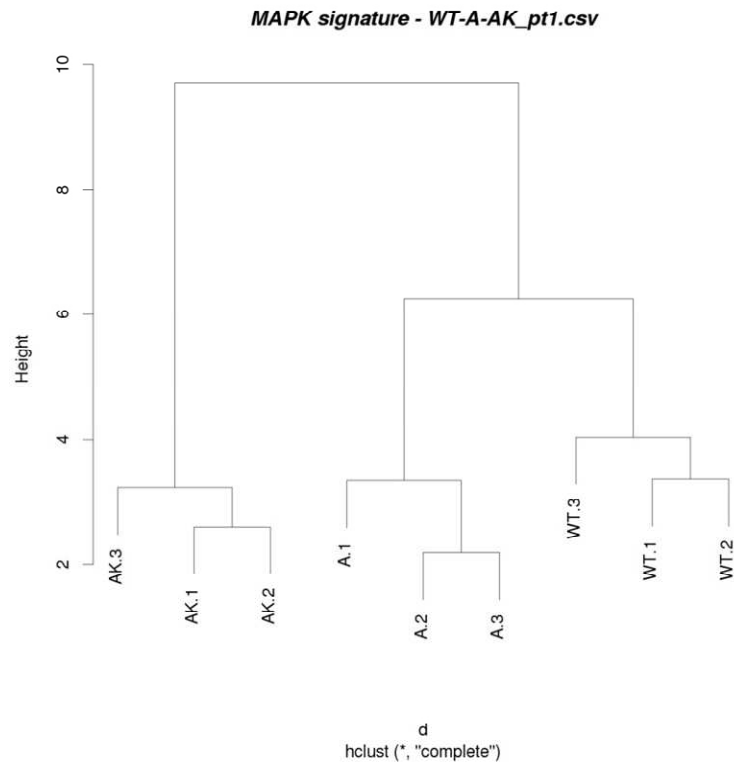
AKDC11040: *VilCreER*⁺ *Apc*^{fl/fl} *KRas*^{LsL-G12D/+} *Dusp6*^{-/-} treated with C11040



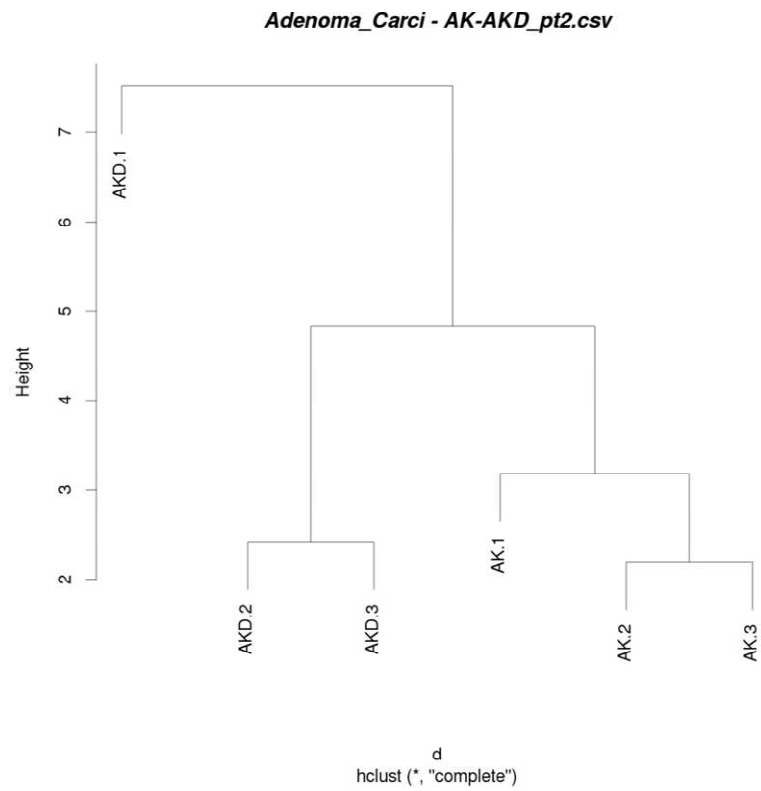
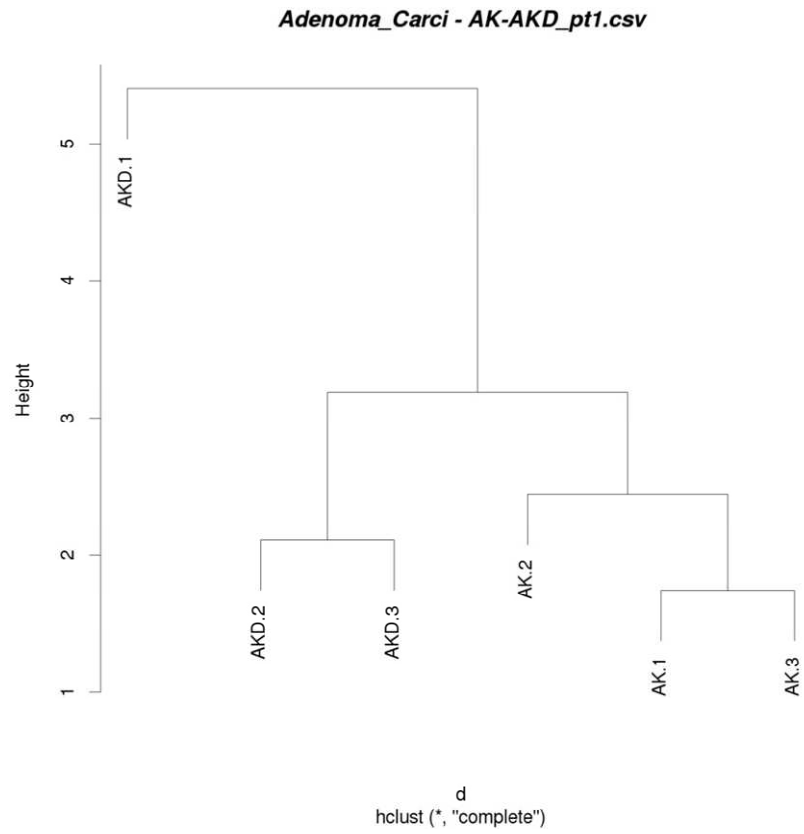
Supplementary figure 1: Wnt signature; Clustering WT, A and AK mice samples



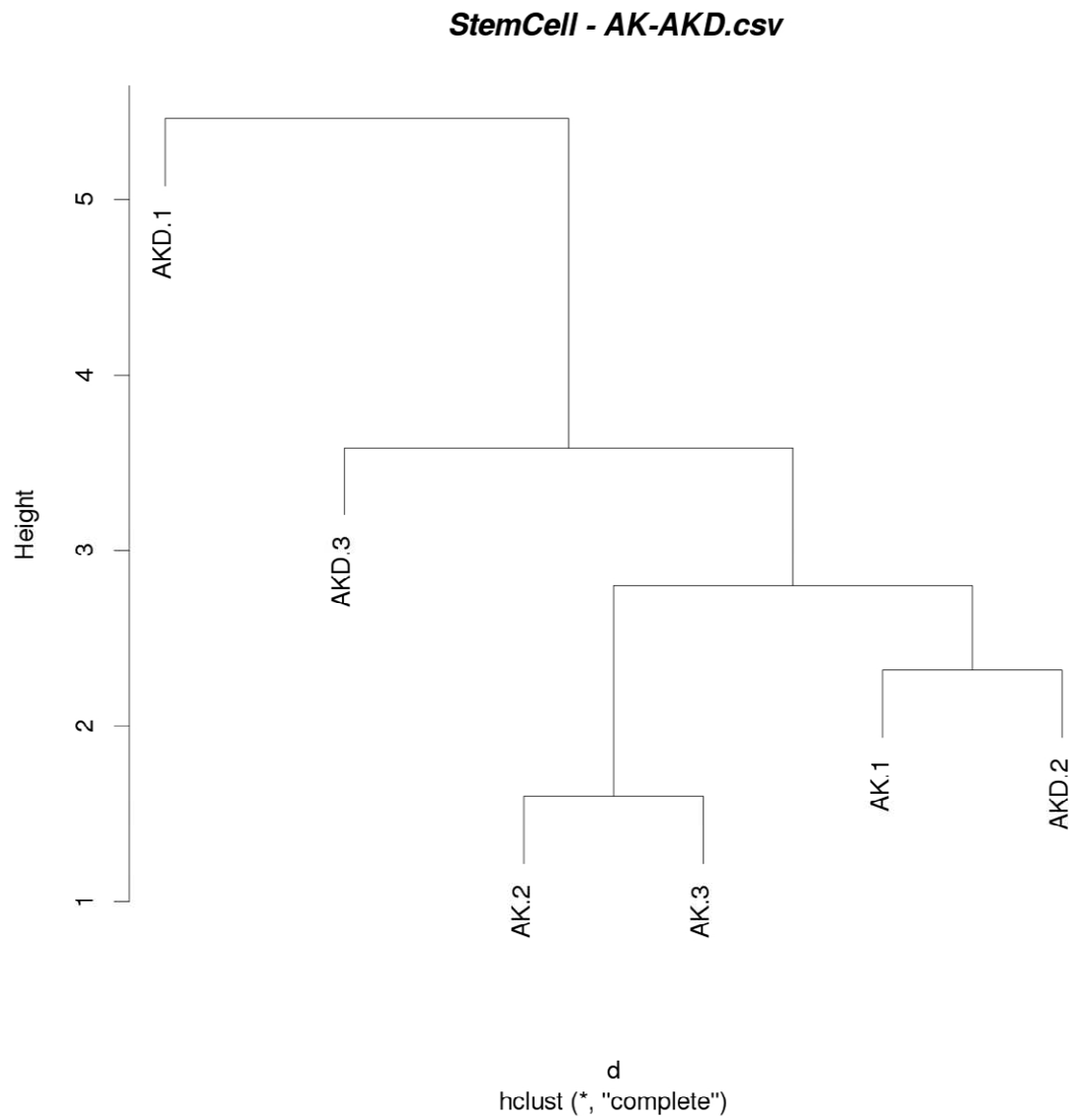
Supplementary figure 2: Stem cells signature; Clustering WT, A and AK mice samples



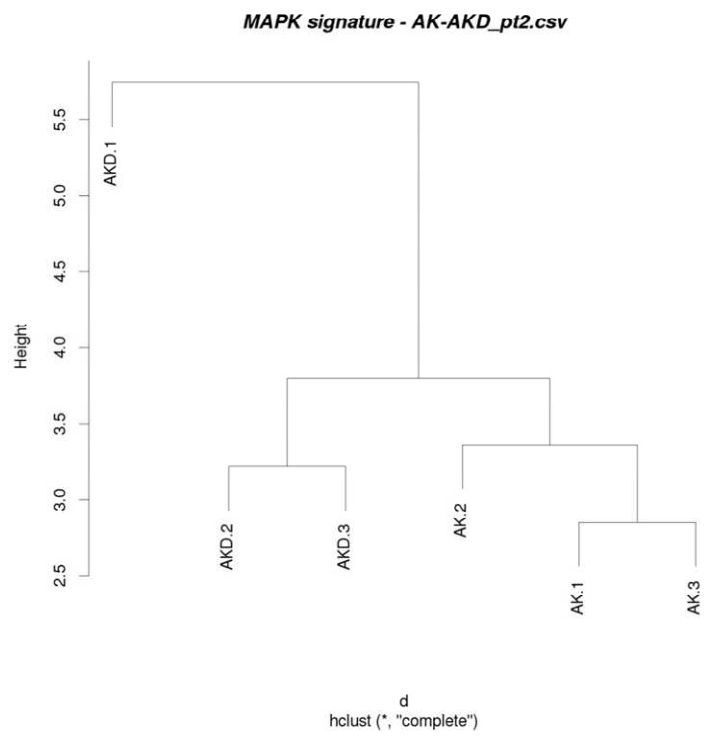
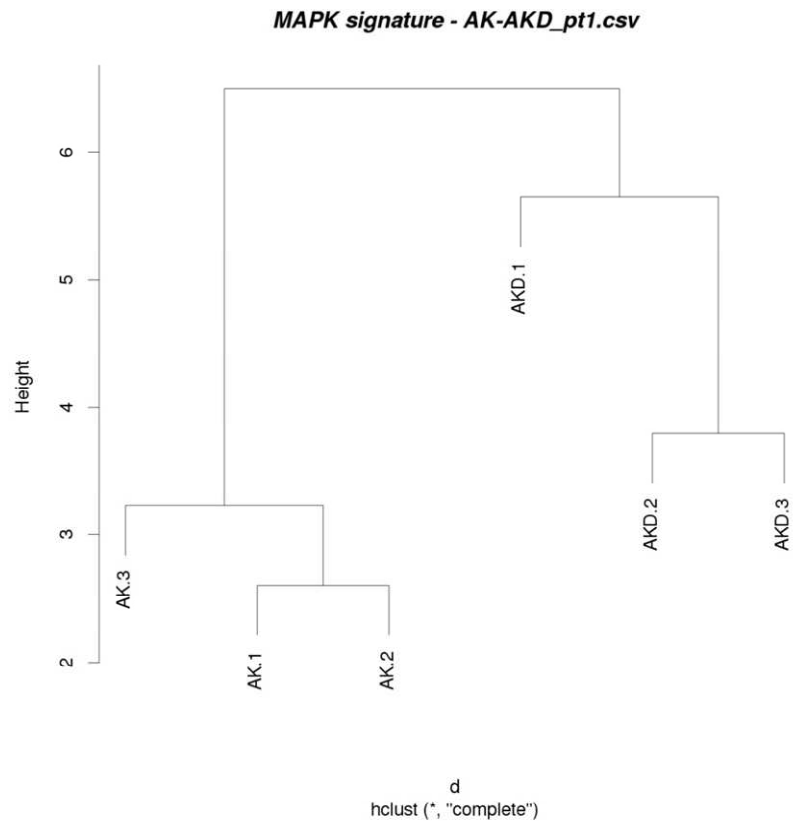
Supplementary figure 3: MAPK signature; Clustering WT, A and AK mice samples



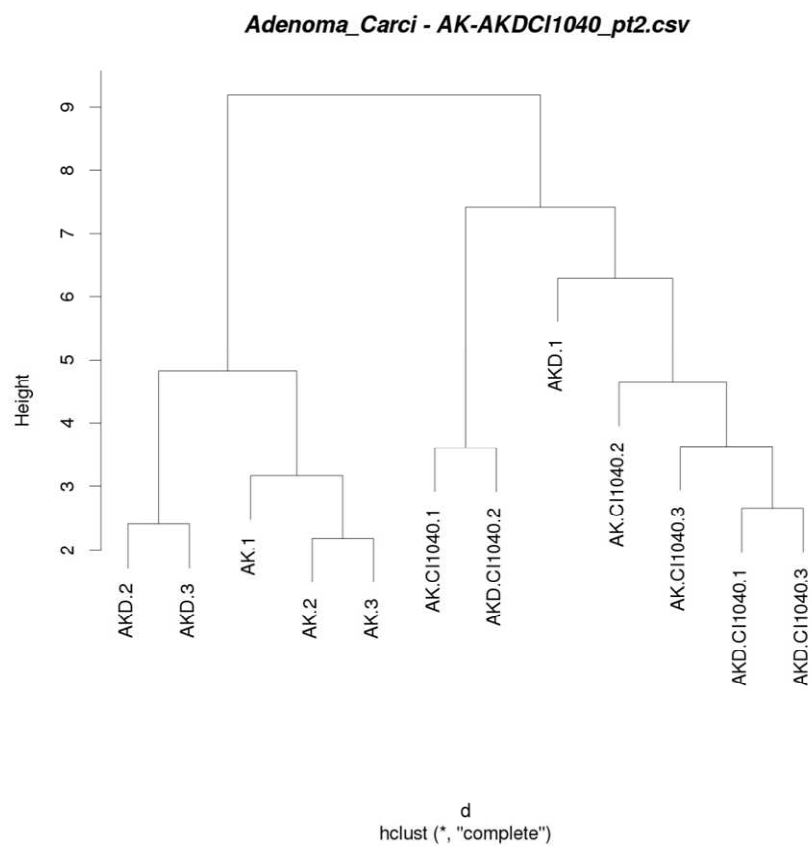
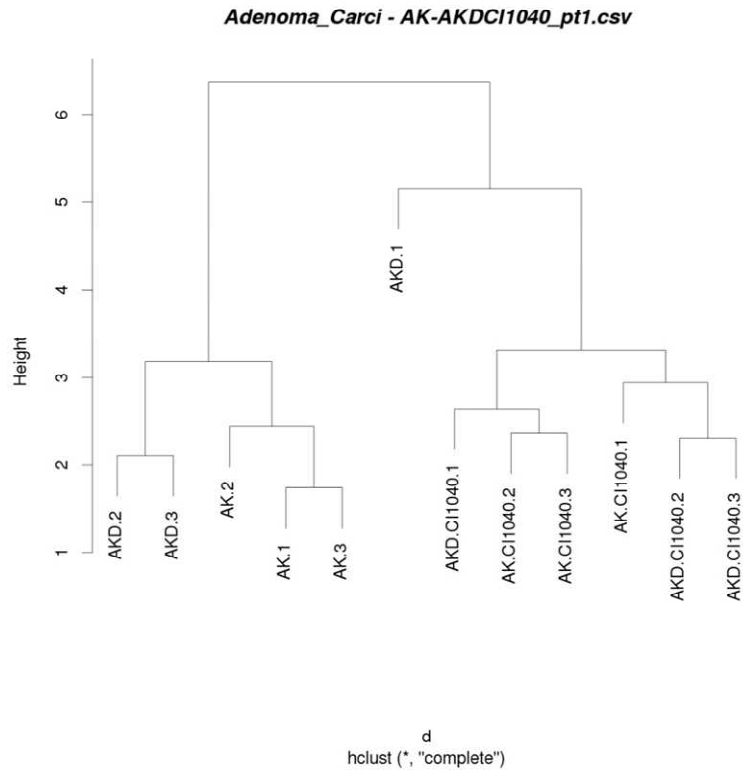
Supplementary figure 4: Wnt signature; Clustering AK and AKD mice samples



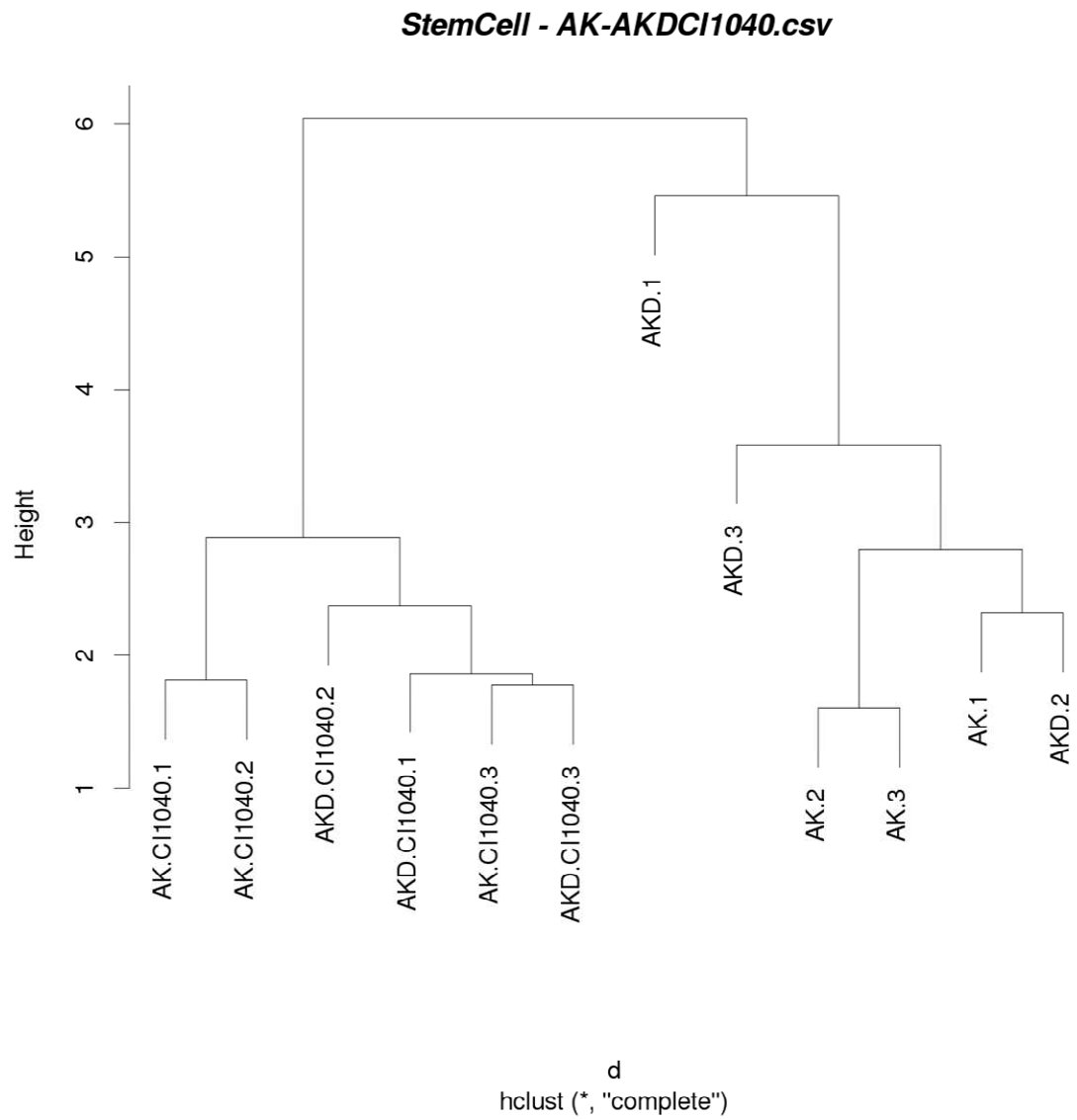
Supplementary figure 5: Stem cells signature; Clustering AK and AKD mice samples



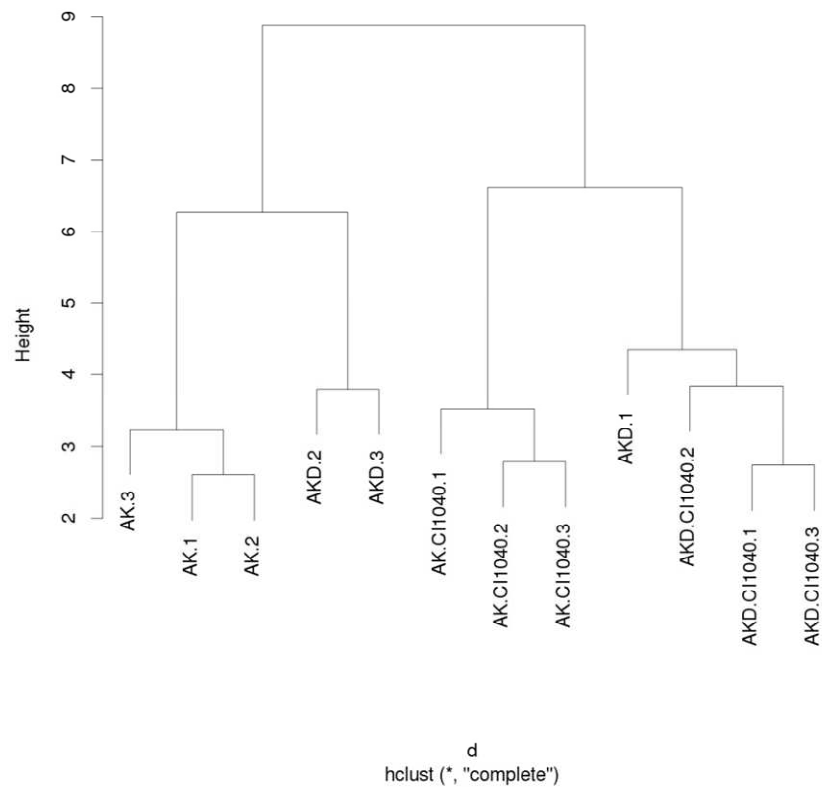
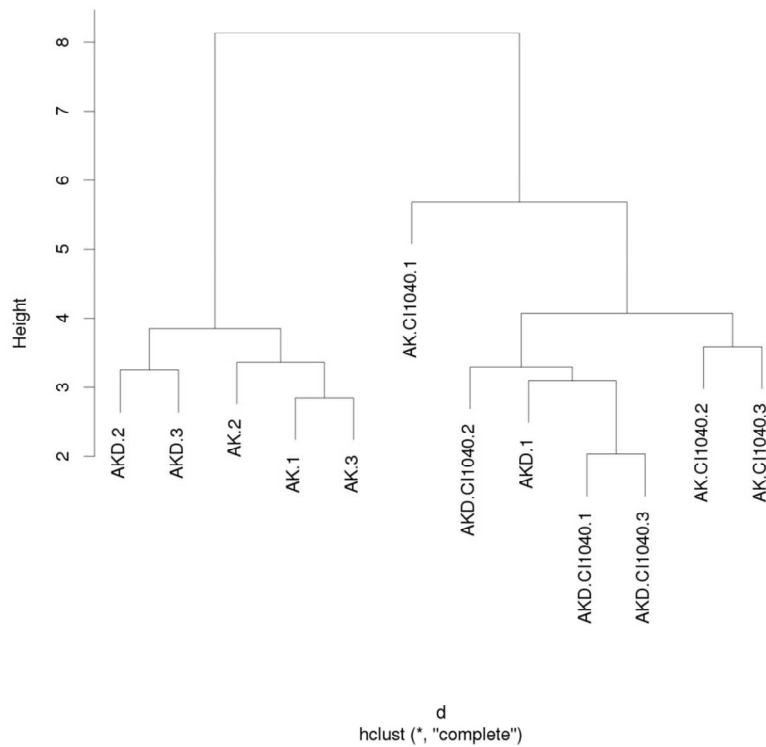
Supplementary figure 6: MAPK signature; Clustering AK and AKD mice samples



Supplementary figure 7: Wnt signature; Clustering AK and AKD mice samples treated with CI1040



Supplementary figure 8: Stem cells signature; Clustering AK and AKD mice samples treated with CI1040

MAPK signature - AK-AKDCI1040_pt1.csv**MAPK signature - AK-AKDCI1040_pt2.csv****Supplementary figure 9: MAPK signature; Clustering AK and AKD mice samples treated with CI1040**

LIST OF REFERENCES

- Aberle, H., A. Bauer, et al. (1997). "beta-catenin is a target for the ubiquitin-proteasome pathway." EMBO J **16**(13): 3797-3804.
- Abremski, K. and R. Hoess (1984). "Bacteriophage P1 site-specific recombination. Purification and properties of the Cre recombinase protein." J Biol Chem **259**(3): 1509-1514.
- Adisheshaiah, P., J. Li, et al. (2008). "ERK signaling regulates tumor promoter induced c-Jun recruitment at the Fra-1 promoter." Biochem Biophys Res Commun **371**(2): 304-308.
- Adisheshaiah, P., M. Vaz, et al. (2008). "A Fra-1-dependent, matrix metalloproteinase driven EGFR activation promotes human lung epithelial cell motility and invasion." J Cell Physiol **216**(2): 405-412.
- Alberici, P., E. de Pater, et al. (2007). "Aneuploidy arises at early stages of Apc-driven intestinal tumorigenesis and pinpoints conserved chromosomal loci of allelic imbalance between mouse and human." Am J Pathol **170**(1): 377-387.
- Allegra, C. J., J. M. Jessup, et al. (2009). "American Society of Clinical Oncology provisional clinical opinion: testing for KRAS gene mutations in patients with metastatic colorectal carcinoma to predict response to anti-epidermal growth factor receptor monoclonal antibody therapy." J Clin Oncol **27**(12): 2091-2096.
- Almoguera, C., D. Shibata, et al. (1988). "Most human carcinomas of the exocrine pancreas contain mutant c-K-ras genes." Cell **53**(4): 549-554.
- Askham, J. M., P. Moncur, et al. (2000). "Regulation and function of the interaction between the APC tumour suppressor protein and EB1." Oncogene **19**(15): 1950-1958.
- Baan, B., E. Pardali, et al. (2010). "In situ proximity ligation detection of c-Jun/AP-1 dimers reveals increased levels of c-Jun/Fra1 complexes in aggressive breast cancer cell lines in vitro and in vivo." Mol Cell Proteomics **9**(9): 1982-1990.
- Baker, S. J., A. C. Preisinger, et al. (1990). "p53 gene mutations occur in combination with 17p allelic deletions as late events in colorectal tumorigenesis." Cancer Res **50**(23): 7717-7722.

- Barker, N. and H. Clevers (2007). "Tracking down the stem cells of the intestine: strategies to identify adult stem cells." Gastroenterology **133**(6): 1755-1760.
- Barker, N., R. A. Ridgway, et al. (2009). "Crypt stem cells as the cells-of-origin of intestinal cancer." Nature **457**(7229): 608-611.
- Barker, N., J. H. van Es, et al. (2007). "Identification of stem cells in small intestine and colon by marker gene Lgr5." Nature **449**(7165): 1003-1007.
- Batlle, E., J. T. Henderson, et al. (2002). "Beta-catenin and TCF mediate cell positioning in the intestinal epithelium by controlling the expression of EphB/ephrinB." Cell **111**(2): 251-263.
- Benhattar, J., L. Losi, et al. (1993). "Prognostic significance of K-ras mutations in colorectal carcinoma." Gastroenterology **104**(4): 1044-1048.
- Bennecke, M., L. Kriegl, et al. (2010). "Ink4a/Arf and oncogene-induced senescence prevent tumor progression during alternative colorectal tumorigenesis." Cancer Cell **18**(2): 135-146.
- Bermudez, O., P. Jouandin, et al. (2011). "Post-transcriptional regulation of the DUSP6/MKP-3 phosphatase by MEK/ERK signaling and hypoxia." J Cell Physiol **226**(1): 276-284.
- Bjerknes, M. and H. Cheng (2005). "Gastrointestinal stem cells. II. Intestinal stem cells." Am J Physiol Gastrointest Liver Physiol **289**(3): G381-387.
- Bodmer, W. F., C. J. Bailey, et al. (1987). "Localization of the gene for familial adenomatous polyposis on chromosome 5." Nature **328**(6131): 614-616.
- Bokemeyer, C., I. Bondarenko, et al. (2009). "Fluorouracil, leucovorin, and oxaliplatin with and without cetuximab in the first-line treatment of metastatic colorectal cancer." J Clin Oncol **27**(5): 663-671.
- Breault, D. T., I. M. Min, et al. (2008). "Generation of mTert-GFP mice as a model to identify and study tissue progenitor cells." Proc Natl Acad Sci U S A **105**(30): 10420-10425.
- Brunet, A., D. Roux, et al. (1999). "Nuclear translocation of p42/p44 mitogen-activated protein kinase is required for growth factor-induced gene expression and cell cycle entry." EMBO J **18**(3): 664-674.
- Cadigan, K. M. and Y. I. Liu (2006). "Wnt signaling: complexity at the surface." J Cell Sci **119**(Pt 3): 395-402.
- Cagnol, S. and J. C. Chambard (2010). "ERK and cell death: mechanisms of ERK-induced cell death--apoptosis, autophagy and senescence." FEBS J **277**(1): 2-21.
- Calcagno, S. R., S. Li, et al. (2008). "Oncogenic K-ras promotes early carcinogenesis in the mouse proximal colon." Int J Cancer **122**(11): 2462-2470.

- Camps, M., A. Nichols, et al. (2000). "Dual specificity phosphatases: a gene family for control of MAP kinase function." FASEB J **14**(1): 6-16.
- Camps, M., A. Nichols, et al. (1998). "Catalytic activation of the phosphatase MKP-3 by ERK2 mitogen-activated protein kinase." Science **280**(5367): 1262-1265.
- Castellano, E. and J. Downward (2011). "RAS Interaction with PI3K: More Than Just Another Effector Pathway." Genes Cancer **2**(3): 261-274.
- Caunt, C. J. and S. M. Keyse (2012). "Dual-specificity MAP kinase phosphatases (MKPs): Shaping the outcome of MAP kinase signalling." FEBS J.
- Chan, D. W., V. W. Liu, et al. (2008). "Loss of MKP3 mediated by oxidative stress enhances tumorigenicity and chemoresistance of ovarian cancer cells." Carcinogenesis **29**(9): 1742-1750.
- Chattopadhyay, S., R. Machado-Pinilla, et al. (2006). "MKP1/CL100 controls tumor growth and sensitivity to cisplatin in non-small-cell lung cancer." Oncogene **25**(23): 3335-3345.
- Chen, H. J., L. S. Hsu, et al. (2012). "The beta-catenin/TCF complex as a novel target of resveratrol in the Wnt/beta-catenin signaling pathway." Biochem Pharmacol **84**(9): 1143-1153.
- Cheng, H. and C. P. Leblond (1974). "Origin, differentiation and renewal of the four main epithelial cell types in the mouse small intestine. I. Columnar cell." Am J Anat **141**(4): 461-479.
- Chi, H., S. P. Barry, et al. (2006). "Dynamic regulation of pro- and anti-inflammatory cytokines by MAPK phosphatase 1 (MKP-1) in innate immune responses." Proc Natl Acad Sci U S A **103**(7): 2274-2279.
- Chuderland, D., A. Konson, et al. (2008). "Identification and characterization of a general nuclear translocation signal in signaling proteins." Mol Cell **31**(6): 850-861.
- Chuderland, D. and R. Seger (2005). "Protein-protein interactions in the regulation of the extracellular signal-regulated kinase." Mol Biotechnol **29**(1): 57-74.
- Clevers, H. (2006). "Wnt/beta-catenin signaling in development and disease." Cell **127**(3): 469-480.
- Conlin, A., G. Smith, et al. (2005). "The prognostic significance of K-ras, p53, and APC mutations in colorectal carcinoma." Gut **54**(9): 1283-1286.
- Cui, Y., I. Parra, et al. (2006). "Elevated expression of mitogen-activated protein kinase phosphatase 3 in breast tumors: a mechanism of tamoxifen resistance." Cancer Res **66**(11): 5950-5959.
- Davies, H., G. R. Bignell, et al. (2002). "Mutations of the BRAF gene in human cancer." Nature **417**(6892): 949-954.

- Davies, S. P., H. Reddy, et al. (2000). "Specificity and mechanism of action of some commonly used protein kinase inhibitors." Biochem J **351**(Pt 1): 95-105.
- Day, C. L. and T. Alber (2000). "Crystal structure of the amino-terminal coiled-coil domain of the APC tumor suppressor." J Mol Biol **301**(1): 147-156.
- de Lau, W., N. Barker, et al. (2011). "Lgr5 homologues associate with Wnt receptors and mediate R-spondin signalling." Nature **476**(7360): 293-297.
- De Palma, M. and D. Hanahan (2012). "The biology of personalized cancer medicine: facing individual complexities underlying hallmark capabilities." Mol Oncol **6**(2): 111-127.
- De Roock, W., B. Claes, et al. (2010). "Effects of KRAS, BRAF, NRAS, and PIK3CA mutations on the efficacy of cetuximab plus chemotherapy in chemotherapy-refractory metastatic colorectal cancer: a retrospective consortium analysis." Lancet Oncol **11**(8): 753-762.
- de Santa Barbara, P., G. R. van den Brink, et al. (2003). "Development and differentiation of the intestinal epithelium." Cell Mol Life Sci **60**(7): 1322-1332.
- de Sousa, E. M. F., S. Colak, et al. (2011). "Methylation of cancer-stem-cell-associated Wnt target genes predicts poor prognosis in colorectal cancer patients." Cell Stem Cell **9**(5): 476-485.
- DeAlmeida, V. I., L. Miao, et al. (2007). "The soluble wnt receptor Frizzled8CRD-hFc inhibits the growth of teratocarcinomas in vivo." Cancer Res **67**(11): 5371-5379.
- DeNicola, G. M., F. A. Karreth, et al. (2011). "Oncogene-induced Nrf2 transcription promotes ROS detoxification and tumorigenesis." Nature **475**(7354): 106-109.
- Denkert, C., W. D. Schmitt, et al. (2002). "Expression of mitogen-activated protein kinase phosphatase-1 (MKP-1) in primary human ovarian carcinoma." Int J Cancer **102**(5): 507-513.
- Dickinson, R. J. and S. M. Keyse (2006). "Diverse physiological functions for dual-specificity MAP kinase phosphatases." J Cell Sci **119**(Pt 22): 4607-4615.
- Drosopoulos, K. G., M. L. Roberts, et al. (2005). "Transformation by oncogenic RAS sensitizes human colon cells to TRAIL-induced apoptosis by up-regulating death receptor 4 and death receptor 5 through a MEK-dependent pathway." J Biol Chem **280**(24): 22856-22867.
- Eblaghie, M. C., J. S. Lunn, et al. (2003). "Negative feedback regulation of FGF signaling levels by Pyst1/MKP3 in chick embryos." Curr Biol **13**(12): 1009-1018.
- Eferl, R., A. Hoebertz, et al. (2004). "The Fos-related antigen Fra-1 is an activator of bone matrix formation." EMBO J **23**(14): 2789-2799.

- el Marjou, F., K. P. Janssen, et al. (2004). "Tissue-specific and inducible Cre-mediated recombination in the gut epithelium." Genesis **39**(3): 186-193.
- Ellis, C. A. and G. Clark (2000). "The importance of being K-Ras." Cell Signal **12**(7): 425-434.
- Fagotto, F., U. Gluck, et al. (1998). "Nuclear localization signal-independent and importin/karyopherin-independent nuclear import of beta-catenin." Curr Biol **8**(4): 181-190.
- Fagotto, F., E. Jho, et al. (1999). "Domains of axin involved in protein-protein interactions, Wnt pathway inhibition, and intracellular localization." J Cell Biol **145**(4): 741-756.
- Farooq, A., G. Chaturvedi, et al. (2001). "Solution structure of ERK2 binding domain of MAPK phosphatase MKP-3: structural insights into MKP-3 activation by ERK2." Mol Cell **7**(2): 387-399.
- Farooq, A. and M. M. Zhou (2004). "Structure and regulation of MAPK phosphatases." Cell Signal **16**(7): 769-779.
- Fjeld, C. C., A. E. Rice, et al. (2000). "Mechanistic basis for catalytic activation of mitogen-activated protein kinase phosphatase 3 by extracellular signal-regulated kinase." J Biol Chem **275**(10): 6749-6757.
- Fodde, R., R. Smits, et al. (2001). "APC, signal transduction and genetic instability in colorectal cancer." Nat Rev Cancer **1**(1): 55-67.
- Frazier, W. J., X. Wang, et al. (2009). "Increased inflammation, impaired bacterial clearance, and metabolic disruption after gram-negative sepsis in Mkp-1-deficient mice." J Immunol **183**(11): 7411-7419.
- Furukawa, T., R. Fujisaki, et al. (2005). "Distinct progression pathways involving the dysfunction of DUSP6/MKP-3 in pancreatic intraepithelial neoplasia and intraductal papillary-mucinous neoplasms of the pancreas." Mod Pathol **18**(8): 1034-1042.
- Gannon, M., P. L. Herrera, et al. (2000). "Mosaic Cre-mediated recombination in pancreas using the pdx-1 enhancer/promoter." Genesis **26**(2): 143-144.
- Givant-Horwitz, V., B. Davidson, et al. (2004). "The PAC-1 dual specificity phosphatase predicts poor outcome in serous ovarian carcinoma." Gynecol Oncol **93**(2): 517-523.
- Glinka, A., C. Dolde, et al. (2011). "LGR4 and LGR5 are R-spondin receptors mediating Wnt/beta-catenin and Wnt/PCP signalling." EMBO Rep **12**(10): 1055-1061.
- Grandis, J. R. and J. C. Sok (2004). "Signaling through the epidermal growth factor receptor during the development of malignancy." Pharmacol Ther **102**(1): 37-46.

- Groden, J., A. Thliveris, et al. (1991). "Identification and characterization of the familial adenomatous polyposis coli gene." Cell **66**(3): 589-600.
- Groom, L. A., A. A. Sneddon, et al. (1996). "Differential regulation of the MAP, SAP and RK/p38 kinases by Pyst1, a novel cytosolic dual-specificity phosphatase." EMBO J **15**(14): 3621-3632.
- Guerra, C., N. Mijimolle, et al. (2003). "Tumor induction by an endogenous K-ras oncogene is highly dependent on cellular context." Cancer Cell **4**(2): 111-120.
- Guerra, C., A. J. Schuhmacher, et al. (2007). "Chronic pancreatitis is essential for induction of pancreatic ductal adenocarcinoma by K-Ras oncogenes in adult mice." Cancer Cell **11**(3): 291-302.
- Gupta, S., A. R. Ramjaun, et al. (2007). "Binding of ras to phosphoinositide 3-kinase p110alpha is required for ras-driven tumorigenesis in mice." Cell **129**(5): 957-968.
- Habets, G. G., E. H. Scholtes, et al. (1994). "Identification of an invasion-inducing gene, Tiam-1, that encodes a protein with homology to GDP-GTP exchangers for Rho-like proteins." Cell **77**(4): 537-549.
- Haigis, K. M., K. R. Kendall, et al. (2008). "Differential effects of oncogenic K-Ras and N-Ras on proliferation, differentiation and tumor progression in the colon." Nat Genet **40**(5): 600-608.
- Hamdi, M., H. E. Popeijus, et al. (2008). "ATF3 and Fra1 have opposite functions in JNK- and ERK-dependent DNA damage responses." DNA Repair (Amst) **7**(3): 487-496.
- Hart, M. J., R. de los Santos, et al. (1998). "Downregulation of beta-catenin by human Axin and its association with the APC tumor suppressor, beta-catenin and GSK3 beta." Curr Biol **8**(10): 573-581.
- Hasselblatt, P., L. Gresh, et al. (2008). "The role of the transcription factor AP-1 in colitis-associated and beta-catenin-dependent intestinal tumorigenesis in mice." Oncogene **27**(47): 6102-6109.
- He, T. C., A. B. Sparks, et al. (1998). "Identification of c-MYC as a target of the APC pathway." Science **281**(5382): 1509-1512.
- Heid, I., C. Lubeseder-Martellato, et al. (2011). "Early requirement of Rac1 in a mouse model of pancreatic cancer." Gastroenterology **141**(2): 719-730, 730 e711-717.
- Hingorani, S. R., E. F. Petricoin, et al. (2003). "Preinvasive and invasive ductal pancreatic cancer and its early detection in the mouse." Cancer Cell **4**(6): 437-450.
- Hingorani, S. R., L. Wang, et al. (2005). "Trp53R172H and KrasG12D cooperate to promote chromosomal instability and widely metastatic pancreatic ductal adenocarcinoma in mice." Cancer Cell **7**(5): 469-483.

- Hoess, R. H. and K. Abremski (1984). "Interaction of the bacteriophage P1 recombinase Cre with the recombining site loxP." Proc Natl Acad Sci U S A **81**(4): 1026-1029.
- Hoornaert, I., P. Marynen, et al. (2003). "MAPK phosphatase DUSP16/MKP-7, a candidate tumor suppressor for chromosome region 12p12-13, reduces BCR-ABL-induced transformation." Oncogene **22**(49): 7728-7736.
- Hruban, R. H., N. V. Adsay, et al. (2001). "Pancreatic intraepithelial neoplasia: a new nomenclature and classification system for pancreatic duct lesions." Am J Surg Pathol **25**(5): 579-586.
- Hruban, R. H., M. Goggins, et al. (2000). "Progression model for pancreatic cancer." Clin Cancer Res **6**(8): 2969-2972.
- Hruban, R. H., A. D. van Mansfeld, et al. (1993). "K-ras oncogene activation in adenocarcinoma of the human pancreas. A study of 82 carcinomas using a combination of mutant-enriched polymerase chain reaction analysis and allele-specific oligonucleotide hybridization." Am J Pathol **143**(2): 545-554.
- Hruban, R. H., R. E. Wilentz, et al. (2000). "Genetic progression in the pancreatic ducts." Am J Pathol **156**(6): 1821-1825.
- Huang, C. Y. and T. H. Tan (2012). "DUSPs, to MAP kinases and beyond." Cell Biosci **2**(1): 24.
- Huang, S. M., Y. M. Mishina, et al. (2009). "Tankyrase inhibition stabilizes axin and antagonizes Wnt signalling." Nature **461**(7264): 614-620.
- Ireland, H., R. Kemp, et al. (2004). "Inducible Cre-mediated control of gene expression in the murine gastrointestinal tract: effect of loss of beta-catenin." Gastroenterology **126**(5): 1236-1246.
- Iitzkovitz, S., A. Lyubimova, et al. (2012). "Single-molecule transcript counting of stem-cell markers in the mouse intestine." Nat Cell Biol **14**(1): 106-114.
- Jackson, E. L., N. Willis, et al. (2001). "Analysis of lung tumor initiation and progression using conditional expression of oncogenic K-ras." Genes Dev **15**(24): 3243-3248.
- Jaffee, E. M., R. H. Hruban, et al. (2002). "Focus on pancreas cancer." Cancer Cell **2**(1): 25-28.
- Janssen, K. P., P. Alberici, et al. (2006). "APC and oncogenic KRAS are synergistic in enhancing Wnt signaling in intestinal tumor formation and progression." Gastroenterology **131**(4): 1096-1109.
- Jin, Y., T. J. Calvert, et al. (2010). "Mice deficient in Mkp-1 develop more severe pulmonary hypertension and greater lung protein levels of arginase in response to chronic hypoxia." Am J Physiol Heart Circ Physiol **298**(5): H1518-1528.

- Jochum, W., E. Passegue, et al. (2001). "AP-1 in mouse development and tumorigenesis." Oncogene **20**(19): 2401-2412.
- Johnson, L., K. Mercer, et al. (2001). "Somatic activation of the K-ras oncogene causes early onset lung cancer in mice." Nature **410**(6832): 1111-1116.
- Jurek, A., K. Amagasaki, et al. (2009). "Negative and positive regulation of MAPK phosphatase 3 controls platelet-derived growth factor-induced Erk activation." J Biol Chem **284**(7): 4626-4634.
- Karlsson, M., J. Mathers, et al. (2004). "Both nuclear-cytoplasmic shuttling of the dual specificity phosphatase MKP-3 and its ability to anchor MAP kinase in the cytoplasm are mediated by a conserved nuclear export signal." J Biol Chem **279**(40): 41882-41891.
- Kawasaki, Y., T. Senda, et al. (2000). "Asef, a link between the tumor suppressor APC and G-protein signaling." Science **289**(5482): 1194-1197.
- Kern, S., R. Hruban, et al. (2001). "A white paper: the product of a pancreas cancer think tank." Cancer Res **61**(12): 4923-4932.
- Keyse, S. M. (2000). "Protein phosphatases and the regulation of mitogen-activated protein kinase signalling." Curr Opin Cell Biol **12**(2): 186-192.
- Kim, H. S., M. C. Song, et al. (2003). "Constitutive induction of p-Erk1/2 accompanied by reduced activities of protein phosphatases 1 and 2A and MKP3 due to reactive oxygen species during cellular senescence." J Biol Chem **278**(39): 37497-37510.
- Kim, K., K. Nose, et al. (2000). "Significance of nuclear relocalization of ERK1/2 in reactivation of c-fos transcription and DNA synthesis in senescent fibroblasts." J Biol Chem **275**(27): 20685-20692.
- Kim, L. C., L. Song, et al. (2009). "Src kinases as therapeutic targets for cancer." Nat Rev Clin Oncol **6**(10): 587-595.
- Kim, S. C., J. S. Hahn, et al. (1999). "Constitutive activation of extracellular signal-regulated kinase in human acute leukemias: combined role of activation of MEK, hyperexpression of extracellular signal-regulated kinase, and downregulation of a phosphatase, PAC1." Blood **93**(11): 3893-3899.
- Kressner, U., J. Bjorheim, et al. (1998). "Ki-ras mutations and prognosis in colorectal cancer." Eur J Cancer **34**(4): 518-521.
- Laderoute, K. R., H. L. Mendonca, et al. (1999). "Mitogen-activated protein kinase phosphatase-1 (MKP-1) expression is induced by low oxygen conditions found in solid tumor microenvironments. A candidate MKP for the inactivation of hypoxia-inducible stress-activated protein kinase/c-Jun N-terminal protein kinase activity." J Biol Chem **274**(18): 12890-12897.
- Lambert, J. M., Q. T. Lambert, et al. (2002). "Tiam1 mediates Ras activation of Rac by a PI(3)K-independent mechanism." Nat Cell Biol **4**(8): 621-625.

- Lavergne, E., I. Hendaoui, et al. (2011). "Blocking Wnt signaling by SFRP-like molecules inhibits in vivo cell proliferation and tumor growth in cells carrying active beta-catenin." Oncogene **30**(4): 423-433.
- Lee, S., N. Syed, et al. (2010). "DUSP16 is an epigenetically regulated determinant of JNK signalling in Burkitt's lymphoma." Br J Cancer **103**(2): 265-274.
- Lenormand, P., J. M. Brondello, et al. (1998). "Growth factor-induced p42/p44 MAPK nuclear translocation and retention requires both MAPK activation and neosynthesis of nuclear anchoring proteins." J Cell Biol **142**(3): 625-633.
- Levy-Nissenbaum, O., O. Sagi-Assif, et al. (2003). "Dual-specificity phosphatase Pyst2-L is constitutively highly expressed in myeloid leukemia and other malignant cells." Oncogene **22**(48): 7649-7660.
- Levy-Nissenbaum, O., O. Sagi-Assif, et al. (2003). "cDNA microarray analysis reveals an overexpression of the dual-specificity MAPK phosphatase PYST2 in acute leukemia." Methods Enzymol **366**: 103-113.
- Levy-Nissenbaum, O., O. Sagi-Assif, et al. (2003). "Overexpression of the dual-specificity MAPK phosphatase PYST2 in acute leukemia." Cancer Lett **199**(2): 185-192.
- Li, W., L. Song, et al. (2012). "Increased levels of DUSP6 phosphatase stimulate tumourigenesis in a molecularly distinct melanoma subtype." Pigment Cell Melanoma Res **25**(2): 188-199.
- Lievre, A., J. B. Bachet, et al. (2008). "KRAS mutations as an independent prognostic factor in patients with advanced colorectal cancer treated with cetuximab." J Clin Oncol **26**(3): 374-379.
- Lievre, A., J. B. Bachet, et al. (2006). "KRAS mutation status is predictive of response to cetuximab therapy in colorectal cancer." Cancer Res **66**(8): 3992-3995.
- Liu, C., Y. Shi, et al. (2005). "Dual-specificity phosphatase DUSP1 protects overactivation of hypoxia-inducible factor 1 through inactivating ERK MAPK." Exp Cell Res **309**(2): 410-418.
- Liu, Y., J. Lagowski, et al. (2007). "Microtubule disruption and tumor suppression by mitogen-activated protein kinase phosphatase 4." Cancer Res **67**(22): 10711-10719.
- Liu, Y., E. G. Shepherd, et al. (2007). "MAPK phosphatases--regulating the immune response." Nat Rev Immunol **7**(3): 202-212.
- Livet, J., T. A. Weissman, et al. (2007). "Transgenic strategies for combinatorial expression of fluorescent proteins in the nervous system." Nature **450**(7166): 56-62.

- Loda, M., P. Capodiceci, et al. (1996). "Expression of mitogen-activated protein kinase phosphatase-1 in the early phases of human epithelial carcinogenesis." Am J Pathol **149**(5): 1553-1564.
- Lynch, H. T. and A. de la Chapelle (2003). "Hereditary colorectal cancer." N Engl J Med **348**(10): 919-932.
- Magi-Galluzzi, C., R. Mishra, et al. (1997). "Mitogen-activated protein kinase phosphatase 1 is overexpressed in prostate cancers and is inversely related to apoptosis." Lab Invest **76**(1): 37-51.
- Malliri, A., R. A. van der Kammen, et al. (2002). "Mice deficient in the Rac activator Tiam1 are resistant to Ras-induced skin tumours." Nature **417**(6891): 867-871.
- Mandl, M., D. N. Slack, et al. (2005). "Specific inactivation and nuclear anchoring of extracellular signal-regulated kinase 2 by the inducible dual-specificity protein phosphatase DUSP5." Mol Cell Biol **25**(5): 1830-1845.
- Mann, B., M. Gelos, et al. (1999). "Target genes of beta-catenin-T cell-factor/lymphoid-enhancer-factor signaling in human colorectal carcinomas." Proc Natl Acad Sci U S A **96**(4): 1603-1608.
- Mao, J., J. Wang, et al. (2001). "Low-density lipoprotein receptor-related protein-5 binds to Axin and regulates the canonical Wnt signaling pathway." Mol Cell **7**(4): 801-809.
- Marchetti, S., C. Gimond, et al. (2005). "Extracellular signal-regulated kinases phosphorylate mitogen-activated protein kinase phosphatase 3/DUSP6 at serines 159 and 197, two sites critical for its proteasomal degradation." Mol Cell Biol **25**(2): 854-864.
- Mark, J. K., R. A. Aubin, et al. (2008). "Inhibition of mitogen-activated protein kinase phosphatase 3 activity by interdomain binding." J Biol Chem **283**(42): 28574-28583.
- Mark, J. K., S. Smith, et al. (2007). "Over-expression and refolding of MAP kinase phosphatase 3." Protein Expr Purif **54**(2): 253-260.
- Masuda, K., H. Shima, et al. (2001). "MKP-7, a novel mitogen-activated protein kinase phosphatase, functions as a shuttle protein." J Biol Chem **276**(42): 39002-39011.
- Matozaki, T., Y. Murata, et al. (2009). "Protein tyrosine phosphatase SHP-2: a proto-oncogene product that promotes Ras activation." Cancer Sci **100**(10): 1786-1793.
- Mechta, F., D. Lallemand, et al. (1997). "Transformation by ras modifies AP1 composition and activity." Oncogene **14**(7): 837-847.
- Merlos-Suarez, A., F. M. Barriga, et al. (2011). "The intestinal stem cell signature identifies colorectal cancer stem cells and predicts disease relapse." Cell Stem Cell **8**(5): 511-524.

- Messina, S., L. Frati, et al. (2011). "Dual-specificity phosphatase DUSP6 has tumor-promoting properties in human glioblastomas." Oncogene **30**(35): 3813-3820.
- Migliardi, G., F. Sassi, et al. (2012). "Inhibition of MEK and PI3K/mTOR suppresses tumor growth but does not cause tumor regression in patient-derived xenografts of RAS-mutant colorectal carcinomas." Clin Cancer Res **18**(9): 2515-2525.
- Millet, C. and Y. E. Zhang (2007). "Roles of Smad3 in TGF-beta signaling during carcinogenesis." Crit Rev Eukaryot Gene Expr **17**(4): 281-293.
- Moncho-Amor, V., I. Ibanez de Caceres, et al. (2011). "DUSP1/MKP1 promotes angiogenesis, invasion and metastasis in non-small-cell lung cancer." Oncogene **30**(6): 668-678.
- Montgomery, R. K., D. L. Carlone, et al. (2011). "Mouse telomerase reverse transcriptase (mTert) expression marks slowly cycling intestinal stem cells." Proc Natl Acad Sci U S A **108**(1): 179-184.
- Mooi, W. J. and D. S. Peeper (2006). "Oncogene-induced cell senescence--halting on the road to cancer." N Engl J Med **355**(10): 1037-1046.
- Morton, J. P., D. S. Klimstra, et al. (2008). "Trp53 deletion stimulates the formation of metastatic pancreatic tumors." Am J Pathol **172**(4): 1081-1087.
- Morton, J. P., P. Timpson, et al. (2010). "Mutant p53 drives metastasis and overcomes growth arrest/senescence in pancreatic cancer." Proc Natl Acad Sci U S A **107**(1): 246-251.
- Moser, A. R., A. R. Shoemaker, et al. (1995). "Homozygosity for the Min allele of Apc results in disruption of mouse development prior to gastrulation." Dev Dyn **203**(4): 422-433.
- Muda, M., U. Boschert, et al. (1996). "MKP-3, a novel cytosolic protein-tyrosine phosphatase that exemplifies a new class of mitogen-activated protein kinase phosphatase." J Biol Chem **271**(8): 4319-4326.
- Muda, M., A. Theodosiou, et al. (1998). "The mitogen-activated protein kinase phosphatase-3 N-terminal noncatalytic region is responsible for tight substrate binding and enzymatic specificity." J Biol Chem **273**(15): 9323-9329.
- Munoz, J., D. E. Stange, et al. (2012). "The Lgr5 intestinal stem cell signature: robust expression of proposed quiescent '+4' cell markers." EMBO J **31**(14): 3079-3091.
- Nateri, A. S., B. Spencer-Dene, et al. (2005). "Interaction of phosphorylated c-Jun with TCF4 regulates intestinal cancer development." Nature **437**(7056): 281-285.

- Nathke, I. S. (2004). "The adenomatous polyposis coli protein: the Achilles heel of the gut epithelium." Annu Rev Cell Dev Biol **20**: 337-366.
- Navas, C., I. Hernandez-Porras, et al. (2012). "EGF receptor signaling is essential for k-ras oncogene-driven pancreatic ductal adenocarcinoma." Cancer Cell **22**(3): 318-330.
- Nishimoto, S., M. Kusakabe, et al. (2005). "Requirement of the MEK5-ERK5 pathway for neural differentiation in *Xenopus* embryonic development." EMBO Rep **6**(11): 1064-1069.
- Nonn, L., D. Duong, et al. (2007). "Chemopreventive anti-inflammatory activities of curcumin and other phytochemicals mediated by MAP kinase phosphatase-5 in prostate cells." Carcinogenesis **28**(6): 1188-1196.
- Normanno, N., S. Tejpar, et al. (2009). "Implications for KRAS status and EGFR-targeted therapies in metastatic CRC." Nat Rev Clin Oncol **6**(9): 519-527.
- Nunes-Xavier, C. E., C. Tarrega, et al. (2010). "Differential up-regulation of MAP kinase phosphatases MKP3/DUSP6 and DUSP5 by Ets2 and c-Jun converge in the control of the growth arrest versus proliferation response of MCF-7 breast cancer cells to phorbol ester." J Biol Chem **285**(34): 26417-26430.
- Nusse, R. and H. E. Varmus (1982). "Many tumors induced by the mouse mammary tumor virus contain a provirus integrated in the same region of the host genome." Cell **31**(1): 99-109.
- Nusslein-Volhard, C. and E. Wieschaus (1980). "Mutations affecting segment number and polarity in *Drosophila*." Nature **287**(5785): 795-801.
- Okudela, K., T. Yazawa, et al. (2009). "Down-regulation of DUSP6 expression in lung cancer: its mechanism and potential role in carcinogenesis." Am J Pathol **175**(2): 867-881.
- Olive, K. P., D. A. Tuveson, et al. (2004). "Mutant p53 gain of function in two mouse models of Li-Fraumeni syndrome." Cell **119**(6): 847-860.
- Owens, D. M. and S. M. Keyse (2007). "Differential regulation of MAP kinase signalling by dual-specificity protein phosphatases." Oncogene **26**(22): 3203-3213.
- Park, K. S., S. H. Jeon, et al. (2006). "APC inhibits ERK pathway activation and cellular proliferation induced by RAS." J Cell Sci **119**(Pt 5): 819-827.
- Patterson, K. I., T. Brummer, et al. (2009). "Dual-specificity phosphatases: critical regulators with diverse cellular targets." Biochem J **418**(3): 475-489.
- Persons, D. L., E. M. Yazlovitskaya, et al. (2000). "Effect of extracellular signal-regulated kinase on p53 accumulation in response to cisplatin." J Biol Chem **275**(46): 35778-35785.

- Pinto, D. and H. Clevers (2005). "Wnt control of stem cells and differentiation in the intestinal epithelium." Exp Cell Res **306**(2): 357-363.
- Pinto, D., A. Gregorieff, et al. (2003). "Canonical Wnt signals are essential for homeostasis of the intestinal epithelium." Genes Dev **17**(14): 1709-1713.
- Polakis, P. (2000). "Wnt signaling and cancer." Genes Dev **14**(15): 1837-1851.
- Pollock, C. B., S. Shirasawa, et al. (2005). "Oncogenic K-RAS is required to maintain changes in cytoskeletal organization, adhesion, and motility in colon cancer cells." Cancer Res **65**(4): 1244-1250.
- Popovici, V., E. Budinska, et al. (2012). "Identification of a poor-prognosis BRAF-mutant-like population of patients with colon cancer." J Clin Oncol **30**(12): 1288-1295.
- Potten, C. S., L. Kovacs, et al. (1974). "Continuous labelling studies on mouse skin and intestine." Cell Tissue Kinet **7**(3): 271-283.
- Potten, C. S. and M. Loeffler (1990). "Stem cells: attributes, cycles, spirals, pitfalls and uncertainties. Lessons for and from the crypt." Development **110**(4): 1001-1020.
- Pouyssegur, J., V. Volmat, et al. (2002). "Fidelity and spatio-temporal control in MAP kinase (ERKs) signalling." Biochem Pharmacol **64**(5-6): 755-763.
- Powell, A. E., Y. Wang, et al. (2012). "The pan-ErbB negative regulator Lrig1 is an intestinal stem cell marker that functions as a tumor suppressor." Cell **149**(1): 146-158.
- Quelard, D., E. Lavergne, et al. (2008). "A cryptic frizzled module in cell surface collagen 18 inhibits Wnt/beta-catenin signaling." PLoS One **3**(4): e1878.
- Regan, C. P., W. Li, et al. (2002). "Erk5 null mice display multiple extraembryonic vascular and embryonic cardiovascular defects." Proc Natl Acad Sci U S A **99**(14): 9248-9253.
- Reya, T. and H. Clevers (2005). "Wnt signalling in stem cells and cancer." Nature **434**(7035): 843-850.
- Rigas, J. D., R. H. Hoff, et al. (2001). "Transition state analysis and requirement of Asp-262 general acid/base catalyst for full activation of dual-specificity phosphatase MKP3 by extracellular regulated kinase." Biochemistry **40**(14): 4398-4406.
- Rijsewijk, F., M. Schuermann, et al. (1987). "The Drosophila homolog of the mouse mammary oncogene int-1 is identical to the segment polarity gene wingless." Cell **50**(4): 649-657.
- Rinehart, J., A. A. Adjei, et al. (2004). "Multicenter phase II study of the oral MEK inhibitor, CI-1040, in patients with advanced non-small-cell lung, breast, colon, and pancreatic cancer." J Clin Oncol **22**(22): 4456-4462.

- Rubinfeld, B., I. Albert, et al. (1996). "Binding of GSK3beta to the APC-beta-catenin complex and regulation of complex assembly." Science **272**(5264): 1023-1026.
- Rubinfeld, B., B. Souza, et al. (1993). "Association of the APC gene product with beta-catenin." Science **262**(5140): 1731-1734.
- Salojin, K. V., I. B. Owusu, et al. (2006). "Essential role of MAPK phosphatase-1 in the negative control of innate immune responses." J Immunol **176**(3): 1899-1907.
- Sancho, E., E. Batlle, et al. (2004). "Signaling pathways in intestinal development and cancer." Annu Rev Cell Dev Biol **20**: 695-723.
- Sangiorgi, E. and M. R. Capecchi (2008). "Bmi1 is expressed in vivo in intestinal stem cells." Nat Genet **40**(7): 915-920.
- Sansom, O. J., V. Meniel, et al. (2006). "Loss of Apc allows phenotypic manifestation of the transforming properties of an endogenous K-ras oncogene in vivo." Proc Natl Acad Sci U S A **103**(38): 14122-14127.
- Sansom, O. J., K. R. Reed, et al. (2004). "Loss of Apc in vivo immediately perturbs Wnt signaling, differentiation, and migration." Genes Dev **18**(12): 1385-1390.
- Sato, T., J. H. van Es, et al. (2011). "Paneth cells constitute the niche for Lgr5 stem cells in intestinal crypts." Nature **469**(7330): 415-418.
- Schreiber, M., Z. Q. Wang, et al. (2000). "Placental vascularisation requires the AP-1 component fra1." Development **127**(22): 4937-4948.
- Sebolt-Leopold, J. S., D. T. Dudley, et al. (1999). "Blockade of the MAP kinase pathway suppresses growth of colon tumors in vivo." Nat Med **5**(7): 810-816.
- Seeling, J. M., J. R. Miller, et al. (1999). "Regulation of beta-catenin signaling by the B56 subunit of protein phosphatase 2A." Science **283**(5410): 2089-2091.
- Seth, D. and J. Rudolph (2006). "Redox regulation of MAP kinase phosphatase 3." Biochemistry **45**(28): 8476-8487.
- She, Q. B., N. Chen, et al. (2000). "ERKs and p38 kinase phosphorylate p53 protein at serine 15 in response to UV radiation." J Biol Chem **275**(27): 20444-20449.
- Shibata, H., K. Toyama, et al. (1997). "Rapid colorectal adenoma formation initiated by conditional targeting of the Apc gene." Science **278**(5335): 120-123.
- Shin, S., T. Asano, et al. (2009). "Activator protein-1 has an essential role in pancreatic cancer cells and is regulated by a novel Akt-mediated mechanism." Mol Cancer Res **7**(5): 745-754.

- Small, G. W., Y. Y. Shi, et al. (2007). "Mitogen-activated protein kinase phosphatase-1 is a mediator of breast cancer chemoresistance." Cancer Res **67**(9): 4459-4466.
- Smit, V. T., A. J. Boot, et al. (1988). "KRAS codon 12 mutations occur very frequently in pancreatic adenocarcinomas." Nucleic Acids Res **16**(16): 7773-7782.
- Smith, A., C. Price, et al. (1997). "Chromosomal localization of three human dual specificity phosphatase genes (DUSP4, DUSP6, and DUSP7)." Genomics **42**(3): 524-527.
- Snippert, H. J., L. G. van der Flier, et al. (2010). "Intestinal crypt homeostasis results from neutral competition between symmetrically dividing Lgr5 stem cells." Cell **143**(1): 134-144.
- Soriano, P. (1999). "Generalized lacZ expression with the ROSA26 Cre reporter strain." Nat Genet **21**(1): 70-71.
- Stanger, B. Z., A. J. Tanaka, et al. (2007). "Organ size is limited by the number of embryonic progenitor cells in the pancreas but not the liver." Nature **445**(7130): 886-891.
- Stelman, L. S., S. L. Abrams, et al. (2008). "Contributions of the Raf/MEK/ERK, PI3K/PTEN/Akt/mTOR and Jak/STAT pathways to leukemia." Leukemia **22**(4): 686-707.
- Stewart, A. E., S. Dowd, et al. (1999). "Crystal structure of the MAPK phosphatase Pyst1 catalytic domain and implications for regulated activation." Nat Struct Biol **6**(2): 174-181.
- Su, L. K., B. Vogelstein, et al. (1993). "Association of the APC tumor suppressor protein with catenins." Science **262**(5140): 1734-1737.
- Suh, E. K. and B. M. Gumbiner (2003). "Translocation of beta-catenin into the nucleus independent of interactions with FG-rich nucleoporins." Exp Cell Res **290**(2): 447-456.
- Sundqvist, A., A. Zieba, et al. (2012). "Specific interactions between Smad proteins and AP-1 components determine TGFbeta-induced breast cancer cell invasion." Oncogene.
- Sung Hee Lee, L.-L. H., Carol Shen, Geom Seog Seo, Scott Herdman, Nissi Varki, Maripat Corr, Jongdae Lee and Eyal Raz (2010). "ERK addiction drives intestinal tumorigenesis in APC^{min/+} mice." submitted.
- Suzuki, H., D. N. Watkins, et al. (2004). "Epigenetic inactivation of SFRP genes allows constitutive WNT signaling in colorectal cancer." Nat Genet **36**(4): 417-422.
- Takeda, K., I. Kinoshita, et al. (2008). "Clinicopathological significance of expression of p-c-Jun, TCF4 and beta-Catenin in colorectal tumors." BMC Cancer **8**: 328.

- Tang, D., D. Wu, et al. (2002). "ERK activation mediates cell cycle arrest and apoptosis after DNA damage independently of p53." J Biol Chem **277**(15): 12710-12717.
- Tanoue, T., T. Moriguchi, et al. (1999). "Molecular cloning and characterization of a novel dual specificity phosphatase, MKP-5." J Biol Chem **274**(28): 19949-19956.
- Tarasewicz, E. and J. S. Jeruss (2012). "Phospho-specific Smad3 signaling: impact on breast oncogenesis." Cell Cycle **11**(13): 2443-2451.
- Tenbaum, S. P., P. Ordonez-Moran, et al. (2012). "beta-catenin confers resistance to PI3K and AKT inhibitors and subverts FOXO3a to promote metastasis in colon cancer." Nat Med **18**(6): 892-901.
- Theodosiou, A. and A. Ashworth (2002). "MAP kinase phosphatases." Genome Biol **3**(7): REVIEWS3009.
- Tian, H., B. Biehs, et al. (2011). "A reserve stem cell population in small intestine renders Lgr5-positive cells dispensable." Nature **478**(7368): 255-259.
- Timpson, P., E. J. McGhee, et al. (2011). "Organotypic collagen I assay: a malleable platform to assess cell behaviour in a 3-dimensional context." J Vis Exp(56): e3089.
- Toualbi, K., M. C. Guller, et al. (2007). "Physical and functional cooperation between AP-1 and beta-catenin for the regulation of TCF-dependent genes." Oncogene **26**(24): 3492-3502.
- Tuveson, D. A., A. T. Shaw, et al. (2004). "Endogenous oncogenic K-ras(G12D) stimulates proliferation and widespread neoplastic and developmental defects." Cancer Cell **5**(4): 375-387.
- Ueda, K., H. Arakawa, et al. (2003). "Dual-specificity phosphatase 5 (DUSP5) as a direct transcriptional target of tumor suppressor p53." Oncogene **22**(36): 5586-5591.
- van der Flier, L. G., A. Haegbarth, et al. (2009). "OLFM4 is a robust marker for stem cells in human intestine and marks a subset of colorectal cancer cells." Gastroenterology **137**(1): 15-17.
- van der Flier, L. G., M. E. van Gijn, et al. (2009). "Transcription factor achaete scute-like 2 controls intestinal stem cell fate." Cell **136**(5): 903-912.
- van Es, J. H., T. Sato, et al. (2012). "Dll1(+) secretory progenitor cells revert to stem cells upon crypt damage." Nat Cell Biol **14**(10): 1099-1104.
- van Es, J. M., M. M. Polak, et al. (1995). "Molecular markers for diagnostic cytology of neoplasms in the head region of the pancreas: mutation of K-ras and overexpression of the p53 protein product." J Clin Pathol **48**(3): 218-222.

- Vial, E., E. Sahai, et al. (2003). "ERK-MAPK signaling coordinately regulates activity of Rac1 and RhoA for tumor cell motility." Cancer Cell 4(1): 67-79.
- Vogelstein, B., E. R. Fearon, et al. (1988). "Genetic alterations during colorectal-tumor development." N Engl J Med 319(9): 525-532.
- Vogelstein, B., E. R. Fearon, et al. (1989). "Allelotype of colorectal carcinomas." Science 244(4901): 207-211.
- Waalder, J., O. Machon, et al. (2012). "A novel tankyrase inhibitor decreases canonical Wnt signaling in colon carcinoma cells and reduces tumor growth in conditional APC mutant mice." Cancer Res 72(11): 2822-2832.
- Wang, H. Y., Z. Cheng, et al. (2003). "Overexpression of mitogen-activated protein kinase phosphatases MKP1, MKP2 in human breast cancer." Cancer Lett 191(2): 229-237.
- Wang, Y., N. Kakinuma, et al. (2006). "Nucleo-cytoplasmic shuttling of human Kank protein accompanies intracellular translocation of beta-catenin." J Cell Sci 119(Pt 19): 4002-4010.
- Wang, Y., A. Sacchetti, et al. (2012). "Identification of quiescent, stem-like cells in the distal female reproductive tract." PLoS One 7(7): e40691.
- Wang, Z., J. Xu, et al. (2006). "Mitogen-activated protein kinase phosphatase-1 is required for cisplatin resistance." Cancer Res 66(17): 8870-8877.
- Warmka, J. K., L. J. Mauro, et al. (2004). "Mitogen-activated protein kinase phosphatase-3 is a tumor promoter target in initiated cells that express oncogenic Ras." J Biol Chem 279(32): 33085-33092.
- Wielenga, V. J., R. Smits, et al. (1999). "Expression of CD44 in Apc and Tcf mutant mice implies regulation by the WNT pathway." Am J Pathol 154(2): 515-523.
- Willert, K., J. D. Brown, et al. (2003). "Wnt proteins are lipid-modified and can act as stem cell growth factors." Nature 423(6938): 448-452.
- Winder, T., A. Mundlein, et al. (2009). "Different types of K-Ras mutations are conversely associated with overall survival in patients with colorectal cancer." Oncol Rep 21(5): 1283-1287.
- Wong, V. C., H. Chen, et al. (2012). "Tumor suppressor dual-specificity phosphatase 6 (DUSP6) impairs cell invasion and epithelial-mesenchymal transition (EMT)-associated phenotype." Int J Cancer 130(1): 83-95.
- Wu, J. J., L. Zhang, et al. (2005). "The noncatalytic amino terminus of mitogen-activated protein kinase phosphatase 1 directs nuclear targeting and serum response element transcriptional regulation." Mol Cell Biol 25(11): 4792-4803.

- Wu, S., Y. Wang, et al. (2011). "Decreased expression of dual-specificity phosphatase 9 is associated with poor prognosis in clear cell renal cell carcinoma." BMC Cancer **11**: 413.
- Xu, S., T. Furukawa, et al. (2005). "Abrogation of DUSP6 by hypermethylation in human pancreatic cancer." J Hum Genet **50**(4): 159-167.
- Yamauchi, J., Y. Miyamoto, et al. (2005). "Ras activation of a Rac1 exchange factor, Tiam1, mediates neurotrophin-3-induced Schwann cell migration." Proc Natl Acad Sci U S A **102**(41): 14889-14894.
- Yan, K. S., L. A. Chia, et al. (2012). "The intestinal stem cell markers Bmi1 and Lgr5 identify two functionally distinct populations." Proc Natl Acad Sci U S A **109**(2): 466-471.
- Yanagawa, S., F. van Leeuwen, et al. (1995). "The dishevelled protein is modified by wingless signaling in Drosophila." Genes Dev **9**(9): 1087-1097.
- Yang, J. Y., C. S. Zong, et al. (2008). "ERK promotes tumorigenesis by inhibiting FOXO3a via MDM2-mediated degradation." Nat Cell Biol **10**(2): 138-148.
- Yeh, J. J., E. D. Routh, et al. (2009). "KRAS/BRAF mutation status and ERK1/2 activation as biomarkers for MEK1/2 inhibitor therapy in colorectal cancer." Mol Cancer Ther **8**(4): 834-843.
- Yeh, T. C., V. Marsh, et al. (2007). "Biological characterization of ARRY-142886 (AZD6244), a potent, highly selective mitogen-activated protein kinase kinase 1/2 inhibitor." Clin Cancer Res **13**(5): 1576-1583.
- Ying, H., A. C. Kimmelman, et al. (2012). "Oncogenic Kras maintains pancreatic tumors through regulation of anabolic glucose metabolism." Cell **149**(3): 656-670.
- Yip-Schneider, M. T., A. Lin, et al. (2001). "Pancreatic tumor cells with mutant K-ras suppress ERK activity by MEK-dependent induction of MAP kinase phosphatase-2." Biochem Biophys Res Commun **280**(4): 992-997.
- Yokoyama, A., H. Karasaki, et al. (1997). "The characteristic gene expressions of MAPK phosphatases 1 and 2 in hepatocarcinogenesis, rat ascites hepatoma cells, and regenerating rat liver." Biochem Biophys Res Commun **239**(3): 746-751.
- Young, M. R. and N. H. Colburn (2006). "Fra-1 a target for cancer prevention or intervention." Gene **379**: 1-11.
- Zehorai, E., Z. Yao, et al. (2010). "The subcellular localization of MEK and ERK--a novel nuclear translocation signal (NTS) paves a way to the nucleus." Mol Cell Endocrinol **314**(2): 213-220.
- Zhang, L., W. Zhou, et al. (1997). "Gene expression profiles in normal and cancer cells." Science **276**(5316): 1268-1272.

- Zhang, W., J. Hart, et al. (2005). "Differential expression of the AP-1 transcription factor family members in human colorectal epithelial and neuroendocrine neoplasms." Am J Clin Pathol **124**(1): 11-19.
- Zhang, Y., J. N. Blattman, et al. (2004). "Regulation of innate and adaptive immune responses by MAP kinase phosphatase 5." Nature **430**(7001): 793-797.
- Zhang, Z., S. Kobayashi, et al. (2010). "Dual specificity phosphatase 6 (DUSP6) is an ETS-regulated negative feedback mediator of oncogenic ERK signaling in lung cancer cells." Carcinogenesis **31**(4): 577-586.
- Zhu, L., P. Gibson, et al. (2009). "Prominin 1 marks intestinal stem cells that are susceptible to neoplastic transformation." Nature **457**(7229): 603-607.
- Ziskin, J. L., D. Dunlap, et al. (2012). "In situ validation of an intestinal stem cell signature in colorectal cancer." Gut.